

# Numerical investigation of the aeration process in the MBR system equipped with a flat sheet membrane module

Dissertation

Zur Erlangung des akademischen Grades Doktor-Ingenieurin (Dr.-Ing.)

vorgelegte Dissertation von Yingchen Cao aus Hubei

Tag der Einreichung: 20.11.2019

Tag der Prüfung: 14.02.2020

Darmstadt — D 17

1. Gutachten: Prof. Dipl.-Ing.Dr. nat.techn. Wilhelm Urban
2. Gutachten: Prof. Dr.-Ing.habil. Yongqi Wang



TECHNISCHE  
UNIVERSITÄT  
DARMSTADT

Institut IWAR  
Fachbereich Bau- und Umweltinge-  
nieurwissenschaften

Numerical investigation of the aeration process in the MBR system equipped with a flat sheet membrane module  
Dissertation

Vorgelegte Dissertation von Yingchen Cao aus Hubei

1. Gutachten: Prof. Dipl.-Ing.Dr. nat.techn. Wilhelm Urban
2. Gutachten: Prof. Dr.-Ing.habil. Yongqi Wang

Tag der Einreichung: 20.11.2019

Tag der Prüfung: 14.02.2020

Darmstadt — D 17

Yingchen, Cao : Numerical investigation of the aeration process in the MBR system equipped with a flat sheet membrane module  
Darmstadt, Technische Universität Darmstadt,  
Jahr der Veröffentlichung der Dissertation auf TUpriints: 2020  
Tag der mündlichen Prüfung: 14.02.2020

Veröffentlicht unter CC BY-SA 4.0 International  
<https://creativecommons.org/licenses/>

---

## Declaration of Dissertation

---

Hiermit erkläre ich, Yingchen Cao, geboren am 02.10.1990 in Hubei, VR China

- dass ich in der Vergangenheit weder an der Technische Universität Darmstadt noch an einer anderen Technische Hochschule oder Universität an einer Promotion gearbeitet oder Ähnliches versucht habe und
- dass meine Dissertation nur unter Einbeziehung der von mir genannten Hilfen von mir selbständig verfasst und angefertigt wurde.

Darmstadt, 20.11.2019

---

(Yingchen Cao)

---



---

## Acknowledgement

---

I want to express my sincere appreciation to Dr. Sonnenburg, who guided me into the field of CFD analysis and set up the cooperation opportunity with the partner company MICRODYN-NADIR GmbH to finance me promotion partly. Without the opportunity, my life path would be totally different, and there is high chance that I cannot conduct research in our departments at IWAR, let alone presenting this dissertation. Throughout my promotion, Dr. Sonnenburg, as my mentor and scientific advisor, supported me with his immense patience and expert guidance and steered me in the right direction whenever I ran into trouble on my research and writing. He also gave me the opportunity to take part in the project with Zweckverband Landeswasserversorgung Wasserwerk Langenau for the modeling of a rapid decarbonization reactor. Working with him is for me a great learning and research experience.

I would also like to take the opportunity to thank Prof. Dr. Urban, who offered me the opportunity to work at Institute IWAR and conduct scientific research under his guidance. Without his encouragement I could never finish my dissertation this year. Thanks very much for the instructive suggestions to my dissertation, to my research and my work. I am deeply grateful that he supported me to attend the summer school in China and the IWA membrane conference in France to present my work there and exchange academic experiences and research with international scientists. Along with Prof. Dr. Urban, I would like to thank Prof. Dr. Wang, my second reviewer, who has given me professional suggestions about my dissertation. The conversations with him were always thought-provoking and helped me to gain a better understanding of the basics of CFD.

This work would not have been possible without the financial support of MICRODYN-NADIR GmbH and the institute IWAR. Besides the financial support, MICRODYN-NADIR GmbH has excited my interest in CFD by offering me the master thesis in the very beginning. My grateful expression goes to Mr. Bareth, who set up the project for me. Along with Bareth, I would like to express my gratitude to Mr. Fischer, Mr. Schreier and Mr. Manuel who offered me valuable help, provided me with experimental data and geometrical data and shared practical experiences with me during my work at IWAR.

I am grateful to all colleges of IWAR, with whom I have had the pleasure to work with during my promotion. Thank you for helping me with the administration staff, giving me valuable suggestions during Doktorand Seminar and caring for me. I also want to acknowledge my master students who researched with me together.

Besides, calculations for this research were conducted on the Lichtenberg high performance computer of the TU Darmstadt. I want to express my thanks to the ones who helped me when I met problems in my cluster.

Last but not least, it is my friends and my family that always give me unconditional love, support, and encouragement whenever I am upset.



---

## Abstract

---

This PhD study is devoted to numerically quantify the hydrodynamic characteristics in FS modules, such as shear stress distribution on the membrane surface and flow field distribution in membrane channels, under different operational and configurational conditions, so that it can provide some hints for the design and the operation of FS membrane modules. For this, interDyMFoam with the volume of fluid (VOF) method for modeling gas-liquid two-phase flow and the self-developed solver (interSolidFoam) coupled with the sludge models for modeling quasi gas-liquid-solid three-phase flow are adopted to simulate the ascent of single bubble and bubble swarms in FS membrane channels with the liquid medium of water and activated sludge, respectively. The critical parameters of the aeration process in FS modules, such as airflow rate, bubble size, superimposed liquid velocity, membrane channel depth, and MLSS concentration, are investigated in numerical models, and their effects are examined fundamentally. The models are validated against the experimental data from the literature in terms of bubble terminal rise velocity, and a good agreement is obtained between them.

Numerical results reveal that the best performance is achieved at the narrowest membrane gap distance investigated, where the maximum shear stress is obtained under the same operational conditions. Therefore, it is recommended that the smallest membrane channel of 6 mm should be applied to the FS membrane modules for better membrane fouling control. Besides, the operational parameters affect the hydrodynamics in the FS membrane module significantly. Among all of the varied parameters, MLSS concentration, namely the rheology of non-Newtonian fluid, affects the bubble ascent behavior most. Airflow rate and superimposed liquid velocity are the parameters that have the most substantial influence regarding area-weighted shear stress, where a generally rising trend is observed with an increase in superimposed liquid velocity or an increase in airflow rate.

**Keywords:** CFD, VOF, shear stress, flat sheet membrane, single bubble, bubble swarms, activated sludge





---

## Contents

---

Contents	v
List of Figures	vii
List of Tables	ix
1 Introduction	1
1.1 Background and motivation . . . . .	1
1.2 Research questions . . . . .	3
1.3 Thesis scope and outline . . . . .	4
2 Literature review	7
2.1 MBR system . . . . .	7
2.2 Research status of MBR . . . . .	10
2.3 Status of CFD research in MBR . . . . .	14
2.3.1 CFD modeling of MBRs on different scales . . . . .	15
2.3.2 CFD modeling of different membrane modules . . . . .	19
2.4 Numerical methods . . . . .	39
2.4.1 Governing equation for single phase . . . . .	39
2.4.2 Turbulence modeling . . . . .	39
2.4.3 Multiphase flow modeling . . . . .	46
2.4.4 Integrated models . . . . .	50
2.5 Discussion . . . . .	61
3 Methods	67
3.1 Solver development . . . . .	67
3.1.1 InterDyMFoam . . . . .	67
3.1.2 Implementation of sludge models . . . . .	70
3.1.3 InterSolidFoam . . . . .	73
3.2 Model Geometry . . . . .	75
3.3 Meshing . . . . .	77
3.3.1 AMR vs. static mesh . . . . .	77
3.3.2 Mesh benchmarking . . . . .	78
3.3.3 Refinement in near-wall regions . . . . .	81
3.4 Turbulence model . . . . .	84
3.5 Material properties . . . . .	85
3.6 Initial and boundary conditions . . . . .	86
3.7 Solution . . . . .	87
3.8 Discussion referring to research questions . . . . .	87

---

4	Results and discussion	91
4.1	Influencing parameters on single bubbles . . . . .	91
4.1.1	Bubble size . . . . .	91
4.1.2	Channel depth . . . . .	99
4.1.3	Superimposed liquid velocity . . . . .	100
4.1.4	MLSS concentration . . . . .	103
4.2	Influencing parameters of bubble swarms . . . . .	106
4.2.1	Bubble swarm dynamics . . . . .	106
4.2.2	Superimposed liquid velocity . . . . .	119
4.2.3	Channel depth . . . . .	121
4.2.4	MLSS concentration . . . . .	122
4.3	Discussion referring to research questions . . . . .	124
5	Summary	129
	References	133

---

## List of Figures

---

1	Sludge caking at membrane sheets in a FS module [source: The MBR Site [16]] . . . . .	2
2	Research roadmap . . . . .	5
3	The MBR process in wastewater treatment plant Hünxe . . . . .	7
4	FS membrane modules installed in submerged MBRs (from left to right: Scheme of a submerged MBR system; Scheme of an aerated submerged FS module (adapted from [61]); Illustration of the channel between two membrane sheets) . . . . .	8
5	Research trends of MBRs: number of MBR-related published papers in key subject areas between 2000 and 2018 . . . . .	11
6	CFD modeling of MRBs: proportion of publications relating to CFD and MBRs in large-scale, in micro-scale, in full-scale (left); proportion of publications using CFD modeling MBRs with the tubular, HF, FS membrane modules (right) . . . . .	16
7	Flowchart of solution sequence of two-phase incompressible flow in interDyMFoam . . . . .	68
8	Model validation against the previous experimental work [253] . . . . .	70
9	Apparent viscosity of activated sludge with a MLSS concentration of 8.83 g/L . . . . .	72
10	Simulated and measured settling curve in 30 minutes at a MLSS concentration of 1.87 g/L .	73
11	Flowchart of solution sequence of three-phase (air-water-sludge) incompressible flow in interSolidFoam . . . . .	74
12	Model geometry in front view (left) and in side view (right) . . . . .	76
13	A sketch of dynamic mesh with the ARM method (left) and a sketch of static mesh (right) .	77
14	Comparison of bubble rising velocity from dynamic and static meshes . . . . .	78
15	Snapshots of 4 mm bubbles at 0.05 s at different mesh refinement levels (refinement level from left to right: 1,2,3,4) . . . . .	79
16	A benchmarking of mesh grids for bubbles of different size in terms of bubble velocity . . . .	80
17	Sketch of dynamic mesh without (left) and with (right) refinement in the near wall regions .	83
18	Comparison of $y^+$ between coarse and fine near-wall meshes . . . . .	83
19	Comparison of the max. SS from coarse and fine near-wall meshes . . . . .	84
20	Comparison of bubble rising velocity from different turbulence models . . . . .	85
21	Snapshot of bubble shapes at different bubble sizes (from small to large, the volumetrically equivalent bubble sizes are 2 - 6 mm, respectively) . . . . .	93
22	Bubble shape classification based on aspect ratio ( $E$ ) and length number ( $Le$ ) . . . . .	94
23	Zones around 4 mm bubble rising in 7 mm membrane channel based on flow fields and SS distribution (arrows correspond to velocity direction of the liquid phase) . . . . .	96
24	Flow fields and SS distribution induced by a 6 mm bubble . . . . .	97
25	Max. SS induced by single bubbles of a diameter ranging from 2 to 6 mm . . . . .	97
26	Max. SS induced by single bubbles of different size in membrane channel with various gap distances . . . . .	99
27	Drag and back diffusion forces acting on a particle near the 6 mm single bubble . . . . .	101
28	Max. SS induced by 3 mm and 6 mm single bubbles under various superimposed liquid velocities . . . . .	102
29	3 mm bubble in water and sludge with a MLSS concentration of 5 g/L . . . . .	103

---

30	3 mm bubble rising velocity in sludge at different MLSS concentrations . . . . .	104
31	Viscosity distribution at membrane walls in sludge with different MLSS concentrations (MLSS concentrations from left to right: 5, 8, 10, 15, 20, 25 g/L) . . . . .	105
32	Max. SS and max. shear rate in sludge with different MLSS concentrations . . . . .	106
33	Ave. SS induced by bubble swarms generated at various gas inlet velocities . . . . .	108
34	Snapshots of 6 mm bubble swarms at different time steps . . . . .	111
35	Snapshot of a giant bubble with a serial of tiny bubbles in the simulation of 6 mm bubble swarm rising in stagnant water (left: in front view; right: in a side view) . . . . .	112
36	Ave. SS induced by bubble swarms with varying sizes in stagnant water at 7 mm spaced membrane channel . . . . .	113
37	Ave. SS induced by 6 mm bubble swarms with varying patching frequencies at 7 mm spaced membrane channel . . . . .	114
38	Snapshot of 6 mm bubble swarms in different scenarios: in 6 mm membrane channel with stagnant water, in 7 mm membrane channel with stagnant water, in 7 mm membrane channel with a liquid velocity of 0.3 m/s, and patching in 7 mm membrane channel with a low frequency(from left to right) . . . . .	115
39	Bubbles size distribution in 6 mm and 7 mm spaced membrane channel . . . . .	117
40	Ave. SS at the same aeration intensity in FS membrane modules with varying distances between the aerators and the bottom of the membrane sheets . . . . .	118
41	Ave. SS on 7 mm spaced membrane sheets with and without bubbling at various liquid velocities . . . . .	120
42	Ave. SS induced by 3 mm or 6 mm bubble swarms in membrane channels with various gap distances . . . . .	121
43	Viscosity distribution around 3 mm bubble swarms at the whole membrane wall in sludge with different MLSS concentrations (from left to right: 5, 8, 10, 15, 20, 25 g/L) . . . . .	122
44	Ave. SS and ave. shear rate of 3 mm bubble swarms rising in sludges . . . . .	123
45	Bubble distribution and shear rate distribution in the top part of the model in water (left two pictures) and in sludge with a MLSS concentration of 5 g/L (right two pictures) . . . . .	124

---

## List of Tables

---

1	Summary of basic information about commercial FS membrane modules (data collected from Judd [14]) . . . . .	9
2	Comparison of SS measurement methods . . . . .	14
3	Overview of previous CFD researches in MBRs in full scale . . . . .	18
4	Overview of previous CFD researches in MBRs with FS membrane modules . . . . .	25
5	Overview of previous CFD researches in MBRs with HF membrane modules . . . . .	33
6	Overview of previous CFD researches in MBRs with tubular membrane modules . . . . .	38
7	Comparison of two-equation RANS turbulence models . . . . .	44
8	Summary of rheological models of MBR sludge . . . . .	51
9	Material properties at 20 °C . . . . .	85
10	Conclusions of classification of bubble shape regimes for different scenarios . . . . .	92
11	SS exerted by a single bubble in the FS membrane module . . . . .	98
12	SS exerted by bubble swarms in the FS membrane module . . . . .	109



---

## Nomenclature

---

### Physical quantities

$\mathbf{R}$	The strain rate tensor
$\boldsymbol{\tau}$	The shear stress (vector)
$\mathbf{f}$	The force (vector)
$\mathbf{g}$	The gravitational acceleration (vector)
$\mathbf{n}$	The surface normal vector
$\mathbf{u}$	The velocity (vector)
$A$	A non-dimensional hydrodynamic parameter
$B$	A non-dimensional hydrodynamic parameter
$b$	Empirical parameter
$Bd$	The Bond number
$C$	The coefficient
$c$	The MLSS concentration
$Co$	The Courant number
$D$	The channel depth
$d$	The diameter
$E$	The aspect ratio
$EO$	The Eötvös number
$f$	The force (scalar)
$Fr$	The Froude number
$g$	The gravitational acceleration (scalar)
$Ga$	The Galileo number
$H$	The height
$I$	The current
$J$	The permeate flux
$K$	The Von Karmans constant

---

$k$	The flow consistency index
$k$	The kinetic energy
$L$	The longest dimension
$Le$	The length number
$m$	The dimensional regularization parameter
$Mo$	The Morton number
$n$	The flow behaviour index
$P$	The production rate
$p$	The pressure
$Q$	The flow rate
$R$	The coefficient of determination with a fixed superscript 2
$r$	The radius
$Re$	The Reynolds number
$SVI$	The sludge volume index
$t$	Time
$U$	The mean velocity of bulk flow
$u$	The velocity (scalar)
$V$	The settling velocity
$W$	The width
$We$	The Weber number
$y$	The indicator with a fixed superscript +
$\mathbf{T}$	The shear stress tensor
$\alpha$	The volume fraction
$\varepsilon$	The energy dissipation rate
$\gamma$	The shear rate with a fixed superscript $\cdot$
$\kappa$	The mean curvature
$\mu$	The dynamic viscosity of fluid
$\omega$	The specific dissipation

---



---

$\rho$	The density of fluid
$\sigma$	The coefficient in turbulent equations
$\sigma$	The surface tension coefficient
$\tau$	The shear stress (scalar)

### Subscripts

$\infty$	Terms related to infinity
0	E.g. $V_0$ represents an empirical parameter
0	Values at initial state, e.g. $\tau_0$ represents the yield shear stress
1p	Single phase values
2p	Two phase values
$\varepsilon$	Terms related to turbulent dissipation rate
$\mu$	Terms related to viscosity
$\tau$	Terms related to friction
B	Terms related to bubble
b	E.g. $\mathbf{f}_b$ represents the body force
bd	Terms related to back diffusion
buo	Terms related to buoyancy
crit	Critical values
drag	E.g. $\mathbf{f}_{\text{drag}}$ represents the drag force
DS	Terms related to dry solids
e	Experimental values
eff	Effective values
g	Terms related to gas phase
i	The $i^{\text{th}}$ phase
in	Terms related to inlet
iner	Terms related to inertial
k	Terms related to kinetic energy
l	Terms related to liquid phase

---

Lev  $C_{\text{Lev}}$  represents the Leveque coefficient

max Terms related to maximum

min Terms related to minimum

o Terms related to orifice

p Terms related to particle

r Relative values

s Terms related to sludge phase

sf Terms related to surface tension

t Terms related to turbulent

w Terms related to water phase

### Superscripts

' Time-varying fluctuating values

· Fixed superscript for the shear rate  $\dot{\gamma}$

^ Unit values or vectors

— Statistic-averaged values

+ Indicator of a non-dimensional values

R E.g.  $\tau^{\text{R}}$  represents the Reynolds stress tensor

T The transpose operator

---

## Abbreviations

---

AMR	Adaptive Mesh Refinement
ASM	Activated Sludge Model
ave. SS	Averaged Shear Stress
CAS	Conventional Activated Sludge
CFD	Computational Fluid Dynamics
CLSM	Confocal Laser Scanning Microscopy
COD	Chemical Oxygen Demand
CPU	Central Processing Unit
CSF	Continuum Surface Force
CT	Computed Tomography
DNS	Direct Numerical Simulation
DO	Dissolved Oxygen
EC	Electro-Coagulation
ENM	Engineered NanoMaterial
EP	ElectroPhoresis
EPS	Extracellular Polymeric Substances
FDG	Fluid Dynamic Gauging
F/M	Food to Mass
FS	Flat-Sheet
FSI	Fluid Structure Interaction
FVM	Finite Volume Method
HBP	Herschel-Buckley model with Papanastasion's adaptation
HF	Hollow-Fiber
HRT	Hydraulic Retention Time
LES	Large Eddy Simulation
max. SS	Maximum Shear Stress

---

MBR	Membrane Bioreactor
MCTP-MP	Micro-Channel Turbulence Promoters with Mirco-Pores
MF	Micro-Filtration
MFC	Microbial Fuel Cell
MLSS	Mixed Liquor Suspended Solids
MULES	Multi-dimensional Limiter for Explicit Solution
N	Nitrogen
N.A.	Not Available
NF	Nano-Filtration
OCT	Optical Coherence Tommography
OLR	Organic Loading Rate
P	Phosphor
PBM	Population Balance Model
PDP	Particle Deposition Propensity
PIV	Particle Image Velocimetry
PISO	Pressure Implicit with Splitting of Operator
PVDF	PolyVinyliDene Fluoride
RANS	Reynolds Averaged Navier-Stokes
RKE	Realizable $\kappa$ - $\epsilon$ model
RMSE	Root Mean Squared Error
RNG	Renormalization Group
RO	Reverse Osmosis
RTD	Residence Time Distribution
SADm	Specific Air Demand per unit of Membrane Area
SIMPLE	Semi-Implicit Method for Pressure-Linked Equations
SKE	Standard $\kappa$ - $\epsilon$ model
SKW	Standard $\kappa$ - $\omega$ model
SMP	Soluble Microbial Products

---

SRT	Sludge Retention Time
SS	Shear Stress
SST	Shear Stress Transport
SVI	Sludge Volume Index
TED	Total Energy Demand
TMP	Trans-Membrane Pressure
TSS	Total Suspended Solids
UF	Ultra-Filtration
VOF	Volume Of Fluid
WWTP	Wastewater Treatment Plant



---

# 1 Introduction

---

## 1.1 Background and motivation

---

Nowadays, with the growth of the global population and the accelerating urbanization process, the demand for drinking water and industrial water has been dramatically increased worldwide, with an accompanying increase in wastewater discharge. Wastewater is usually treated through the conventional activated sludge (CAS) process, whose general arrangement is an aeration tank mainly for organic matter removal and followed by a settling tank for the separation of sludge from the treated wastewater. Despite the disadvantage of higher operation cost [1] over CAS process, the membrane bioreactors (MBR) system, a combination of a CAS process with a membrane filtration process, usually micro-filtration (MF) or ultra-filtration (UF), which replaces the secondary sedimentation, is becoming increasingly favored and has been used as a promising alternative to CAS process [2–5], due to the well-recognized advantages [4–8]: high effluent quality; low sludge production; small footprint and flexible implementation.

Due to all these advantages and a decrease in the production cost of membranes year by year [9, 10], MBRs have been widely applied in the environmental and industrial fields [5, 11], especially in municipal wastewater treatment [2, 5, 10]. The global MBR market has experienced a high rate of expansion with a compound annual growth rate (CAGR) of 10.5% from 2008 to 2013 [2], a higher CAGR of 12.8% from 2014 to 2019 [12] and appears to expand at an even higher CAGR of about 15% from 2018 to 2026 [10, 13]. Europe is one of the principal MBR markets and holds a large share of the global MBR market [14], where Germany plays the most crucial role in it [14, 15]. The leading German membrane manufacturers and suppliers are export-orientated and entered foreign markets with the successful experience of MBR applications at home.

While the membrane production cost has exponentially decreased from \$400/m<sup>2</sup> in 1992 to \$10/m<sup>2</sup> over the past decades [9], membrane fouling has become the main contributor to overall capital expenditure and operational expenditure in MBRs. Membrane fouling is formed by the blocking of membrane pores by colloidal particles and deposition of solids as a cake layer on the membrane wall due to solids straining during the filtration, resulting in declining flux, increasing the trans-membrane pressure (TMP), and frequent membrane replacement due to frequent backwashing [12]. Fig. 1 exemplarily presents the sludge caking at membrane sheets in a flat sheet (FS) module. With the cake layer blocking the pores of membrane sheets, water cannot go through them. At its worst, the sludge caking becomes extremely thick and compacted, which can clog the channel between membrane sheets. As a result, the feed cannot go through the channel, and the operation of MBRs needs to be interrupted.

Thus, an amount of studies [3, 12, 17, 18] has been devoted to membrane fouling to investigate fouling mitigation methods. Among all fouling mitigation methods, aeration scouring is the simplest but most effective way to limit the formation of the cake layer and to alleviate membrane fouling without stopping the filtration operation and thus widely implemented in MBRs. Aeration, i.e. air injection into the mixed liquor, can mitigate membrane fouling by exerting shear stress (SS) along membrane surfaces and scoring the accumulated particles away during the ascent of bubbles. When gas sparging is introduced in the MBR system to control fouling, the membrane filtration is reported to be enhanced [19, 20], the permeate flux is reported to increase by 43% [21], and the critical flux is reported to be improved up to 1.7 times greater [22]. Despite the beneficial effect of bubbling in MBR systems reported in numerous studies [19–



Figure 1: Sludge caking at membrane sheets in a FS module [source: The MBR Site [16]]

27], high energy demand of aeration, leading to high operating cost, is the main limitation hindering the MBR application, since aeration represents respectively up to 60% - 70% [5, 28, 29] of the total energy demand in MBR plants and about 80% [28] of the total energy demand in the FS module in MBR systems. Therefore, optimization of operating parameters and a deeper understanding of the hydrodynamics during the aeration process in aerated FS membrane modules are necessary to make the process efficient resulting in saving energy and cost.

Computational fluid dynamics (CFD), a computer-based method involving fluid dynamics, heat and mass transfer, chemical reaction, transport process, etc. by means of numerical methods and algorithms [30], has become a leading tool for process modeling and analysis of flows in many fields since 1970s [31, 32]. As the computation power of computers grew, their prices dropped and the CFD software has been developed rapidly. Besides, the advantages offered by CFD such as the reduction of lead times and costs [30, 33], the ability to modify geometrical and operational parameters easily [33, 34], and to provide detailed insights into the processing system [35, 36], etc., make it a vital component for design and analyze the industrial products and processes [30]. It has been widely applied in the areas [30, 36]: aerodynamics of aircraft and vehicles, electronics, turbo-machinery, power plants, chemical process engineering, biomedical engineering and many other fields [31, 32]. In the field of water and wastewater treatment, CFD has been applied from the modeling of hydraulic elements such as pumping stations, storm overflows, screens, etc. to the modeling of physical, chemical, and biological treatment processes such as disinfection tank, activated sludge basin, digester, etc. The use of CFD tools is either to achieve a successful design and operation of treatment tanks with better hydraulic flow patterns and high pollutant removal efficiency, or to improve the existing treatment unit for better performance with low energy consumption.



---

With the development of computer science, CFD provides possibilities for quantification of hydrodynamic characteristics that can hardly be done experimentally, such as SS distribution, flow field distribution under different operating conditions in different FS membrane modules, etc. This enables numerical studies on the MBR system to shed light on the characterization of two-phase flow in MBRs. Successful application of CFD to investigate the gas-liquid two-phase flow in MBR systems have been reported by a lot of researchers [33, 37–40]. Despite numerous fundamental studies on the hydrodynamic characteristics of two-phase flow in MBR system, there has been only limited corresponding fundamental studies on bubble interactions with the FS membrane. Thus, the hydrodynamics such as the flow conditions, bubble behaviors, in submerged FS membranes are still not fully understood due to the complicated multi-phase flow in the system. To design the FS module and optimize aeration process for the desired flow regime to mitigate membrane fouling is currently mainly based on empirical techniques and experiences [41], since no universally applicable models for designing and operating MBR tank exist. In the commercially available FS modules, membrane sheets separation ranges from 5.5 to 16 mm [14], and the recommended membrane aeration rate ranges from 0.15 to 1.1 Nm<sup>3</sup>/h per m<sup>2</sup> membrane [14]. The massive difference in these parameters indicates that neither design of the FS membrane nor aeration process in the MBR system has been systematically optimized yet. There is, therefore, a need to investigate the aeration process in the FS membrane module fundamentally to gain a more in-depth insight into mechanisms involved in flux enhancement and membrane fouling control. The motivation for this research arose from the importance of optimizing the configuration of the FS module and the operational conditions in the MBR system for membrane fouling mitigation. The hydrodynamic conditions such as bubble size, gas flow rate, nozzle size, superimposed liquid velocity, the concentration of activated sludge and membrane gap distance in FS membranes are investigated in this research, since such information is vital for a basic understanding of air scouring effect in submerged FS membranes. And a fundamental understanding is the basic premise for the improvement in the design and operation of the FS membrane module and ultimate reduction in operation and capital costs. CFD provides an efficient way to bridge the gap, to overcome the shortcomings, and to achieve the optimum in the FS membrane module by examining the effects of configurational and operational parameters on membrane performance under various conditions.

**The overall aim of this thesis** is to achieve a deeper understanding of the aeration process in the FS module through fundamental investigation of bubbles, so that improvement of the performance of MBRs with the FS module can be accomplished by merely modifying individual parameters.

---

## 1.2 Research questions

---

Even after decades of research in MBRs, membrane fouling, which is the biggest obstacle impeding the broader application of MBRs owing to high energy consumption for fouling control and high capital cost for frequent membrane replacement due to mechanically and chemically backflushing for fouling mitigation [7, 14], remains the most important subject of numerous MBR studies and is becoming the hottest topic [9, 15, 42] among all the issues relating MBRs. On the other hand, CFD has become a powerful tool to design products and analyze the treatment process. In the field of water and wastewater treatment, CFD models can provide detailed insights into the treatment processes by presenting the overall hydrodynamic in each treatment unit. Hassan et al. [43] and Tong et al. [44] investigated the flow distribution through various manifolds configurations to attain outflow uniformity. McNamara et al. [45] and Sonnenburg et al. [46,

---

47] studied, evaluated, and improved grit removal technologies to achieve high grit removal efficiency. In the activated sludge basin, simulations are carried out on activated sludge mixing properties with bubbling [48] or with surface aerators and submerged impellers [49]. Other researchers including Le Moullec et al. [50–52], Rehman [53] and Lei et al. [54] have focused their studies on the physical-chemical-biological process in activated sludge systems by coupling CFD with activated sludge model (ASM). Lei et al. [54] used CFD coupled with species transport and biological process models to predict the concentration map of mixed liquor suspended solids (MLSS), dissolved oxygen (DO), chemical oxygen demand (COD), nitrogen (N) in the oxidation ditch. Given the rheological behavior of the activated sludge, the Takacs’ double exponential settling function [55] is usually coupled with CFD for the solid phase, e.g. in the simulations of oxidation ditch by Xie et al. [49]. Since MBR and CAS have many common issues [56], this raises the question, **how to apply CFD tools to optimize the design and the operation process of an aerated FS membrane module regarding of membrane fouling control performance?**

Activated sludge is an extremely complex mixture, which contains 98% - 99.7% water, suspended flocs with various forms, microorganisms, and its products (i.e. extracellular polymeric substances (EPS)), particulate wastewater constituents and dissolved nutritious substances for biomass [57]. Due to the complex in the composition of activated sludge, its rheological and settling behavior is much more complicated than the Newtonian fluid. The properties of activated sludge have a substantial influence on hydrodynamics in MBRs, membrane fouling, and membrane filtration process [57, 58]. However, most CFD studies perform simulations with Newtonian fluid instead of activated sludge. This raises the question, **how to include the activated sludge properties into the CFD simulations of an aerated FS membrane module?**

Aeration process is the most energy consuming part in an FS membrane module. Thus, a deep understanding of the aeration process is a must for a better design and operation of MBRs. As activated sludge contains liquid and solid phase, the aeration process in MBRs is characterized by the multi-phase flow. Due to the complexity of multi-phase fluid, the present knowledge of hydrodynamic characteristics of multi-phase flow in an FS membrane module is still limited. To gain a comprehensive understanding of the aeration process in the FS membrane module, one should know, **which parameters can affect the hydrodynamics in an aerated FS membrane module, and how do they affect the SS.**

---

### 1.3 Thesis scope and outline

---

In this work, aeration process in the MBR system equipped with an FS membrane module has been addressed via 3D transient simulation of bubbles’ behavior during their ascent in the FS channel with adequate length by using the open-source software OpenFOAM. The flow field in the membrane channel and the SS on the FS membrane surface are analyzed under different geometrical and operating conditions, particularly regarding the impacts of membrane gap distance, nozzle configuration, bubble size, aeration pattern, and liquid velocity. Specifically, the simulations in this study are carried out in interDyMFOam with a volume of fluid (VOF) approach, which is an interface tracking method capable of tracking the motion of bubbles in the FS membrane channel with an adequate rising length. A 3D geometry is built in OpenFOAM with a height of over 1500 mm. To save computing resources and shorten calculation time, the finer mesh is applied for gas phase and the coarse mesh for liquid. Additionally, mesh size independence is done to make sure the mesh size is fine enough to capture the interface between bubbles and liquid adequately. The resolution in the near-wall region is sufficient for calculating SS accurately. Besides, the

modeling results obtained from the 3D model are validated with the data from the literature. Furthermore, a third solid phase is added in the self-developed solver *interSolidFoam* to evaluate the effect of activated sludge concentration on the membrane fouling reduction process by taking into consideration of the settling behavior of activated sludge, as shown in Fig. 2. This new solver is developed in the OpenFOAM framework based on the existing *driftFluxFoam* and *interDyMFoam*. Subsequently, the optimization of the operational parameter, MLSS concentration, is examined based on the modified 3D transient CFD model.

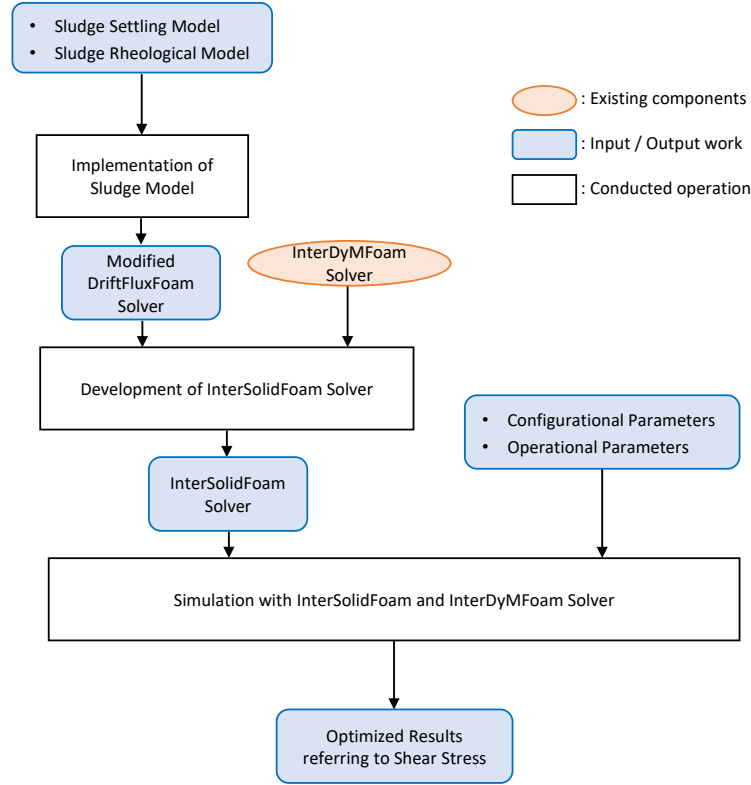


Figure 2: Research roadmap

This thesis contains five chapters whose contents are described below respectively:

Chapter 1 presents the general background and overall aim of this research, research questions, scope and outline of this thesis.

Chapter 2 introduces MBR basics, FS membrane modules, basic CFD principles. It also provides a brief analysis of the MBR research status and a comprehensive literature review on CFD research in MBRs. All references related to CFD and MBRs that can be found are reviewed on different scales, in different membrane modules, and with various numerical methods.

Chapter 3 describes the methodology used for the study. The explanations for choices concerning multi-phase modeling, turbulence models, etc. are presented here. The dynamic mesh methods, the boundary conditions, and the implementation of a third solid phase into the VOF method are described here in detail. The developed sludge model describing the rheological and settling behavior of activated sludge is presented in this chapter. Moreover, the numerical results are validated against the experimental results from the literature.

Chapter 4 deals with the numerical results from different simulations, including the simulation of a single bubble rising in a narrow channel under different conditions, the simulation of the rise of bubble swarms in

---

the FS membrane channel under different conditions and the simulation of bubble growth through different diffusers and then ascent in the channel. The results from the simulation of single bubbles regarding the effect of bubble size, membrane sheets separation, superimposed liquid velocity, MLSS concentration are presented here first. Subsequently, the results from the modeling of bubble swarms are presented. Apart from the parameters mentioned above, the impact of airflow rate, and bubble frequency are included in this part. Besides, the influences of aerator configuration on membrane fouling control are presented here, as well.

Chapter 5 summarizes the outcomes drawn from this study, along with recommendations for the possible future work.

---

## 2 Literature review

---

### 2.1 MBR system

---

MBR is a biological wastewater treatment process using activated sludge composed of bacteria and protozoa to treat municipal and industrial wastewater, and using membrane as a filter to reject solid materials. An MBR system commonly includes an aerated bioreactor and membrane modules directly submerged in the tank, as shown in Fig. 3. In wastewater treatment plant (WWTP) Hünxe, the MBR tank has two large membrane modules, and each contains 8 membrane cassettes. The microorganisms in activated sludge suspended in the tank feed on organic matters contained in the feed wastewater. The introduction of air into the system is to provide these microorganisms with sufficient oxygen, and at the same time, to create beneficial hydraulic conditions in MBRs. Solid matters and liquid phase in the feed are separated by MF or UF. The operation of an MBR system is displayed in the leftmost picture in Fig. 4.



Figure 3: The MBR process in wastewater treatment plant Hünxe

Compared to the CAS process, the secondary sedimentation tank is replaced by membrane modules, the advantages are obvious:

- High effluent quality. MF or UF with pore sizes ranging from  $0.05 - 0.4 \mu\text{m}$  [8] are used as the separation process to reject particles whose size are larger than the membrane pore sizes, such as most of the suspended solids, bacteria, large organic matters, etc. As a result, the produced effluent has a relatively high quality with a low concentration of suspended solids (usually  $\leq 5 \text{ mg/L}$ ) [4]. Besides, MBRs run typically at a lower Food to Mass (F/M) ratio or a lower organic loading rate (OLR) in the range of  $0.08 - 0.24 \text{ kgCOD}/(\text{kgMLSS}\cdot\text{d})$ , which is approximately a third to a half of OLR values in the CAS process [59]. Under the food-stringent condition, slowly degrading organics can be better treated. As a result, the MBR effluent is characterized with a lower concentration of COD, Phosphor (P) and N [59, 60].
- Small footprint. A high MLSS concentration, generally in the range of  $10 - 20 \text{ g/L}$  [9], allow the size reduction of bioreactors. And the footprint of wastewater plant is even primarily reduced since the



secondary settling tank in the CAS process is replaced with the compact configurations (membrane modules). With a small footprint, the MBR system can retrofit and update the old existing WWTP easily.

- Low sludge production. MBRs operate at a high MLSS concentration and a long retention time (SRT) of 12 - 30 days [59], which leads to an increase in the relative portion of the endogenous respiration and low sludge yield, resulting in a sludge reduction.
- Flexible implementation and installation in WWTP owing to their compact configurations.

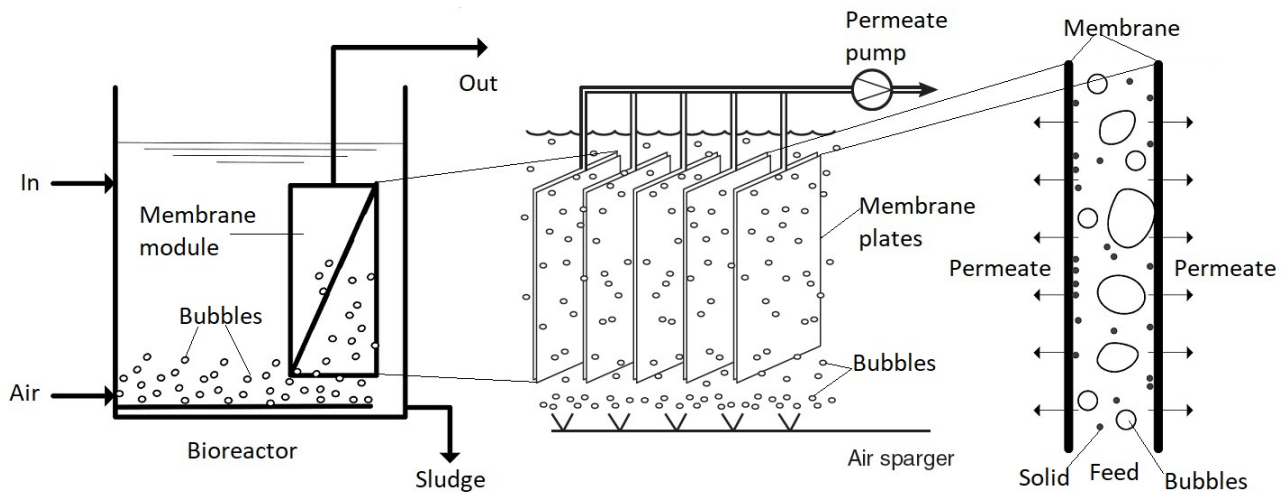


Figure 4: FS membrane modules installed in submerged MBRs (from left to right: Scheme of a submerged MBR system; Scheme of an aerated submerged FS module (adapted from [61]); Illustration of the channel between two membrane sheets)

One of the most important assemblies in MBR system is membrane - a perm-selective layer - which acts as a strainer to separate particles from liquid by forcing liquid going through the tiny pores on the membrane surface under adequate pressure, while solids remaining in the stream. Just like any other surface separation processes, a deposition layer also known as cake layer can be formed due to the straining effect on the membrane surface during the filtration, resulting in the blockage of membrane pores. Some particles can even go deeper into the membrane pores and then be adsorbed by membrane walls within the pores. This process, cake layer formation, blockage of membrane pores and adsorption by membrane materials, is membrane fouling. The rightmost picture in Fig. 4 displays this process, where the fluid goes through the membrane, while solids deposit at the membrane surfaces.

Two principal configurations are mainly employed in the commercially available MBR modules: Hollow fiber (HF) and FS modules. HF membranes have a bundle of 0.5 - 3 mm fibers [14] acting as the filtration media. During the membrane filtration, clean water is extracted from the feed via the HF wall into or out of the HF and then flows inside the fiber or otherwise, at last exits at the open fiber ends. FS has many planar and rectangular sheets or panels directly installed in the tank with the feed mixture, displayed in Fig. 4. During the membrane filtration, since a vacuum is applied on the inner side of membrane plates as a driving force, the permeate is forced to flow from the feed stream via filter media into the inside of the panel, and then collected from the pipes connecting all the membrane plates and the concentrate is returned to the mixed liquor stream. The channel between two membrane sheets, also presented in Fig.

4, generally ranges from 6 to 10 mm in membrane products provided by larger suppliers. e.g. Huber Technology, Kubota and MICRODYN-NADIR, etc. [14], as listed in Table 1.

Table 1: Summary of basic information about commercial FS membrane modules (data collected from Judd [14])

Company	Membrane height [mm]	Membrane length [mm]	Membrane thickness [mm]	Channel depth [mm]	Aeration [ $\text{Nm}^3/\text{h}$ ]
Kubota	1560	575	6	N.A.	0.29
A3 Water	700	1040	6	7	0.685
Brightwater	950	950	7	9	0.69
Ecologix	1000	490	6	6	0.72 - 1.0
	1000	320	3	6	0.5 - 0.8
Huber	1000	1000	8	6	0.15 - 0.25
	800	400	4	8	0.6 - 0.8
Lantian Peier	1190; 1789; 2000	518	15	7	0.41 - 0.72
LG Electronics	1200	490	4	7	0.6 - 0.9
MICRODYN-NADIR	1000; 2000	500; 1000	2	8	0.2 - 0.6
MegaVision	930	610	16	16	0.75
Sinap	1000; 1800	490; 650	7; 10	7	> 0.9
Toray Industries	1620; 2320	810; 515	6.5	7	0.56; 0.67
Weise Water Systems	492	165	2	5.5	N.A.
	490	375	3.5	6	N.A.

Aeration: recommended aeration rate by membrane manufacturers [ $\text{Nm}^3/\text{h}$ ] per  $\text{m}^2$  membrane

MegaVision: Shanghai MegaVision Membrane Engineering & Technology Co., Ltd

Sinap: Shanghai Sinap Membrane Science & Techonology Co., Ltd

Lantian Peier: Jiangsu Lantian Peier Memb. Co., Ltd

HF modules, compared to FS modules, are generally cost-effective to manufacture [62], have a higher packing density allowing higher flux [8, 63], are more prone to fouling [8, 62] thus cleaning mechanically and chemically more frequently [63, 64]. Concerning energy consumption, Iglesias et. al. [28] reported that regarding the overall energy need in one wastewater treatment plant, the total energy consumption during the operation of FS modules, such as aeration, recirculating pumping, backwashing pumping, permeate pumping and priming pumping, makes up a more substantial portion of WWTP's total energy demand (TED) than that of HF modules. However, for both modules, energy needed for aeration accounts for the largest share in TED in MBR systems, respectively, 60% of the TED in HF modules and 80% in FS

---

modules [28]. Since aeration in FS modules consumes more energy [10], optimizing the constructional and operational parameters for the aeration process in the FS membrane module offers excellent opportunity to reduce the TED in MBRs. Besides, in the commercial FS membrane modules, the recommended aeration intensities are total different from membrane manufactures to manufactures, as displayed in 1, which implies an high potential improvement in the optimization of aeration process in the FS module. Thus, more efforts should be paid to it in research related to aeration in the FS membrane module.

---

## 2.2 Research status of MBR

---

Many researches have been conducted on the topic of MBR. A comprehensive review of scientific research conducted in MBR technologies based on Scopus since 2000 reveals the rising research trends in MBRs [9]. The bar chart (Fig. 5) illustrates the changes in the number of MBR-related published articles in Scopus searching membrane bioreactor over the period from 2000 to 2018, where it reveals a rapid upward trend from 2000 to 2008 and from this year on, the number of publications remained relatively stable with slight fluctuations. As demonstrated in Fig. 5, around 700 research articles related to MBR in the field of wastewater treatment are published per year in the last decade. Within this data set searching the secondary key subject areas, it is found that fouling, taking up more than 50% in the recent publications in 2018, remains the most prevalent subject among the MBR research topics, which is also proven by word cloud analysis from other researchers [9, 14, 65]. As shown in the black line in Fig. 5, the number of publications in the subject of fouling in MBR research goes sharply up year by year to around 500, revealing its rising popularity. Similarly, we can see from the chart (Fig. 5) that the subject of energy has also attracted more attention in recent years by MBR researchers, implying that studies [6, 66, 67] focus more on operating cost in MBRs.

As shown in Fig. 5, many studies have been devoted to membrane fouling investigating fouling characterization and fouling mitigation methods to make the MBR technology even more attractive. In a number of critical reviews published on the past decade by Wang et al. [68], Drews et al. [69], Le-Clech et al. [8], Wang et al. [17], Du et al. [18] and most recently published by Meng et al. [3], Schmitt et al. [9], Besha et al. [1], krzeminski et al. [12], etc. focusing on the topic of fouling in MBRs, following issues are discussed:

1. Mechanisms responsible for fouling [70]:

- Pore narrowing due to the adsorption of small particles such as natural organic matter (NOM) to membrane wall, when particles are small enough to enter the membrane pores.
- Pore plugging due to straining of particles at membrane surfaces when particles have a size similar to or larger than membrane pore size.
- Cake layer formation due to the accumulation of stained solids on the membrane's surface and this cake layer acts as a dynamic filter media resulting in cake filtration when small particles are retained by a cake of solids even though they are small enough to pass through the membrane pores.

2. Type of membrane fouling:

- Based on the nature of membrane foulants:
  - a. Biofouling deposition of microorganisms



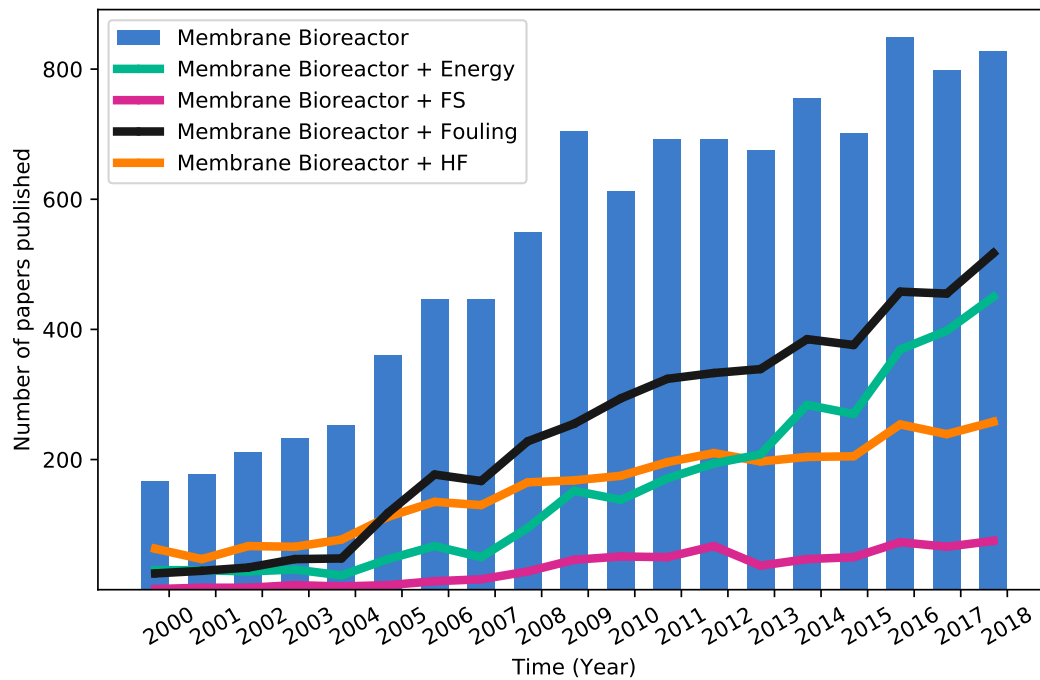


Figure 5: Research trends of MBRs: number of MBR-related published papers in key subject areas between 2000 and 2018

- b. Organic fouling deposition of proteins, humic acids, polysaccharides, and other organic substances
- c. Inorganic fouling chemical precipitation of inorganic crystals
- Based on the strength of foulants attached to membranes:
  - a. Reversible fouling removable or temporary fouling that can be removed mechanically
  - b. Irreversible fouling fouling that can only be removed chemically
  - c. Residual fouling fouling that cannot be removed mechanically or chemically but can be removed by recovery cleaning
  - d. Irrecoverable fouling irrecoverable or permanent fouling that cannot be removed by any means

### 3. Characteristics of membrane fouling:

- The primary membrane foulant in MBR systems is polysaccharides due to their large size and gelling properties
- Proteins and humic substances may lead to serious membrane fouling through the formation of bio-molecular assemblies, termed as EPS and soluble microbial products (SMP) depending on if they are bound to flocs or suspended in mixed liquor.
- Bio-cake formation due to the considerable amount of bacteria and microorganisms in sludge, which tends to adhere on the membrane surface forming a bio-film allowing bio-degradation

---

during membrane filtration, is another characteristic of membrane fouling. As fouling or TMP increase, dead cells of microorganisms and EPS have become the major foulants [9].

4. Parameters affecting fouling:

- The mixed liquor properties. The items in mixed either colloidal or soluble, is reported to be clearly related to membrane fouling [71]. The use additives such as coagulants forming sludge flocs, polyelectrolytes, adsorbing agents such as zeolite and activated carbon adsorbing colloidal and soluble substances, is to modify the mixed liquor properties in order to mitigate membrane fouling.
- The membrane characteristics. Chemically modified membranes such as an anti-fouling coating on membrane surface, or composite membranes using different chemical additives may improve MBR performance.
- The properties of sewage. Application of suitable pre-treatment to feed wastewater may improve the MBR performance by changing the properties of mixed liquor.
- The operating conditions: backflushing or relaxation, bubble aeration, backwashing with or without aeration, chemical cleaning, hydraulic load, sludge retention time, and hydraulic retention time (HRT), etc.

5. Fouling control methods:

- Physical methods:
  - a. Hydraulic cleaning, backflushing and relaxation, air scouring, ultrasonic cleaning, fluid dynamic gauging (FDG), turbulence promoters, etc.
  - b. Mechanically cleaning, vibrations or rotation, adding suspended particles and carriers, scraping, etc.
  - c. Application of pre-treatment for feed wastewater
- Chemical methods:
  - a. Chemical cleaning of membranes and chemical enhanced backflushing with chemical agents such as caustic soda, hydrochloric, sulfuric, citric, hypochlorite, hydrogen peroxide, etc.
  - b. Chemical modification in membrane characteristics such as an anti-fouling coating on the membrane surface, the enlargement of the membrane pore size or adding engineered nano-materials (e.g. ENMs) in membranes, etc.
  - c. Chemically modifying the properties of mixed liquor.
- Biological control of bio-fouling
  - a. Through optimization or modification of bio-cake
  - b. Through the degradation of SMP and EPS
- Electrically-assisted fouling mitigation
  - a. Through the electro-coagulation (EC) process to inhabit bio-cake

- b. Through the electro-phoresis (EP) process to create an electric repulsive force between membrane and foulants
- c. Through microorganisms to generate electricity biologically in the MBR system combined with microbial fuel cells (MFC)

Among all of these fouling reduction methods, aeration is still one of the simplest but most effective ways to control membrane fouling. However, aeration process in MBRs, particularly in the FS membrane module, is highly energy consuming. Hence, optimizing the constructional and operational parameters for the aeration process in the FS module offers excellent opportunity to reduce the TED in MBR systems. Therefore, more efforts should be paid to it in research related to aeration in the FS module. However, large amounts (802) of published paper are found using aeration and hollow fiber membrane searching on 11. Oct. 2018 in Scopus, the largest database of peer-reviewed literature, while only 184 articles with the words aeration and flat sheet membrane are found. While numerous fundamental studies [72–80] are carried out in HF modules about its hydraulic conditions, aeration optimization, fouling etc., the literature [23, 81–83] on fouling, aeration, hydrodynamics, etc. in the FS modules is still limited, despite the rising trend year by year in the number of published papers about the FS membrane, as exhibited in Fig. 5, where the publications on HF outnumbered the publications on FS every year. In research works, HF modules in MBRs are often overemphasized, shadowing the importance of FS modules. Thus, more studies should be taken in the FS module, since the number of municipal WWTP installed with FS modules is as high as that with HF modules. And the number of FS products worldwide is not far from that of HF products [15], implying that the FS module is as essential as HF module. Furthermore, in the German market, the amount of HF products is far less than that of FS products. Most of the large companies supplying membrane units, such as MICRODYN-NADIR, Huber Technology, Martin Membrane Systems AG, Weise Water Systems GmbH, etc., are FS suppliers, reflecting the prevalence of FS in Germany.

As an effective membrane fouling control strategy, air sparging can induce SS at membrane surfaces, as bubbles rise in membrane gaps. The induced shear forces prevent the deposition of particles due to particle back transport and aid in scouring the accumulated particles from the deposited layer, thus reducing the membrane fouling and increasing the permeate flux. A great number of studies [76, 77, 84–89] show that SS is a good indicator for membrane performance, and in general, an increase in SS can reach an increase in permeate flux. Therefore, many researches have been done to characterize SS experimentally [85, 90–92] and numerically [77, 93, 94].

Electrodifusion method (EDM), particle image velocity (PIV), and direct shear sensor measurement are the common methods for SS measurement. The basic principles, advantages, and disadvantages of these experimental measurements are listed in Table 2. In the EDM method, SS is indirectly obtained by mass transfer theory, where the shear rate is related to the limiting diffusion current, and SS is determined through the shear rate. More details of the principle can be found in previous studies [85, 90]. The EDM method can be only applied to an electrolytic solution. Moreover, the applied voltage on electrolytes should be accurately controlled, since a too low voltage may affect the measurement of the current, and a too high voltage may cause the hydrolysis process [90]. Besides, surrounding devices, pumping process, and other reagents in the flow system could affect the accuracy of the measurement of the current [90]. PIV method is an optical visualization method to obtain the velocity field in the MBR system. During the measurements, a laser sheet is projected to the flow, and the seeding particles in the flow scattering the laser light are

captured by a high-speed camera. Based on the captured position of the seeding particles and the fixed interval time, the velocity field in the MBR system can be determined [18]. After the determination of the velocity field, SS can be calculated by the velocity gradients near membrane walls. Thus, this method is able to determine the SS distribution along the membrane walls. The seeding particles are essential elements for the experiment since they should be large enough to absorb sufficient laser light and at the same time, small enough to accurately respond to the flow conditions. To get the 3D velocity field, more than one high-speed camera is needed for the measurement, resulting in a complicated experimental setup. Due to cameras and Lasers, the cost of experiment rigs is relatively high. Another way to get shear stress is by the direct measurement of shear force through shear force sensors [92]. Then SS is calculated as the ratio of the measured shear force to the measured area. This method is more flexible than other methods, as shear force sensors are easily removed and installed at the target position. There is no specific requirement of solutions [18]. However, the measured points are limited, similar to the EDM method.

Table 2: Comparison of SS measurement methods

Experimental measurements	Electrodiffusion method (EDM)	Particle image velocity (PIV)	Shear force sensor measurement
Measured quantities	Limiting diffusion current	Velocity field	Shear force
Principles	Mass transfer theory $\tau_e = \mu C_{Lev}^{-3} \cdot I^3$	Velocity gradient $\tau_e = \mu \frac{\partial u}{\partial y}$	shear force divided to measured area
Advantages	Relatively low cost	Provide more information such as SS distribution	Flexible installation No restriction of solutions
Disadvantages	Electrolytic solutions with a known viscosity Limited measure points Affected by surroundings	Solutions with a known viscosity Complexed experiment setups for 3D velocity field high cost safety constraints	limited measure points

$u$  refers to a certain component of the vector  $\mathbf{u}$

Unlike experimental methods, CFD can provide detailed insights into MBR systems by presenting the overall hydrodynamic conditions such as flow fields and SS distribution. It can change the geometry of the MBR system and the operational conditions easily. As there are no experimental rigs, it can also reduce the cost. All these advantages make it a powerful analytical tool for designing and optimizing the operation process in MBRs.

### 2.3 Status of CFD research in MBR

A considerable amount of CFD research has been done in MBR field during the last decade. By searching membrane bioreactor and CFD in Scopus, 278 publications in total came out. After reviewing these publications one by one, it is found out that barely 100 published papers are modeling MBR using CFD. While examining this literature, other related papers that are mentioned in the reviewed papers and not included in the research results can be found. All of these MBR-CFD related literature will be used as a database to analyses the CFD research trends in MBRs and to perform the literature review. Based on

the searching results, the first study on MBRs using CFD was carried out by Ndinisa et al. [25, 26] in 2006. Actually, the pioneer work can be traced to Essemiani et al. [95] in 2001, who modeled the spherical cap bubble in the FS module in a 2D simulation, however, apart from the shape and location of bubbles, nothing else was gained numerically. Later, in 2003, a more meaningful numerical study was conducted by Cui et al. [19, 20], who performed a detailed 2D axi-symmetric modeling of bubble flow in tubes for UF. Then came the investigations by Ndinisa et al. [25, 26] in 2006, who characterized the gas-liquid two-phase flow in submerged flat sheet. The numerical investigation of a full-scale MBR system is followed by Brannock et al. [41, 96–99] around 2010. The numerical study of rotating MBR systems, tubular, HF, hollow sheet modules is followed by Ratkovich's group [38, 100–108] around 2012. Since then, numerous studies have been inspired by those forerunners, and the subject has been extensively explored. As the popularity of CFD analysis in MBR systems grows steadily, more and more publications have been seen worldwide, particularly in China. Liu's research group [37, 94, 109] worked on modeling HF membranes and Wang's group [40, 83] and Yang's group [39, 58, 110] simulated the FS membrane module with CFD to identify the optimized design and operation for enhancement on fouling migration hydraulically.

---

### 2.3.1 CFD modeling of MBRs on different scales

---

The simulations of MBRs are carried out on different scales. Based on the CFD-MBR literature, a pie chart (Fig. 6) is made. This pie chart depicts the percentage of publications where CFD simulations are conducted in MBRs on different scales and in different modules, i.e. in micro scale, in lab scale, in full scale, in tubular, in HF, and FS membrane module. As presented in the left picture of Fig. 6, a significant majority of the numerical methods developed so far, particularly for two-phase or three-phase problems are applied only in lab-scale MBR research, which accounts for about 90% of all numerical investigations on the MBR system. It is followed by the MBR research in full scale, with about 10%. Unlike large scale and lab scale researches, few studies focused on the MBR system in micro-scale employing CFD, while many researchers [35, 111–114] modeled the high pressure membrane filtration process, i.e. reverse osmosis (RO) processes, in micro scale, where flow distribution, mass transfer, soluble transport are investigated in spiral-wound membrane modules with different spacer designs using approaches based on CFD. After reviewing all the literature in the database, a summary of CFD researches relevant to MBR in different scales is presented here.

#### **Modeling MBRs in micro scale**

Limited researches [115–117] are modeling MBRs in micro-scale with a focus on cake layer formation during the membrane filtration process. In the study by Yu et al. [115], confocal laser scanning microscopy (CLSM) was performed to scan the structure of the cake layer, to obtain the fluorescent images for reconstructing the three-dimensional structure of cake layer in CFD software. With the geometry of the cake layer in ANSYS, its permeability could be calculated numerically. Their results agreed with the experimental data well and their model could predict the permeability accurately. Similarly, Fortunato et al. [116] used optical coherence tomography (OCT) to extract the profiles of bio-film structure and these extracted profiles was converted into the CFD software as the model geometry. Based on all these data, flux was calculated numerically, which was in good agreement with the flux obtained experimentally. Poostchi et al. [117] determined the velocity field and SS distribution on the dynamic membrane. Besides, researchers investigated the MF through the porous membrane at a small scale. Rahimi et al. [118] implemented

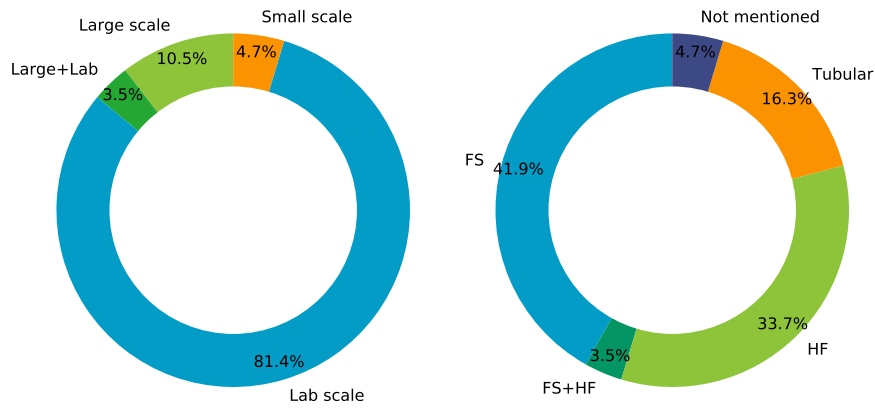


Figure 6: CFD modeling of MRBs: proportion of publications relating to CFD and MBRs in large-scale, in micro-scale, in full-scale (left); proportion of publications using CFD modeling MBRs with the tubular, HF, FS membrane modules (right)

the Darcy equation into the numerical methods to predict the local permeate flux through the porous membrane sheet during MF process for various input-output pressures and in different membrane cell geometries.

#### Modeling MBRs in lab scale

Most of simulations are conducted in lab scale not in full scale due to the high computing resource for the full-scale MBR system, particularly for multi-phase simulations. Compared to large-scale simulations, lab-scale simulations either have smaller membrane module configurations or have limited membrane sheets or fibers to save computing time and resources. It should be noted that the simplifications in the model might lead to a disagreement between the corresponding numerical results and the real situation. Kang et al. [119] reported a huge difference between lab-scale system and full-scale system in terms of mixed liquor velocity and air velocity. Compared to the lab-scale system, mixed liquor velocity and air velocity for a plant system is about 50% - 80% lower and 15% - 40% lower, respectively. This observation indicated that the hydrodynamics in the MBR system is overestimated in lab scale. This conclusion can be proven by comparing the lab-scale simulations [120, 121] with a full-scale simulation [39]. The existence of baffles improved SS in MBRs by 6.67% in a full-scale application [39]. Under the same condition, it's up to roughly 20% in lab scale [39]. The beneficial effect of the inclusion of baffles in membrane module on SS was found 38.9% higher [121] and 74% higher [120] than that without baffles in a lab-scale MBR system with a more simplified model. The results from simulations of MBRs in lab scale will be discussed in the next section in different membrane module in detail.

#### Modeling MBRs in full scale

A summary of publications concerning the modeling of full-scale MBRs is presented in Table 3, where only limited studies performed simulations in full scale due to high computing time. To shorten the calculation time, the whole membrane module in full scale is usually regarded as one zone either with an impermeable block or with a porous media. Studies [122] proved that numerical results are more accurate if the CFD model is coupled with a porous zone instead of impermeable block. With such simplification of porous media representing membrane module, Ratkovich et al. [123] compared the air distribution in

---

airlift MBR systems with a ring aerator and with a disk aerator and found the disk aerator could provide better air distribution. Brannock et al. [41, 97, 99] evaluated the mixing performance in different full-scale MBRs configured with varying membrane modules by comparing the residence time distribution (RTD). By examining the inside configuration where the membrane modules are directly installed in bioreactors with the outside configuration where membrane modules are submerged in an external filtration tank, they found more pronounced internal circulation velocity in the outside configuration and thus concluded that the outside configuration is less prone to membrane fouling than the inside configuration. They also discovered that aeration dominated mixing in MBRs for both inside and outside configurations. Moreover, the position of inlets is found to be crucial for the mixing properties in MBR units. Less short circuiting and dead zones were found in the system if the inlet was placed near the aeration vessel center. As for membrane modules, they found that the mixing degree was high for both HF and FS modules, with HF modules slightly closer to complete mixing. In another study [124], HF membranes are identified to require 20% less total energy and 50% less aeration energy for the same amount of permeate obtained. With the assumption of a porous zone representing FS modules, Wu et al. [125] identified the optimal position of the FS module in the MBR tank by evaluating the self-defined risk velocity in different cases. With similar CFD approach where HF modules are represented by porous media, Saalbach and Hunze [126] reported the importance of aeration on flow field in the MBR tank and Kang et al. [119] found that hydrodynamic conditions were improved merely by enlarging the size of the MBR tank.

Apart from recommendations for design and operation of the MBR system in full scale, studies also focus on the comparison between full scale results and lab scale results, since lab scale simulations cannot be fully consistent with full scale simulations due to the huge difference in module configurations and sizes. Kang et al. [119] investigated differences in hydrodynamic characteristics of pilot- and full-scale MBRs with the simplification of hollow-fiber modules as homogeneous porous media. Mixed liquor and air velocity were found roughly 50% - 80% and 15% - 40% lower in the full-scale system than in lab scale, respectively. The differences between lab-scale and large-scale simulations were also discussed in the study by Yang et al. [39]. They found that the averaged shear stress (ave. SS) in full-scale simulations is much less sensitive to geometrical parameters, such as inclusion of baffles and membrane spacing, than that in lab scale simulations. In full-scale MBRs, SS was found 6.67% higher in FS modules with the presence of baffles compared to that without baffles, while in lab scale, it is 19.53% higher in MBRs with 5 membrane sheets. In other studies of lab-scale MBRs, the presence of baffles in the FS membrane module with one membrane channel was reported to be able to increase the SS by up to 74% [121]. The contradictory results from simulations of MBRs for lab-scale application and for full-scale application could be attributed to the difference in the number of membrane sheets. Studies [83] have shown that SS on the membrane surface of each membrane sheet was found to be related to membrane sheets numbers. Besides, the addition of one baffle in the FS membrane module with only one baffle would change the hydrodynamics in this system significantly, while the addition of one baffle in the FS membrane module with many membrane sheets will not change the hydraulic conditions in the system much.

Table 3: Overview of previous CFD researches in MBRs in full scale

Author	Membrane module	Dimension [mm]	Phases	Modeling method	Implementation	Results
Brannock et al. [41]	inside/outside	$L$ : 2020 $D$ : 950	gas-liquid	Eulerian	Porous media	aeration is the main mixing mechanism; inlet position is crucial for the mixing properties
Brannock et al. [99]	FS/HF	N.A.	gas-liquid	Eulerian	Mass transfer; Species transport	CFD model coupled with activated sludge model was validated
Brannock et al. [97]	FS/HF	N.A.	gas-liquid	Eulerian	MLSS	turbulent viscosity rather than the sludge rheology only has a significant effect on the hydrodynamic conditions.
Wang et al. [122]	HF	N.A.	gas-liquid	Eulerian	Porous media; MLSS	CFD model coupled with porous zone could get more accurate results; Velocity decreased as MLSS concentration increased
Kang et al. [119]	N.A.	N.A.	gas-liquid	Eulerian	Porous media; MLSS	huge difference was observed in terms of velocity drop in full scale system and in pilot scale system
Wu et al. [125]	FS	2000; 2700; 1250	gas-liquid	Eulerian	porous media	configuration of FS membrane module was studied and an optimum was identified
Yang et al. [39]	FS	2360; 1390; 4400	gas-liquid	Eulerian	DO	lab-scale and full-scale AEC-MBRs are compared with CFD simulation; Cyclic aeration modes would be a better aeration strategy
Ratkovich et al. [123]	HF	N.A.	gas-liquid	VOF	Porous media	disk aerator can create a better air distribution in two phase flow than ring aerator.
Saalbach and Hunze [126]	HF/FS	N.A.	gas-liquid	N.A.	Porous media, ASM	aeration has a great impact on flow field
Amini et al. [33, 127]	FS	500; 1000; 8	gas-liquid-biomass	Eulerian	PBM; MLSS	outmost membranes are most prone to fouling; optimal bubble size was 3 mm; higher MLSS concentration lead to more fouling
Liu et al. [128]	HF	$L$ : 1500	gas-liquid-biomass	N.A.	Porous media	bubble size distribution showed that most bubbles are 3 - 5 mm in diameter; small bubbles induce higher absolute value of vertical velocity in membrane module

Dimension:  $L$  represents length;  $D$  represents diameter; when there is no letter, three numbers stand for the length, width and height or the channel gap distance

MLSS: implementation of MLSS expression; PBM: implementation of population balance model

DO: implementation of DO models

N.A.: not available



---

### 2.3.2 CFD modeling of different membrane modules

---

Much work has been reported on CFD modeling of MBRs in different membrane modules. The literature reviewed revealed that CFD had been widely used in FS modules, HF modules, and tubular membrane modules, as illustrated in the pie chart on the right side in Fig. 6. Most of the reviewed literature in the database mentioned above studied hydrodynamics in the FS membrane modules using CFD which accounts for more than 40% of the total CFD-MBR related publications. In the literature, researchers are mainly focused on the optimal design of FS modules and on operational parameters.

Next comes HF membrane modules with nearly 35% of the total. More HF studies are carried out in 2D in cylinder coordinate to predict the permeate flux or nutrient removal efficiency by implementing self-developed models, and no such studies are found in FS modules. This is attributed to the mathematical model for permeate flux prediction in porous media, which is developed in cylinder coordinate and only suitable for simulations in a HF module. Besides, research on backwashing process was found in HF modules and cannot be found in FS modules. In the literature, a vast of researchers regarded the whole HF module as porous media for simplifying the real situation, while this simplification can be found only in one study by Wu et al. [125] in the FS module. This can be attributed to the high packing density in HF modules and low packing density in FS modules. With a high packing density, it might make sense to view the whole HF module as a porous media as a whole. However, this treatment might not be well applied in FS, since the channel distance between membrane sheets are relatively high. Therefore, the same method in the FS module might lead to untrustable numerical results. Besides, backwashing process [129, 130] and cake layer growth process [131] are also included in the HF module.

Many studies concerning simulations of tubular membranes or rotating membrane can be found in the database, even though tubular modules are not widely applied in the MBR system as HF and FS modules. This might be attributed to the tubular geometry of this membrane module, which can be simplified as a 2D axi-symmetric system to save the computing resources. In early studies [19, 20, 132, 133], mainly two-phase problem included, simulations are undertaken to investigate hydrodynamics in tubular membrane module and their effect on membrane filtration performance. With the advance in the computer, later researches [134–136] can solve more complex problems with more complex configurations equipped with the impeller. Numerical results showed that the effects of bubbling [19, 100, 132, 133] and turbulence promoter [137] in tubular membrane are similar to that reported in HF and FS modules.

#### **FS membrane module**

The majority of the relevant literature studied hydrodynamics in the FS membrane modules using CFD. A summary of the previous studies concerning simulations of FS membrane modules is reviewed below and listed in Table 4, where it can be seen that researches have made great efforts into modeling FS modules to achieve optimum by analyzing the following constructional and operational parameters.

##### 1. Configurations of FS: membrane plates

The presence of the FS module could affect the hydrodynamics in the MBR tank. However, this effect is still in dispute. Moraveji et al. [138] revealed that the presence of membranes could increase gas hold up, whereas Prieske et al. reported that [139–141] with the FS module in the MBR tank, the total gas holdup is lower than that without the FS module. Besides, they found that the presence of membrane plates had a significant deceleration effect for bubbles in a certain size range.

Moreover, the location of the FS module installed in the MBR tank is proven to affect the fouling control for full-scale MBRs in simulations by Wu et al. [125], who proposed a risk water velocity to judge membrane fouling potential and identified an optimal membrane location in the MBR tank. Khalili et al. [142] suggested to shorten the liquid level, i.e. the distance between the membrane unit top and water surface, so that the mixing intensity and liquid velocity distribution in the riser could be improved. However, these results might not be in consist of the results from Yang et al. [39], who also investigated the FS module location in the full-scale MBR tank and revealed that the relative location of the FS module does not affect the surface SS that much for a full-scale MBR application. Comparing these CFD studies, the results from Yang et al. [39] are more plausible, for they modeled the FS module at full-scale directly and used SS as indicators.

When it involves multi membrane sheets in CFD studies, efforts [33, 40, 83] are made to identify which membrane sheets are most prone to membrane fouling. Amini et al. [33] found out that the outermost membranes are more vulnerable to membrane fouling because the SS and the cross-flow velocity between the outmost membrane sheets and the module wall are lower than elsewhere. Moreover, in their three-phase simulation, biomass tends to be accumulated near the module wall, particularly near the outermost membranes. This discovery that outmost membranes are prone to fouling was confirmed by Wang et al. [40, 83] who simulate the bubble slug in 14 channels and identified that the lowest SS was on the outmost membranes.

One of the most popular geometrical parameters of the FS module is membrane gap distance, which plays a dominant role in hydrodynamics in submerged FS membranes [25]. Generally speaking, SS increases as membrane gap distance decreases. Prieske et al. [139–141] found SS decreased significantly with an increase in the distance between the two membrane plates and the optimal condition for the FS membrane is found to be 5 mm bubbles with a channel depth of 5 mm. Wang et al. [40, 83] identified the optimal configuration was at a membrane channel gap of 6 mm. However, in the study conducted by Wei et al. [93], the optimal gap distance was around 8 mm. While strong influence of membrane spacing distance on SS is found in lab-scale MBRs, SS is not that much sensitive to membrane gap distance in full scale MBRs, where SS increased only by 4.2% as membrane space decreased from 10 to 7 mm, reported by Yang et al. [39].

## 2. Configurations of FS: baffle configuration

Baffles are proven to play a vital role in membrane fouling control for the FS module in the lab-scale MBR system both in simulations and experiments [25, 26, 121]. Ndinisa et al. [25, 26] are the first to investigate the effect of baffle installed in FS membrane modules experimentally and numerically. They revealed experimentally that baffles could decrease fouling rate and increase critical flux significantly. Their numerical results showed that the presence of baffles could affect the hydraulic conditions in FS modules significantly. Kim, D. C. and K. Y. Chung[143] found that the SS between the membrane and the baffle was higher than the SS between membrane sheets. Their results are in contrary to the numerical results in a previous study by Amini et al. [33] who revealed that the SS was lower between the outmost membrane sheet and tank wall than that between membrane sheets in their research. The reason for this contradiction between these two conclusions might lie in the presence of baffles, to be precise, the distance between the outmost membrane sheet

---

and tank wall or baffle wall. In the former CFD study, baffles were installed into the MBR tank and the distance between the outmost membrane sheet and baffle was identical to the gap distance between membrane sheets, while in the later, there were no baffles and the distance between the outmost membrane sheet and tank wall was 3 times as large as the gap distance. Anyway, both studies proved the importance of baffles in hydrodynamics in lab-scale MBRs.

Yan et al. [121] made detailed research on baffles and investigated the effect of baffle configuration, baffle location and baffle sizes on the hydrodynamics in an airlift FS module in bench scale. The results indicated that the baffle location and size have a significant impact on MBRs hydrodynamics, particularly at lower aeration intensities. In their later CFD study published in 2016 [120], they concluded that the ave. SS on the membrane surface in MBRs with baffles was 74% higher than that without baffles. However, the results in other studies [40, 83] revealed that the ave. SS on the membrane surface is related to membrane sheets numbers. And the simulations conducted by Yan et al. [121] was performed with only one or two membrane sheets in their studies, where the effect of the presence of baffles might not be accurately predicted for real situations where there are plenty of membrane sheets in one FS module, for example, 50 membrane sheets are installed in BIO-CEL<sup>®</sup>, a product provided by Microdyn-Nadir GmbH. In this case, the flow in these channels would be much stable than that in one channel, which is proven by the results conducted by Yang et al. [39] in MBRs with 5 membrane sheets. SS was 6.67% higher with baffles than without baffles in full-scale MBRs, while it was 38.9% higher and 74% higher in lab-scale MBRs, investigated by Yan's earlier and later study, respectively. Therefore, the effect of baffles on hydrodynamics in the MBR system tends to be overestimated at a lab scale.

Khalili et al. [144] made a further study on the effect of the baffles by changing their angles on the membrane resistances, which is highly correlated with SS on the membrane surface. The numerical results demonstrated that by changing the baffle angle from 90° to 85° the SS increased, which can migrate the membrane fouling.

### 3. Configurations of FS: turbulence promoter

One of the most popular hydrodynamic techniques under study for membrane fouling control and improvement in membrane flux is to increase the turbulence intensity in the flow channel by the introduction of turbulence promoter, which is inserted inside membranes, fixed on membrane surface or placed between membrane sheets [145–147]. Based on numerical results, the introduction of turbulence promoter in MBRs showed an enhancement in hydrodynamics in the FS module, as well.

Early work by Cao et al. [148] provided a numerical evaluation of flow pattern in a spacer-filled narrow channel with FLUENT. They reported that the inclusion of turbulence promoters could promote turbulence and local surface SS. This research group also observed the concentration boundary layer significantly affected by the recirculation regions between the two spacers in another study [149]. Karode et al. [150] carried out CFD simulations for fluid flow through FS channels filled with different types of spacers. Their numerical results showed that Spacers with a constant diameter resulted in a higher pressure drop and more uniform shear rate distribution.

Xie et al. [151–156] systematically investigated the enhancement effect of the presence of micro-channel turbulence promoters with micro-pores (MCTP-MPs) and its shapes, sizes, and positions

in submerged flat-sheet MBRs on hydrodynamics performance numerically. The numerical results showed that velocity, SS, turbulence intensity, and gas hold up are enhanced in the channel of the FS membrane equipped with MCTP-MPs than that without MCTP-MPs. Even though their 2D numerical results have shown similar tendency to their experimental results and have provided valuable insights into the flow conditions in the channel of FS membranes with MCTP-MPs, the numerical results in their work might not be reliable, as illustrated in the work of Iwatsu et al. [157] that 2D simulations cannot truthfully describe the realistic characteristics of 3D flow at a high Reynolds numbers ( $Re$ ). In the studies of MCTP, their subject is to enhance flux by creating more turbulence from MCTP, where  $Re$  is high.

#### 4. Aeration process in FS: bubble characteristics

Bubble size is another focus in the CFD-FS related literature. Increasing bubble size has a positive effect on flux enhancement [26]. Ndinisa et al. [26] explained that by increasing bubble diameter, the degree of meandering of gas increased resulting in more turbulence or mixing in the system, which helps the improvement of flux and the reduction of membrane fouling. Numerical results from Wei et al. [93] have shown that SS is more intensive in wake region where secondary flow behind the bubble is generated by bubble's motion [20]. As larger bubbles create stronger secondary flow effect, which can promote local mixing near the membrane surface, hence, enhance permeate flux, higher SS at membrane surfaces is normally induced by larger bubbles, as reported by Yamanoi and Kageyama [92] reported that compared to the mm bubbles (3.710 mm), the large cm bubbles (1121 mm) in the membrane channel could result in higher SS. Ibrahim [158] confirmed that higher SS was gained at higher bubble sizes. Wei et al. [93] simulated the rise of single large bubbles with various sizes in stagnant liquid using the VOF method to investigate the corresponding SS at the membrane surfaces and reported an increase in bubble size leading to an increase in SS. Moreover, the SS is found to increase quickly at first as bubble size increases and then slowly and even stop rising above a specific bubble diameter. There might be an optimum in bubble size with a combination of other parameters. Amini et al. [33] reported that in 8 mm membrane channel at an air velocity of 1.5 m/s the optimal bubble size is 3 mm in terms of the max. SS. Yang et al. [58] pointed out that the optimal bubble diameter was at around 4.8 mm.

Apart from membrane filtration performance, bubble size is reported to be able to affect DO concentration. Yang et al. [110] incorporated simplified bio-kinetics into CFD framework to predict the DO concentration in an airlift external circulation MBR system equipped with the FS module and found an increase in DO concentration with increasing bubble diameter.

#### 5. Aeration process in FS: aerator

A proper arrangement of aeration nozzle might be the simplest but effective way to improve SS along membrane surface in the FS membrane module, since the aerator spacing distance, the location, and orientation of nozzles affected hydrodynamics in MBRs significantly, particularly for full-scale MBRs. Yang et al. [39] reported an increase in SS and a more even bubble distribution by simply decreasing the aerator spacing distances. The experimental results from Ndinisa et al. [25] presented that at a given air flow rate, by increasing nozzle size could enhance the scouring effect by bubbling.

As for the location of nozzles, Prieske et al. [139, 140] reported a higher superficial liquid velocity in the modified MBR system by merely locating the aerators at the bottom of the MBR tank compared to the conventional MBR system where aerator is placed at the entrance of the FS module. Similarly, Wang et al. [40] pointed out that the superior hydrodynamic performance was achieved when the membrane plate centrally located above the aerator and Yang et al. [39] discovered that higher SS are gained in lab scale when aeration pipes are parallel placed to membrane sheets than perpendicular to membrane sheets, and they determined the optimal vertical distance between nozzle and membrane bottom edge of being 300 mm [110]. Result from Zhang [159] demonstrated that by increasing the ratio of the distance between aerator and membrane unit bottom to the total static depth of the MBR tank, the cross-flow velocity becomes more uniform in FS modules. However, for full scale this height is less important [39] since membrane sheets in practice are very high, and the change in the ratio of aerator-sheets distance to membrane height is much smaller in full-scale MBRs.

#### 6. Aeration process in FS: gas flow rate

An improvement in permeate flux is achieved in the FS module at a higher gas flow rate due to the greater mixing or more turbulence in the tank created by them [25, 26]. As the air flow rate increases, Wei et al. [93] and Amiraftabi et al. [160] reported an increase in critical flux and Bayat et al. [161] and Boyle-Gotla et al. [162] observed an increase in SS. A power-law relationship between gas flow rate and SS was found in CFD researches [110, 121]. Yang et al. [110] discovered a power-law correlation between the ave. SS on membrane surfaces and superficial aeration velocity projected cross-section area. Yan et al. [121] also found that the ave. SS presented a power relationship with the aeration intensity described as the specific air demand per unit of membrane area (SADm) with specific coefficients depending on membrane configurations.

However, a further increase in air flow rate above a certain velocity seems to have a minor effect on membrane filtration performance. Ndinisa et al. [25, 26] pointed out that with increasing air flow rate, membrane fouling decreased up to a given value and then stayed stable beyond this critical air flow rate. This observation is consist to the experimental research from Boehm et al. [82], who reported an increase in critical flux with increasing gas flow rate in the FS module at first and then no further increase in critical flux was observed with a further rise in gas flow rate.

#### 7. Aeration process in FS: aeration pattern

Intermittent aeration is experimentally proven to be more energy-saving for the same extent of membrane fouling reduction [163]. However, very limited studies are found to investigate this numerically. Yang et al. [39] used the cyclic aeration model to evaluate the corresponding SS numerically in the FS module and found more fluctuation in observed SS with an intermittent aeration model than continuous aeration. The higher amplitude of SS is expected to control fouling better, hence save energy consumption significantly for the same fouling control effect under the cyclic compared to the conventional aeration pattern.

Apart from intermittent aeration, the bubbling regimes (slug flow and bubbly flow) are often discussed in the literature. Javid et al. [164] compared the permeate flux under different aeration pattern in the FS membrane and found an increase in permeate flux by 78% and 30% with a slug flow and a bubbly flow, compared to that without bubbling. The beneficial effects on anti-fouling performance

---

in the FS membrane module is proven experimentally by Zhang et al. [165], who reported that compared to the bubbly flow, slug bubbling was a more energy saving aeration strategy, which was more effective to flux enhancement and could achieve a better anti-fouling performance at the same aeration intensity. Based on their conclusions, Wang et al. [40, 83] developed and optimized a novel slug aeration approach where large-sized coalescent bubbles generated periodically by an aerator below membranes broke into small bubbles which rose between membrane plates.

#### 8. Aeration process in FS: cross flow velocity

Flow conditions are necessary factors for fouling control [162] since it can determine the critical particle diameter, at which smaller particles tend to deposit on membrane surface resulting membrane fouling. Amini et al. [33, 127] revealed that higher cross-flow velocity has an advantageous effect on membrane fouling mitigation. The significant effect of cross-flow is proven by Drews et al. [141], who analyzed the drag and lifted forces in a relationship with cross-flow on single particles theoretically based on CFD and found that critical particle diameter decreased by increasing liquid velocities. In the same study, they also investigated the effect of cross-flow velocity on flux enhancement and saw more than 50% higher SS with bubble rising in moving water than in stagnant water. Boehm et al. [82] made a further experimental study to identify the optimal conditions where the max. SS was gained at a velocity of 0.1 m/s with bubbles ascent in 7 mm spaced membrane sheets. Prieske et al. [139, 140] modified the Chisti model to calculate the bulk liquid velocity accounting for the effect of a cross-section of up-flow and down-flow in MBRs with the FS module.

#### 9. sludge conditions in FS: MLSS

Depending on the implementation methods of MLSS, some researchers found the minor effect of activated sludge viscosity on SS, while other researchers revealed more membrane fouling at a higher MLSS concentration due to lower cross-flow velocity. Wei et al. [93] found that the effect of activated sludge viscosity was minor and concluded that water could be used for CFD simulations to simplify the problem. However, in their studies, they investigated the rheological behavior of activated sludge through simply changing the overall values representing the properties of the fluid to be modeled. Due to the minor differences between the density and viscosity of water and activated sludge, there is an only slight difference in the numerical results of SS calculated from their simulations. Thus, these results are in contrast with the findings from other researchers [33, 58, 161], who proved the critical role of activated sludge rheology in membrane fouling control. Bayat et al. [161] reported an increase in the MLSS concentration resulting in an increase SS. Yang et al. [58] carried out 15 CFD simulations with varying inputs such as air flow rate, biomass concentration, and bubble diameter and the results demonstrated that among all of these input factors, sludge concentration is the most potent influence factor regarding SS and particle deposition propensity (PDP). According to their research, the MLSS concentration of 8820 mg/L is identified to be optimal for fouling control. Amini et al. [33] introduced a CFD model to study the effect of the MLSS concentration on the membrane SS in the FS module. They found that a higher MLSS concentration leads to lower cross-flow velocity, thus more membrane fouling, since cross-flow velocity plays a dominant role in the determination of the critical particle diameter, at which smaller particles tend to be attracted to the membrane surface and accumulated there forming cake layer.

Table 4: Overview of previous CFD researches in MBRs with FS membrane modules

Author	Dimension [mm]	Phases	Turbulence model	Modeling method	Implementation	Brief description of main results in the literature
Wang et al. [40, 83]	510; 1200; 4 - 8	gas-liquid	RKE	VOF	No	critical height for bubble development was around 250 m; SS by slug bubbles are 6 fold stronger than that from single bubbles
Xie et al. [151–156]	72; 320	liquid/ gas-liquid	RNG	Eulerian	No	enhancement was achieved in FS with MCTP-MPs; vertical orientated micro channel turbulence promoter is better than horizontal oriented regarding enhancement effect
Yang et al. [39, 58, 110]	220; 320; 10	gas-liquid	RNG	Eulerian	MLSS; DO	sludge concentration is the most influencing for SS; high nitrogen removal efficiency (> 90%) was achieved by high recirculation
Kim et al. [143]	500; 460; 10	N.A.	N.A.	N.A.	No	SS between the membrane and the baffle was higher than that between membrane sheets
Wu et al. [125]	N.A.	gas-liquid	SKE	Eulerian/	Porous media; MLSS	most of velocity is in the range of 0.245 - 0.275 m/s; optimal design was at the indexes equaling 0.6
Yan et al. [120, 121]	250; 200; 10	gas-liquid	SKE	Eulerian	No	baffle location and size affect MBR hydrodynamics, particularly at lower aeration intensities; ave. SS in MBRs with baffles was 74% higher than that without baffles
Ibrahim et al. [158]	N.A.	gas-liquid	SKE	Eulerian/ VOF	No	higher SS values were obtained from higher bubble diameters with elevated bubble rising velocities
Bayat et al. [161]	N.A.	gas-liquid	SKE	Eulerian	PBM;MLSS	SS increases with an increase in MLSS concentration; bubble size increased during it rise from aerator to free liquid surface and larger bubbles tend to be near membrane surface and tank walls
Amini et al. [33, 127]	500; 1000; 8	gas-liquid- biomass	SKE	Eulerian	PBM; MLSS	higher cross-flow velocity benefits membrane fouling mitigation; out-most membranes are most prone to membrane fouling; optimal bubble size was 3 mm; higher MLSS concentration lead to more membrane fouling

continued ...



... continued

Author	Dimension [mm]	Phases	Turbulence model	Modeling method	Implementation	Brief description of main results in the literature
Jajuee et al. [167]	720; 960; 10	liquid	LES	N.A.	Porous media	the effect of surface jet is superimposed to the local effect of hydrostatic-pressure difference
Boyle et al. [162]	N.A.	gas-liquid	N.A.	Eulerian	No	at higher overall SS, cake layer is thinner and more uniform
Wei et al. [93]	150; 600; 10	gas-liquid	RKE	VOF	No	an increase in bubble size leads to an increase in SS; SS in wake region was more intense; Optimal gap was obtained at 8 mm; activated sludge viscosity effect found to be minor
Moraveji et al. [138]	355; 820; (5; 7; 9)	gas-liquid	SKE	Eulerian	No	the presence of membranes increase gas hold up; as gap distance increased, gas hold up decreased and the liquid circulation velocity increased
Khalili et al. [142, 144]	310; 230; 8	gas-liquid	SKE	Eulerian	No	baffle angle has significant impact on SS; ave. SS increases by increasing gas flow rate
Drews et al. [141]	N.A.	gas-liquid	N.A.	VOF	MLSS	the presence of membrane plates has a significant deceleration effect for bubbles in certain size range; SS decreased significantly with an increase in gap distance; the optimal condition is found to be 5 mm bubbles with a channel depth of 5 mm
Prieske et al. [139, 140]	820; 100; 3-7	gas-liquid	SST	Eulerian/ VOF	No	the highest shear rates are obtained in the smallest channels; an increase of bubble size above a certain diameter does not yield higher SS; the position of aerators affects the hydrodynamics
Boehm et al. [166]	N.A.	N.A.	N.A.	N.A.	No	good agreement between numerical results and experimental results
Javid et al. [164]	100; 300; 6	gas-liquid	SKE	VOF	No	slug flow and bubbly flow could increase the permeate flux by 78% and 30%, compared to that without bubbling; bubble wake region and increasing velocity gradient could enhance SS

continued ...



... continued

Author	Dimension [mm]	Phases	Turbulence model	Modeling method	Implementation	Brief description of main results in the literature
Ndinisa et al. [26]	N.A.	gas-liquid	N.A.	Eulerian	No	identifying the most effective flow profiles for fouling control
Essemiani et al. [95]	N.A.	gas-liquid	N.A.	VOF	No	an isolated spherical cap bubble can be observed
Amirafatabi et al. [160]	N.A.	N.A.	N.A.	N.A.	No	the jet injection can partially remove cake layer, hence, increase the permeate flux
Rahimi et al. [118]	80; 30	liquid	RNG	N.A.	Porous media	CFD can predict the permeate flux in water filtration but not be able to predict realistic cases in sludge filtration
Cao et al. [148]	N.A.	liquid	RNG	N.A.	No	the inclusion of turbulence promoters could promote turbulence and local surface SS
Saalbach and Hunze [126]	N.A.	gas-liquid	N.A.	N.A.	Porous media; ASM	aeration has a great impact on flow field
Karode et al. [150]	25; 35	liquid	N.A.	N.A.	No	spacers with constant diameter resulted in higher pressure drop and more uniform shear rate distribution.
Wiley et al. [149]	N.A.	liquid	N.A.	N.A.	No	the concentration boundary layer is affected significantly by the re-circulation regions between the two spacers.
Brannock et al. [97, 99]	N.A.	gas-liquid	N.A.	Eulerian	MLSS	the overall mixing performance in both FS and HF seems to be complete mixing; the effect of sludge rheology in the system is minor

MLSS: implementation of MLSS expression; PBM: implementation of PBM model; ASM: implementation of ASM model

SKE: Standard  $k - \varepsilon$  model; RKE: Realizable  $k - \varepsilon$  model; RNG: RNG  $k - \varepsilon$  model; SST: SST  $k - \omega$  model

Dimension: three numbers stand for the length, width and the channel gap distance

N.A.: not mentioned

---

## HF membrane module

While studies on HF modules outnumbered studies on FS modules in the literature, researchers focused more on FS modules than HF modules numerically, as shown in Fig. 6. Similar to the research on FS modules, many numerical studies have been carried out on HF modules with the aim of achieving optimum by analyzing the following parameters. A review and a summary of the previous studies is presented below and in Table 5.

### 1. Configurations of HF: HF module

Researchers discussed the size and orientation of the HF module in the MBR tank in detailed. Liu et al. [37] compared the vertical and horizontal aligned HF module, and found that under the same condition, the vertical aligned HF module could improve the area-weighted average liquid velocity along membrane surface (0.129 m/s) up to 33%, compared to the horizontally aligned HF module (0.097 m/s). Besides, the MBR system with vertical orientated hollow fibers produced higher SS along the membrane surface and less resistance to the flow. They also investigated the relative size of the HF module in the MBR tank. An improvement in area-weighted liquid velocity near the membrane surface was observed when the ratio of the distance between the HF module and wall to the width of the HF module increased from 0.2 to 0.6, and no further improvement was followed by a further increase in this ratio. The beneficial effect of the large tank is also found by Kang et al. [119]. They compared the hydrodynamic characteristics in two MBR tanks of different size and found out that by merely enlarging the tank size, mixed liquor and air velocities could be improved by approximately 50%.

By increasing packing density, Praneeth et al. [168] reported an dramatic decrease in the permeate flux, while Liu et al. [109] observed a sharp increase in SS. However, Liu et al. [109] denied their conclusion because in their model fluid motion and SS was dominated by fiber movement instead of by bubbles, and the resistance of fibers on fluid was not taken into consideration. More researchers revealed an optimum in packing density. Guenther et al. [169, 170] found that at a moderate packing density, relatively more homogeneous axial flux profile and higher filtration flux could be obtained. Zhuang et al. [171] and Lim et al. [172] employed a 2D CFD based model proposed by Zhuang et al. [171] to study the relationship between permeate flux and packing density in dead-end outside-in HF modules. Zhuang et al. [171] recommended that packing density should be less than 0.6 to keep uniform flux distribution and efficient energy utilization. Lim et al. [172] did an expended study on packing density and concluded that optimum in permeate flow rate was achieved at a packing density of 0.5 for short fibers (0.5 m and 1.0 m fibers) and 0.6 for long fibers (1.5 m and 2.0 m fibers). Nowee et al. [173] also investigated the effect of fiber numbers through the same model and found the optimal number of fibers at round 10. Despite the different numerical methods, similar conclusions could be found in another 3D CFD study [78] with vibrating membrane walls, where it revealed that the optimal distance between fibers for the max. shear rate was around 0.6 mm.

As for fiber arrangement in the HF bundle, Zamani et al. [78] investigate hydrodynamics numerically in the HF module with two different configurations: staggered configuration and in-line configuration. They observed higher SS in a staggered configuration. In their study, the fiber arrangement was regular, while in practice the fiber position is usually irregular. Buetehorn et al. [174] investigated

---

the impact of the irregular arrangement of the hollow fibers with a novel geometry modeling approach based on X-ray computed tomography (CT) scanning technology to map instantaneous fiber displacement in the HF bundle. The developed model allowed prediction of the effect of the irregular arrangement of fibers on the flow pattern in the HF bundle by the introduction of the concept of porosity. Their results showed that the distribution of cross-flow velocity is highly dependent on the local porosity. In regions of higher local porosity where the fiber concentration is lower, the local velocity is higher which indicated that these regions are less prone to membrane fouling.

## 2. Configurations of HF: fiber

HF modules consist of a bundle of fibers. The properties and arrangement of fibers are important factors influencing the hydrodynamics in the MBR system equipped with HF modules. The HF membrane porosity is one of the key parameters. Nowee et al. [173] look into its effect on phenol removal efficiency based on a comprehensive mathematical model by introduction the ratio of membrane porosity to tortuosity and found a high phenol removal efficiency at a high ratio. Sanaeepur et al. [175] observed the same trend for nitrate removal efficiency: the MBR efficiency for nitrate removal improved as the pore diameter increased. Besides, low membrane permeability would increase the pressure drop during membrane filtration [176].

Liu et al. [109] simulated the impact of the stiffness and outer diameter of polyvinylidene fluoride (PVDF) fibers with the assumption of isotropic homogeneous material on the ave. SS. Their results revealed a reduction in the ave. SS with increasing fiber stiffness. They found that the ave. SS at 1.3mm fiber (o.d.) was more than 2.5 times to that at 1.0 mm fiber (o.d.). On the contrary, higher shear rates were obtained in vibrating fibers with a smaller diameter in another research by Zamani et al. [78], who investigate the shear profile for single phase under laminar conditions. Comparing these two studies, the results from fluid structure interaction (FSI) model might be more reliable, since air bubbling, lateral movement, and turbulent conditions were included in the FSI model, which might be closer to the real situation.

Taken the outer radius of fiber alone, decreasing this radius is not only beneficial for SS but also phenol removal efficiency [173]. By merely decreasing the outer fiber diameter, Nowee et al. [173] observed an improvement in phenol removal and Sanaeepur et al. [175] found the enhancement in nitrate removal. They explained this observation by an increase in membrane thickness, hence an increase in membrane resistance, when the fiber outer diameter increased. As for the internal diameters, Zhuang et al. [171] found a significant increase in energy efficiency when the inner diameter increased from 0.1 to 0.7 mm, and they recommended that the internal fiber size should be larger than 0.4 mm in dead-end outside-in HF modules. Lim et al. [172] revealed a positive linear correlation between permeate output flow rate and fiber inner diameter. Enlarging the fiber inner radius also led to an enhancement of the system performance due to the reduction of membrane thickness, to be precise, membrane resistance [173]. They also identified the optimal fiber inner diameters depending on fiber lengths to achieve the max. output flow rate, which could be obtained when the internal fiber diameter is 1.25 mm for 1 m long fibers, 1.5 mm for 1.5 m long fibers and 1.875 mm for 2 m long fibers, respectively. Ghidossi et al. [176] proposed a pressure loss correlation as a function of internal fiber diameter based on Hagen-Poiseuille law for flow through the hollow fiber. This relationship

---

and numerical simulations showed excellent agreement. As indicated from this relationship, pressure drop increased significantly, as internal diameter decreased. In short, decreasing the outer radius and increasing the inner radius of fibers could enhance the membrane filtration performance.

Tao et al. [177] found a non-uniform distribution of liquid velocity along fiber length and the highest velocity magnitude at 3 m both in their simulations and in their experiments. Zhuang et al. [171] observed a decrease in permeability, a decrease in energy efficiency and an increase in non-uniformity of flux distribution with an increase in fiber length. When fiber length went beyond 2000 mm, a significant increase in the non-uniformity of flux distribution can be observed, which indicated that fibers longer than 2000 mm are more vulnerable to irreversible membrane fouling. Therefore, they recommended fibers in dead-end outside-in HF modules should be shorter than 2000 mm. Using a similar method, Lim et al. [172] identified that the optimal fiber length was 1 m in terms of the max. permeate flux in the HF module. Besides, The model proposed by Nowee et al. [173] enable the researchers to analyze the effect of fiber length on phenol removal efficiency. They revealed that an extension in membrane length from 157 to 942 mm was followed by more significant improvement removal efficiency of phenol, quantitatively around 24%. This enhancement of system performance is attributed to a longer contact time and a larger contact surface in the reactor with longer fibers. The authors pointed out that there should be an optimum in fiber length if the pressure loss were taken into consideration because pressure dropped linearly along fiber length based on the pressure loss equation derived by Ghidossi et al. [176].

### 3. Configurations of HF: baffle

The presence of baffles has a substantial effect on hydrodynamics in the FS module, particularly for the lab-scale application. Similar to that in the FS module, the presence of baffles in the HF module is believed to improve the membrane hydraulic performance. Researchers [37, 178] investigated how strong will the existence of baffles affect the flow conditions in the HF module, as well. Liu et al. [37] found an enhanced shear effect up to 30% in the upper section of the membrane module, i.e. the regions that are more susceptible to membrane fouling, with the inclusion of baffles in a pilot-scale MBRs. Wang et al. [178] compared bubble distribution, velocity field in two HF modules configured with and without baffles. They reported that the baffle effect on gas hold-up was minor, but on flow field characteristics was significant. It should be noted that the improvement might be not so substantial in the FS module on a large scale. As indicated in the study by Kang et al. [119], the hydrodynamic characteristics in full-scale MBRs are much lower than that in a pilot system.

### 4. Aeration process in HF: bubble characteristics

The effect of bubble size on membrane filtration performance is controversy among researchers. One researcher group [179] concluded based on their numerical results that bubble size is irrelevant to membrane fouling control. This conclusion might not be accurate, for it is in contrast to a vast of studies in the literature database [21, 180]. Some thought small bubbles are more beneficial based on their researchers. They revealed that fine bubbles could induce higher absolute value of vertical velocity [37], higher cross flow [37], and higher SS [37]. Some believed that large bubbles should be recommended for aeration in the MBR system to achieve a better hydraulic condition. In an experimental study by Culfaza et al. [181], they recommended large, cap-shaped bubbles in HF,

---

since these bubbles have better performance compared to small bubbles. Braak et al. [182] also reported that coarse bubbles are more beneficial for fouling control since higher SS could be induced by larger bubbles. Ratkovich et al. [100] found out that a periodic slug bubbling (coarse bubbles) is found to be able to provide better hydrodynamics than free bubbling.

#### 5. Aeration process in HF: gas flow rate

The gas flow rate is proven to be a determining parameter controlling membrane fouling. In most of the studies, it is confirmed that a high air flow rate could enhance the scouring effect by air bubbling in MBRs to migrate membrane fouling. Xing et al. [183] investigated the impact of air flow rate in the HF module and found a beneficial effect on membrane filtration performance, which agrees well with conclusions from other studies [93, 141, 160, 162]. They reported that membrane surface liquid velocity increased gradually, gas hold-up on membrane surface increased and bubble distribution become more uniform along membrane surface, hence the scouring effect of bubbling on membrane fouling was enhanced, as aeration intensity increased. Braak et al. [182] also found the enhanced effect of gas flow rate. Increasing aeration intensity, bubble size and velocity increased, which might lead to higher SS on membrane surface resulting in better membrane performance. Ratkovich et al. [38] and Li et al. [184] also reported the ave. SS because of an increase in gas flow rate.

#### 6. Aeration process in HF: aerator

Liu et al. et al. [37] simulated the impact of aeration design variables, including orientation of the air diffusers, alignment of the aerator pipes to the membrane, the distance between aerator tubes and the distance between the nozzle and the base of the HF module. They placed aerator with the nozzle facing downwards towards the tank bottom and facing upwards towards the HF module in their simulations and discovered a more homogeneous bubble distribution and a 12% increase in SS if the nozzles were facing downwards instead of upwards because vortices were created hence turbulence was promoted before bubble entering the the HF module if the nozzles are oriented facing the MBR tank bottom. They also compared the flow condition in the HF module with parallel and perpendicular oriented aerator pipes. Their numerical results showed a more even liquid velocity distribution and a slightly higher averaged cross flow in upper regions of the air diffusers were parallel aligned to the membrane cassettes.

As for the distances, Liu et al. [37] performed simulations by varying the distance between aerator and membrane curtains. Results showed that the liquid velocity distribution along the membrane surface was more homogeneous and the area-weighted velocity increased by 11% when this distance increased from 20 to 100mm. Moreover, the same authors observed a more evenly distributed bubbles in the HF module with increasing the vertical distance from aerator pipes to the HF module bottom edge in another CFD study [94].

Nozzle size could affect control of fouling in the FS module, which is proven experimentally by Ndinisa [25]. This effect is investigated by Xing et al. [183] in the HF module numerically. Their results showed that at a given aeration rate, the max. velocity decreased with enlarging the aeration aperture. The max. liquid velocity was 0.45 m/s for nozzles with a diameter of 1mm, 0.4 m/s for nozzles with a diameter of 2 mm and 0.39 m/s for nozzles with a diameter of 3mm, respectively.

---

Moreover, the aeration system with smaller nozzles can produce more intense turbulence along the membrane surface, improve SS and promote mass transfer between gas and liquid phases.

## 7. Operational process in HF: MLSS

Since the MLSS concentration determined the rheological properties of the fluid, hydrodynamics such as SS and cross-flow velocity highly depend on the MLSS concentration. Ratkovich et al. [102] observed that the ave. SS is about 3.5 times greater in mixed liquor than in water, indicating that viscosity of activated sludge should be included in the experiment and simulations for the analysis of SS in MBRs. They found a linear relationship between MLSS concentration and SS [185]. Braak et al. [182] also revealed that both the ave. and the max. SS are in the order of magnitude higher in fluid representing activated sludge than in water. Liu et al. [37] implemented dynamic viscosity expressions representing the rheological properties of activated sludge into their CFD model. Their results indicated that the area-weighted ave. SS increased significantly when the MLSS concentration increased from 3.1 to 12.3 g/L.

However, bubble induced velocity is found to be 18% - 26% lower in mixed liquor than in pure water [182]. As the MLSS concentration increased, liquid velocities in the HF module dropped [122], the turbulent viscosity decreased [174]. They also observed that the impact of the MLSS concentration on liquid velocity distribution seemed to be relatively weak [174]. The minimal effect of mixed liquor was observed by Brannock et al. [97], as well. They explained this observation by high turbulence viscosity ratio above 3 in the 70% of the system, indicating the dominant effect of turbulence on hydrodynamics in the MBR system.

## 8. Operational parameter in HF: cross flow velocity

Liquid flow rate could affect the filtration performance and the contaminants removal efficiency in the HF module. At high cross flow rate, the mass and the thickness of the cake layer is expected to decrease, while the pressure drop would increase. Buetehorn et al. [174] investigated the effect of superficial inlet velocity on filtration performance. By increasing the inlet velocities, they found more pronounced turbulence and an increase in total pressure loss at the same time. This observation confirmed the pressure loss correlation for the HF module as a function of inlet velocity derived by Ghidossi et al. [176]. Based on their proposed model equation, pressure dropped significantly as inlet velocity increased. Nowee et al. [173] modeled the phenol removal efficiency under different flow rate. Due to the effect of flow rate on mass transfer coefficient and concentration gradient at the interface, high removal efficiency of phenol could be achieved at a high flow rate. A similar model was applied in the study by Sanaeepur et al. [175] for modeling nitrate removal efficiency. However, they observed the opposite trend: the efficiency reduced by increasing the feed flow rate. They explained this observation by the decrease in residence time in the fluid.

Table 5: Overview of previous CFD researches in MBRs with HF membrane modules

Author	Dimension [mm]	Phases	Turbulence model	Modeling method	Implementa- tion	Brief description of main results in the literature
Cui et al. [129]	<i>Rin</i> : 0.3; <i>Rext</i> : 0.5; <i>L</i> : 1800	liquid	N.A.	N.A.	Porous media; MT; ST	membrane fouling degree could affect backwashing velocity in fiber lumen, thus backwashing length
Nowee et al. [173]	<i>Rin</i> : 1.4; <i>Rext</i> : 2.2; <i>L</i> : 410	liquid	N.A.	N.A.	Porous media	increase in flow rate, membrane length, ratio of membrane porosity to tortuosity, and inner radius of the membrane lead to high phenol removal efficiency; the optimal number of fibers at round 10
Braak et al. [182]	<i>Rin</i> : 1.25; <i>Rext</i> : 1.85; <i>L</i> : 450	liquid/ gas-liquid	N.A.	VOF	MLSS	bubble velocity in water is higher than in mixed liquor; the mean and max. SS is one order of magnitude higher in in mixed liquor than in water
Wang et al. [131]	<i>Rin</i> : 0.12; <i>Rext</i> : 0.22; <i>L</i> : 250	liquid	N.A.	N.A.	Porous media; MLSS	an increase in cake layer porosity led to a thicker cake layer, a higher permeate velocity and a more non-uniform permeability
Liu et al. [109]	<i>Rext</i> : 1.0 <i>Rin</i> : 1.3 <i>L</i> : 300	gas-liquid	RNG	Eulerian/ FSI	No	ave. SS at 1.3 mm fiber (o.d.) was more than 2.5 times to that at 1.0 mm fiber (o.d.); ave. SS decreased with increasing fiber stiffness
Zamani et al. [78]	<i>Rext</i> : 0.4; <i>L</i> : 400	liquid	N.A.	N.A.	Vibrating walls	optimal distance between fibers is 0.6 mm; higher SS was found in sagged configuration, in vibrating fibers with a smaller diameter
Liu et al. [37]	250; 250; 500	gas-liquid	RNG	Eulerian	Porous media; MLSS	vertical aligned HF module could improve average liquid velocity up to 33%; SS in the upper section of HF increased by 30% with the inclusion of baffles
Liu et al. [94]	500; 1000; 2200	gas-liquid	N.A.	Eulerian	Porous media; MLSS	SS increased by 12% when coagulants were added in filtration zone other than in primary anoxic zone
Zhuang et al. [171]	<i>Rin</i> : 0.7; <i>Rext</i> : 1.3; <i>L</i> : 100	liquid	N.A.	N.A.	Porous media	Optimum: fiber length should be shorter than 2000 mm, packing density should be lower than 0.6 and an internal diameter should be wider than 0.4 mm of the fiber
Tao et al. [177]	1000; 500; 1700	liquid	SKE	N.A.	Porous media	distribution of liquid velocity was not uniform; highest velocity magnitude at 3 mm both in their simulations and in their experiments

continued ...

... continued

Author	Dimension [mm]	Phases	Turbulence model	Modeling method	Implementa- tion	Brief description of main results in the literature
Lim et al. [172]	<i>Rin</i> : 0.625; <i>Rext</i> : 1.5; <i>L</i> : 500 - 2000	liquid	N.A.	N.A.	Porous media	the optimum length is 1 m; a proportional increase in permeate flow rate with an increase in fiber inner diameter
Wang et al. [178]	1720; 150; 3000	gas-liquid	N.A.	Eulerian		the baffle effect on gas hold-up was minor, but on flow field characteristics was significant
Xing et. al. [183]	1000; 500; 1700	gas-liquid	N.A.	Eulerian	Porous media	membrane surface liquid velocity increased gradually, gas hold-up on membrane surface increased and bubble distribution become more uniform along membrane surface as aeration intensity increased
Praneeth et al. [168]	<i>Rin</i> : 0.5; <i>Rext</i> : 0.75; <i>L</i> : 3	gas-liquid	N.A.	Eulerian	Porous media	permeate flux decreased dramatically with a increase in the packing density.
Guenther et al. [169, 170]	<i>Rin</i> : 1.25 <i>Rext</i> : 2.1 <i>L</i> : 125	liquid	N.A.	N.A.	Porous media	the flow velocity will be higher in top area resulting in a better removal of particles in this area at a low packing density compared to that at a high packing density
Guo et al. [130]	<i>Rext</i> : 1.1 <i>L</i> :400	gas-liquid	RNG	Eulerian	Porous media	the cleaning effect by backwashing process was better in upper membrane region than middle and lower regions
Buetehorn et al. [174]	<i>L</i> : 850; 1400	liquid/ gas-liquid	RNG	VOF	Porous media; MLSS	the local velocity was higher, at a higher local porosity; turbulent viscosity and pressure loss decreased as MLSS concentration increased, as inlet velocity decreased
Sanaeepur et al. [175]	<i>Rin</i> : 0.55 <i>Rext</i> : 0.85 <i>L</i> : 380	liquid	N.A.	N.A.	Nitrate transport equation	the MBR efficiency for nitrate removal improved as the pore diameter increased; the efficiency reduced by increasing the feed flow rate
Saalbach et al. [126]	N.A.	gas-liquid	N.A.	N.A.	Porous media; ASM	aeration has a great impact on flow field
Ratkovich et al. [123]	tube with HF	liquid/ gas-liquid	N.A.	VOF	Porous media	disk aerator could provide a better bubble distribution in the membrane module than the ring aerator

continued ...



... continued

Author	Dimension [mm]	Phases	Turbulence model	Modeling method	Implementa- tion	Brief description of main results in the literature
Ratkovich et al. [108, 185]	N.A.	liquid/ gas-liquid	SST	N.A.	No	a linear relationship between the MLSS concentration and SS was observed; rotational MBRs without air injection has the highest energy consumption
Ratkovich et al. [38, 106]	2180; 850; 470	gas-liquid	N.A.	Mixture model	No	hollow sheet has a higher energy consumption than HF; SS by empirical expression is 38% overestimated; viscosity has a strong effect; ave. SS increases wiht increasing gas flow rate
Martinelli et al. [179]	N.A.	gas-liquid	N.A.	Eulerian/ VOF	No	filtration performance is not strongly depended on which kind of bubbles were injected in HF module; a more severe fouling was found at the highest local gas flow rate
Liu et al. [128]	<i>L</i> : 1500	gas-liquid	N.A.	N.A.	Porous media	bubble size distribution showed that most bubbles are 3 - 5 mm in diameter; small bubbles induce higher absolute value of vertical velocity in membrane module
Li et al. [184]	<i>Rext</i> : 2.8 <i>L</i> : 900	gas-liquid	SST	Eulerian	No	accurate results obtained at a low air flow rate; large error obtained at a high air flow rate; time ave. SS increased with an increase in air flow rate.
Kang et al. [119]	N.A.	gas-liquid	N.A.	Eulerian	Porous media; MLSS	liquid and air velocities in full-scale MBRs were 50% - 80% and 15% - 40% lower than in pilot system; velocities could be improved by about 50% by enlarging tank
Wang et al. [122]	N.A.	gas-liquid	N.A.	Eulerian	Porous media; MLSS	CFD model coupled with porous zone could get more accurate results; velocity in membrane module decreased as MLSS concentration increased
Brannock et al. [97, 99]	N.A.	gas-liquid	N.A.	Eulerian	Porous media; MLSS	The overall mixing performance in both FS and HF seems to be complete mixing; the effect of sludge rheology in the system is minor

*L*: length; *Rin*: internal radius; *Rext*: external radius; when there is no letter, three numbers in dimension column stand for the length, width and height

SKE: Standard  $k - \varepsilon$  model; RKE: Realizable  $k - \varepsilon$  model; RNG: RNG  $k - \varepsilon$  model; SST: SST  $k - \omega$  model

MLSS: implementation of MLSS expression; ASM: implementation of ASM model

MT: Mass Transfer; ST: Species transport

N.A.: not available

---

## Modeling tubular membrane module

Even though tubular modules are not as widely applied in the MBR system as HF and FS modules, much literature concerns two-phase flow in tubular membranes could be found in the database. This could be explained by the fact that the earliest numerical studies are carried out with the simplified 2D tubular system to save the computing resources, e.g. Cui et al. [19, 20] studied slug bubbling in tubular membrane module in early days. Later, as computer technology advanced, the modeling problem gets more complicated, e.g. the modeling of the impeller in the tubular membrane module can be found in several studies [134–136, 186]. These previous studies are reviewed below and summarized in Table 6.

### 1. Configurations of tubular membrane module: impeller

Trad et al. [134, 135] carried out simulations for MBR reactor with two mixing impellers in lab scale, and they found out that the top and bottom impellers interacted weakly with each other, resulting in two different mixing regions in the MBR reactor. With an improving configuration design in their later study, they found the advantageous effect of the large top impeller on liquid circulation. They also recommended the rotation speed at 200 rpm, for it can prevent vortex formation and promote a homogeneous distribution of mixed liquor. Vlaev et al. [136, 186] used a similar model to study the SS and its homogeneity induced by the rotation of a radial mixing impeller in a stirred MBR vessel. They found that the impeller speed instead of gas flow rate played a vital role in fouling-reducing in a tubular membrane module, as the impeller speed could increase the fluid velocity gradients significantly, while gas flow rate was found to decrease the mean shear rate in the near-wall regions. Apart from the fouling mitigation effect, the authors considered the appropriate operating conditions for the activated sludge, hence recommend that rotational speed of the flat-blades should be less than 600 rpm to ensure high operational quality with a mild biological performance.

### 2. Configurations of tubular membrane module: inclined tubes

Taha et al. [132, 133] carried out a numerical study to examine the single Taylor bubbles and their effect on UF performance in vertical tubes. They found a highest the wall shear rate at the inclined tubes with an angle of  $45^\circ$  from the horizontal position.

### 3. Configurations of tubular membrane module: Baffles

Baffles in membrane tubes could promote turbulence and increase SS, hence significantly reduce fouling [187]. After comparing SS under different baffle designs, they found higher SS in central baffle with decreasing baffle spacing or increasing baffle diameter. Ahmed et al. [137] undertook a very similar numerical study on turbulent flow in membrane tubes configured with a set of baffles. Their observations are also similar. They found the baffle size and arrangements could affect the hydrodynamics in tubular membrane modules significantly and hence addressed the importance of optimization of baffles in tubular membrane modules.

### 4. Configurations of tubular membrane module: Spacer thickness

Li et al. [188] used CFD to simulate the fluid flow through disk membrane modules with varying collection-tube sizes and spacer thicknesses. After comparing 24 structure configurations, they identified that the optimum condition could be achieved when the collection-tube is 15 - 20 mm and

---

the spacer thickness is 0.75 - 1.0 mm, where the highest volumetric flow rates of permeate could be obtained.

#### 5. Aeration process: bubble characteristics

Bubble's size and bubbling frequency are found to be able to affect the permeate flux experimentally in the study of Taha et al. [132]. They revealed that injecting bubbles enhanced the permeate flux and increasing the bubble size led to an increase in permeate flux. For a given bubble volume, increasing the bubbling frequency could improve the permeate flux, but with a further rise in bubbling frequency, the permeate flux increased only slightly.

#### 6. Aeration process: slug flow

Taha et al. [132] proved an enhancement in permeate flux when slug flow is introduced into the tubular membrane module and further discovered the mixing zone beneath the slug bubbles. Cui et al. [19, 20] revealed the bubble-induced secondary flow could promote local mixing and hence enhance membrane filtration and observed the link between permeate flux enhancement and the transient SS. Ratkovich et al. [100] undertook numerical studies to examine the effect of slug flow on SS across the membrane surface in the tubular membrane module, as well. The hydrodynamics of slug flow in tubes from their CFD models is similar to that reported by Cui et al. [20]. They revealed that SS increased along the film zone gradually and decreased in the wake zone dramatically. However, Ratkovich et al. [100] also reported that their CFD simulations tend to over-predict the slug bubble induced SS in the tubular membrane module. Yang et al. [189] investigated the mass transfer characteristics at the membrane surface under slug-flow conditions in the tubular membrane module, which is as a side stream anaerobic membrane bioreactors (AMBRs). Their numerical results showed that mass transfer capacity was higher in the regions at the noses of slug bubbles than that in the tails of slug bubbles.

#### 7. Operational process: MLSS

Ratkovich et al. [107] investigated the SS in a tubular vessel with different impellers of different numbers of blades. They observed a more than ten times difference in SS values obtained from simulations with water and with activated sludge, respectively. He suggested that the non-Newtonian behavior of activated sludge must be included in the simulation of MBR systems, as the CFD model with water viscosity will under-predict SS. Bentzen et al. [104] carried out simulations with similar models and also found the significant effect of activated sludge concentration on the ave. SS. He made a further investigation and developed an approximation based on empirical relationships, which determines the ave. SS as a function of angular velocity and the activated sludge concentration. This relationship illustrated that an increase in the concentration of activated sludge would increase the ave. SS significantly. Yang et al. [189] investigated the mass transfer characteristics in tubular membrane module with water and with activated sludge and found that the mass transfer capacity in water and activated sludge are inconsistent.

Table 6: Overview of previous CFD researches in MBRs with tubular membrane modules

Author	Dimension	Phases	Turbulence model	Modeling method	Implementation	Brief description of main results in the literature
Trad et al. [134, 135]	two impellers	N.A.	Corrected KE	VOF /Mixture model	MRF	top and bottom impellers interact weakly resulting in two different mixing regions; using a large top impeller is an advantage for liquid circulation
Vlaev et al. [136, 186]	six flat-blade impellers	gas-liquid/ single phase	RKE/ SST/ SKE	Eulerian	MRF	impeller speed is key factor in fouling-reducing; the rotational speed of the flat-blades should be less than 600 rpm
Bentzen et al. [104]	rotational cross-flow MBRs	N.A.	SST	N.A.	No	the ave. SS is a function of angular velocity and the activated sludge concentration; an increase in the concentration of activated sludge, will increase the ave. SS significantly
Ratkovich et al. [100, 107]	$L$ : 2000 $D$ : 4.95	N.A.	laminar; SST; SKE	N.A.	No	more than 10 times difference between water and sludge in terms of SS; SS is over predicted
Yang et al. [189]	$L$ : 1000 $D$ : 5.2	gas-liquid	RNG	VOF	No	mass transfer capacity in water and in activated sludge are inconsistent
Taha et al. [19, 132, 133]	one tube	gas-liquid	RNG	VOF	No	the bubble-induced secondary flow could enhance membrane filtration; injecting bubbles enhanced the permeate flux; permeate flux increases with increasing bubble size and bubbling frequency; highest wall shear rate was at the inclined tubes with an angle of 45°
Li et al. [188]	$L$ : 92.5 $D$ : 0.2	single phase	N.A.	N.A.	No	optimum condition could be achieved when the collection-tube is 15 - 20 mm and the spacer thickness is 0.75 - 1.0 mm
Ahmed et al. [137]	$L$ : 200 $D$ : 15	single phase	RNG	N.A.	No	baffles in membrane tubes could promote turbulence and increase SS; an increase in ave. SS was observed with a decrease in baffle spacing or an increase in baffle diameter
Liu et al. [187]	$L$ : 200 $D$ : 15	single phase	SKE	N.A.	No	higher SS was found in central baffle than in wall baffle

SKE: Standard  $k - \varepsilon$  model; RKE: Realizable  $k - \varepsilon$  model; RNG: RNG  $k - \varepsilon$  model; SST: SST  $k - \omega$  model

Dimension: three numbers stand for the length, width and the channel gap distance

MLSS: implementation of MLSS expression

N.A.: not available

---

## 2.4 Numerical methods

---

Computational Fluid Dynamics is a computer-aided engineering tool which is capable of analyzing problems involving fluid dynamics, transport process, and heat and mass transfer process by using different numerical methods and algorithms. It can optimize the design and the operating conditions by changing the geometry of the reactor and the operational conditions easily [33, 34]. In this way, the lead times and costs could be reduced dramatically [30, 33]. Besides, it can provide detailed information about flow at any position and time [35], and some of them are experimentally not accessible. With so many advances over experiments, CFD has to become a leading analysis tool in examination of MBRs. The basic principle and models will be introduced and reviewed in this section.

---

### 2.4.1 Governing equation for single phase

---

All fluid dynamics are based upon the fundamental governing equations, namely the continuity and momentum equations. They are a mathematical statement of physical conservation laws for all fluid dynamics [190, 191]: the conservation of mass and the conservation of momentum. For incompressible flow they can be described by Eq. 1 and Eq. 2, respectively [35].

$$\nabla \cdot \mathbf{u} = 0 \quad (1)$$

$$\frac{\partial \rho \mathbf{u}}{\partial t} + \nabla \cdot (\rho \mathbf{u} \mathbf{u}) = -\nabla p + \nabla \cdot (\mu (\nabla \mathbf{u} + \nabla \mathbf{u}^T)) + \mathbf{f}_b \quad (2)$$

where  $\rho$  is the fluid density,  $\mathbf{u}$  denotes the velocity,  $p$  is the pressure,  $\mu$  is the dynamic viscosity of the fluid, and  $\mathbf{f}_b$  denotes the body forces including the gravitational body force and other external body forces.

The application of single-phase flow in the FS membrane module is dominantly in early studies around 2002 to model the cross-flow or recirculation flow in water filtration [118, 149] or to model the turbulence and local SS induced by turbulence promoters [148, 150]. Single phase flow simulation is not so popular in the simulations of the tubular membrane module, either. It is only used for the simulation of turbulence promoters [137, 187] and rotational impellers or disks [134, 135, 188]. However, in the HF membrane module, it is prevalent, particularly in combination with a porous media [129, 131, 169–174, 177, 182]. With such combination, it is capable of predicting the backwashing process, of predicting the permeate flux, to evaluate the phenol removal efficiency, to investigate the effect of membrane porosity, tortuosity, membrane length, radius, etc. When the vibrating walls model is incorporated, the effect of vibrating walls on SS could be examined, as well [78]. Compared to single-phase simulations with multi-phase simulations in the MBR system, it is found out that the multi-phase simulations dominate since the flow in the MBR system is indeed a multi-phase flow.

---

### 2.4.2 Turbulence modeling

---

Most flows in engineering practice are turbulent flows, which are unstable, chaotic, time-dependent and could produce vortex and mixing rapidly [192]. The unsteady turbulence develops at a large  $Re$  above a certain critical  $Re$ , while the relative stable laminar flow is at a small  $Re$  under critical  $Re$ . The concept "energy cascade" plays a vital role in the study of turbulence. Based on the Kolmogorov theory [193, 194],

---

turbulence consists of eddies with different sizes. The largest eddies possess most of the kinetic energy, while smaller eddies contain less energy. An energy cascade refers to the hand down of kinetic energy from the largest eddies to progressively smaller eddies. These newly formed eddies will continue to break up into even smaller eddies and transfer energy to them. The energy cascade continues until the size of eddies is sufficiently small that the molecular viscosity is effective at dissipating kinetic energy. Turbulence can be approached typically in three ways: direct numerical simulation (DNS), large eddy simulation (LES), and Reynolds averaged Navier-Stokes (RANS).

### DNS

DNS could calculate the turbulence at large and small scales directly, without any simplifications or approximations of the turbulent flow. To do that, the mesh grids should be smaller than the smallest eddies and the time step interval should be shorter than the shortest turbulent fluctuations. The mesh points number, which is necessary for a sufficient simulation of eddies at a small scale, grows as a function of Reynolds number ( $Re^{\frac{9}{4}}$ ) and the time steps number increases following power law of Reynolds number, as  $Re^{\frac{1}{2}}$  [192, 195, 196]. The computing time, which is directly proportional to mesh points number and time steps number, is approximately proportional to  $Re^3$  [192, 195, 196]. The larger the  $Re$  is, the finer the mesh and the greater the computing effort have to be [196]. That means DNS requires a very large computer memory capacity due to the extremely fine mesh grids and very long calculating time due to the short time step size. Thus, the possibility of DNS is out of reach even for the simple turbulent flow [196], let alone for a practical application. Thus no one simulated the MBR system with DNS. However, when DNS is performed to simulate the turbulent flow, all scales of flow motion could be directly computed without any further assumptions of the kinetic energy and the turbulent eddies viscosity. DNS would be a good approach for simulating the not fully developed turbulent flow, i.e. membrane filtration conditions [197].

### LES

Since DNS is infeasible for a practical application, two main alternative approaches are employed to compute the turbulent flow in practice: LES and RANS. LES is based on space filtered equations. In this filtering process, small eddies with a size smaller than the filter width will be filtered out effectively [195]. Thus, only the large unsteady eddies are directly computed, while smaller eddies are modeled instead, resulting in a reduction in computing cost compared to DNS. In another class (RANS) of modeling turbulence, statistically averaged variables associated with their fluctuation terms are applied in the governing equations, resulting in a new unknown term, Reynolds stress tensor [195]. The modeling of turbulent flow is transformed into the calculation of Reynolds stress tensor. To solve it, additional transport equations are introduced for the closure of the system. In this approach (RANS), all large and small eddies are modeled, where the modeling is more complex than that in LES, where large-scale turbulence is computed directly [198]. This, on the other hand, causes more mesh refinements in LES than that in RANS [198].

Little work has been done in applying the LES turbulence modeling technology in the membrane modules modeling. In the literature, only one study [167] is found, where LES can be employed to calculate the liquid velocity field of single-phase flow in the MBR system. For the modeling of two-phase turbulent flow in the MBR system, no research is found to perform the simulations with an LES approach, despite that LES might be the best approach for two-phase flow due to its unsteady behavior [30, 130]. However, the requirement of a very fine mesh by this method makes it infeasible or unfavorable among researchers for the simulation of MBRs, especially for modeling a train of bubbles [30, 130].

## RANS

RANS equations for incompressible flow are based on variables such as velocity  $\mathbf{u}$  and pressure  $p$ . These fields can be decomposed into a mean component  $(\bar{\mathbf{u}}, \bar{p})$  and a fluctuating component  $(\mathbf{u}', p')$ , as shown in Eq. 3 [192]:

$$\mathbf{u} = \bar{\mathbf{u}} + \mathbf{u}' \quad ; \quad p = \bar{p} + p' \quad (3)$$

Substituting the variables of velocity and pressure by their decomposed expressions above in the incompressible continuity (Eq. (1)) and momentum (Eq. (2)) equations, the Reynolds averaged equations are given by,

$$\nabla \cdot \bar{\mathbf{u}} = 0 \quad (4)$$

$$\frac{\partial \rho \bar{\mathbf{u}}}{\partial t} + \nabla \cdot (\rho \bar{\mathbf{u}} \bar{\mathbf{u}}) = -\nabla \bar{p} + \nabla \cdot (\mu(\nabla \bar{\mathbf{u}} + \nabla \bar{\mathbf{u}}^T) - \rho \overline{\mathbf{u}' \mathbf{u}'} + \bar{\mathbf{f}}_b) \quad (5)$$

Comparing Eq. (4) and Eq. (5) with Eq. (1) and Eq. (2), the RANS equations are similar to the fundamental conservation equations except for the additional term  $(-\rho \overline{\mathbf{u}' \mathbf{u}'})$ . The averaged products of the fluctuating components are known as the Reynolds stress tensor  $\boldsymbol{\tau}^R$ , whose expanded form is expressed in Eq. 6.

$$\boldsymbol{\tau}^R = -\rho \begin{pmatrix} \overline{u'u'} & \overline{u'v'} & \overline{u'w'} \\ \overline{u'v'} & \overline{v'v'} & \overline{v'w'} \\ \overline{u'w'} & \overline{v'w'} & \overline{w'w'} \end{pmatrix} \quad (6)$$

Due to the additional term, Reynolds stress tensor, the system is not closed. The modeling of turbulence is transferred to the modeling of Reynolds stress tensor. To predict the turbulent flow, numerous models are developed, since there is still no universal turbulence model available that can be applied to all the turbulent flows correctly [199]. Each turbulence model can predict some turbulent flows satisfactorily but can not be successfully applied to other turbulent flows due to their limitations and deficiencies [199]. The most important models are grouped into [192, 198]:

- Algebraic (Zero-Equation) Models

Using algebraic expressions to solve the Reynolds stresses without any additional differential equation.

- One-Equation Models

Solving only one transport equation for the turbulent variable ( $k$ ) to calculate Reynolds stress.

- Two-Equation Models

Using two extra transport equations for the calculation of Reynolds stress.

- Second-Order Closure Models

The second-order closure models [192], also known as the Reynolds-stress models (RSM), are the most computationally expensive among all of these models, since modeled all the components of the Reynolds stress tensor are modeled as separate transport equations (6 equations) [199].

Zero-equation models, one-equation models and second-order closure models are rarely applied into the simulation of the MBR system of practical interest, while two-equation models are the most popular among researcher in the simulation of industrial applications such as the modeling of MBRs, since they can provide more accurate predictions. Two-equation turbulence models are based on the Boussinesq hypothesis. For incompressible flow, it is provided as,

$$\tau^R = -\rho \overline{\mathbf{u}'\mathbf{u}'} = \mu_t(\nabla \bar{\mathbf{u}} + \nabla \bar{\mathbf{u}}^T) - \frac{2}{3}\rho k \mathbf{I} \quad (7)$$

The term  $-\frac{2}{3}\rho k \mathbf{I}$  is normally computed combined with the pressure gradient term by defining a new term called turbulent pressure  $p_t$  as,

$$p_t = \bar{p} + \frac{2}{3}\rho k \quad (8)$$

Eq. (5) is now,

$$\frac{\partial \rho \bar{\mathbf{u}}}{\partial t} + \nabla \cdot (\rho \bar{\mathbf{u}} \bar{\mathbf{u}}) = -\nabla p_t + \nabla \cdot (\mu_{\text{eff}}(\nabla \bar{\mathbf{u}} + \nabla \bar{\mathbf{u}}^T)) + \bar{\mathbf{f}}_b \quad (9)$$

where, the  $\mu_{\text{eff}}$  in the equation above consists of material dependent viscosity  $\mu$  and flow dependent turbulent viscosity  $\mu_t$ , as,

$$\mu_{\text{eff}} = \mu + \mu_t \quad (10)$$

With the Boussinesq assumption [198, 200], the turbulent problem is transformed into the determination of the turbulent viscosity  $\mu_t$  and the turbulent kinetic energy  $k$ . The closure of the system is still not fulfilled, since these variables are unknown variables. To model these two variables, numerous models are developed. These models are mainly grouped into two categories:  $k - \varepsilon$  models and  $k - \omega$  models. In  $k - \varepsilon$  models, the turbulent viscosity  $\mu_t$  is modeled in terms of the turbulent kinetic energy  $k$  and the energy dissipation rate  $\varepsilon$ , where  $k$  determines the energy of turbulence and  $\varepsilon$  determines the scale of turbulence. In  $k - \omega$  models, the new variables, i.e. the turbulent kinetic energy  $k$  and the specific dissipation  $\omega$  are introduced to compute Reynolds stress tensor. For both models, the newly introduced variables could be solved through the two additional transport equations for suitable turbulent quantities ( $k$  and  $\varepsilon$  or  $k$  and  $\omega$ ).

**Standard  $k - \varepsilon$  (SKE) model**, proposed by Launder and Spalding [202], is one of the most common two-equation models, since it is robust, economic and accurate for a large range of the turbulent flow [201]. The  $k - \varepsilon$  models are semi-empirical models. The computing of turbulent flow was transformed into the determination of two transported quantities, i.e., the kinetic energy,  $k$  and the turbulent dissipation rate,  $\varepsilon$ . These two variables determine the energy processing by the turbulence and the scale of the turbulence, respectively. In  $k - \varepsilon$  models,  $k$  and  $\varepsilon$  are assumed to be in equilibrium [196] and the turbulent viscosity  $\mu_t$  could be modeled through a further assumption which relates  $\mu_t$  to  $k$  and  $\varepsilon$ .

$$\mu_t = C_\mu \rho \frac{k^2}{\varepsilon} \quad (11)$$



To compute the kinetic energy,  $k$  and the dissipation rate,  $\varepsilon$ , two additional transport equation for both quantities are set up. These two extra transport equations have a form of a general scalar transport equation only with specific source and sink terms [192, 196]. To simplify the notation, the overbar symbol is left out from the average variables.

$$\frac{\partial \rho k}{\partial t} + \nabla \cdot (\rho \mathbf{u} k) = \underbrace{\nabla \cdot (\mu_{\text{eff},k} \nabla k)}_{\text{diffusive term}} + \underbrace{P_k}_{\text{source term}} - \underbrace{\rho \varepsilon}_{\text{sink term}} \quad (12)$$

$$\frac{\partial \rho \varepsilon}{\partial t} + \nabla \cdot (\rho \mathbf{u} \varepsilon) = \underbrace{\nabla \cdot (\mu_{\text{eff},\varepsilon} \nabla \varepsilon)}_{\text{diffusive term}} + \underbrace{C_{\varepsilon 1} \frac{\varepsilon}{k} P_k}_{\text{source term}} - \underbrace{C_{\varepsilon 2} \rho \frac{\varepsilon^2}{k}}_{\text{sink term}} \quad (13)$$

where,

$$\mu_{\text{eff},k} = \mu + \frac{\mu_t}{\sigma_k} \quad ; \quad \mu_{\text{eff},\varepsilon} = \mu + \frac{\mu_t}{\sigma_\varepsilon} \quad (14)$$

where  $P_k$  denotes the production rate of turbulent kinetic energy. And  $C_{\varepsilon 1}$ ,  $C_{\varepsilon 2}$ ,  $C_\mu$ ,  $\sigma_k$ ,  $\sigma_\varepsilon$  are determined experimentally for fundamental turbulent flows and have been found to work fairly well for a wide range of free shear flows [201]. They are assigned in the standard model the following values [192, 196, 201]:

$$C_{\varepsilon 1} = 1.44, C_{\varepsilon 2} = 1.92, C_\mu = 0.09, \sigma_k = 1.0, \sigma_\varepsilon = 1.3$$

SKE model, as one of the most established and validated turbulence models [30] is also computationally inexpensive. However, in the derivation of this model, the flow is assumed to be fully turbulent, and the effect of molecular viscosity is supposed to be negligible in the far field [201]. Therefore, the SKE model is valid only for the fully developed turbulent free shear flow with a high  $Re$  [201]. To overcome the weakness of the SKE model and improve its performance, two variants, i.e. the RNG  $k - \varepsilon$  and the Reliable  $k - \varepsilon$  model are proposed.

**RNG  $k - \varepsilon$  (RNG) model**, derived using "renormalization group" (RNG) methods, differs slightly in form to the SKE model. It includes an additional term to improve the accuracy for the rapidly strained flow significantly [201] and a modified viscosity term with a differential formula derived analytically to account for the turbulent flow with a low  $Re$  and the near-wall flow [201]. Thus, RNG model is more accurate and reliable for a wider range of the turbulent flow than the SKE model [201]. However, computations with the RNG model tend to consume 10% - 15% more CPU time than the SKE model because of the extra treatments [201].

**Reliable  $k - \varepsilon$  (RKE) model** is another widely used improved  $k - \varepsilon$  model. To overcome the deficiencies in other  $k - \varepsilon$  models, the RKE model is adopted with an improved dissipation ( $\varepsilon$ ) equation and a new eddy viscosity formulation with a variable  $C_\mu$  instead of a constant  $C_\mu$  [201]. The variable  $C_\mu$  is a function of the mean flow and the turbulence [201] to ensure the positivity of normal stresses (realizable), which conforms to the physics of turbulent flow [201]. The RKE model could provide superior performance over the SKE model for both planar and round jets, the rotating flow, the separated flows, the channel and boundary layer flow [201]. In addition, the RKE model could provide the best performance over other models in the family of  $k - \varepsilon$  models for the flow with complex secondary flow features [201].

**Standard  $k - \omega$  (SKW) model** belongs to another widespread two-equation class, i.e. the family of  $k - \omega$  models, which is also based on the Boussinesq hypothesis and has a similar form with  $k - \varepsilon$  models. In  $k - \varepsilon$  models, the transport equations of the turbulent energy ( $k$ ) and the dissipation rate ( $\varepsilon$ ) are solved, while in  $k - \omega$  models the transport equation of dissipation rate,  $\varepsilon$ , is replaced by the differential equation of the specific turbulence dissipation,  $\omega$ .

SKW is based on the Wilcox  $k - \omega$  model [203]. And the transport equations solve  $k$  and  $\omega$  [192, 201]. By replacing the transport equation of  $\varepsilon$  with the transport equation of  $\omega$ , the turbulence model is more robust, and can perform better in the flow with a low  $Re$  without additional damping functions, and in the flow with adverse pressure gradients [192]. The main drawback of the SKW model lie in its sensitivity to the free-shear flow. A modified variant, the SST model, includes a cross-diffusion source term and a blending function to remove this sensitivity [201].

**Shear Stress Transport  $k - \omega$  (SST) model**, developed by Menter [204], combines the formulation of the SKW model for the modeling of the near-wall flow and the formulation of the  $k - \varepsilon$  to model the turbulent flow in the far field. Hence, the SST model is capable to model turbulent flow with a low  $Re$  without any further modifications and to model the free-stream turbulence, as well [192]. To achieve this, a blending function ( $F$ ) is introduced to combine these two models and the  $k - \varepsilon$  model is converted into a similar formulation as the  $k - \omega$  model. This transformed model multiplied by  $(1-F)$  is then added with the SKW model multiplied by  $F$ . In this way, the SST model acts as the SKW model in the near-wall regions, since the blending function is assigned as 1 in this regions, while it acts as the  $k - \varepsilon$  model in the far-field zones, where  $F$  is assigned to be 0. These features make the SST model more applicable for a wider range of the turbulent flow than the SKW model.

A summary and comparison of the RANS turbulence models mentioned above is presented in Table 7.

Table 7: Comparison of two-equation RANS turbulence models

Model	Advantages and disadvantages	Applications
SKE	<ul style="list-style-type: none"> <li>+ most common models[201], most established and validated turbulence models[30]</li> <li>+ robust, economic and accurate for a large range of the turbulent flow[201]</li> <li>+ computationally inexpensive[201]</li> <li>- neglect molecular viscosity[201]</li> </ul>	fully developed turbulent free shear flows with a high $Re$ [201]
RNG	<ul style="list-style-type: none"> <li>+ more reliable and accurate for a wider range of turbulent flows [201]</li> <li>- less stable[31] and 10% - 15% more CPU time consumption</li> </ul>	<ul style="list-style-type: none"> <li>rapidly strained flows</li> <li>for turbulent flows with a low <math>Re</math></li> <li>for near-wall flows</li> </ul>
RKE	<ul style="list-style-type: none"> <li>+ ensure the positivity of normal stresses</li> <li>- consume more CPU time</li> </ul>	both planar and round jets, rotating flows, separated flows, channel and boundary layer flows[201] for flows with a secondary flow[201]
SKW	<ul style="list-style-type: none"> <li>+ more robust</li> <li>- more sensitive to free-shear flows</li> </ul>	<ul style="list-style-type: none"> <li>flow with a low <math>Re</math> number</li> <li>flows with adverse pressure gradients</li> </ul>

continued ...

... continued

Model	Advantages and disadvantages	Applications
SST	+ most accurate two-equation models[31] + accounts for the transport of the principal SS[31]	near-wall flows flow with a low $Re$ number flows adverse pressure gradients free-stream turbulence

SKE: Standard  $k - \varepsilon$  model; RKE: Realizable  $k - \varepsilon$  model; RNG: RNG  $k - \varepsilon$  model; SKW: Standard  $k - \omega$  model; SST: SST  $k - \omega$  model

RANS is employed in almost the entire research related to turbulent flow simulation in membrane modules. In addition, two-equation models have been employed in RANS method except one study [184], where the  $k - \varepsilon$  model is applied to the liquid phase and zero equation is applied for the modeling of turbulence of gas phase to calculate SS in the HF membrane module at different gas flow rates. However, the numerical results did not agree well with experimental results, especially at a high gas flow rate. The authors attributed that to the vibration of hollow fibers in the experiments. The application of this turbulence model might be one of the reasons for the disagreement between numerical and experimental results. As reported in the study carried out by Liu et al. [37], the modified turbulence model is thought to be capable to get more accurate results by including the bubble-induced turbulence, but turned out to be less satisfying, for this modified model caused more significant errors based on their experimental and numerical results. Therefore, they concluded that this model is not suitable for the simulation of the aerated HF membrane module, which is regarded as a porous zone.

Flows in HF and FS modules are normally characterized with a low  $Re$ . As analyzed above, the SKE model and the RKE model have deficiencies in prediction of turbulent flow with a low  $Re$ . The RNG model and the SST model, suitable for flow with a low  $Re$  and the near-wall flow, are preferred and hence widely applied in the simulations of MBRs. The RNG model is used to model the movement of bubbles, aeration process, fiber arrangement. The SST model is used to predict the circulation velocity at different gas flow rates in a pilot-scale MBR by Prieske et al. [139]. Cao et al. [148] chose the RNG model to simulate the turbulence in approach in net-type spacers in a narrow channel, because it is more suitable for turbulent flow with a relatively low  $Re$  and the near-wall flow than other turbulent models in the family of  $k - \varepsilon$  models. Liu et al. [37] compared the SST model and the RNG model in their simulation and found that the RNG model is more suitable, since the mean flow velocities predicted by this model are slightly closer to the velocities measured by PIV. However, both models could not predict the random vorticity at a small scale accurately, since the bubble induced turbulence has a mixing length scale much smaller than the mesh size [37]. Despite that, they believed that their model with the RNG model is capable to predict hydrodynamics in the HF membrane module, based on the satisfying agreement between simulated mean flow velocities and measure values at different x and y locations [37].

In tubular membrane modules, researchers reported no huge difference between turbulence models. Ratkovich et al. [107] measured SS at membrane surfaces with an electrochemical approach to validate the CFD models with different turbulence models (the RNG model and the SST model). A good agreement with an error less than 9% was obtained by comparing the numerical results from both turbulence models with the analytical and the measured results. In their simulations, both models performed quite well and little difference was observed by applying different turbulent models. Later, Vlaev et al. [136, 186] also conducted simulations of rotational impellers in the tubular membrane module to calculate the shear rate

---

and SS at membrane surfaces. They also found out that numerical results involving SS and shear rate from the SST model, the SKE model and the RKE model are similar. By comparing the SS from the SKE model and the SST model at different  $Re$ , they observed an averaged deviation of 6%, the highest deviation of 14% at a relative low  $Re$  and the lowest deviation of 0% at the highest  $Re$ .

To conclude, the RNG model and the SST model are more suitable for the prediction of turbulence near membrane wall. The SKE model can be applied for turbulence modeling when the numerical model requires high computational consumption.

---

### 2.4.3 Multiphase flow modeling

---

Flows encountered in the MBR system are a mixture of phases. With the presence of activated sludge, suspended solids, and other substances in the mixed liquor in the MBR system, the fluid is a mixture of liquid and solids. As bubbling is introduced into the MBR system to control membrane fouling and to serve biomass with sufficient oxygen, the gas phase should be considered in the MBR system. Thus, the flow in the aerated MBR system is a gas-solid-liquid multi-phase flow.

Trajectory models and two-fluid models are generally applied to simulate dispersed multi-phase flow [205]. Trajectory models treat the mixed fluid as a continuum and tracks each particle and bubbles individually from a certain point of time, which requires extensive computing resources [24]. This approach is suitable for the simulation of spray dryers or liquid fuel combustion, where the volume fraction of the second phase can be neglected. However, the volume fraction of other phases, e.g. relatively large bubbles, activated sludge flocs, of mixed liquor in the MBR system, cannot be ignored. That might be the reason why no study in the database can be found using this method for the simulation of the MBR system.

Two-fluid models are more suitable for the practical application, hence widely used in the simulations of multi-phase flow in MBRs. It treats all phases mathematically as interpenetrating continua. The disperse phase is regarded as a second continuous phase interacting with the primary continuous phase [205]. In this case, the concept of volumetric fraction of each phase is introduced into these models, and the sum of the volumetric fraction of all phases should be equal to 1. Generally, three multi-phase models are available: the Eulerian model, the Mixture model, and the VOF model [201].

#### **Eulerian method**

The Eulerian model is the most complicated among these three multi-phase models. It solves the mass conservation equation and momentum conservation equation for each phase separately. All phases in the mixture are coupled through the shared pressure and the inter-phase exchange coefficients [201]. This method is widely used to model the aeration process in the MBR system, taking up more than 80% of the total multi-phase flow in the FS and HF membrane modules. In theory, the Eulerian method can model any number of secondary phases, if the computing memory is sufficient and the convergence behavior is good. A few studies [161] in the database could be found that performed a simulation of the MBR system with the Eulerian method for the mixture of bubbles, water and activated sludge. However, for such complex multi-phase flow, the solution might not converge, and the required computing resource is enormous. Thus, the simulation is limited to small and simple models. In the Eulerian model, the phases in the multi-phase flow are treated as inter-penetrating continua by the introducing the concept of volume fractions  $\alpha_i$ . Hence, the sum of all phases is equal to one. Each phase (the  $i^{\text{th}}$  phase) is governed by the laws of mass conservation and momentum conservation individually.

---

Considering gas-liquid flow, the relative motion between bubbles yields local pressure and SS gradients. The forces between different phases, which are the additional source term in the momentum equation, are the drag force, the lift force, the virtual mass force, etc. As the predominant force is drag force, it must be considered and the effect of other forces could be neglected [138].

### **Mixture method**

The mixture method, also referred to as the algebraic slip model or slip mixture model, is the simplest multi-phase model among these three multi-phase models. This simplification is due to the assumption of small Stokes number, where local equilibrium of primary fluid and secondary fluids can be achieved over short spatial length scales, i.e. their velocities are almost the same in both magnitude and direction [201]. However, this method allows different phases to move at different velocities by introducing the concept of algebraic slip velocities, which assumes that all phases in a mixture move at different velocities but with a local equilibrium between them. In this case, the relative velocities between phases are prescribed instead of solved. The momentum equation and the continuity equation are solved for the mixture. As a result, the mixture method is much simpler than Eulerian or VOF models. But the relative velocity must be defined to describe the dispersed phases [135]. As in many multi-phase flows, for example, the separated flow, the relative motion of different phases is closely related to pressures and velocity gradients, the mixture methods cannot be applied in such situations [205]. This approach is usually not well accepted in the simulation of the multi-phase flow, whose relative velocity between phases are not well known [206]. Thus, only two studies used this method [38, 106] for the simulation of bubble-water two-phase flow in the database. Despite that this model is widely used to solve the water and activated sludge mixture in the fields of water and wastewater treatment [31], only one study concerning the solid phase used this method for the modeling of the tubular membrane module in the MBR system.

### **VOF method**

The VOF approach is a surface tracking method that could capture the interface of two or more immiscible fluids by tracking the volume fraction of each phase in each computation cell throughout the domain. As this method is capable of tracking the motion of bubbles in water [100, 133], it can be found in the simulation of MBRs to observe the bubbles' behavior in aerated membrane modules, to develop novel aeration pattern [40, 83], to compare bubbly flow and slug flow [40, 83, 93, 164], to investigate the effect of bubble shape and trajectory [19, 95, 100, 132, 133, 141, 189]. However, all of these simulations are limited in small models, since the VOF method requires very fine grid size to better describe the interface of the gas and liquid phases. Besides, most of the simulations are conducted in a tubular membrane module in 2D models, where they can be set as 2D axi-symmetric swirl space to save computing resources. Only a few studies utilize the VOF method to carry out simulations in FS or HF membrane modules, while most of them used the Eulerian method when it concerns gas-liquid two-phase flow in the MBR system. Reviewing the literature with the VOF method in the database, there exists none that performed the simulation for gas-liquid-solid multi-phase flow in MBRs, and there are only simulations for bubbles' rise in Newtonian or non-Newtonian fluid. This might be attributed to the fact that VOF is suitable for immiscible fluids, for example, gas and liquid. And activated sludge and water in the MBR system are not immiscible fluids. Even though they could be regarded as immiscible fluids and using the VOF method for simulation, there is not sufficient data and no model available for the solid phase to describe the activated sludge.

The VOF model is first published in the journal in 1981 by Hirt and Nichols [207] with the basic concept of determination of the volume fraction of the liquid phase in the grid cell. The volume fraction for each grid cell in two-phase flow is defined as [208]:

1.  $\alpha_l = 1, \alpha_g = 0$ , the cell is full with liquid, but empty of gas;
2.  $\alpha_l = 0, \alpha_g = 1$ , the cell is full of gas, but empty of liquid;
3.  $0 < \alpha_l < 1, 0 < \alpha_g < 1$ , the interface of two fluids.

All variables and fluid properties in the equations are cell-averaged using volume fraction [164]. Mixture properties (e.g. density and viscosity) are weighted by the volume fraction, as shown in Eq. 15.

$$\rho = \alpha_l \rho_l + \alpha_g \rho_g \quad ; \quad \mu = \alpha_l \mu_l + \alpha_g \mu_g \quad (15)$$

where  $\rho$  and  $\mu$  denote the density and the dynamic viscosity of the mixture, respectively.  $\rho_l$  and  $\rho_g$  are the density of the liquid phase and gas phase, respectively.  $\mu_l$  and  $\mu_g$  represent the dynamic viscosity of the liquid phase and gas phase, respectively.  $\alpha_l$  and  $\alpha_g$  are the volume fraction of liquid phase and gas phase. The sum of them should be one, as illustrated in Eq. 16.

$$\alpha_l + \alpha_g = 1 \quad (16)$$

The volume fraction is determined by solving the additional equation (Eq. 17) [164].

$$\frac{\partial \alpha_l}{\partial t} + \nabla \cdot (\alpha_l \mathbf{u}) = 0 \quad (17)$$

In this model, all phases share a single set of mass and momentum equations [100, 133]. The single set of conservation equations for the incompressible flow is expressed in Eq. 18 and Eq. 19.

$$\nabla \cdot \mathbf{u} = 0 \quad (18)$$

$$\frac{\partial \rho \mathbf{u}}{\partial t} + \nabla \cdot (\rho \mathbf{u} \mathbf{u}) = -\nabla p + \nabla \cdot (\mu (\nabla \mathbf{u} + \nabla \mathbf{u}^T)) + \mathbf{f}_b \quad (19)$$

In the momentum equation, the term of body force  $\mathbf{f}_b$  contains the gravitational force and the surface tension forces between gas and liquid phases. It can be written as in Eq. 20.

$$\mathbf{f}_b = \rho \mathbf{g} + \mathbf{f}_{sf} \quad (20)$$

where  $\mathbf{f}_{sf}$  represents the surface tension force at the interface of gas-liquid two-phase fluids. In the VOF model, the velocity field is assumed to be continuous across the interface, but the surface tension produces pressure jump across the interface, resulting in a discontinuous pressure field [209]. This discontinuity in the pressure field makes the simulation of the interfacial flow complex. The VOF model used continuum

surface force (CSF) model, proposed by Brackbill et al. in 1992 [210], to calculate the surface tension force. In the CSF model, the surface tension force is added to the momentum equation as a component of the body force [208]. Supposing the surface tension along the interface is constant and only considering the forces normal to the interface, the boundary condition at the interface or the pressure drop across the interface can be stated as displayed in Eq. 21 [201, 208].

$$p_2 - p_1 = \sigma \left( \frac{1}{r_1} + \frac{1}{r_2} \right) \quad (21)$$

where  $p_1$  and  $p_2$  are the pressures on either side of the interface.  $\sigma$  is the surface tension coefficient.  $r_1$  and  $r_2$  are radii in orthogonal directions at the interface. The interface curvature  $\kappa$  is defined as in Eq. 22.

$$\kappa = \frac{1}{r_1} + \frac{1}{r_2} \quad (22)$$

In the CSF model, the surface tension force  $\mathbf{f}_{\text{sf}}$  is calculated from the surface curvature, which is a function of the local surface normal at the interface. And the surface normal  $\mathbf{n}$  is given in Eq. 23.

$$\mathbf{n} = \nabla \alpha_1 \quad ; \quad \hat{\mathbf{n}} = \frac{\mathbf{n}}{|\mathbf{n}|} \quad (23)$$

The interface curvature is computed as the divergence of a normal unit field  $\hat{\mathbf{n}}$ , as shown in Eq. 24 [190].

$$\kappa = \nabla \cdot \hat{\mathbf{n}} \quad (24)$$

For the incompressible two-phase flow, the surface tension force  $\mathbf{f}_{\text{sf}}$  is calculated with Eq. 25 [211].

$$\mathbf{f}_{\text{sf}} = \sigma \kappa \nabla \alpha_1 \quad (25)$$

Reviewing the CFD-MBR related literature, it is found out that the modeling the interaction between bubbles with a sufficient rising length using the VOF approach still lacked, due to high consumption of computing resource. In the literature, large models are normally simulated with the Eulerian method. Taking example of studies conducted by Amini et al. [33, 127], full-scale simulations were performed in a large model with a height of 1000 mm. However, they used the Eulerian approach for modeling the gas-liquid two-phase flow in the FS membrane. With this approach, the bubbles' motion and interaction with water and membrane sheets are not included in the simulation. Besides, a basic premise of this method is that for the dispersed phase (bubbles), the characteristic length of the interface should be much smaller than the grid size [212], which means one mesh cell should contain a lot of bubbles. However, the membrane sheets separations in commercial FS membrane modules are usually in the range of 6 - 10 mm [14]. If each membrane sheets separation has one mesh cell with a size of 6 - 10 mm in the same direction as the membrane sheets separation, the characteristic length of the interface of gas-liquid phases are even



larger than the grid size in this direction for larger bubbles with a diameter above 10 mm. Hence, the mesh cell cannot contain such a bubble completely.

---

#### 2.4.4 Integrated models

---

Apart from the general-purpose CFD approaches, there are many studies combined with other models to serve the different purpose of the simulations. Most of the integrated models take the effect of permeable properties of the membrane and the non-Newtonian behavior of activated sludge into consideration to make the simulated problem closer to the real situation. Wu et al. [125] integrated porous media to simulate the MBR tank in full-scale by treating the whole FS membrane module as porous zone instead of impermeable block. Similarly, Liu et al. [37, 94] carried out two-phase simulations in the MBR tank equipped with the FS membrane module, which was simplified as a porous zone. Jajuee et al. [167] also simulated the two-phase flow in a FS membrane module, where the boundary conditions of membrane sheets were set as porous media. Particularly in the HF membrane module, the porous media is usually implemented into the numerical methods to predict the effect of packing density and fiber geometry on permeate flux or contaminated species removal [169, 171–173].

##### **Porous media**

For the full-scale simulation of MBRs, the mesh grids can be too fine to be used for simulations. Wu et al. [125] found a compromise to save the computational resource, making it feasible to model the full-scale MBRs. They used the integrated porous media models to treat the whole FS membrane module as a porous zone by adding a source term into the momentum conservation equation. The coefficients needed for their model came from published research, which were determined experimentally. In this way, the mesh required for the computational domain is reduced dramatically, and the simulation of full-scale MBRs is feasible. Comparing the models with and without porous zones, they found out that the liquid velocity profiles depend on the CFD models greatly and the flow motion in the MBR tank predicted by the integrated models is closer to the real flow motion. Liu et al. [37, 94] did the same treatment and found an improvement in the accuracy of their simulations when they are incorporated with a porous media model. However, this integrated model might be suitable for the simulation of the HF membrane module, but its application in the FS membrane module might not be appropriate, since the HF membrane module has a relatively high packing density, while membrane sheets in the FS membrane module are 6 - 10 mm separated.

To represent the permeable properties of membrane plates in the FS membrane module, Jajuee et al. [167] implemented Darcy's law to describe the boundary condition of the porous membrane, as Darcy's law is an equation that states the flow through a porous medium. In their integrated boundary condition, the driving force that forces fluid flowing through the porous membrane is the hydro-static pressure differences at the membrane surface in the riser zone and the downcomer zone. The hydro-static pressure difference is found to be linked to the gas holdup in the riser and the relative pressure, which were measured to determine the pressure gradient.

Other researchers [169, 171–173] utilized Darcy's law in the HF membrane to determine the permeate flux distribution along one hollow fiber within a bundle, where the fibers are regularly spaced. The computational domain is the lumen of the fiber, the porous membrane wall and the external channel, where the feed region, the membrane filtration region and the permeate region are included in the model.



The flow is assumed to be steady, incompressible and uniformly distributed at both ends of the fiber. The porous membrane is considered as porous media with a constant membrane permeability, where Darcy's law is applied by adding momentum sink into the governing equations. The model is further simplified when it is simulated in the 2D axi-symmetric model instead of a 3D model. Besides, the packing density is linked to the geometry of the models with analytical expressions, and the geometry can be easily modified. With this numerical approach, researchers can study the effect of the design features of the HF membrane including the packing density, the fiber diameter, the fiber length, etc. on the permeate flux distribution and permeate outflow rate.

### Sludge rheological model

It is observed experimentally by Rosenberger et al. [213] that the MBR sludge exhibited strongly pseudoplastic behavior indicating that activated sludge should be treated as non-Newtonian fluid. The non-Newtonian behavior in MBRs is a crucial fluid property that has a substantial impact on hydrodynamics, oxygen transfer, mass transfer rate, membrane fouling, and membrane filtration process in MBRs, due to its essential role in the flow pattern, sludge viscosity and shear rate [57, 58]. The sludge viscosity, the most common parameter used to describe the rheological properties of activated sludge, is known to be affected by a vast of factors, such as the MLSS concentration, temperature, shear forces induced by mixing or aeration [57], pH, substrates concentration [94] and particle size distribution, etc. Among all of these factors, the MLSS concentration is the decisive factor of the viscosity of mixed liquor [57]. A series of MBR sludge models have been proposed to describe their relationship, which is illustrated in Table 8.

Table 8: Summary of rheological models of MBR sludge

Model	General formulation	Specific expressions	Applied MLSS [g/L]	Reference
Bingham	$\tau = \tau_0 + k\dot{\gamma}$	$\mu = 10^{-3} \times (\frac{28.939c}{\dot{\gamma}} + 0.233c + 1)$	3.7 - 22.9	Laera et al.[214]
Power-Law	$\tau = k\dot{\gamma}^n$	$\tau = 0.001e^{2c^{0.41}}\dot{\gamma}^{1-0.23c^{0.37}}$	10 - 50	Rosenberg et al.[213]
		$\tau = 0.0431c^{0.89}\dot{\gamma}^{0.68}$	3 - 8	Liu et al.[94]
		$\tau = 0.0412c^{1.64}\dot{\gamma}^{0.45}$	8 - 16	
Ostwald-de Waele	$\mu = k\dot{\gamma}^{n-1}$	$\mu = 10^{-3}e^{0.822c^{0.494}}\dot{\gamma}^{-0.05c^{0.631}}$	3.7 - 22.9	Laera et al.[214]
		$\mu = 10^{-3}e^{1.17c^{0.61}}\dot{\gamma}^{-0.13c^{0.63}}$	4 - 10.2	Duran et al. [215]
		$\mu = 32.36c^{1.359}\dot{\gamma}^{-0.807}$	2.8 - 10.2	Yang et al.[216]
		$\mu = 1 + 3.25c^{1.03}\dot{\gamma}^{-0.124c^{0.359}}$	9 - 25	Pollice et al. [217]
Herschel-Bulkley	$\tau = \tau_0 + k\dot{\gamma}^n$	$\tau = 0.149(1 - e^{-44.7\dot{\gamma}}) + 0.0137\dot{\gamma}^{0.783}$	N.A.	Brannock et al.[97]
		$\tau = 0.00686c^{2.08413}(1 - e^{-0.03355\dot{\gamma}}) + 0.00001c + 0.00028\dot{\gamma}^{1.46224}$	6 - 16	Rios et al.[218]
Sisko model	$\mu = \mu_\infty + k\dot{\gamma}^{n-1}$	$\mu = 6.35 \times 10^{-4} + 2.73 \times 10^{-3}c^{1.65}\dot{\gamma}^{-0.46}$	3 - 18	Yang et al.[58]
Alternative models		$\mu = 1.0477\mu_w e^{0.0754c}$	$\leq 9.122$	Yang et al.[58]
		$\mu = \mu_w(0.0254c^2 - 0.1674c + 1.5918)$	$> 9.122$	

$\tau$  is the SS (Pa) and  $\dot{\gamma}$  is the shear rate ( $s^{-1}$ ),  $\tau_0$  is the yield SS (Pa) and  $k$  is the flow consistency index ( $Pa \cdot s^n$ ), and  $n$  is the flow behaviour index (-),  $\mu_\infty$  is the infinite rate apparent viscosity ( $Pa \cdot s$ ), and  $\mu_0$  is the viscosity at a low shear rate ( $Pa \cdot s$ ).

Table 8 shows that in the literature there are numerous rheological models to predict the viscosity of one fluid with different degrees of complexity depending on the fluid properties. The most simple one is for

the Newtonian fluid, of which the SS is linearly proportional to the strain rate. Therefore, the viscosity is constant, which is defined by Eq. 26 [57].

$$\mu = \frac{\tau}{\dot{\gamma}} \quad (26)$$

where  $\tau$  is the SS (Pa) and  $\dot{\gamma}$  is the shear rate ( $\text{s}^{-1}$ ). It should be noted that  $\mu$  is a scalar,  $\tau$  is a vector, and  $\dot{\gamma}$  is a tensor. In OpenFOAM and in Eq. 26, all variables are treated as scalars, which means the expression uses the modulus of the vector and the modulus of the tensor.

However, the relationship between the SS and the shear rate for non-Newtonian fluids is non-linear. Thus, the viscosity also refers to as apparent viscosity [57], being a function of shear rate. The models for the prediction of the viscosity of non-Newtonian fluids also become more complex, as shown in Table 8. Most of them are empirical models, and their parameters are usually determined experimentally. Among all of these models, the Bingham model and the Power-Law model are the most basic, most common and most widely used rheological models. The Herschel-Bulkley model and the Sisko model, which are popular to predict the apparent viscosity of activated sludge in the MBR system, are combined versions of the Bingham model and the Power-Law model.

#### 1. Bingham model

Activated sludge exhibits plastic behavior or pseudoplastic behavior [219] since the aggregated particles could be broken up by shear force. The plastic behavior of fluids is prescribed in analog to the plastic behavior of solids. The deformation of plastic materials occurs until the yield stress  $\tau_0$  (Pa) is achieved. In activated sludge there exists a interconnected 3D network of flocs that has the cohesion Van-Der-Waals forces as resistance oppose to deformation [220]. The applied stress needs to overcome the Van-Der-Waals forces and once it exceeds the yield stress, the fluids start to flow. The Bingham model is considered to be one of the most appropriate models to describe the rheological behavior of activated sludge [219, 221], since the yield stress component is included in this model. Eq. 27 shows the general form of the Bingham model.

$$\tau = \tau_0 + k\dot{\gamma} \quad (27)$$

where  $\tau_0$  is the yield SS (Pa) and  $k$  is the flow consistency index ( $\text{Pa}\cdot\text{s}$ ).

In general, a higher value of the consistency index reflect a higher viscosity of the fluids. These two parameters could be determined experimentally. As sludge concentration contributes significantly to SS [57], the main parameters in empirical rheological models, such as the yield SS  $\tau_0$ , the flow consistency index  $k$  is usually expressed as a function of the MLSS concentration. Besides, they are known to be affected by temperature. At high temperature, the molecules can move more freely due to the weaker bounce to each other, resulting in a more flowable fluid, hence a lower value in the viscosity of the fluid. Researchers [216, 222, 223] proposed the main parameters based on the influencing variable, i.e. sludge concentration. Therefore, this review focuses on the rheological behavior of activated sludge in the MBR system.

Laera et al. [214] took the activated sludge sample from a bench-scale MBR system and measured the ave. SS under various shear rates to determine the parameters of the Bingham model, i.e. the

yield stress and the flow consistency index. The parameters of the Bingham model are proposed as a function of the MLSS concentration, as demonstrated in Eq. 28 and Eq. 29.

$$\tau_0 = 2.8939 \times 10^{-2}c \quad (28)$$

$$k = 10^{-3} \times (0.233c + 1) \quad (29)$$

where  $c$  is the MLSS concentration (g/L).

## 2. Power-Law model

The Power-Law model is another basic rheological model applied widely in the description of the sludge rheological behavior. Eq. 30 shows the general form of the Power-Law model. [57].

$$\tau = k\dot{\gamma}^n \quad (30)$$

where  $k$  is the flow consistency index ( $\text{Pa} \cdot \text{s}^n$ ), and  $n$  is the flow behaviour index (-), which indicates the tendency of shear-thinning or shear-thickening behavior of fluids. When  $0 < n < 1$ , fluids show shear-thinning behavior and their apparent viscosity decreases with an increase in shear rate. When  $1 < n < \infty$ , fluids show shear-thickening behavior. For shear-thickening fluids, their apparent viscosity increases as the shear rate increases. Activated sludge has been identified by many studies [57, 216, 220] as shear-thinning fluids.

Rosenberg et al. [213] took activated sludge samples from 9 MBRs and examined their rheological behavior. They found a strong pseudo-plastic behavior of activated sludge in all samples and the dominant influence of the MLSS concentration on apparent viscosity. The measured data were fitted to a the Power-Law model, and its main parameters expressed as a function of the MLSS concentration in Eq. 31 and Eq. 32:

$$k = 0.001e^{2c^{0.41}} \quad (31)$$

$$n = 1 - 0.23c^{0.37} \quad (32)$$

where,  $n$  is between 0 and 1, indicating the shear-thinning behavior of activated sludge.

Liu et al. [94] measured the viscosity of activated sludge from a pilot-scale MBR at different sludge concentrations. The fitting equations took the form displayed in Eq. 33.

$$\tau = \begin{cases} 0.0431c^{0.89}\dot{\gamma}^{0.68} & \text{for } 3 \text{ g/L} \leq c < 8 \text{ g/L} \\ 0.0412c^{1.64}\dot{\gamma}^{0.45} & \text{for } 8 \text{ g/L} \leq c \leq 16 \text{ g/L} \end{cases} \quad (33)$$

where  $c$  is the MLSS concentration (g/L),  $\tau$  is the SS (Pa) and  $\dot{\gamma}$  is the shear rate ( $\text{s}^{-1}$ ). All of them are scalars.

With this equation implemented into their CFD models, they found out that the ave. SS increased, as the MLSS concentration increased. This is attributed to the direct increase in sludge viscosity due to the MLSS concentration increase. With a further rise in the MLSS concentration, SS decreased due to the low liquid velocity near the membrane surface at a high viscosity. In the CFD-MBR related literature, Wu et al. [125] also incorporated this rheological model for activated sludge in MBRs in their CFD model.

### 3. Ostwald-de Waele model

The Ostwald-de Waele model is a modified version of the Power-law model. The rheological studies of activated sludge in the MBR system conducted by Hasar et al. [223] revealed that the Ostwald-de Waele model was the most suitable model to describe the rheological behavior of activated sludge in a submerged MBR. The Ostwald-de Waele model has the following formula, as shown in Eq. 34.

$$\mu = \frac{\tau}{\dot{\gamma}} = k\dot{\gamma}^{n-1} \quad (34)$$

where  $k$  and  $n$  are the flow consistency index ( $\text{Pa} \cdot \text{s}^n$ ) and the flow behaviour index (-), respectively.

Laera et al. [214] used the obtained experimental data to fit the Power-Law model, and found slightly better results obtained by the Bingham model in terms of statistical analysis. The main parameters of the Ostwald-de Waele model determined by the authors have a similar formulation (Eq. 35 and Eq. 36) to that obtained by Rosenberg et al. [213].

$$k = 10^{-3} e^{0.822c^{0.494}} \quad (35)$$

$$n = 1 - 0.05c^{0.631} \quad (36)$$

Duran et al. [215] also investigated the non-Newtonian behavior of activated sludge in MBRs and used the Ostwald-de Waele model to describe the sludge rheology. They gave the rheological parameters of this model ( $k$  and  $n$ ) the expressions displayed in Eq. 37 and Eq. 38.

$$k = 10^{-3} e^{1.17c^{0.61}} \quad (37)$$

$$n = 1 - 0.13c^{0.63} \quad (38)$$

The rheological parameters above are also similar to that proposed by Rosenberg et al. [213].

Yang et al. [216] carried out a rheological study of activated sludge in submerged MBRs and proposed a mathematical model based on the Ostwald-de Waele model to describe the sludge rheological behavior. The main parameters at the temperature of 20 °C are expressed as a function of the MLSS concentration (Eq. 39 and Eq. 40).

$$k = 32.36c^{1.359} \quad (39)$$

$$n = 0.193 \quad (40)$$

Pollice et al. [217] characterized the rheological behavior of the MBR sludge with a MLSS concentration ranging from 9 to 25 g/L with the Ostwald-de Waele model since it fitted the experimental data most accurately compared to other modules. The parameters of the Ostwald-de Waele model are given by Eq. 41 and Eq. 42.

$$k = 1 + 3.25c^{1.03} \quad (41)$$

$$n = 1 - 0.124c^{0.359} \quad (42)$$

#### 4. Herschel-Bulkley model

The Herschel-Bulkley model (Eq. 43) is one of the most popular models applied for the description of the rheological behavior of activated sludge in the MBR system, as it is a combination of two basic rheological models: the Bingham model and the Power-law model.

$$\tau = \tau_0 + k\dot{\gamma}^n \quad (43)$$

where  $\tau_0$ ,  $k$  and  $n$  the yield SS ( $Pa$ ), the flow consistency index ( $Pa \cdot s^n$ ), and the flow behaviour index (-), respectively.

Brannock et al. [97] measured the activated sludge rheological properties directly in the pilot-scale MBR tank at a MLSS concentration of 8.0 g/L at a constant temperature of 25 °C and fitted the experimental data with the Herschel-Buckley model with Papanastasiou's adaption [224, 225], as it can match the experimental rheological data for the MBR sludge very well. The Herschel-Buckley rheological model with Papanastasiou's adaption fitted to the experimental data is shown in Eq. 44:

$$\tau = 0.149(1 - e^{-44.7\dot{\gamma}}) + 0.0137\dot{\gamma}^{0.783} \quad (44)$$

Then, Brannock et al. [97] implemented this sludge viscosity model into CFD simulations to investigate the effect of sludge rheology on the bulk mixing in the MBR system, and they found this effect was small compared to the mixing effect by turbulence, as a turbulent viscosity ratio above 3 existed in 70% of the MBRs. It should be noted that in their sludge model, the concentration of activated sludge is constant at a MLSS concentration of 8 g/L everywhere in the MBR tank, and the sludge viscosity is only affected by shear rate. That might be attributed to the minor effect of the activated sludge rheology on the bulk mixing.

Rios et al. [218] took activated sludge samples from a lab-scale side-stream MBR and then concentrated or diluted to get 11 different concentrations of total suspended solids (TSS). Four models were used to fit the experimental data, and the Herschel-Buckley model with Papanastasiou's adaptation (HBP) is found to be the best one to model the settling behavior of activated sludge in MBRs. The HBP model is expressed in Eq. 45 [224, 225].

$$\tau = \tau_0(1 - e^{-m\dot{\gamma}}) + k\dot{\gamma}^n \quad (45)$$

where  $m$  is the dimensional regularization parameter.

Based on their measurement, the parameters of the HBP model are given by Eq. 46, Eq. 47 and Eq. 48.

$$\tau = 0.00686c^{2.08413} \quad (46)$$

$$k = 0.00001c + 0.00028 \quad (47)$$

$$m = 0.03355 \quad ; \quad n = 1.46224 \quad (48)$$

## 5. Sisko model

The Sisko model, a combination of the Bingham model and the Ostwald-de Waele model, takes the form as demonstrated in Eq. 49.

$$\mu = \mu_{\infty} + k\dot{\gamma}^{n-1} \quad (49)$$

where  $\mu_{\infty}$  is the infinite rate apparent viscosity (Pa·s).

Yang et al. [58] obtained the expression (Eq. 50) at a temperature of 20 °C, and a MLSS concentration between 3 and 18 g/L can be described as a function of the MLSS concentration.

$$\mu = 6.35e^{-4} + 2.73e^{-3}c^{1.65}\dot{\gamma}^{-0.54} \quad (50)$$

It should be noted that in the source code of some CFD software, such as OpenFOAM, "e" represents 10, while in mathematics "e" represents natural constant. If "e" was natural constant in the expression above, the viscosity of water, when the MLSS concentration equals to 0 g/L, would be 0.116 Pa·s, while the dynamic viscosity of water should be at about  $8.90 \times 10^{-4}$  Pa·s. Thus, it makes more sense, if "e" represents 10 in the expression instead of the natural logarithm. Yang et al. [58] used the model to investigate the effect of sludge concentration on hydrodynamics in MBRs, and their results revealed that the MLSS concentration is the most vital influencing factors on hydrodynamics in MBRs.

## 6. Alternative models

The most popular empirical rheological model derived the apparent empirical viscosity directly from the sludge concentration. The apparent viscosity is believed to be a function of the MLSS concentration. As the MLSS concentration increases, the electrostatic forces between solid particles increase. As a result, the sludge floc has a higher degree of the cross-linking network, and the fluid has a higher apparent viscosity [94]. The model is given by Eq. 51 [33, 119, 127, 174, 226].

$$\mu = \begin{cases} 1.0477\mu_w e^{0.0754c} & \text{for } c \leq 9.122 \text{ g/L} \\ \mu_w(0.0254c^2 - 0.1674c + 1.5918) & \text{for } c > 9.122 \text{ g/L} \end{cases} \quad (51)$$

where  $\mu_w$  is the water viscosity.

Kang et al. [119] and Buetchorn et al. [174] took the effect of the MLSS concentration on mixed liquor viscosity into account by using this model. Amini et al. [33, 127] also used this model to calculate the dynamic viscosity at various sludge concentrations. Besides, they estimated the density corresponding to sludge concentration according to Eq. 52.

$$\rho = c + 1000\left(1 - \frac{c}{\rho_{DS}}\right) \quad (52)$$

where  $\rho_{DS}$ , the specific density of dry solids, equals to 1250 kg/m<sup>3</sup>.

However, the mixed liquor is still assumed to be a Newtonian fluid; only the dynamic viscosity changed in their studies. .

Despite various rheological studies of activated sludge in the MBR system, the effect of activated sludge on hydrodynamics in MBRs is still not clear. Brannock et al. [97] revealed that the activated sludge rheology has only a slight impact on the bulk mixing in the MBR system compared to the mixing effect caused by turbulence in the membrane module. The results from Buetchorn et al. [174] and Amini et al. [33, 127] also showed a minor effect of dynamic viscosity of activated sludge on hydrodynamics in the MBR system. However, in their studies, the mixed liquor was regarded as a Newtonian fluid, and they simplified the rheological problem by merely changing the viscosity of the fluids. Wei et al. [93] also found that the ave. SS induced by bubbles was only slightly increased even at a sharp increase in viscosity by 10.7%. Experimental investigation undertook by Boehm et al. [82] also found that the rheology of the mixed liquor is minor in MBRs, as the fluctuation of SS is stronger in water compared to that in the non-Newtonian fluid. However, other researchers found the rheology of activated sludge was vital to hydrodynamics in MBRs. Yang et al. [58] used response surface method to compare the effect of the MLSS concentration, aeration intensity and bubble size on hydrodynamic in MBRs including SS, particle deposition, strain rate, sludge viscosity. They found out that the MLSS concentration was the most important influencing factors among all these investigated factors. Sludge rheology has been shown experimentally to affect the hydrodynamic regime in the MBR system, the energy consumption, membrane filtration [213, 223].

### Sludge settling model

The settling behavior of the MBR sludge is normally not taken into consideration in the modeling of MBRs. In all the CFD-MBR related literature, none studied the settling behavior of the MBR sludge or

implemented sludge settling models into their CFD models. However, the sedimentation characteristics of the activated sludge are well investigated in the literature. As early as in 1952, Kynch [227] has developed the theory of gravitational sedimentation and classified the sludge sedimentation into four categories based on solid concentration. At a low sludge concentration ( $c < 0.6\text{--}0.7$  g/L) [228], i.e. in the free settling zone or in the discrete settling zone, the suspended solids are supposed to settle down freely, and the settling velocity are supposed to be constant or dependent on particle properties. Francois et al. [229] studied the settling curve of activated sludge during its settlement and observed a constant velocity in the settling phase. Li et al. [230] correlated the settling velocity with the shape of flocs as shown in Eq. 53, Eq. 54 and Eq. 55.

$$V_s = 0.35 + 1.77D \quad (53)$$

$$V_s = 0.33 + 1.28L \quad (54)$$

$$V_s = 1.47L^{0.55} \quad (55)$$

where  $V_s$  is the settling velocity (mm/s) representing the component of relative velocity  $u_r$  in  $z$  direction.  $D$  and  $L$  are the cross-sectional diameter (mm) and the longest dimension (mm), respectively.

But at a high sludge concentration with a MLSS concentration larger than 0.6 - 0.7 g/L, i.e. in the hindered settling zone or the compression zone, the settling velocity decreases with increasing sludge concentration [231]. Thus, the settling velocity is typically expressed as a function of sludge concentration. Francois et al. [229] observed a decreasing velocity in the compression phase when the concentration is high enough for flocs to interfere with each other and form a more complex structure.

In an activated sludge tank or a MBR system, the sludge concentration is relatively high, being in the range of 2 - 4 g/L for conventional activated sludge and 10 - 20 g/L for the MBR sludge [9]. The settling velocity models suitable for activated sludge are either based on the Vesilind model or derived from the Carman-Kozeny equation, which is an analytical formula for flow through a packed bed. Among these models, the function of Vesilind [232] or its extended form is the most commonly used model [233]. The Vesilind settling model describes the relationship between the settling velocity of the sludge blanket and the concentration of solids, as demonstrated in Eq. 56.

$$V_s = V_0 e^{bc} \quad (56)$$

where  $c$  represents the solid concentration,  $V_0$  and  $b$  are an empirical parameter, which defines the settling characteristics of sludges. Researchers [234–236] have determined the constants  $a$  and  $b$  in the Vesilind model as a function of sludge volume index ( $SVI$ ). Daigger et al. [234] measured 236 individual settling velocities, correlated the empirical parameters with  $SVI$  and determined the settling velocity expression, as shown in Eq. 57.

$$V_s = 7.80e^{(0.148+0.00210 \cdot SVI)c} \quad (57)$$



Haertel et al. [235] developed dynamic simulation models for the activated sludge settling and thickening process based on the Vesilind model [232]. Their settling model is given by Eq. 58 and Eq. 59.

$$V_0 = 17.4e^{-0.0113 \cdot SVI} + 3.931 \quad (58)$$

$$b = 0.9834e^{-0.00581 \cdot SVI} - 1.043 \quad (59)$$

Akca et al. [236] determined the empirical parameters (in Eq. 60 and Eq. 61), so that it could provide guidelines for the design of a secondary clarifier in activated sludge plants.

$$V_0 = 28.1 \cdot SVI^{-0.2667} \quad (60)$$

$$b = 0.177 + 0.0014 \cdot SVI \quad (61)$$

Zhang et al. [237] developed a mathematical expression based on the Vesilind equation for the compression settling process of activated sludge (in Eq. 62), and proved that the Vesilind model is capable of predicting the compression settling velocity when the parameters are appropriately estimated.

$$V_s = \begin{cases} 6.79e^{0.345c} & \text{for } c \leq 5.846 \text{ g/L} \\ 64.2e^{-0.667c} & \text{for } c > 5.846 \text{ g/L} \end{cases} \quad (62)$$

Other researchers modified the basic settling model of Vesilind for a broader application [184, 223] or turbulent flow conditions [231]. Among all these extended model, the Takacs model [55], expressed in Eq. 63, is identified to be the best by Grijspeerdt et al. [238], as it accounts for the decrease in settling velocity when solids concentration approaches zero [239] and hence it can describe the settling behavior of suspensions at both dilute and concentrated solutions [240].

$$V_s = V_0e^{-r_h c} - V_0e^{-r_p c} \quad (63)$$

Apart from the exponential model, the cho settling model is another empirical models for the settling velocity used in practice [241]. The formula is developed based on the Carman-Kozeny equation [241, 242]. To verify the settling models, Cho et al. [241] took activated sludge samples from WWTP and measured the settling velocity. They found that the exponential model could fit the experimental data best. Besides, their settling model with 4th order of the sludge concentration could fit the experimental data better than the 3rd order equation proposed by Scott [242].

A comparison between Cho models, the Vesilind model and the Takacs function was given by Vanderhasselt et al. [243], who found that the Takacs model is suitable for a broader range of solids concentrations, whereas the Vesilind model is more efficient describing the settling velocity in dilute suspensions. Cho functions were found to be better in describing the complete batch settling curve. As the Vesilind model and the Takacs function are more popular in the literature, they are chosen for further research in this study.

---

## Other implementation

Apart from the most popular models, i.e. the porous model and sludge rheological models, the transport species model and the population balance model (PBM) could be found in one or two studies, which incorporated the models into their CFD simulations of the MBR system. Concerning the simulation of membrane filtration, the transport species model are more popular in the simulation of high-pressure membrane filtration process (RO and NF) to describe the mass transfer during membrane filtration, to model the micro-structure of the membrane, to predict the solutes rejection, to resolve concentration polarization effect or to analyse the flow conditions [244], while its application in the modeling of the MBR system is rare. Sanaeepur et al. [175] developed a mathematical model for the two-dimensional nitrate transport through the membrane to predict the effect of design features on the nitrate removal efficiency. They used the simplified mass conservation equation for the nitrate transport with several assumptions, e.g. the flow in the lumen side was assumed to be fully-developed laminar flow, to calculate the nitrate concentration. Cui et al. [129] included the convective mass transfer and diluted species transport equation into their 2D CFD models to investigate the backwashing process in MBRs with the aim to guide the backwashing process. Yang et al. [110] used the advection-dispersion species transport equation with a source term of the oxygen mass transfer rate for oxygen consumption, and the submodels for nitrogen transformation to predict the 3D steady state DO and the ammonia distribution in MBR tanks. The model is capable of predicting the species concentration with an acceptable accuracy, compared to the measured data. Actually, in this study, the simplified ASM is applied in the source term in the species transport equation. In the ASM framework, the biological reaction in MBRs could be simulated. This study is the first one to incorporate the ASM model into a CFD model to simulate the biological reaction in MBRs. Most CFD models coupled with the ASM model are applied into the simulation of activated sludge tanks [50, 51, 245] to predict the species concentration, such as COD, DO, and ammonium, etc.

Nearly all CFD simulations of gas-liquid flow in MBR systems are assuming a constant bubble size instead of bubble size distribution to simplify the simulation. However, in the MBR system, the bubble size has a wide range during operation. And the bubble size has a significant influence on bubble behaviors. The PBM model, which can be coupled into the CFD, turns out to be a practical approach to predict the bubble size distribution. Wang et al. [246] developed a CFD-PBM coupled model with consideration of bubble breakup and coalescence, which was able to predict the hydrodynamics in complex flow regime. It is found that at a low gas flow rate the bubbles are small and had a narrow size distribution and a relatively uniform gas hold-up profile. With an increasing gas flow rate, the effect of bubble coalescence becomes stronger, and a lot of large bubbles are formed. Wang [247] used this CFD-PBM coupled model to simulate the bubble columns to investigate the fundamental hydrodynamic characteristics in it. The simulated bubble size distribution and gas hold up for bubble columns both in the homogeneous and heterogeneous regime showed good agreement with experimental data. The activated sludge flocs and bubbles could be regarded as ensembles of populations of individual entities with specific properties [31]. Both the interactions between the individual entities and the interaction between the individual entities and their environment should be taken into consideration. However, to reduce the computing consumption, the individual entities are usually assumed to be the same, e.g. the fixed bubble diameter [37, 120] or uniform floc size [248]. And the mutual interactions between individual entities, e.g. the coalescence and breakups are usually ignored. CFD model incorporated with the PBM model can describe the variations

in individual entities and mutual interactions. Nopens et al. [249] used the PBM model to investigate the activated sludge flocculation process by taking the floc size, floc aggregation and breakage rate of flocs into consideration. However, their model could not describe the floc size distribution accurately and seems to lack flexibility. In the MBR-CFD related literature, only two studies could be found using the PBM model to describe the sludge floc or bubbles. However, One of them [161] did not state clearly, which PBM model was used for which phase and only the name of PBM was mentioned in their study. The other one [127] coupled the PBM model into the Eulerian model to describe the population of bubbles including the effect of bubble breakup and coalescence, so that the numerical prediction could be closer to the real situation. Their results revealed that an increase in the MLSS concentration could lead to an increase in the mean diameter, while aeration is insignificant. Besides, the sparger configuration is found to play a more critical role in the mean diameter of generated bubbles than the air flow rate.

---

## 2.5 Discussion

---

More and more research groups utilize CFD to assist the design of the MBR system and to shed light on the phenomena taking place in this system. And with the rapid development in computing technology and the steady advances in CFD software packages, the problems in CFD studies in the MBR field have become more complex. In the earliest study [95], the model was 2D with a small domain, and the results from simulations are limited, e.g. SS could not be solved by software, while nowadays, membrane vibration employing the two-way FSI approach [109] with more mesh cells could be simulated in 3D and 3D simulations for full-scale MBRs coupled with bio-kinetics [39] could be found in the literature. The CFD studies on MBRs in the future may include more complex mechanisms such as mass transfer between bubbles and fluid, the permeable wall conditions and large-scale membrane vibration. The models in future CFD studies may match the real MBR system better. The bench-scale models e.g. single fiber [109] or single membrane channel [120] will be replaced.

Previous studies on hydrodynamics in MBRs using CFD are critically reviewed. Based on the review and the results from this research, CFD has shown significant advantages in predicting and investigating hydrodynamic conditions in MBRs and has been proven to be a powerful tool for designing and optimizing MBRs. Therefore, more and more CFD researches on the hydrodynamics of the aeration process in the FS membrane module will appear in the Future. For this purpose, the following issues related to potentials, limitations, and future CFD study of the aerated FS membrane module need to be addressed.

1. Lack of systematic numerical investigation of the aeration process in the FS membrane module

Researchers, e.g. Boehm's group, did conduct a systematic hydrodynamic investigation experimentally to study bubble behaviors in the FS membrane module. But their studies are mainly for single bubbles [81, 166, 250–252]. And only a few studies [82, 91] are on bubble swarms. Besides, the max. SS measured by three sensors in the experiment might not be sufficient to represent the max. SS along the membrane surface. Still, they studied the hydrodynamics in the FS module systematically by conducting a series of experiments for single bubbles and bubble swarms. However, a corresponding numerical study is still lacked in the literature.

As a result, controversial conclusions are drawn regarding key parameters affecting the aeration process in MBRs. The effects of the critical parameters, e.g. bubble size, and MLSS concentration,

---

are still controversial. Air bubbling in MBRs is typically divided into aeration with fine and coarse bubbles. Sofia et al. [180] reported a more beneficial effect of fine bubbles on membrane filtration performance in the FS membrane module than coarse bubbles, while other research groups recommended [26, 33] coarse bubble for aeration in the FS membrane module to achieve better hydrodynamic conditions and a better cleaning effect on the membrane surface. Since the aeration process in MBRs consumes high energy [1], a systematical and comprehensive understanding of this process in the aerated FS membrane modules would be of great importance to innovate novel aeration pattern for fouling control, with the aim of operating the wastewater treatment plant at low cost.

## 2. VOF approach in large models

To include the interaction between bubbles, the VOF method would be a great choice. Considering the enormous computational resource required by the VOF method, a 3D model with a height over 1500 mm is very rare to be found in previous literature. Prieske et al. [140, 166] did conduct a simulation to model a single bubble movement with a height of the domain of 1500 mm. However, in their model, only half of the bubble and half of the channel was simulated. Therefore, the simulation might not be accurate for small bubbles whose center is not always on the symmetry plane, which happens all the time as bubbles rise. Most models from the literature are similar to the model from Ndinisa et al. [26] with a small height of 290 mm, which is too short compared to the real height (about 1000 - 2100 mm) [140] of the membrane in FS modules. With such a short height, some information about bubble dynamics might be lost, since the critical height for bubble development was identified to be 250 mm by Wang et al. [40]. According to the previous study [253], the phenomena of bubble bouncing against the membrane wall could not be observed in small models and could be only observed in large models with a sufficient height.

Since the VOF method requires very fine mesh grid, it is infeasible to simulate large 3D model with this method. To save computing resources, some authors like Essemiani et al. [95] used a 2D model for simulations, the results from which might not be accurate. Because in Fluent there are two options to simplify a 3D problem to a 2D problem: planar space or axi-symmetric swirl space. With the simplification of planar space, the bubble will be a horizontal cylinder instead of a sphere in 3D. And using axi-symmetric swirl space, the membrane wall will become a tube in 3D. Both cases cannot represent the real situation, i.e. a spherical bubble in a rectangular vertical channel.

Regarding all the references, only one research group [40, 83] conducted simulations in a large model with a height of 1200 mm with the VOF approach to track the interface of two-phases. However, a novel aeration strategy with large slug bubbles was addressed in their studies, and the conventional aeration with a bubbly flow was not investigated.

Thus, it is still a gap in the literature to investigate the fundamental rising behavior of bubbles and the corresponding hydrodynamics with the VOF method in MBRs, particularly in the FS membrane module, with a sufficient rising length.

## 3. Bubble swarms modeling with the VOF method

SS is a crucial parameter indicating the membrane cleaning process. However, little is known about SS related to bubbly flow [92]. Only a few studies are conducted in the literature to examine the

---

SS on the FS membrane surface generated by bubble swarms [82]. All of them [82, 89, 92] carried out simulations in the lab scale, and most of them [89, 92] are in small scale. As for the numerical studies, the majority performed simulations with the Eulerian approach. In these numerical methods, bubbles are considered as spherical bubbles with constant diameters, and the interaction between bubbles cannot be accounted for. Bubbles' breakup and coalesce are not included in the simulation, let alone the effect of bubbles' deformation. Due to the absence of bubbles' behavior in numerical studies, SS was reported to disagree with experimental results [100].

#### 4. Nozzle size in aerated FS modules

Concerning nozzle size, it is proven experimentally by Ndinisa [25] that the nozzle size could affect membrane fouling reduction process in FS modules. No numerical studies are found in the literature to investigate the effect of nozzle size on hydrodynamics in the FS module. Only one study conducted by Xing et al. [183] examined this effect in the HF module numerically. However, in their studies, they performed simulations with the Eulerian method. The bubbles through different nozzle size are with a constant diameter, which is inconsistent with the common sense that large bubbles are generated through large diffusers. The shortcoming in this study makes their simulation incapable of providing a reliable evaluation of the effect of nozzle size. Future work can be done with the VOF approach to investigate the effect of nozzle size on bubble dynamics in aerated FS membrane modules.

#### 5. Benchmarking of the turbulence models

An industrial flow has a nature of turbulence. Turbulence plays a vital role in mixing, in species transport, in mass transfer and in fouling control in MBRs. As it is so essential, the turbulence model should be chosen with care, so that it can reduce the computing effort while providing an accurate prediction of the turbulent flow in MBRs. Different turbulence models are introduced and reviewed in section 2.4.2. The RANS method is the most popular option for modeling turbulence in industrial flow simulations. Nearly all the simulation of MBRs concerning turbulence used this method in the literature. In the RANS method, numerous turbulence sub-models are available for the specific turbulent flow, since there is no general turbulence model that can be applied for all kinds of turbulent flows. Among all the sub-models in the RANS method, two-equation models are the most popular one and widely used in the simulation of MBRs, since they are economic, robust and can provide reasonable and satisfying results. In the family of two-equation models, the SKE model, the RNG model, and the SST model are most frequently used by many authors in their simulations. Higuera et al. [254] compared the SKE model and the SST model in interFoam, from which no significant difference can be observed. Ratkovich et al. [107] and Vlaev et al. [136, 186] found no significant difference in the rotational flow predicted by these two turbulence models. Liu et al. [37] reported more accurate mean flow velocities in the HF membrane module predicted by the RNG model despite poor accuracy at a small scale provided by both models. A comparison between different turbulence models applied in the simulation of FS membrane modules cannot be found in the literature. Future work can be done to fill the gap.

#### 6. Activated sludge

---

Activated sludge is a very complex mixture containing water, sludge flocs, microorganisms, and other dissolved and suspended matters. Regarding all integrated models in the modeling of MBRs, the settling behavior of activated sludge is ignored in the literature, since the modeling of real activated sludge in MBRs is rather tricky [174] in the simulation. Most CFD studies used water instead of mixed liquor in their simulations for simplification. However, activated sludge behaves as a non-Newtonian fluid [97], which is different from water, a Newtonian liquid. To account for the rheological behavior of activated sludge mixture, many studies adopted simplified methods by incorporating the correlations between the MLSS concentration and the fluid viscosity into the CFD model. Indeed, the rheological behavior of activated sludge is included in the simulations. However, another important property of activated sludge, the settling behavior, is absent in the majority of literature. Only one research group [33, 127] took the settling behavior of mixed liquor into consideration by using the Eulerian three-phase model for modeling the mixture of gas, liquid, and biomass. The Eulerian approach, coupled with the PBM model, is also able to simulate sludge flocs by treating them as ensembles of populations of individual entities. However, given the small membrane channel depth, the Eulerian approach is not suitable for MBRs, as analyzed in section 2.4.3.

In theory, these flocs could be treated as individual entities like the individual bubbles in this study. However, these flocs usually have various forms and properties. Without sufficient experimental data, it is impossible to simulate the behavior of flocs in the MBR system.

In a word, more attention should be paid on the properties of activated sludge and its effect on hydrodynamics in MBRs.

## 7. Validation of models

In most CFD studies, SS is only calculated and not validated against measured values, as SS is difficult to measure. PIV, EDM, and direct shear sensor measurement are used in the literature to measure SS. However, the measured values are highly dependent on the measurement methods. The limitation of SS measurement methods due to the complicated geometry and flexible membrane affects the accuracy of experimental data and further hinders the validation of numerical models. Developing reliable measurement techniques for SS on the membrane surface would be highly expected in future work. More experimental research of SS on membrane wall under various geometrical and operational conditions is required to validate the numerical model directly.

## 8. Indicator

SS is used in most CFD studies, including this one, to indicate membrane fouling control performance. In these studies, various configurational and operational parameters are studied to achieve high SS, which ensures an enhanced scouring effect. However, high SS does not always have a beneficial effect on the MBR system. The main drawback of high SS is the breakup of sludge flocs, which is caused by high aeration intensity [255, 256]. The breakage of sludge flocs can lead to an increase of colloids and soluble components from microbial flocs to sludge suspension. Due to the smaller size of colloidal particles and solutes, this might cause a severe pore blocking problem or a rapid loss in membrane permeability. Besides, high shear forces can lead to membrane damage, resulting in a high expenditure cost by frequent replacement of membrane modules. Therefore, ranges of SS, which are beneficial for membrane fouling control, are required through experiments in future work to guide

---

the CFD simulations. It is worth mentioning that SS is not a good indicator for fouling mitigation performance, when it involves fluid viscosity, as SS is directly proportional to fluid viscosity. Shear rate turns out to be a better indicator, as it is independent on fluid viscosity. More attention should be given on shear rate and its link to membrane fouling control performance in future research.

## 9. Flexible membrane

Future work for CFD simulations of hydrodynamics in MBRs should focus on the effect of the flexibility and vibration of membrane on flow hydrodynamics. The impact of membrane movement on SS is observed by many researchers experimentally. However, to save computing resources and to simplify the numerical problem, membranes are considered as rigid walls without considering the membrane motion in most numerical studies. In the literature, only very few studies investigated SS induced by membrane vibrating with the FSI approach. One study conducted by Liu et al. [109] took the effect of the flexibility of membrane in HF modules into consideration. The previous study [253] simulated flexible FS membranes with a very small model. In both studies, the two-way FSI approach is used to model the interaction between fluid and solid. Results from both studies show that membrane vibration is promoting SS significantly. Therefore, the FSI approach should be used in future work to take the membrane vibration into consideration, so that the hydrodynamics in MBRs is closer to the real situation. However, it should be noted that with the two-way FSI approach the computing complexity is considerably upgraded. Given the computing resources, the simulations of the flexibility of membranes are still limited in small scopes, such as one fiber or tiny FS membranes. Besides, both studies used ANSYS for modeling. OpenFOAM might not be suitable for FSI simulations involving gas-liquid two-phase fluids, since standard solvers for solving such a system are not available. Even though codes coupling the FSI approach with the VOF method can be found in the OpenFOAM community, but the codes are not yet validated.





---

## 3 Methods

---

### 3.1 Solver development

---

The development of the CFD models of the FS membrane module is presented in this chapter. The Open source CFD toolbox OpenFOAM (Open Field Operation And Manipulation) is applied to carry out various simulations. OpenFOAM, a free source CFD package based on the finite volume method (FVM), written in C++ and implemented with adequate numerical methods [257], is able to solve complex multi-phase problems. Unlike commercial computational fluid packages, the open source feature of OpenFOAM makes it possible to modify the source code or to implement of other functions for research purpose [254, 258, 259]. Its characteristics of robust, advanced CFD code, cost-saving features, and capability for solving specific problems, make it very suitable for applications in industry [254, 258, 259]. Compared to commercial packages, OpenFOAM can provide comparable results [260]. However, the main drawback lies in the high learning cost from users, since the mainstream OpenFOAM tools are without graphical user interface (GUI).

---

#### 3.1.1 InterDyMFoam

---

InterDyMFoam is a predefined solver included in OpenFOAM for solving a two-phase incompressible flow with additional functions handling the dynamic mesh [259]. This solver uses a finite volume discretization and the VOF method to solve three-dimensional Navier-Stokes equations for the incompressible multi-phase flow [259]. The principles of the VOF method has been introduced in the last chapter. In this method, each phase occupies mesh cells with a volume fraction. For gas-liquid fluid, the volume fraction of the continuous phase (water) is normally denoted as *alpha.water*, and the dispersed phase (gas phase) is denoted as *alpha.air* in this solver. The interface of gas-liquid is tracked by calculating the *alpha.water* fields, since the interface, locates in the mesh cells with a value of *alpha.water* between 0 and 1 ( $0 < \alpha.water < 1$ ). Thus, to carry out fundamental research on bubble's behavior in aeration process in MBRs, VOF would be the best choice, as it can track bubbles' path, bubbles' shape in any time in the system. But bubbles have a size in mm range and are very small compared to the size of the MBR tank or the membrane cassette. VOF requires relative fine mesh to track the interface of bubbles. The function of dynamic mesh motion in interDyMFoam can only refine the mesh at the interface to save computing resource. The finer grids at the interface can move with bubbles based on the updated *alpha.water* field from last step. The algorithm of a solution of the incompressible multi-phase flow code in interDyMFoam is shown in Fig. 7 and can be summarized as follows.

1. Initialize fields. After building the geometry and mesh, setting up boundary conditions and patching fields in initial mesh cells, all these input parameters will be read for calculating and initializing fields, for example, the flux field.
2. Start time loop.
3. Start PIMPLE loop for each time step.
4. Refine mesh based on the *alpha.water* field calculated in last time step.

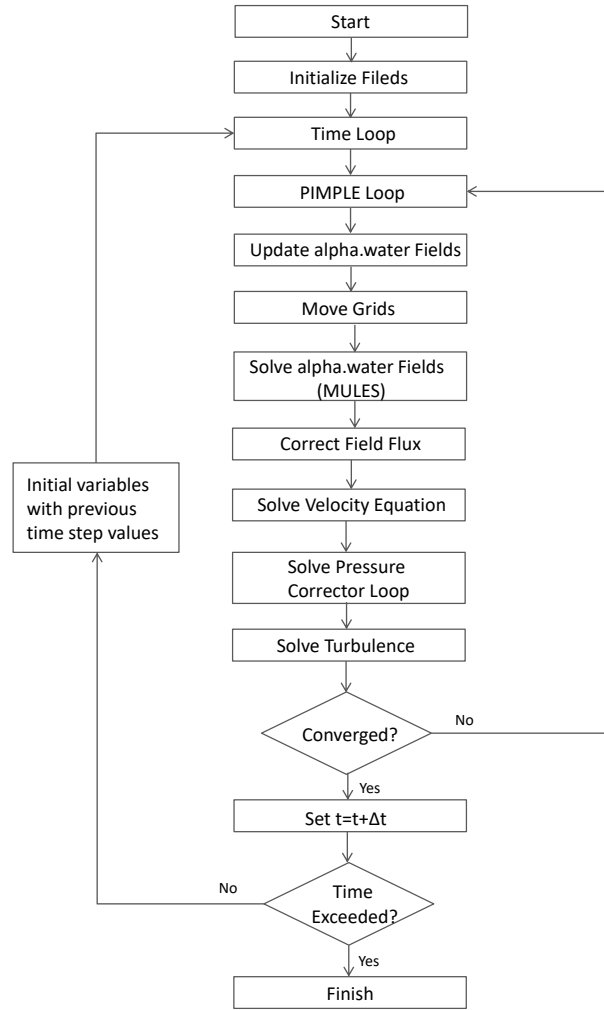


Figure 7: Flowchart of solution sequence of two-phase incompressible flow in interDyMFoam

5. Solve *alpha.water* iteratively until it is converged or the iteration steps exceed the user-defined the max. iteration steps.
6. Correct *alpha.water* field in the multi-dimensional limiter for explicit solution (MULES) solver.
7. Correct field flux.
8. Calculate an intermediate velocity field by solving the discretized momentum equation.
9. Loop for pressure-velocity coupling until the pressure residual is small enough or the user-defined the max. iteration steps are reached; correct the velocity fields based on the new pressure field.
10. Solve turbulence.
11. Go to step 3, if the convergence is not reached.
12. Advance the time.
13. Go back to step 2 and repeat until the prescribed time is reached.

The solution sequence is based on the PIMPLE algorithm, which is a merged algorithm of PISO (Pressure Implicit with Splitting of Operator) algorithm and SIMPLE (Semi-Implicit Method for Pressure-Linked Equations) algorithm. These are numerical techniques for solving the pressure-velocity coupling system, so that the navier-stokes equation can be solved numerically [261]. The procedure is: predict the velocity field first, then solve the pressure equation in a correction loop and correct the velocity field based on the pressure field from the last step. A SIMPLE algorithm is applied for steady-state calculations, while PISO and PIMPLE algorithms are used for the transient flow [261]. However, PISO algorithm is expensive to solve the transient problem, when it deals with a large number of time steps, as the time step is strictly limited by Courant number ( $Co$ ) [258], which should be smaller than 1. PIMPLE algorithm, combining PISO and SIMPLE algorithms, uses under-relaxation for a steady-state solution and outer correction loops to ensure convergence [259]. In this way, PIMPLE algorithm can be used for solving the transient problem with a large  $Co$  ( $Co \gg 1$ ) less expensively since the time step increases dramatically [261]. MULES (multidimensional universal limiter for explicit solution), as mentioned above, is a solver in OpenFOAM which uses a limited factor on the fluxes to make sure that the value of *alpha.water* falls between 0 and 1 [259].

## Validation

Bubble velocity is as an indicator evaluating the model through the whole chapter. The numerical solutions from this work are compared against the published experimental data. The first validation study is performed between the numerical results from the CFD model built in interDyMFOam and the experimental data from the experiments [253], where the rising velocities of bubbles of different size were measured. The membrane channel is 8 mm spaced and 500 mm high, filled with still water. To model these experiments, the CFD validation model has two 8 mm spaced membrane walls with a height of 500 mm. 30 mm instead of the same membrane width in the experiment is used in the CFD validation model to save computing time. Geometry independence benchmarking is performed to identify the minimum width of the geometry, above which the width will not affect the numerical results significantly. 30 mm is proven to be the minimum width, which has no significant influence on the ascent of bubbles ranging from 2 to 6 mm. In the region near membrane walls, the mesh is refined, so that more reliable results can be obtained. Mesh size is fine enough to get accurate results. SKE model is used in the CFD validation model. A comparison of rising velocity of bubbles of different sizes is demonstrated in Fig. 8, where the modeling velocities (orange line) are compared to the corresponding measured bubble rising velocity (blue line), as well as the rising velocities of freely moving bubbles from Clift's study [262], where experiments were performed in stagnant clean water (gray line) and stagnant, contaminated water (gray dot line). As can be observed from Fig. 8, numerical results agree with its corresponding experimental results very well, which means that the presented CFD validation model can reproduce the bubble rise behaviors in membrane channel observed experimentally. The measured velocity in pure water in Clift's study [262] is higher than the measured velocity in the previous work [253] due to the slow down effect of small spaced membrane walls on bubbles' motion. In the experiment conducted in the previous work [253], the bubble rose in small membrane channel, while in Clift's study, bubbles rose in a container without any restraint of walls. Besides, the water used in the experiments was tap water or slightly contaminated water. Therefore, the measured bubble rising velocities lie between the bubble velocities in pure water and contaminated water from Clift's study [262].

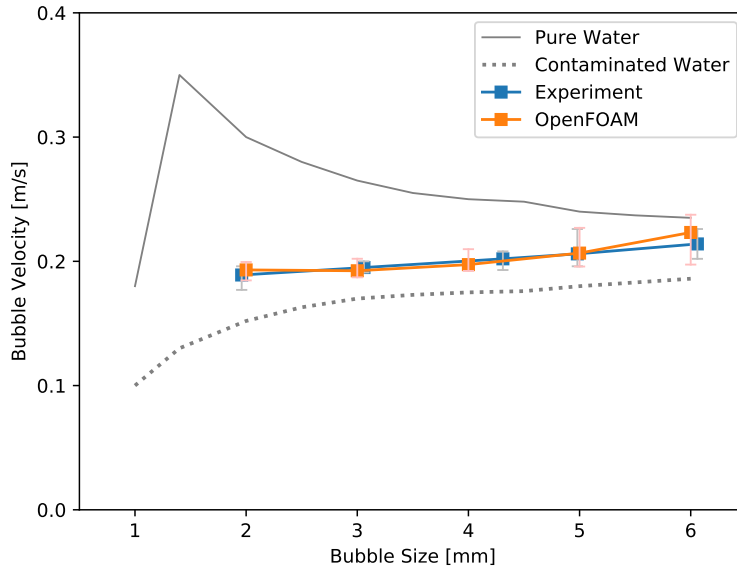


Figure 8: Model validation against the previous experimental work [253]

The second validation study is conducted by comparing numerical values and experimental results measured from Boehm [91]. Boehm [91] used PIV to measure the bubble velocities in a 7 mm spaced membrane channel. His experimental rig is identical to the model geometry in the simulations throughout the whole work. They are 1500 mm high, 160 mm wide and 7 mm deep. The settings of this CFD model is identical to the CFD validation model, as described before. The simulated rising velocity of 3 mm bubble is 0.204 m/s, while the measured value is 0.2 m/s. For the single bubble with a diameter of 5 mm, the measured velocity is 0.19 m/s and the simulated value is 0.198 m/s. A perfect agreement can be obtained between the measured bubble velocities in his study [91] and the simulated velocities from this CFD model. This proves the ability of this CFD model for obtaining reliable results, at least in terms of bubble velocity.

Different studies are used to validate the CFD model, and numerical results match closely to the experimental data. Thus, the validation studies demonstrate that the presented CFD model built in interDyMFoam can reproduce the rise behavior of bubbles in membrane channel accurately. However, this solver is not capable of predicting bubble rising behavior in activated sludge. To add the function of describing the sludge effect in interDyMFoam, following works are done: development of sludge model in driftFluxFoam and implementation of driftFluxFoam into interDyMFoam.

---

### 3.1.2 Implementation of sludge models

---

The activated sludge in the MBR system is a complex mixture containing the liquid phase (water), the solid phase (microorganisms, particles, sludge aggregation) and dissolved species (dissolved organic carbon (DOC), nitrate, DO, etc.). As the solid phase has a large range in size from  $\mu\text{m}$  (the size of bacteria) to cm (the size of sludge floc), the settling velocities and density of these particles are not the same. Thus, a modeling of the sedimentation of the solid phase is very difficult in such a system, let alone the interactions between individual solids. It requires massive computational resources in terms of CPU usage and memory of computers along with long computing times [31]. Even if only sludge floc is considered, the size, density

and, distribution of the individual sludge flocs should be given as the properties for the solid phase in the simulation. However, these data are usually not available. Even though the simulation could be done, the computing effort would be considerable. Thus, the activated sludge is usually regarded as a mixture containing water and solid as a whole rather than separated phases. The sedimentation behavior and the rheological behavior of activated sludge could be described with empirical expressions as a function of the MLSS concentration, as adequate empirical formula concerning these two properties of activated sludge could be found in the literature.

DriftFluxFoam, based on the mixture method, is a solver suitable for the modeling of activated sludge. Its core principle is the relative velocity between phases, which can be assigned as the settling velocity of the solid phase in activated sludge mixture as a function of the MLSS concentration. Moreover, the density and the mixture viscosity can also be implemented with experiment obtained expressions as a function of the MLSS concentration. There are several sludge settling models and sludge rheological models available in driftFluxFoam. These are models for slurry sludge, plastic sludge, but not particular models for activated sludge. The activated sludge model implementation involves the implementation of sludge settling model and sludge rheological model.

#### **Implementation of sludge rheological model**

Among all these models analyzed in chapter 2.4.4, Laera model [214] is chosen to describe the rheological behavior of activated sludge in this work, as the investigated MLSS concentration in their study is suitable for MBRs. Besides, the Bingham and HBP models are used to fit the experimental data with sludge samples from the wastewater treatment plant in Griesheim and Eberstadt. The experiments were carried out by former colleagues for one of the projects in our department IWAR WV. In this project, they measured momentum in the process-viscometer at different rotational speeds and at different MLSS concentrations. Then with the measured data, viscosity, SS and shear rate were calculated accordingly. The detailed description of the experiment can also be found in work by Brenda [263]. With the calculated SS and shear rate, the fitted expressions of Bingham model and HBP model are given by Eq. 64 and Eq. 65, respectively.

Bingham model:

$$\tau = 1.08 \times 10^{-7} c^{8.854} + 0.00353 c^{0.3885} \cdot \dot{\gamma} \quad , \quad R^2 = 0.98 \quad (64)$$

HBP model:

$$\tau = 2.44 \times 10^{-7} c^{10.44} (1 - e^{-1.24 \dot{\gamma}}) + 0.000775 c + 0.0044 \dot{\gamma}^{0.975} \quad , \quad R^2 = 0.99 \quad (65)$$

To choose the best model among these three rheological models for describing the rheological behavior of activated sludge in MBRs, apparent viscosity of activated sludge with a MLSS concentration of 8.83 g/L is modeled at various rotational speeds in a model that matches the process-viscometer used in the experiment. The simulated viscosity of the MBR sludge are then compared to the measured data. Fig. 9 presents the modeled apparent viscosity obtained from different sludge models. The HBP model over-predicts the apparent viscosity at various rotational speeds, as shown in the green line and the blue line in Fig. 9. Comparing the Bingham model and the Laera model with the measured data, the Laera model agrees better with experimental data at a low or a high rotational speed. In the middle range of rotational

speed, the Bingham model seems to be the most accurate, as displayed in Fig. 9. Since the best model is different at different rotational speeds, the root mean squared error (RMSE) [217] is applied to evaluate the agreement between the simulated and the measured data, so that the best model with the lowest RMSE values can be found. After calculating the RMSE values, it is found out that the Laera model is the one with the lowest RMSE value. Therefore, the Laera model is used for the simulations to investigate the sludge effect.

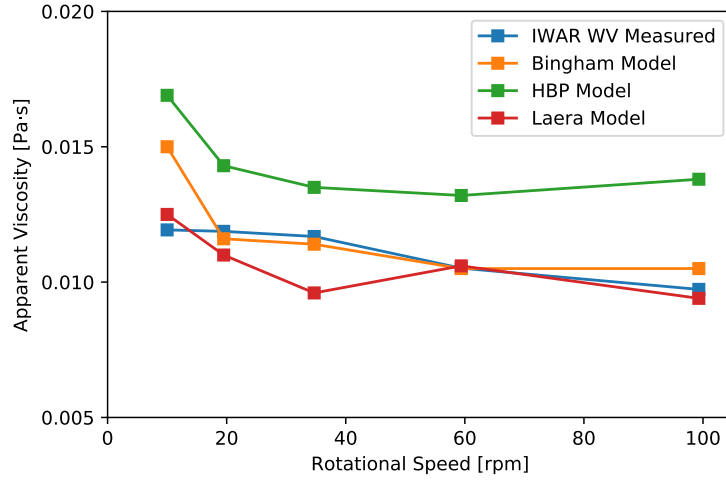


Figure 9: Apparent viscosity of activated sludge with a MLSS concentration of 8.83 g/L

### Implementation of sludge settling model

In this research, the Vesilind model and the Takacs model are chosen to fit the experimental data, where the sludge samples for the settling test were taken from two wastewater treatment plants in Eberstadt and Griesheim in Germany. A standard 1 L cylinder was used for the settling test experiment, and every sludge was settled down for 30 min. A detailed description of the experiment and how the settling velocity was obtained can be found in the research of Brenda [263]. With these experimental data and the necessary formulas describing the settling behavior of activated sludge, empirical constants of different models can be determined in Matlab. The best-fit expressions are Eq. 66 and Eq. 67.

Vesilind model:

$$u_{r,z} = 0.003835e^{-0.649c} \quad , \quad R^2 = 0.95 \quad (66)$$

Takacs model:

$$u_{r,z} = 0.0089(e^{-0.9609c} - e^{-1.7666c}) \quad , \quad R^2 = 0.966 \quad (67)$$

where,  $u_{r,z}$  is the settling velocity (m/s), which is the component of relative velocity  $u_r$  in  $z$  direction. Other components of relative velocity  $u_r$  are 0.

These expressions are directly implemented in OpenFOAM for modeling the settling behavior of activated sludge. To choose the best model, settling tests simulations analog to experiments are conducted in the 1 L standard cylinder, where homogenous sludge mixture settles down for 30 mins. The sedimentation course of the suspension with a MLSS concentration of 1.87 g/L is demonstrated in Fig. 10, where it can

be observed that the sludge blanket level decreases with time. After 5 min, sludge is concentrated near the bottom. Besides, a comparison between the simulated and the measured data is also presented in Fig. 10, where the blue line represents the measured settling curve of activated sludge, and other lines represent the simulated settling curves. It is observed from this diagram that the settling curve from the Takacs model agrees with the measured one better than that from Vesilind model. Simulations are also conducted at a MLSS concentration of 7.73 g/L and Takacs model is also found to agree with the experiment better. Therefore, the Takacs model is chosen to conduct the simulations to investigate the sludge effect.

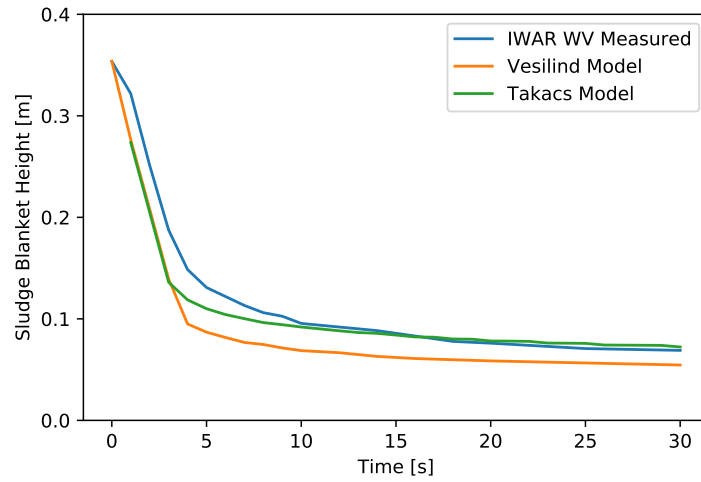


Figure 10: Simulated and measured settling curve in 30 minutes at a MLSS concentration of 1.87 g/L

### 3.1.3 InterSolidFoam

The flow in the aerated FS membrane module is gas-liquid-solid three-phase flow. Since the activated sludge is modeled with mixture method, where the solid phase and liquid phase in the activated sludge system is treated as a whole rather than separated phases, the flow in MBRs (activated sludge + bubbles) is simplified as a pseudo-three-phase flow, where the mixed liquor and bubbles are two separated phases and the solid and liquid phases in activated sludge is treated as a mixture. Still, there is no solver available in OpenFOAM to simulate this pseudo-three-phase flow with the focus on bubbles behavior. Combining the interDyMFoam and the driftFluxFoam solver, a new solver, named interSolidFoam, is developed within the OpenFOAM framework in this work to investigate the effect of the MLSS concentration on bubbles rising behavior. The base solver is interDyMFoam, where the mixed liquor is the continuous phase, whose volume fraction is denoted as *alpha.mixture* and bubbles are the dispersed phases, whose volume fraction is denoted as *alpha.air*. The sum of both volume fractions of mixed liquor and gas phase is 1 in the VOF method, as explained in the last chapter. In this base solver, the interface of mixed liquor and bubbles can be tracked, and the dynamic mesh around the interface can be refined. By merging driftFluxFoam into interDyMFoam, the mixed liquor has the additional ability to present the activated sludge properties as a function of the MLSS concentration. Only the core solution procedures, i.e. the drift velocity equation, the transport equation of solid volume fraction, the settling and the rheological models of activated sludge, are implemented in the base solver. The details of the solution sequence of interSolidFoam are provided in Fig. 11 and can be summed up as follows:

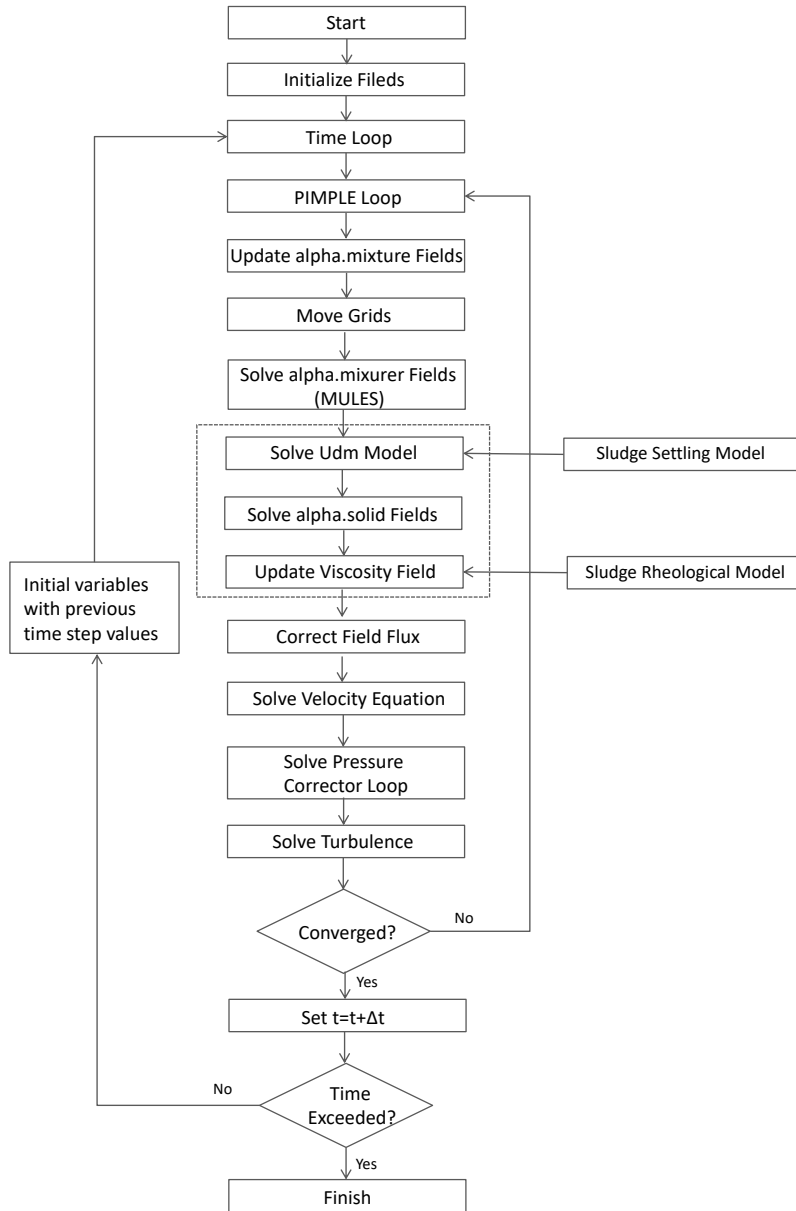


Figure 11: Flowchart of solution sequence of three-phase (air-water-sludge) incompressible flow in interSolidFoam

1. Initialize fields after setting the properties for mixed liquor and bubbles.
2. Start time loop.
3. PIMPLE loop. They are the main structure of the solution code and similar to that in interFoam.
4. Refine mesh based on the *alpha.mixture* field calculated in last time step. This step is an additional function for mesh refinement around the interface of mixed liquor and bubbles. They are similar to that in interDyMFoam.
5. Loop for solving *alpha.mixture* until it is converged or the iteration steps exceed the user-defined the max. iteration number and correct the field in MULES solver.



- 
6. Solve drift velocity, *alpha.solid* and update viscosity and density. These steps are the core solution procedures in driftFluxFoam that are implemented in the interDyMFoam. Even though the mixed liquor is treated as a whole, it still deals with the solid-liquid two-phase flow. The primary principle for solving these two phases is calculating the drift or the relative velocity between these two phases with an experiment based sludge settling model, which is explained in the last section. In this mixed liquor, water is a continuous phase, while the solid phase is the dispersed phase, whose volume fraction is denoted as *alpha.solid*. The sum of the volume fraction of both solid and liquid phases equals to the value of *alpha.mixture* calculated in step 4. After solving the *alpha.solid*, the viscosity and density fields of mixed liquor and this pseudo-three-phase mixture will be updated based on the latest *alpha.solid* and *alpha.mixture* fields.
  7. Correct fields, solve the pressure-velocity coupling problem and then solve turbulence. These steps are similar.
  8. Go to step 3, if not yet converged.
  9. Advance the time, if the prescribed time is not reached, back to step 2 and repeat.

---

### 3.2 Model Geometry

---

This work is devoted to investigate the aeration process for fouling control in the MBR system equipped with a FS membrane module fundamentally. The model geometry of this research is initially thought to have the same size as the MBR tank applied in wastewater treatment. And in the membrane tank, individual bubbles would be simulated and investigated. However, this thought is not feasible due to the limit in computing cost and resource. In practice, the membrane tank should be equipped with multiple FS membrane cassettes, and each cassette contains dozens or hundreds of membrane sheets, like in the commercial FS membrane products. As VOF requires very fine mesh to track bubbles, the simulation of bubbles in the MBR tank with the VOF method is not feasible at the moment. For the commercial FS membrane module with channel depths ranging from 6 to 10 mm, as listed in Table 1, the Eulerian approach is not suitable, as analyzed in chapter 2.4.3. A compromise is to model the system partially instead of taking it as a whole. The most basic model consisting of a 3D rectangular membrane channel with two impermeable membrane walls is general enough to represent the membrane geometries for the FS membrane module with the purpose of investigating the bubbles' rising behavior and its fouling control effect on membrane surfaces.

Therefore, this configuration consisting vertical channels of rectangular cross-section is applied. As shown in Fig. 12, there are two zones from bottom to top. The bottom zone is the membrane channel. The zone above the top edges of the membrane is defined as the exit zone. Bubbles are patched or generated at the bottom and rise through the membrane channel due to buoyancy force and leave the membrane channel entering into the exit zone at last.

The dimension of the model can be observed in Fig. 12, where it shows that the membrane sheets are 1500 mm in height, and 160 mm in length and the membrane sheets are 7 mm separated from each other. The choice of 7 mm as the channel gap is attributed to the fact that most of the commercial FS membrane modules have a membrane sheets separation of 7 mm. As listed in Table 1 above, the membrane sheets

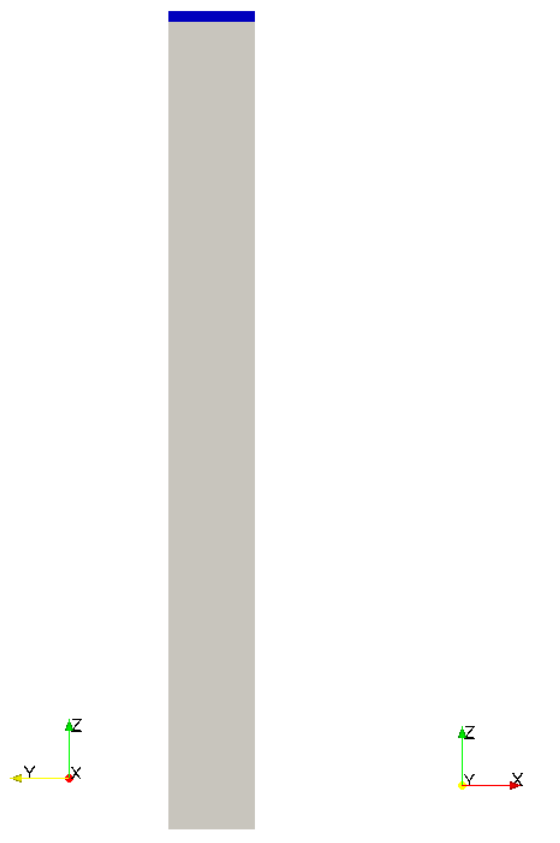


Figure 12: Model geometry in front view (left) and in side view (right)

are spaced from 6 to 10 mm in the commercial FS membrane modules. To investigate the effect of the membrane sheets separation on hydrodynamics in the membrane module, this range will be selected to conduct simulations. The dimension of membrane sheets varies significantly from product to product. As listed in Table 1, the height ranges from 490 to 2320 mm, and the length varies from 165 to 1040 mm. A height of 1500 mm and a length of 160 mm is chosen for the membrane sheets. Another reason for this dimension is that an experimental study carried out by Boehm [91] used the same configuration to investigate the bubble rising behaviors and the SS in an aerated FS membrane module. And with the identical geometry, the applied model can be validated against his experimental results. The membrane sheets in the model are then 1500 mm high and 160 mm long. The exit zone is 160 mm in length, 7 mm in width, and 100 or 20 mm in height, whose effect is proven to be minor. Thus, the different heights of exit zone does not affect the investigated parameters. Hence, the geometry of the model is 1600 or 1520 mm high in total, 160 mm long and 7 mm wide.

For the simulation of single bubbles and bubble swarms, bubbles are patched in the entrance zone, and the bottom face of the model is the velocity inlet of liquid phase, where liquid flows through it and moves upwards when the upwards inlet velocity of the liquid phase is not equal to 0. For the cases of bubbles generation, the aerator is of different dimensions placed at the bottom face of the model. These aerator faces are the velocity inlet of the gas phase. To investigate the effect of the aerator geometry and aeration intensities, various dimensions of aerators are applied under different gas flow rates.

---

### 3.3 Meshing

---

The grid size can affect the numerical results significantly since inaccurate results can be obtained due to coarse grids. With a fine mesh, one can get much better results compared to a coarse mesh since the VOF method needs an adequate resolution of grids at the gas-liquid interface, which should have a thickness of at least a few cells due to the numerical diffusion for solving the transport equation of volume fraction [264]. And it is evident that the mesh cells at the interface should be as small as possible, so that the interface can be resolved more accurately. However, it takes larger memory and longer computing time with a fine mesh, particularly for such large models described above. A local adaptive mesh refinement (AMR) technique, which can address this problem, is introduced in CFD models to track the interface accurately. AMR allows a relatively coarse grid for the pure liquid phase or pure gas phase and a local mesh refinement at the interface. In this way, the solution accuracy at the interface of the gas-liquid phases are enhanced with the minimum computational cost [265], and the simulations in such large models with the VOF method is then feasible.

---

#### 3.3.1 AMR vs. static mesh

---

The accuracy of the AMR technique has been tested in many studies for the gas-liquid two-phase flow [264, 265]. Theodorakakos and Bergeles [265] performed various test simulations to evaluate the accuracy of the AMR approach with the VOF method and found an adequate accuracy in numerical results provided by AMR approach. Cooke et al. [264] used the VOF method to study the film flow with static mesh techniques and dynamic AMR techniques, respectively. They found a better agreement between experimental results and numerical results with adaptive mesh refinement. They also proved an improvement in simulation accuracy and a reduction in computational effort with AMR techniques.

In this research, benchmarking simulations are performed to compare the numerical results from both models with the static mesh and with the ARM approach. A sketch of the mesh cells for these two benchmarking simulations with the static mesh approach and with the ARM method, in the beginning, is presented in Fig. 13, where it can be seen that the static mesh has a uniform mesh density globally and dynamic mesh has relatively coarse mesh cells in pure water phase or pure air phase, but very fine mesh cells around the interface.

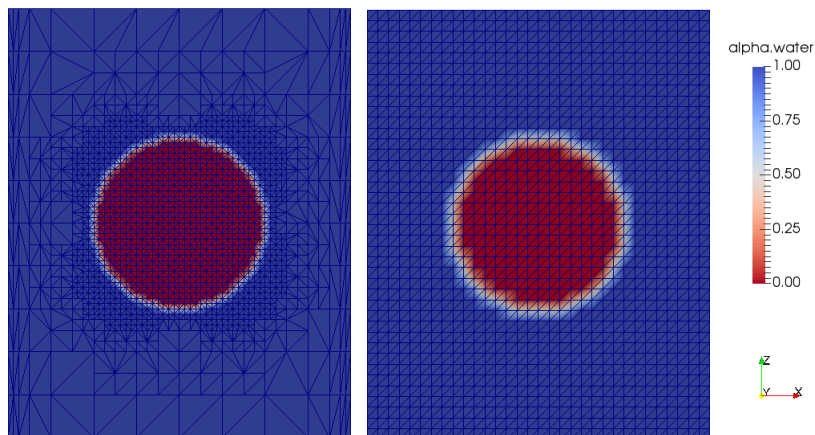


Figure 13: A sketch of dynamic mesh with the ARM method (left) and a sketch of static mesh (right)

Bubble velocity is a very good parameter for validation of numerical results against experimental data, as it is easier to measure. The velocities of a 4 mm bubble from two simulations with the static and dynamic meshes are illustrated with two statistic boxplots in Fig. 14, where the orange line in the boxes represent the median value (50<sup>th</sup> Percentile) of bubble velocities at different time steps. The box stands for interquartile range, where the bottom of the box is the first quartile (25<sup>th</sup> Percentile), and the top of the box is the third quartile (75<sup>th</sup> Percentile). The size of this box implies the data variation, where a small box means a high level of data agreement. The bottom and the top black horizon lines represent the minimum and the maximum, respectively. Comparing the box plots of bubble velocity at different time steps obtained with dynamic and static meshes, their median bubble velocities are around 0.2 m/s, and bubbles' velocities in static mesh show a higher level of agreement, as its box is smaller.

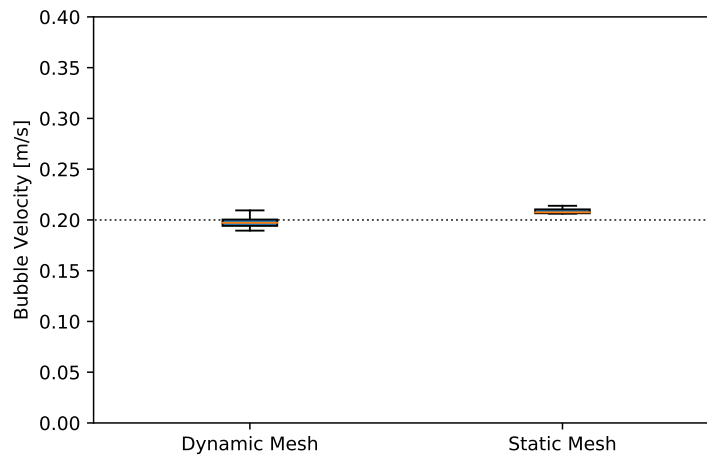


Figure 14: Comparison of bubble rising velocity from dynamic and static meshes

The gray horizontal dot line in Fig. 14 is the 4 mm bubble velocity obtained experimentally in the literature. The benchmarking model here has a height of 500 mm, a membrane gap distance of 8 mm, which are precisely the same as the geometry of membrane channel in the experiment. Despite the different scale in width of models, benchmarking of model width is carried out to determine an appropriate width for the simulation of a single bubble rising. A width of 30 mm is proven to be adequate for bubbles with a diameter ranging from 1 - 6 mm. Comparing numerical results and experimental results, a good agreement can be seen from Fig. 14, where the velocity boxes lie closely near the horizontal line. These have proven that both simulations with dynamic and static meshes can get reliable results.

In conclusion, simulations with the ARM method can provide adequate accuracy, as the simulated velocities and the experimental velocity show good agreement. Comparing the simulations with static and dynamic meshes, it can be found that simulations with the ARM approach can obtain almost the same results but with less computing time required, as it took 2 min to complete a time step with the ARM method, while it took 20 min with the static mesh under the same conditions.

### 3.3.2 Mesh benchmarking

When gas is injected into fluid, bubbles are formed. The size of bubbles generated are linked to the sparger geometry and the gas flow rate [20]. Based on the bubble size, bubbles generated through orifices in the

MBR system, can be roughly divided into two groups, i.e. fine bubbles and coarse bubbles. Fine bubbles have a diameter from 2 to 5 mm, while coarse bubbles sizes range from 6 to 10 mm [14]. However, it does not mean that bubbles in MBR systems have a size range only between 2 - 10 mm. Actually, the bubble size is found experimentally by Liu et al. [128] to vary in a wide range, from 0.2 to 50 mm. The majority of bubble sizes in their experiment is found to be in the range of 3 - 5 mm, which belongs to fine bubbles according to the rough grouping. In this work, bubbles with a diameter ranging from 2 to 6 mm are investigated.

A benchmarking of mesh grids is carried out under various refinement levels for different bubble sizes to determine the appropriate max. refinement level for each bubble, to ensure the simulation accuracy while using as less computing resource as possible. Mesh resolution studies are conducted by comparing the shapes of bubbles at different mesh sizes around the interface. The snapshots from left to right in Fig. 15 show the forms of 4 mm bubbles with a max. refinement level of 1, 2, 3 and 4, respectively.

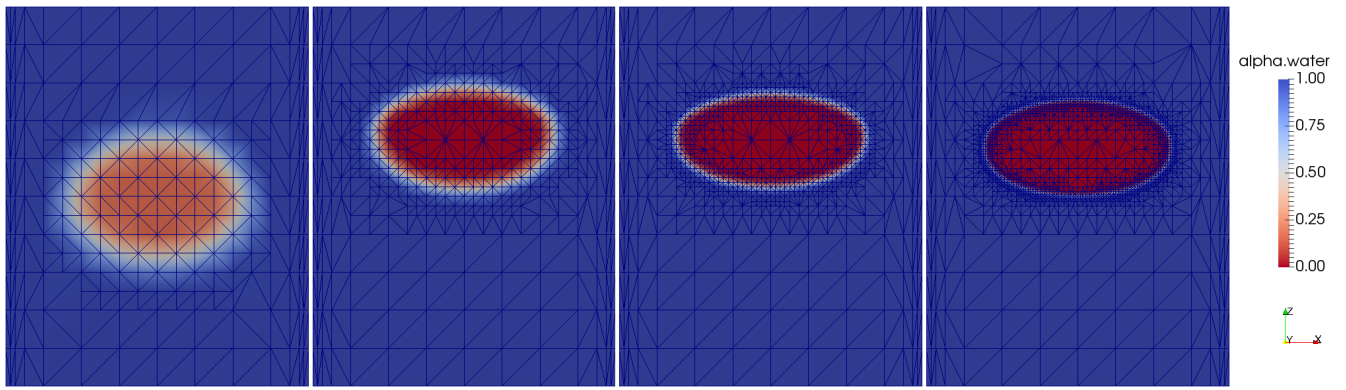
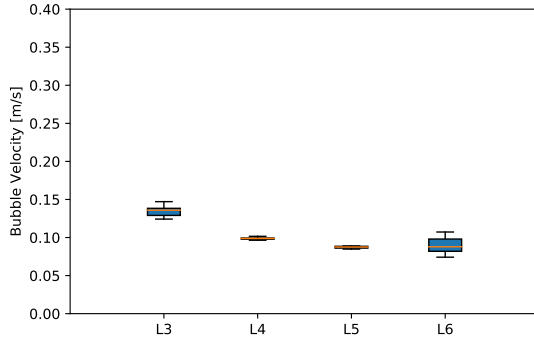


Figure 15: Snapshots of 4 mm bubbles at 0.05 s at different mesh refinement levels (refinement level from left to right: 1,2,3,4)

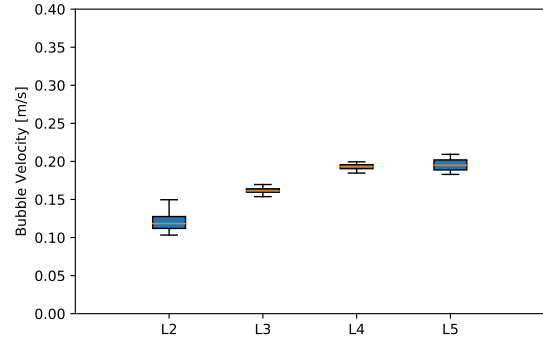
From Fig. 15 it can be observed that with an increase in the max. refinement level, the mesh cells around the interface become smaller, and at the interfaces of the bubble become sharper. At the min. refinement level, the interface of gas-liquid phases cannot be solved adequately, so that the whole bubble is treated as an interface, while at the max. refinement level, the interface is extremely thin. Despite a thicker interface, the 3 mm bubble can keep its shape at a max. Refinement level of 2.

Grid independence is studied through simulations of varying max. refinement levels for bubbles with a diameter ranging from 2 to 6 mm. Fig. 16 illustrates the effect of mesh resolution at the interface on bubble velocity. As can be seen from Fig. 16, mesh resolutions for bubbles with different sizes are different. In general, small bubbles require finer mesh at the interface for keeping the spherical shape. 2 mm bubble needs a max. refinement level of at least 4 to ensure accurate prediction of bubble velocity, while 5 or 6 mm bubble requires only a max. refinement level of 2. Thus, for 2 mm bubble, a refinement level of 4 is used in the simulation, and a max. refinement level of 2 is used for the simulation of large bubbles with a diameter of 5 or 6 mm. For medium bubbles (3 and 4 mm), a max. refinement level of 2 seems sufficient to predict the bubble velocity accurately. However, a max. refinement level of 3 is chosen for them, as the computing time does not increase much when the max. refinement level increased from 2 to 3.

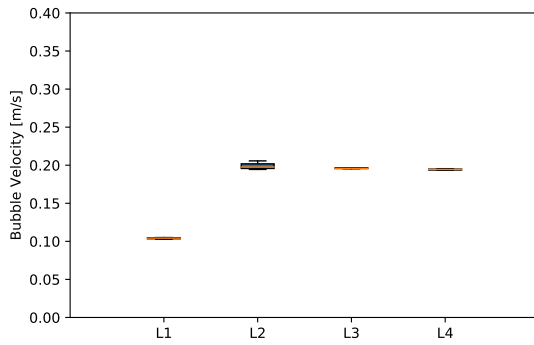
Therefore, a max. refinement level of 4 is adopted for 2 mm bubble, 3 is selected for 3 and 4 mm bubbles, and 2 is chosen for large bubbles with a diameter of 5 and 6 mm.



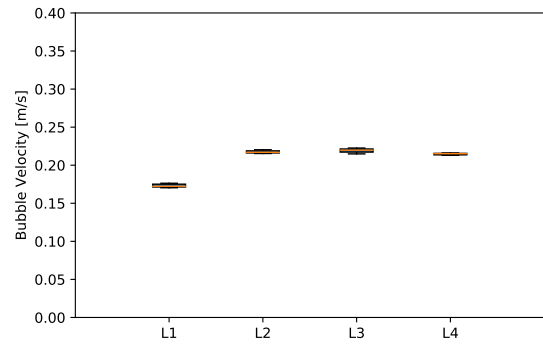
(a) 1 mm Bubble



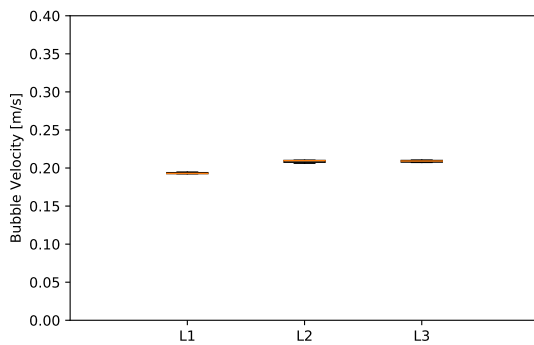
(b) 2 mm Bubble



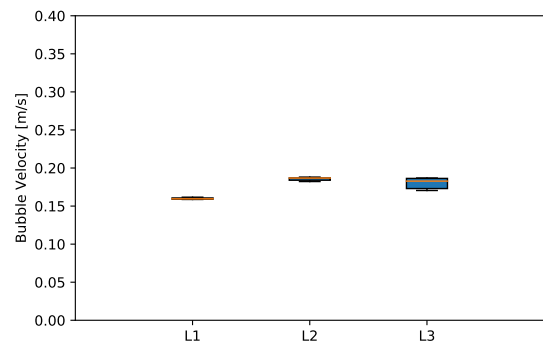
(c) 3 mm Bubble



(d) 4 mm Bubble



(e) 5 mm Bubble



(f) 6 mm Bubble

Figure 16: A benchmarking of mesh grids for bubbles of different size in terms of bubble velocity

### 3.3.3 Refinement in near-wall regions

As flow approaches a wall, there exists a thin layer of fluid where the velocity decreases from the mainstream velocity to zero at the wall, due to the strong viscous effect resulting in high velocity gradient normal to the wall [192]. This thin layer is called the boundary layer. Based on the boundary layer theory for the turbulent flow, the boundary layer has three zones in its inner layer: viscous sub-layer next to the wall, a transition layer or a buffer layer in the middle and a log-layer far away from the wall. The subdivisions of the near-wall regions are based on the value of  $y^+$ , which is the non-dimensional distance to the wall and can be calculated with Eq. 68, Eq. 69 and Eq. 70.

$$y^+ = \frac{\rho u_\tau y}{\mu} \quad (68)$$

$$u_\tau = \sqrt{\frac{\tau_w}{\rho}} \quad (69)$$

$$u^+ = \frac{U}{u_\tau} \quad (70)$$

where  $\tau_w$  is the SS on the wall;  $u_\tau$  is the friction velocity;  $y$  is the distance to the wall,  $u^+$  is the non-dimensional velocity and  $U$  is the mean velocity.

In these three zones,  $u^+$  can be expressed as a function of  $y^+$  [30].

- Viscous sub-layer ( $y^+ < 5$ )

The viscous sub-layer is extremely thin and dominated by the viscous effect. The SS in this layer can be assumed to be constant. Thus in this thin layer, the relationship between  $u^+$  and  $y^+$  is linear, as shown in Eq. 71.

$$u^+ = y^+ \quad (71)$$

- Buffer layer ( $5 < y^+ < 30$ )

Due to the complex velocity profile, there is no direct expression between  $u^+$  and  $y^+$  available in this region. Normally, if  $y^+ < 11.63$ , this part is regarded as a viscous sub-layer, and if  $y^+ > 11.63$ , logarithmic profile (introduced below in log-layer) will be applied. The intersection of linear and logarithmic approximations lies in  $y^+ = 11.63$ .

- Log-law layer ( $y^+ > 30$ )

In this region, both the viscous effect and the turbulent effect are essential for the flow. The velocity  $u^+$  varies slowly as a logarithmic function of  $y^+$ , as demonstrated in Eq. 72.

$$u^+ = \frac{1}{\kappa} \cdot \ln(y^+) + B \quad (72)$$

where  $\kappa$  is the Von Karman's constant, equals to 0.41 and constant  $B$  equals to 5.5 approximately.

Ideally, the first computing cell should lie in this very thin viscous sub-layer, and a sufficient fine mesh should be used to resolve the near wall layer. But this usually is at the cost of using a large number of grids if high accuracy of the numerical solution in the near wall region is required. To address this problem, wall functions, another approach to modeling near-wall regions, are introduced in OpenFOAM to ensure an accurate solution of turbulent flow with a relative coarse mesh near the wall. Wall functions used semi-empirical formulas or functions to solve the variables in the near-wall mesh cells with a reasonable accuracy. A wall-function approach is a popular option for flow simulation in practice, as it is robust and economic. However, wall functions might not be adequate for the simulations involving low Reynolds number [201]. Besides, this wall function approach is suitable for relatively large  $y^+$ , e.g. the first cell center is in the log-law layer. At a low dimensionless wall distance, mesh refinement can be adopted, while at a high dimensionless wall distance, wall functions would be an option. But if  $y^+$  falls in the buffer layer, both approaches cannot provide accurate solutions of turbulent flow. Therefore, the first cell center should avoid being located in the buffer layer.

In this research, SS is a crucial parameter investigated. SS is calculated with Eq. 73.

$$\mathbf{T} = \mu \mathbf{R} \quad (73)$$

where  $\mathbf{T}$  is the SS tensor (Pa),  $\mu$  is the apparent viscosity,  $\mathbf{R}$  denotes the strain rate tensor ( $s^{-1}$ ), which is given by Eq. 74.

$$\mathbf{R} = \nabla \mathbf{u} + \nabla \mathbf{u}^T \quad (74)$$

SS is then calculated with Eq. 75.

$$\tau_w = \hat{\mathbf{n}} \cdot \mathbf{T} \cdot \hat{\mathbf{t}} \quad (75)$$

where  $\hat{\mathbf{n}}$  and  $\hat{\mathbf{t}}$  are the unit normal and tangent vectors referring to wall,  $\tau_w$  is SS (Pa) on the wall. In the following context, the value of SS refers to the module of a SS vector.

Therefore, to get reliable values of SS, the turbulent flow and the velocity gradient in the near wall regions should be resolved with a high accuracy. For successful computations of turbulent flow in the near wall regions, a very fine mesh resolution is required there, which cannot be fulfilled for flows in relative large models usually. However, in this model, the first mesh cell center can be located in the viscous sublayer, since the membrane sheets separation is small and the base mesh is relatively fine. Still, two benchmarking simulations are performed in this section with and without mesh refinements in the near wall regions. For the case with mesh refinement, the first cell near walls is refined three times in the direction normal to membrane walls. The settings of these two simulations are identical, and the only difference lies in the near wall treatment. A sketch of the mesh near walls in these two cases is displayed in Fig. 17, where the left picture shows the base mesh of membrane channel without mesh refinement at the adjacent membrane wall, while the right one presented the mesh refinement in the near wall region. The min. distance of the first cell center normal to the wall is 0.5 mm in the cases without any wall treatment, while it is only 0.0625 mm in the case with mesh refinement near the wall. The geometry of these two benchmarking cases is the



same as the cases for mesh independence test.  $y^+$  induced by the motion of 4 mm bubble is compared between these two cases.

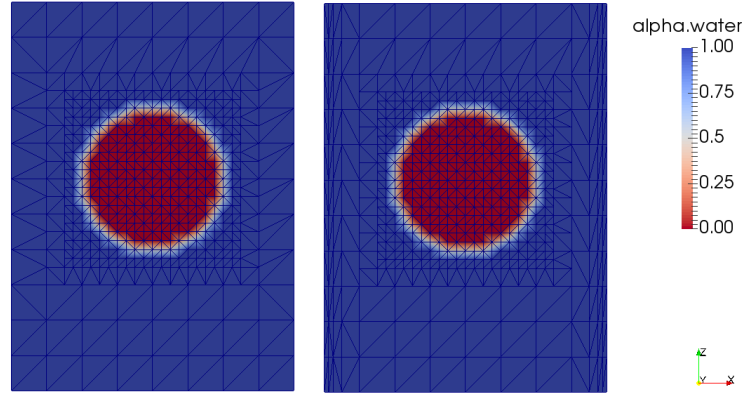


Figure 17: Sketch of dynamic mesh without (left) and with (right) refinement in the near wall regions

$y^+$  is calculated and presented in Fig. 18, where it can be seen that the max.  $y^+$  for the case without mesh refinement is in the range  $5 < y^+ < 30$ , which means its first layer cells near walls lie in the buffer region, where wall functions are not suitable, either. Its average  $y^+$  are smaller than 5 with most of the values in the magnitude of 1, where the dot line in Fig. 18 represents  $y^+ = 1$ . This means that the majority of the first layer cell is in the viscous sublayer, while the mesh cells where the max.  $y^+$  occurs are in the buffer region. As the max. SS is the key parameter investigated in this research and it is positively related to  $y^+$ , which can be concluded from Eq. 68 and Eq. 69, the max. SS and max.  $y^+$  occur in the same place with a high possibility. These cells are in the buffer region, where turbulence can not be accurately predicted, resulting in an inaccurate prediction of the max. SS. Therefore, the first mesh layer should be refined. For the case with mesh refinements in the near-wall regions, the max.  $y^+$  and the averaged  $y^+$  are less than 1. The first refined mesh cells near walls lie perfectly in the viscous sub-layer, which means the refined mesh is fine enough to resolve the turbulence in the near wall region and to predict the max. SS accurately.

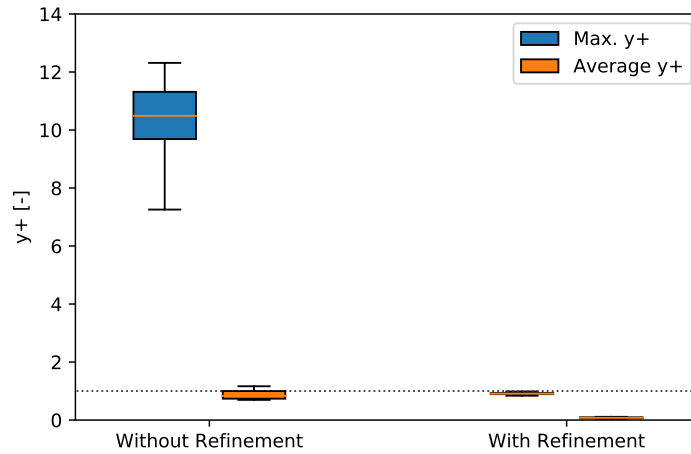


Figure 18: Comparison of  $y^+$  between coarse and fine near-wall meshes

As analyzed before, the first layer cell, where the max. SS occurs, lies probably in buffer region and viscous sub-layer region, for the case without and with wall treatments, respectively. There might exist a difference between these two cases in terms of the max. SS. To prove this, the max. SS from these two cases is calculated and shown in Fig. 19, where the max. SS calculated with the sufficiently refined mesh is almost two times as that from the unrefined mesh. The results with the finer near-wall mesh should be reliable, while the max. SS cannot be predicted accurately with the coarser near-wall mesh.

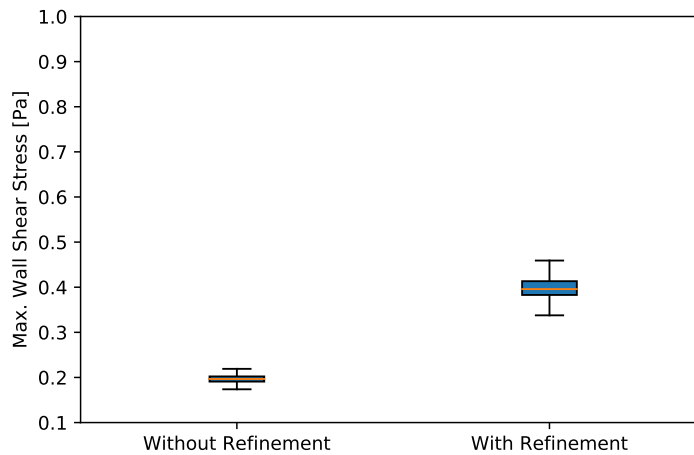


Figure 19: Comparison of the max. SS from coarse and fine near-wall meshes

The bubble velocities from these two cases are compared, and no significant difference can be observed. And both agree well with the measured rising velocity of a 4 mm bubble in the literature. Because the mesh cells containing gas phase are not in the first layer near walls. And the averaged  $y^+$  demonstrates that the majority of the mesh cells near the wall can resolve turbulence accurately. Therefore, bubble velocities are almost the same for both cases.

In conclusion, the model without wall treatment can provide accurate results in terms of bubble velocity. However, to gain a reliable max. SS, the first layer mesh cell should be refined. As with the refined mesh near walls, the max. SS is more accurate, the simulations throughout the research are carried out with mesh refinement in the near-wall region.

### 3.4 Turbulence model

In this section, simulations with various turbulent models are performed to check the derivation in numerical results caused by different turbulence models. The model is the same as the model with mesh refinement in the near wall region in the last section. During the simulation, these bubbles rise to the top. Other settings are identical for all simulations in this section. The only difference between all benchmarking simulations lies in the turbulence models. The SKE model, the RNG model, and the SST model are benchmarked. The numerical results in terms of bubble velocity is demonstrated in Fig. 20, where no significant difference can be observed in terms of bubble velocity predicted by different turbulence models. Besides, the boxes of bubble velocities from the RNG model and the SST model are almost identical in terms of the median value and the deviation of the data set. Comparing these three bubble velocities with an experimental velocity of a single bubble with the same diameter, only the bubble velocity predicted with the SKE model agrees

with the experiment (the dot line in Fig. 20) the best. Bubble velocities predicted by other turbulence models are a little higher. Therefore, the SKE model is chosen for the subsequent simulations of bubble's rise in a membrane channel, as it is capable of providing the most accurate numerical results.

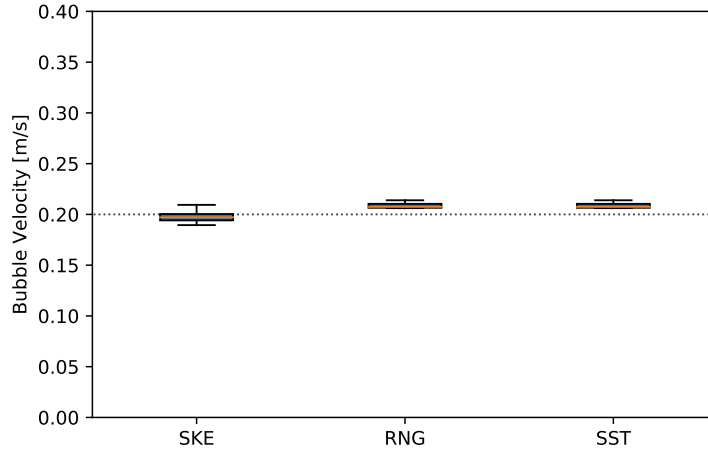


Figure 20: Comparison of bubble rising velocity from different turbulence models

### 3.5 Material properties

Temperature plays a vital role in the physical properties of gas and liquid phases. It can affect not only the viscosity of the fluids but also the surface tension. In this study, the effect of temperature on bubble dynamics is not included. The physical properties of the fluids listed in Table 9 are assumed to be at a temperature of 20 °C. As pointed out in the study by Brenda [263], the density of dry sludge ranges from 1200 to 1500 kg/m<sup>3</sup>. Keudel [266] and Schumacher [267] measured the density of dry sludge in the range of 1400 to 1500 kg/m<sup>3</sup>. In this study, the dry sludge density is assumed to be 1450 kg/m<sup>3</sup>. Other properties of activated sludge have been demonstrated previously. The Takacs settling model exhibits good fit to the experimental data, and the Bingham model has shown good agreement with the measured viscosity for the MBR sludge.

Table 9: Material properties at 20 °C

Physical properties	Value
Water density [kg/m <sup>3</sup> ]	998.2
Water kinematic viscosity [m <sup>2</sup> /s]	$1.0034 \times 10^{-6}$
Air density [kg/m <sup>3</sup> ]	1.204
Air kinematic viscosity [m <sup>2</sup> /s]	$1.516 \times 10^{-5}$
Surface tension [kg/s <sup>2</sup> ]	0.0728
Dry sludge density [kg/m <sup>3</sup> ]	1450

---

### 3.6 Initial and boundary conditions

---

The computing domain has always boundaries, where values implying some specific physical quantities have to be assigned at the faces. Initial and boundary conditions are additional constraints to specify the numerical solution of Navier-Stokes equations. Improper treatment of initial and boundary conditions can negatively affect the accuracy, the stability and the converging speed of the simulation [191].

Common boundaries in OpenFOAM are wall (for solid walls), symmetry (for symmetry planes) and patch (used for inlets or outlets). Boundary conditions are specified at the patches. Commonly used boundary conditions are `fixedValue`, which specify a value at the patch, `zeroGradient`, which means the normal gradient is zero, `noSlip`, which allows flows tangentially to walls and the velocity components normal to walls is zero. In this research, the bottom of the model studied is set as the velocity inlet with the `fixedValue` boundary condition, which describes velocities at the inlet. The value and direction of the velocity vector can be defined in the solver. In the simulations to investigate the effect of liquid velocities, upwards inlet velocity of 0.1, 0.2, 0.3 m/s in the z-direction are assigned at the velocity inlet, so that the liquid phase can move upwards in the membrane channel, as it is in reality. For the simulation of bubble generation, the small patch at the bottom of the model is defined as gas velocity inlet, where the velocity of the gas phase can be specified. The boundary for the top of the computational domain is configured as channel outlet, where the combination of `pressureInletOutletVelocity` boundary condition on velocity and the `totalPressure` condition on pressure is specified at this patch, where reversed flow may occur. The `totalPressure` condition determines a fixed pressure, and the `pressureInletOutletVelocity` condition specifies `zeroGradient` of velocity for outflow at the channel outlet. And a symmetry condition is used for the vertical planes in the exit zone, where bubbles are not constrained by walls.

Flat membrane sheets are normally regarded as rigid walls in simulations for simplifications, while in reality they are thin sheets with a thickness of several mm and can swag with the bubbly flow. Even though this membrane movement can scour the solids from the membrane surface to achieve a better fouling control [109], the effect of flexibility of membrane sheets is not in the scope of this work. Hence, the membrane sheets are treated as rigid walls in this research, as well. During the membrane filtration process, water flows through the membrane pores and membrane walls are permeable. In this work, they are considered as impermeable in the simulation for simplification. The membrane walls treated as impermeable, stationary walls, are represented by using no-slip boundary conditions, which is set by default for the viscous flow. With this boundary condition, the velocity component normal to the wall is zero, and the velocity components tangential to the wall gives rise to the SS. `zeroGradient` boundary conditions are imposed to the pressure on membrane walls, since there is no flow through the wall and hence no pressure gradient as driving force exists.

The whole computing domain is filled with water or mixture, and for the simulation of single bubbles, a bubble is patched in the system in the beginning, whose center is 6 mm above the model bottom and in the middle of the model in terms of width and depth. The bubble rises from bottom to top due to buoyant force. For the simulations of bubble swarms, the computing domain is also full of water or mixture, and a single bubble is patched in the same position at every certain time step. If bubbles are generated through the gas velocity inlet, only water or mixture is patched in the computing domain in the beginning.

---

### 3.7 Solution

---

Transient simulations are conducted with small time steps for accurate capture of the unsteady bubble behavior in the membrane channel. The adjustable time step is calculated based on the specified  $Co$ , which depends on the cell-size, velocity and time step. If  $Co$  is less than and equal to one, the fluid can flow from one mesh cell at most to the neighboring mesh cell at each time step, otherwise the fluid can flow through more mesh cells within one time step, resulting in problems in convergence. The max.  $Co$  is specified as one and the min. time step can be calculated accordingly. The time step for the simulation of 1 mm bubble in the membrane channel with a mesh refinement level of 3 is around  $4 \times 10^{-4}$  s, while it is as small as  $1 \times 10^{-5}$  s when the mesh refinement level increases to 6.

---

### 3.8 Discussion referring to research questions

---

#### **How to apply CFD tools to optimize the design and the operation process of an aerated FS membrane module regarding of membrane fouling control performance?**

As analyzed in section 2.1, previous studies [76, 77, 84–89] show that SS can indicate the membrane fouling control performance and the numerical calculation of SS has many advantages over the experimental measurement, since there exist various insufficiency in each experimental methods. This study characterizes SS numerically and uses it as an indicator for membrane fouling mitigation performance. In general, a high value in SS means a high potential membrane fouling removal. Chapter 3 describes the procedures and considerations of building CFD models, so that SS along membrane walls can be calculated based on the built models. The SS calculation method is also introduced in detail in section 3.3.3. And it implies that SS depends greatly on hydraulic conditions in the FS membrane module. Parameters affecting the MBR hydrodynamics can be regarded as inputs by modifying the model geometries, i.e. configurational parameters, or changing the boundary conditions or the initial conditions, i.e. operational parameters. The output here is SS values, and optimum is considered to be achieved at the highest SS under different conditions.

CFD investigation of hydrodynamics in FS membrane modules regarding these parameters are reviewed in section 2.3.2 in detail. Chapter 2 (Section 2.5) also points out the gaps in the literature. In order to fill some of the gaps and overcome the shortcomings, this thesis performs CFD simulations to investigate the aeration process in an FS membrane module, accounting for the following aspects.

- Systematical study of aeration process in the FS membrane module

This study starts from single bubble movement in an FS membrane channel to bubble swarms in FS modules, taking into account of all critical parameters in MBR systems: bubble size, aeration rate, module geometry and activated sludge properties, which have decisive effects on SS along membrane surfaces. It gives a comprehensive insight into the aeration process in an FS module regarding all these parameters. This work will be the first numerical study to examine the hydrodynamics in the FS membrane module systematically.

- VOF approach and a sufficient model height

This study is the first numerical study to examine the multi-phase flow profile and SS along membrane surface in a large model with a height of over 1500 mm, including the bubbles' deformation and motion

---

during their rise in the FS membrane channel. As the VOF method requires adequate resolution of grids to solve the gas-liquid interface, the number of grids of a large model is enormous. And so are the computing time and required computing resource. AMR technique is used in this study to get a finer mesh at the interface and a relatively coarser mesh in the liquid phase. In this way, the amount of grids is significantly reduced, and the computing time of such a large model is then acceptable when simulations are conducted with high-performance computers.

- Bubble swarms

Bubble behaviors can be modeled in this work with the VOF method, and the developed CFD model for aeration process is capable of simulating thousands of bubbles of different size and with consideration of the effect of bubble coalesce and breakup, which have not been studied previously.

- Nozzle size

In this work, simulations of bubble generation through nozzles are performed with the VOF method and the impacts of the nozzle size and the nozzle position are accurately assessed. Therefore, this work can provide new insights into the aeration process in the FS membrane module, including the effects of the nozzle size and its position.

- Activated sludge models

A new solver named `interSolidFoam` is developed for the simulation of gas-liquid-solid three-phase fluid by implementing the sludge model into the VOF method. The implemented sludge model is capable of describing the rheological and settling behavior of activated sludge since the sludge settling model is obtained from experimental data, and the rheological model comes from the literature special for activated sludge. Subsequently, simulations are conducted using the new solver `interSolidFoam` to examine the effect of activated sludge on aerated submerged membrane filtration and to optimize the MLSS concentration in MBRs. This work is the first research that carries out simulations with sludge models that accounts for both settling and rheological behavior of activated sludge.

### **How to include the activated sludge properties into the CFD simulations of an aerated FS membrane module?**

The flow in the aerated FS membrane module is gas-liquid-solid three-phase flow. Activated sludge is a very complex mixture containing water, sludge flocs, microorganisms, and other dissolved and suspended matters. In this simulation, for simplification, the activated sludge is regarded as a continuous phase using the rheological model and the settling model to describe the properties of activated sludge. The sedimentation behavior and the rheological behavior of activated sludge are described with empirical expressions as a function of the MLSS concentration based on experimental data. By performing benchmarking simulations, the best fit models are chosen, when the numerical results agree the experimental data the best. Then these chosen models are implemented into the new solver `interSolidFoam`, as described in Section 3.1.2.

With the simplification that the solid phase and liquid phase are treated as a mixture, the gas-liquid-solid three-phase flow is then only pseudo-three-phase flow, where the solid-liquid mixture and bubbles are two separated phases. As in the OpenFOAM framework there is no solver available, which uses the VOF approach to simulate bubbles behavior, a new solver `interSolidFoam` combining the VOF method and the

---

mixture model is developed to solve the gas-liquid-sludge three-phase problem in the FS membrane module. This new solver is developed by combining the `interDyMFoam` and the `driftFluxFoam` in `OpenFOAM`. Detailed work of this implementation is described in section 3.1. The new solver is capable of investigating the effect of the MLSS concentration on bubbles' rising behavior and on the induced SS.





---

## 4 Results and discussion

---

### 4.1 Influencing parameters on single bubbles

---

Given its relationship to membrane fouling control performance, SS is chosen in this work as a criterion to evaluate membrane performance. Bubble size [93, 141], bubble shape [179], gap distance [82, 93, 141], rheological behavior of activated sludge [33, 58, 161] are reported to have an effect on SS in FS membrane modules. The effects of these parameters will be discussed in this chapter.

---

#### 4.1.1 Bubble size

---

Bubble size is a determining parameter that affects the hydrodynamics in the MBR system significantly, such as bubble shapes, rising velocities, wake region and SS.

##### **Bubble shape regimes**

Decades of efforts have been made to research into bubble dynamics in gas-liquid two-phase flow, and achievements have been accomplished in studies [20, 262, 268–270], indicating that the dynamics and behavior of bubble rising in the liquid are governed by the following forces, i.e. inertial force  $f_i$ , viscous force  $f_\mu$ , buoyancy force  $f_{buo}$  and surface tension force  $f_{sur}$ . Bubbles can rise in the liquid medium due to buoyancy force and deform because of inertial force and surface tension force. The basic three dimensionless variables based on the ruling forces: Reynolds number  $Re_B$ , Eötvös number  $Eu$  and Morton number  $Mo$  characterize the dynamics and morphology of bubbles in liquid [262]. All these dimensionless parameters are fundamental to develop an understanding of the role of bubbles in the hydrodynamics of a gas-liquid two-phase system, as these dimensionless variables can be used to estimate the bubble shape [262], which is one of the most critical parameters affecting the bubble hydrodynamics. Because the deformation of bubbles can result in an increase in the interface between two phases. Hence an enhance in mass, momentum, and energy transfer [271]. For a deeper understanding of hydrodynamics in aerated FS membrane modules, it is necessary to characterize bubble shape regimes.

The bubble terminal rising velocity [262], which is termed as the velocity attained at a steady state when all applied forces on this bubble are balanced, is around 0.2 m/s for the investigated bubbles in this study, depending on bubble sizes only slightly. With a relative constant bubble rising velocity of 0.2 m/s, the dimensionless numbers can be calculated for the investigated bubbles in this study.

1. The Reynolds number of the bubble  $Re_B$  (Eq. 76), which is an indicator of relative importance between the flow inertial compared to its viscosity [262].

$$Re_B = \frac{f_i}{f_\mu} = \frac{\rho_l u_t d_B}{\mu_l} = 400 - 1200 \quad (76)$$

where,  $u_t$  is the bubble terminal rising velocity and is assumed to be 0.2 m/s.  $\rho_l$  and  $\mu_l$  are the density and the dynamic viscosity of the liquid phase, respectively.  $d_B$  [m] is the bubble diameter. The bubble shape is linked to  $Re_B$  [272], as illustrated in Table 10. Based on this classification, investigated bubbles should be ellipsoidal.

Table 10: Conclusions of classification of bubble shape regimes for different scenarios

Scenario	Features	Spherical bubbles	Ellipsoidal bubbles	Spherical-cap bubbles
Free moving bubbles	Bubble size [mm] [20]	$d_B < 1$	$1.5 < d_B < 15$	$d_B > 15$
	Weber number [273]	$We \ll 1$	$We \sim 1$	$We \gg 1$
	Reynold number [272]	$Re_B < 400$	$400 < Re_B < 3200$	$Re_B > 3200$
	Aspect ratio [273]	$0.9 < E < 1$	$0.25 < E < 0.9$	$0 < E < 0.25$
Bubbles in tubes	Length number [274, 275]	$Le < 0.125$	$0.125 < Le < 0.6$	$Le > 0.6$
Bubbles in a wide channel	Length number [274, 275]	$Le < 0.07$	$0.07 < Le < 0.4$	$Le > 0.4$

2. The Eötvös number  $Eo$ , which describes the correlations between the buoyancy force  $f_{buo}$  and the surface tension force  $f_{sur}$  [262].  $Eo$  (Eq. 77) in this study is about 0.54 - 13.4 for bubble diameters between 2 - 10 mm under normal condition and room temperature.

$$Eo = \frac{f_{buo}}{f_{sur}} = \frac{(\rho_l - \rho_g)g(d_B)^2}{\sigma} \quad (77)$$

where,  $\rho_g$  is the density of gas phase,  $g$  is gravitational acceleration, and  $\sigma$  is the surface tension between gas and liquid phases.

3. The Morton number  $Mo$ , which describes mainly the fluid properties and the relationship between all the forces [262]. The Morton number is calculated to be  $2.55 \times 10^{-11}$  for water.
4. The Froude number  $Fr$ , which is the ration of the flow inertia force  $f_i$  to the buoyancy force  $f_{buo}$ .
5. The Weber number  $We$  (Eq. 78), which relates to the inertial force  $f_i$  and the surface tension force  $f_{sur}$  and is well suited to characterize the bubble deformation [276].

$$We = \frac{f_i}{f_{sur}} = \frac{\rho_l(u_t)^2 d_B}{\sigma} = 1.1 - 3.3 \quad (78)$$

As mentioned above, Weber number indicates the bubble shape change. It is summarized in the study by Loth [273] that the correlations between bubble shape and Weber number can be qualitatively expressed, as shown in Table 10. Since the Weber number is between 1.1 and 3.3, the investigated bubbles should have an ellipsoidal shape.

In this study,  $We$  is around 1.1 - 3.3 and  $Re_B$  is between 400 and 1200, which means bubbles will have an oblate ellipsoidal shape if they move freely without the constraint of channel walls. However, apart from ellipsoidal bubbles (smallest Bubble in Fig. 21), spherical-cap shaped bubbles (largest bubble in Fig. 21) can be observed in this work, as well. The snapshots of investigated bubbles at around 1.0 s are displayed in Fig. 21, where it reveals that the deformation of bubbles increases, as bubble size increases.

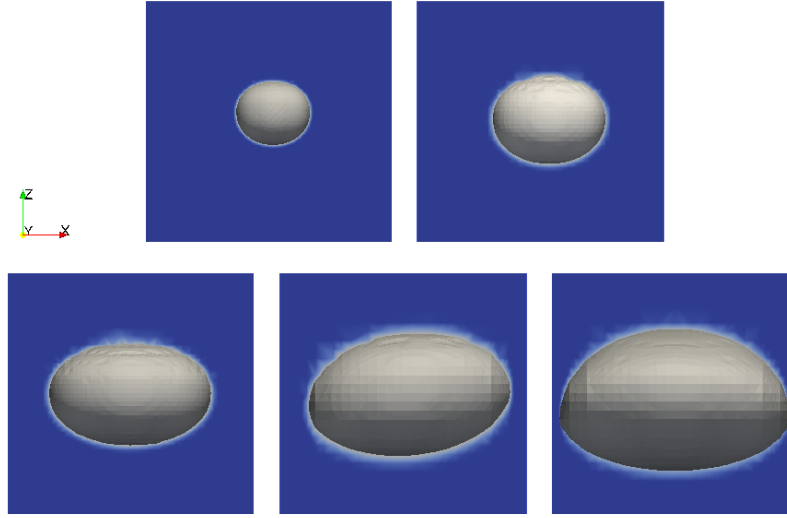


Figure 21: Snapshot of bubble shapes at different bubble sizes (from small to large, the volumetrically equivalent bubble sizes are 2 - 6 mm, respectively)

Besides, based on their shape presented in Fig. 21, 2 - 4 mm bubbles can be grouped into ellipsoidal bubbles, and 5 - 6 mm bubbles seem to show different forms. They seem to show a spherical-cap shape, or to be precise, they are in a transient shape regime between ellipsoid and spherical-cap. However, based on general classification, 6 mm bubbles have generally a ellipsoidal shape, as only large bubbles whose diameter are larger than 15 mm show a spherical-cap form, as shown in Table 10. This contradiction between the conclusions drawn in this study and in the literature is due to the existence of membrane walls. The narrow channel constrains the development of bubbles in the horizontal direction normal to the vertical placed membrane sheets, while bubbles in the unconfined environment will have a larger width in this direction and would be flatter. Thus, the general classification criterion of bubble shape regime based on the bubble size,  $We$  or  $Re$  is not suitable for bubbles when they rise in narrow channels. When 2 - 6 mm bubbles rise in narrowly spaced membrane channels, 2 - 5 mm bubbles present ellipsoidal shape and 6 mm bubbles are spherical-cap shaped.

On the other hand, aspect ratio ( $E$ ) characterizes the deformation of bubbles directly.  $E$  is defined as the ratio of the max. vertical to the max. horizontal dimension of a bubble [262]. Aybers and Tapucu [272] and Loth [273] grouped bubble shapes based on  $E$ , as demonstrated in Table 10. In this study,  $E$  of all bubbles lies between 0.25 and 0.9. Based on the classification in Table 10, they should have a ellipsoidal shape.  $E$  is also found out to decrease as the bubble becomes larger. Additionally, a dramatic reduction can be observed when the bubble diameter increases from 5 to 6 mm. This dramatic decline can be attributed to the presence of walls. As the membrane walls constrain the deformation of bubbles, the horizontal axes of this bubble are 6.46 mm in the directions perpendicular to membrane sheets, and 7.86 mm in the direction parallel to membrane walls. The projected area of the 6 mm bubble to the horizontal

plane is a flat ellipsoid, while other bubbles have a more or less circular projected area. Based on these vast differences, the classification of bubbles in a 7 mm spaced channel should be ellipsoidal bubbles (2 - 5 mm) and spherical-cap bubbles (6 mm).

Simulations are also performed at different channel depths. Spherical-cap bubbles (orange crosses in Fig. 22) have a relatively low  $E$ , while a high  $E$  can be observed with ellipsoidal bubbles (blue dots in Fig. 22). From Fig. 22 it can be seen that  $E$  alone is not a good criterion to classify bubble shape regimes. As bubbles rise in a confined environment, to account for the constraining effect of walls on bubbles, another non-dimensional number  $Le$  (length number) is introduced in this study.  $Le$  is defined as the ratio of the bubble equivalent diameter ( $d_B$ ) to the conduit diameter or channel depth ( $D$ ), as shown in Eq. 79.

$$Le = \frac{d_B}{D} \quad (79)$$

$Le$  can be used to roughly classify the bubble shape in a confined environment with consideration of wall effect. At a low  $Le$ , bubbles can move relatively freely, while at a high  $Le$ , due to the limit of membrane walls, the deformation of bubbles mainly occurs horizontally in the direction parallel to the membranes. Fig. 22 illustrates the classification of bubble regimes between ellipsoid and spherical-cap, based on  $Le$  and  $E$ . Bubbles are spherical-cap shaped at a  $Le$  above 0.8 and an  $E$  below 0.55. Krishna et al. [274, 275] used the same parameters to group bubble shapes in tubes and channels, as listed in Table 10, where the critical  $Le$  for different scenarios are different. In their studies, the bubbles investigated are relatively large, while in this study the investigated bubbles are relatively small, as well as the channel depths.

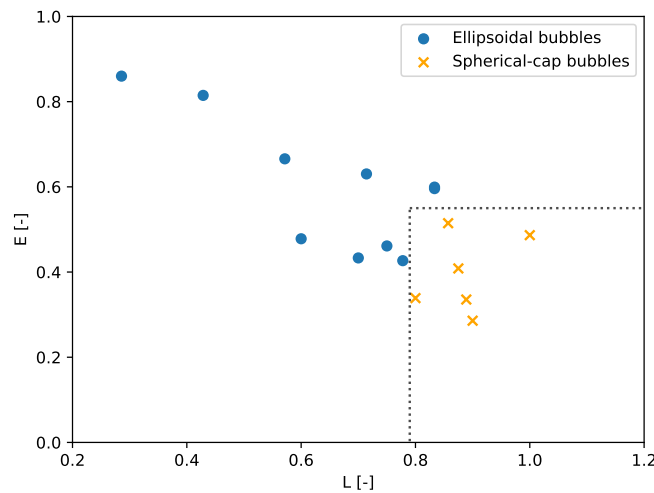


Figure 22: Bubble shape classification based on aspect ratio ( $E$ ) and length number ( $Le$ )

The classification of bubble shape regimes is concluded and listed in Table 10. Non-dimensional numbers  $Le$  and  $E$  are used as indicators. In previous studies [273–275],  $Le$  and  $E$  are used alone to group bubbles. It is found out that for bubbles rising in 6 - 10 mm channels, the criterium is not suitable anymore. A new classification based on the combination of  $Le$  and  $E$  can be applied in this situation.

$E$ , together with  $Le$ , can be used to group bubbles. As  $E$  is not so straightforward to specify, it is usually derived from other dimensionless numbers, since these numbers, such as  $We$  and  $Eo$ , can be calculated

based on fluid properties. Since  $E$  is related to the bubble size and surface tension,  $We$  [276] and  $Eo$  [277] are generally employed to anticipate bubble shape empirically. It is also found out that  $We$  is more critical than the  $Eo$  when it comes to predicting  $E$  [270]. However, since  $Eo$  is more straightforward to specify, it is frequently used to indicate  $E$ . Based on Loth [273], the buoyancy force included in  $Eo$  is not directly responsible for bubble deformation. For that reason, the  $Eo$  should be applied when the equilibrium conditions are reached, where the buoyancy force equals drag force. The empirical link for the  $E$  in terms of  $Eo$ , is originally developed by Wellek [270] for non-oscillating drops in contaminated liquids. However, researchers [277] have confirmed that this model can be applied to the oscillating bubbles rise in low-viscosity liquids as well. Analog to their equation [277] and considering wall effects on bubbles' shapes, the relationship between  $E$  and  $Eo$ ,  $Le$  is given by Eq. 80.

$$E = \frac{1}{1.204 + 0.1066Eo^{1.287}}(1/Le)^{0.02755}, \quad R^2 = 0.9868 \quad (80)$$

### Terminal rise velocity

Bubble shape regime determines the terminal rise velocity, vortex wake [20]. Several studies [20, 262, 278–280] have been conducted to build the terminal rise velocity models. Theoretical models are available for very small spherical bubbles and large spherical-cap bubbles freely rising in infinite water. Based on their model, the terminal rise velocities for 2 - 6 mm bubbles range from 0.235 (6 mm bubble) to 0.295 m/s (2 mm bubble) [262]. When 3 mm or 5 mm single bubbles rise in the narrow membrane channel with a space of 7 mm, the modeled terminal rise velocity is around 0.2 m/s, agreed well with the measured bubble rise velocity in 7 mm spaced membrane channel [91], which is also close to 0.2 m/s.

The difference in the velocity of bubbles rising in confined and unconfined environments is attributed to the deceleration effect of membrane walls. Aybers et al. [272] also observed this wall effect experimentally, when bubbles rose in tubes. They found out that the bubble rising velocity is lower with the presence of plexiglass cylinder around bubble than that without cylinder. And the wall effect vanished at a  $Le$  smaller than 0.055. Drews et al. [141] also observed the deceleration effect of walls on bubbles, when the  $Le$  is less than 1. Bozzano and Dente [281] found a lower rising velocity of bubbles in tubes for relative large bubbles, as well. They explained that the flow rate in bubble wake is upwards. Because of continuity, the flow rate in the cross-section between bubbles boundary and the tube wall should be downwards. It is the descend velocity that slows down the bubbles.

Therefore, classic models predicting bubble rising velocity are not suitable for 2 - 6 mm bubbles rising in small gaps. To accurately predict bubble terminal rise velocity of bubbles rising in membrane channel with various gap distances filled with stagnant water, the declaration effect of membrane walls should be taken into consideration. It can be done by introduction the concept of safe factor analogy to that in previous studies [282], who proposed a velocity model for bubbles rising in very thin gaps.

### Wake regions

Direct visualization of flow fields of membrane gap cross-section, and SS distribution along the right edge of this slice is presented in Fig. 23, where three district zones can be observed based on the flow field and SS distribution. These three zones are:

- Bubble front zone, which is the region ahead of bubble nose. The flow is uniform upwards.

- Bubble influence zone, where SS is significantly higher. The velocity of gas phase is higher than that of the surrounding liquid phase. The velocity of the gas phase is mainly upwards, while the velocity of the liquid flow experiences a transition from upward to downward flow, then a liquid film flow and at last a change from downward to upward flow, as shown in Fig. 23. This zone can also be divided into liquid falling film zone (bubble body region surrounded by a falling liquid film) and wake zone (wake region behind bubble), which originates from the circular wall jet [19, 133, 283] and generates vortices. In the falling film region, the velocity is downwards, which confirms the suspect of Bozzano and Dente [281] about the descent velocity in the falling film region.
- Bubble tail zone below the wake region. Here is a mainly upwards flow.

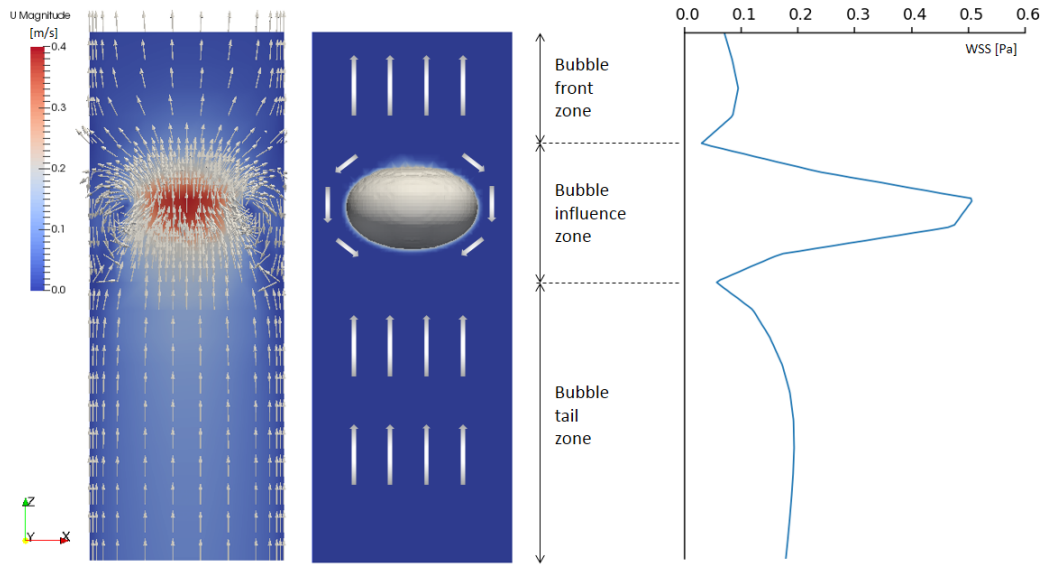


Figure 23: Zones around 4 mm bubble rising in 7 mm membrane channel based on flow fields and SS distribution (arrows correspond to velocity direction of the liquid phase)

Apart from flow field distribution, the SS values in these three zones differ significantly, as shown in Fig. 23, where SS is relatively low in the bubble front zone and bubble tail zone, while it dominates in the bubble influence zone. Here, the SS increases rapidly from nearly zero to maximum values and then decreases rapidly to nearly zero. The peak of SS exists within the falling film regions that separate the bubble and membrane walls. As the shear contributes to fouling control, hence a flux enhancement during membrane filtration, this zone is likely to be the regions mainly responsible for the air-scouring effect. However, in most of the previous studies, SS is found to be more intensive in wake regions [19, 20]. The contradiction is attributed to the sizes of investigated bubbles. Because the bubble size, to be exact, bubble shape affects the hydrodynamics significantly and bubbles with different shapes can induce different flow fields and SS distribution around them. Fig. 24 demonstrates the SS profile along the left edge of the membrane gap cross-section with a 6 mm bubble passing through it. Two SS peaks can be observed in Fig. 24, instead of only one peak of SS in Fig. 23. The SS peaks generated by 6 mm bubbles locate in the falling film region and the wake region. SS in the wake region is more intensive and covers a larger area, compared to that in the falling film region, which indicates the dominant air-scouring effect in the wake region [93, 103, 284].

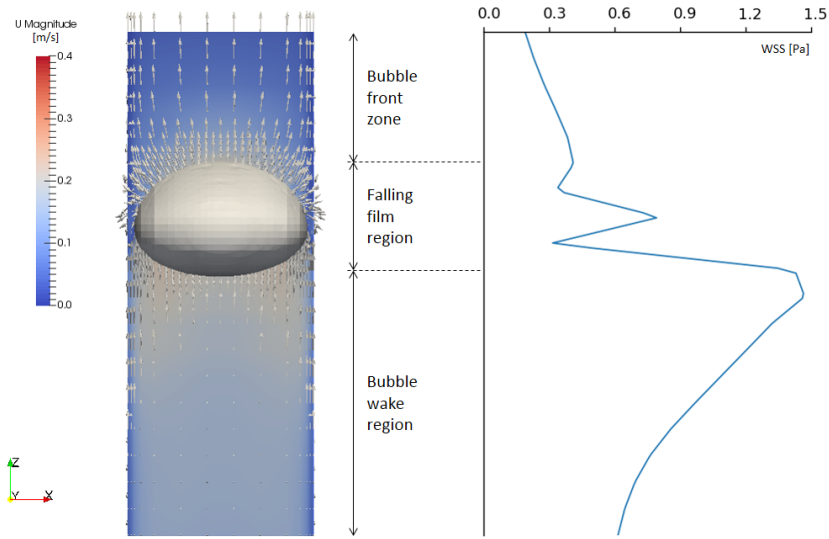


Figure 24: Flow fields and SS distribution induced by a 6 mm bubble

### Shear stress

Comparing SS peaks in Fig. 23 and Fig. 24, the max. SS induced by the 6 mm bubble is nearly two times higher than that exerted by 4 mm bubble. As for the locations of SS peaks, the max. SS occurs in film falling regions at the same height where the 4 mm bubble is located, while for the 6 mm bubble the max. SS exists in the wake region behind the bubble body. The second peak of SS induced by 6 mm bubble is also in the film region. The value of this peak is much lower than the other one, but still higher than that induced by the smaller bubble. As bubble size affects the max. SS significantly, the relationship between them is depicted in Fig. 25, where it reveals a general increase in the max. SS as bubble size increases. This is in agreement with what observed by Ndinisa et al. [25, 26], Prieske et al. [140] and Boehm [91].

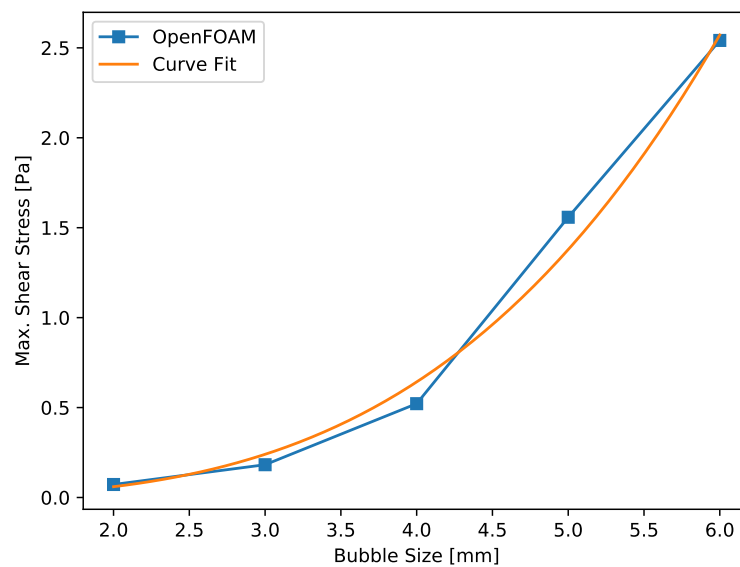


Figure 25: Max. SS induced by single bubbles of a diameter ranging from 2 to 6 mm

As bubbles grow, the liquid film between bubbles and the membrane wall becomes smaller. At the same time, the values of the descend velocity in the falling film region increase as bubble size increases [281]. Thus, SS, as a function of velocity gradient, is high at a large bubble size in fixed channel depth. The empirical expression for prediction of the max. SS ( $\tau_{max.}$ ) concerning bubble size ( $d_B$ ) in the membrane channel with a fixed gas distance of 7 mm is expressed in Eq. 81.

$$\tau_{max.} = 1.026 \times 10^8 d_B^{3.421} \quad , \quad R^2 = 0.9886 \quad (81)$$

The power-law correlation suggests that the larger bubbles are, the higher SS is exerted. It should be noted that the empirical relationship is only valid for bubbles with a diameter in the range of 2 - 6 mm. In this range, the highest and the lowest SS are 0.07 and 2.54 Pa, respectively. SS induced by single bubbles in this research and in previous studies are collected and listed in Table 11, which demonstrates that SS obtained in this study is in the same order of magnitude as the values reported in the literature.

Table 11: SS exerted by a single bubble in the FS membrane module

Reference	Methods	Geometry $d \times w \times h$ [mm]	System	Bubble size	SS magnitude
Wei et al. [93]	Num.	(6, 8, 10, 20)×100 ×1000	Water + sludge	5 - 200 mL	Ave. 0.5 - 2.4 Pa Max. 1.0 - 5.0 Pa
Drews et al. [141]	Exp. + Num.	(3 - 10)×160×700	Water + sludge	3 - 24 mm	Max. 2.5 - 6 Pa 0 - 4 Pa in still water
Boehm et al. [81, 91, 250]	Exp.	(3, 5, 7)×160×1500	Water	3, 5, 7, 9 mm	0 - 3.1 Pa in still water 0 - 1.95 Pa at 0.2 m/s
Preksie et al. [140]	Exp. + Num.	(3 - 11)×160×700	Water	3 - 10 mm	Max. 0.2 - 4.4 Pa
Wang et al. [83]	Num.	(4 - 8)×510×1200	Water	> 100 mm	Ave. 0.2 - 5.0 Pa

The max. SS exerted by single bubbles depending on bubble sizes can be 0 - 5.0 Pa [93, 141]. In this study, the SS induced by 3 - 6 mm bubbles in stagnant water agrees well with that reported by Prieske et al. [140] and Drews et al. [141], who also simulated the single bubbles' rise behavior in a 7 mm membrane channel. Boehm et al. [81, 91, 250] continued this work and investigated bubbles in membrane channel experimentally. Compared to the measured SS, the simulated values in this work are slightly higher but still in the same order of magnitude. This deviation in maximum values is due to the shortcomings of the experimental technique, as the resolution of measured points is not comparable with the resolution of CFD simulations. Wang et al. [40, 83] found the ave. SS in the range of 0.2 - 5.0 Pa, which is considerably higher than the ave. SS in this study. The difference can be attributed to model geometries and more importantly, to bubble sizes. They simulated slug bubbles with a diameter above 100 mm rising in multiple membrane channels with smaller membrane sheets, whereas relative smaller bubbles are modeled in a channel with larger membrane sheets in this study.



---

#### 4.1.2 Channel depth

---

Wall effect of membrane sheets is considered using  $Le$ . At a low  $Le$ , bubbles can rise relatively freely, while at a high  $Le$ , membrane walls constrain the deformation of bubbles and slows down bubbles due to the decent velocity in the falling film region. As gap distance increases, the cross-section between bubbles' rim and membrane walls increases correspondingly. As the falling film thickness increases, the descend velocity becomes smaller. The finding in this study confirms the theory of Bozzano and Dente [281].

In terms of the max. SS, Fig. 26 demonstrates the effect of gap distance on SS induced by bubbles ranging from 2 to 6 mm. Given a constant bubble size, the max. SS decreases, when the gap distance increases from 6 to 10 mm. When 2 mm bubble rises in 10 mm separated membrane sheets, the SS is only 0.02 Pa, while the SS induced by 6 mm bubble rise in 6 mm wide channel is as high as 3.06 Pa. The SS ranges from 0.02 to 3.06 Pa, which agrees well with the SS values reported in previous studies, as shown in Table 11. The drop of the max. SS by widening gap distance is also observed in previous studies [25, 26, 140]. And Ndinisa et al. [25, 26] found a decrease in fouling reduction by at least 40% experimentally, as the channel depth increased from 7 to 14 mm.

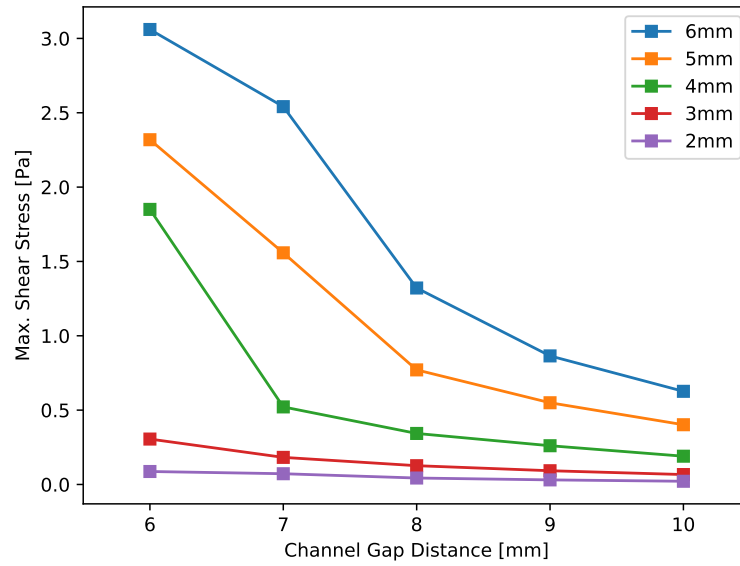


Figure 26: Max. SS induced by single bubbles of different size in membrane channel with various gap distances

Regarding to the sizes of single bubbles, the max. SS induced by 2 mm bubbles is affected by the channel gap distance slightly, while this distance has a significant effect on the max. SS induced by large bubbles. The max. SS increases by a factor of about 4, from 0.63 to 3.02 Pa, when the space between two membrane sheets decreases from 10 to 6 mm. It can also be seen from Fig. 26 that a very sharp decrease in the max. SS induced by 3 and 4 mm bubbles occurs as channel depth increases from 6 to 7 mm, while the steepest decrease of that by 6 mm bubbles existed when channel depth increases from 7 to 8 mm. All of them suggest that channel depth and bubble size together determine the max. SS. With the non-dimensional

parameter  $Le$ , the max. SS is characterized as a function of bubble size and channel gap, as demonstrated in Eq. 82.

$$\tau_{max.} = 0.0776d_B^{-0.7415}(1/Le)^{-3.229} \quad , \quad R^2 = 0.9425 \quad (82)$$

---

#### 4.1.3 Superimposed liquid velocity

---

When air is injected into the feed channel, cross flow is generated is in the range of 0.1 to 0.3 m/s [139, 141] in submerged MBRs. Both the motion of liquid and gas phases can induce shear forces on the membrane surface, which generates the back transport of the deposited particles from the membrane surface into the bulk flow. The mechanisms of particle back transport theory [58, 285, 286] involve concentration polarization concept (Brownian molecular diffusion) mainly for small particles, shear-induced diffusion due to cross flow velocity and inertial back diffusion forces for large particles. The convective force on particles towards the membrane surface is a drag force of permeation flow. The movement of particles depends on the forces acting on them. If the drag forces towards the membrane surface are larger than the total back transport forces, the particle will deposit on the membrane surface and form the cake layer. Otherwise, a settled layer of particles will travel back into the bulk flow. A detailed description of the theory can be found in the studies of Vyas et al. [287] and Altmann et al. [288]. Depending on the resultant net force from various forces, acting on the spherical particle at the membrane surface, particles can move towards membrane and depot on the membrane surface or remain in the feed flow. Of all these forces, the balance between the back diffusion force and drag force of permeate flux determines the particle movement during the filtration process in the FS membrane. Based on Stock's equation, the drag force due to permeation flow can be estimated with Eq. 83.

$$f_{drag} = 3\pi\mu d_p J \quad (83)$$

where,  $f_{drag}$  is the drag force [ $\text{kg} \cdot \text{m}/\text{s}^2$ ],  $\mu$  is the dynamic viscosity of the feed flow [ $\text{Pa} \cdot \text{s}$ ],  $d_p$  is the particle diameter [ $\text{m}$ ], and  $J$  is the permeate flux [ $\text{m}/\text{s}$ ].

The main force leading to detaching of particles on the membrane surface is related to SS. According to Eq. 84, an increase in SS can reduce the particle deposition effectively, thus controlling membrane fouling effectively. It is proven by Wray et al. [87] that large pulse bubble sparging can reduce fouling by up to 80% compared to conditions where no air sparging was applied. Another study conducted by Wray et al. [289] also confirms the fact that high SS increases permeate flux. The back diffusion force  $f_{bd}$  can be calculated according to Rubin (Eq. 84) [290] (cited in [287, 288] ).

$$f_{bd} = 0.761\tau_w^{1.5}d_p^3\rho^{0.5}/\mu \quad (84)$$

where,  $f_{bd}$  is the back diffusion force [ $\text{kg} \cdot \text{m}/\text{s}^2$ ],  $\tau_w$  is SS [ $\text{Pa}$ ], and  $\rho$  is the fluid density [ $\text{kg}/\text{m}^3$ ].  $f_{bd}$  is proportional to the third power of particle diameter and  $f_{drag}$  is only proportional to the first power of particle diameter. Therefore, small particles attach to the membrane surface easier, and large particles tend to travel back to the feed stream. Once particles attach to the membrane surface, the adhesion and friction forces might be higher than hydrodynamic forces [288] especially for small particles. Balancing  $f_{drag}$

and  $f_{bd}$ , the critical particle diameter  $d_{p,crit}$  can be calculated. Below  $d_{p,crit}$ , particles will be transported to the membrane surface and deposit there, while particles with a diameter above  $d_{p,crit}$  tend to travel back to the feed. The critical flux was found to be  $J_{crit} \approx 8 \text{ L}/(\text{m}^2 \cdot \text{h})$ , and  $J_{crit} \approx 6 \text{ L}/(\text{m}^2 \cdot \text{h})$  without aeration at a superimposed liquid velocity of 0.2 and 0.3 m/s, respectively [141]. With these permeate fluxes, the drag forces are calculated with Equation 83 and plotted in Fig. 27. The SS induced only by the liquid phase is about 0.5 Pa at a flow rate of 0.2 m/s and 1.0 Pa at 0.3 m/s. The ave. SS on membrane surfaces in the influence zone of 6 mm bubbles is 0.9 and 1.4 Pa respectively, as they rise in the liquid media with a velocity of 0.2 and 0.3 m/s. The influence zone is defined with a length of 3 times of bubbles horizontal axes, a height of 3 times of vertical axes, and a width of channel depth. With the CFD-based SS,  $f_{bd}$  is determined based on Eq. 84 and plotted in Fig. 27. Based on force balance, the critical particle size is  $0.63 \mu\text{m}$ , when this particle is in the influence zone of 6 mm bubble in the liquid with a velocity of 0.3 m/s, while it is  $1.57 \mu\text{m}$ , when the flow velocity is 0.2 m/s without bubbling. Drews et al. [141] and Boehm [91] also analyzed the critical particle size, and their values are in the same magnitude of values in this study. But from a long-term perspective, a low critical particle size does not necessarily guarantee a better fouling control performance, as small particles tends to cause a higher resistance [91, 141].

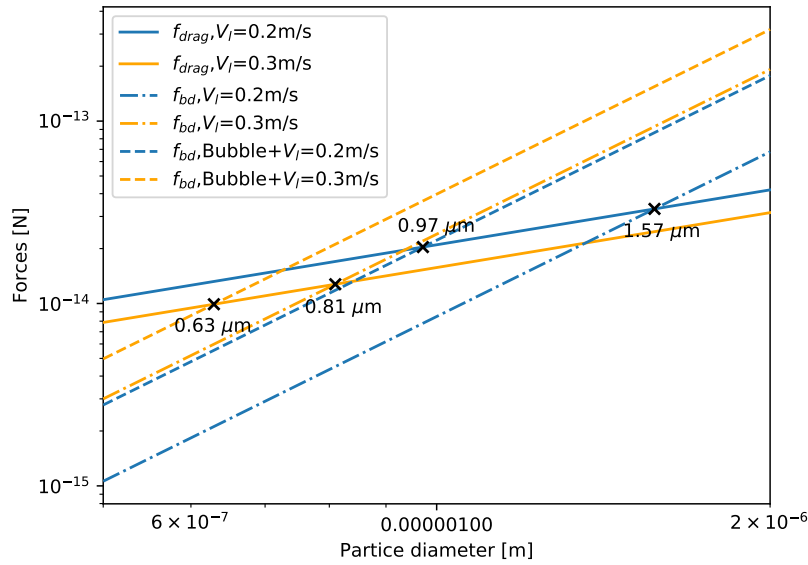


Figure 27: Drag and back diffusion forces acting on a particle near the 6 mm single bubble

Apart from SS values, flux enhancement is also found to be linked to SS fluctuation in gas-liquid two-phase flow [88, 89, 91]. A non-dimensional hydrodynamic parameter  $B$  (Eq. 85), which quantifies the SS fluctuation and indicates the relative increase in SS induced by gas phase compared to liquid phase, is defined as the ratio of the SS amplitude in two-phase flow to that in the liquid phase [88, 89]:

$$B = \frac{(\tau_{max.} - \tau_{min.})_{2p}}{\tau_{1p}} \quad (85)$$

Ducom et al. [88, 89] found that a higher value of parameter  $B$  could lead to a high flux enhancement of FS membrane filtration. To determine the parameter  $B$  in this study, SS in water and two-phase flow

induced by 3 and 6 mm bubble is calculated. The SS of single phase flow at a superimposed liquid velocity of 0.1, 0.2, and 0.3 m/s are 0.17, 0.50, and 0.95 Pa, respectively. The max. SS induced by 3 and 6 mm bubble with superimposed liquid velocity ranges from 2.35 to 9.53 Pa, which is much higher than that of single phase, as shown in Fig. 28. This is also found in the study by Boehm [91].

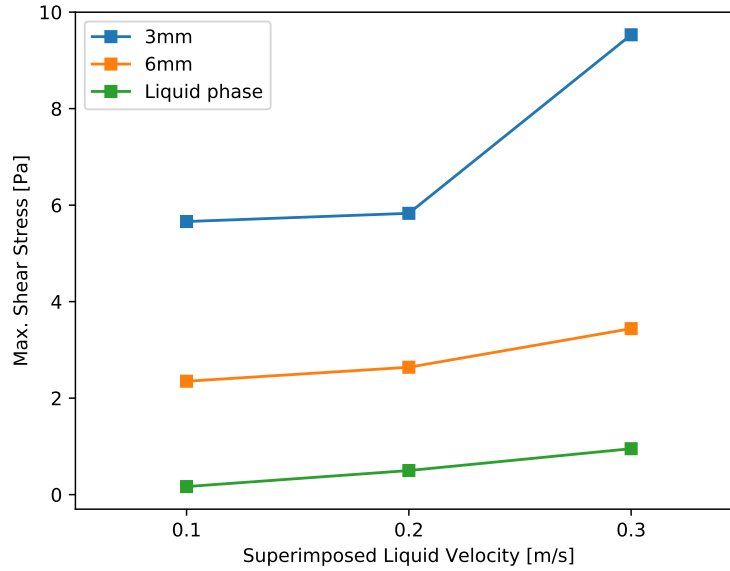


Figure 28: Max. SS induced by 3 mm and 6 mm single bubbles under various superimposed liquid velocities

Besides, the max. SS induced by 3 mm bubbles is much higher than that induced by 6 mm bubbles under the same conditions, as demonstrated in Fig. 28. This agrees well with the findings of Boehm et al. [81], who found out that single small bubbles with a diameter of 3 mm could generate a higher max. SS in the probability range of 90% - 99% on 7 mm spaced membrane sheets than that by 5 mm or 7 mm single bubbles at a liquid flow rate of 0.2 m/s. The possible reason for this phenomenon is the oscillation amplitude of bubbles. It is observed that the oscillation amplitude of small bubbles is larger than that of large bubbles. As small bubbles rise towards the membrane sheets, the liquid film between bubbles rim and membrane wall becomes thinner, resulting in a higher max. SS. Furthermore, the max. SS (5.83 Pa) generated by 3 mm bubble in 7 mm membrane channel with a superimposed liquid velocity of 0.2 m in this study lie in the 90% - 99% probability range of the measured max. SS and is close to the 99% value (approx. 6.4 Pa), noted as  $\tau_{max}$  by the researcher, under the same conditions as in Boehm's study [91].

Since the minimum SS is approximately equal to 0 Pa, the parameter  $B$  can be calculated as the ratio of the time-averaged max. SS to the SS of a single phase. The parameter  $B$  is found in the range of 3.6 - 34 in this study, which is close to the range of 5 - 40 as parameter  $B$  values calculated by Ducom et al. [88, 89]. Besides, the parameter  $B$  is found to decline as the superimposed liquid velocity increases or bubble size increases. Based on this trend and the conclusion by Ducom et al. [88, 89] that higher flux enhancement could be achieved at a high parameter  $B$  values due to aeration, small bubbles with a low superimposed liquid velocity are recommended, where the parameter  $B$  is larger, and the contribution of air sparging on flux enhancement is larger.

---

#### 4.1.4 MLSS concentration

---

In previous studies, water is usually used to investigate SS in MBRs both experimentally and numerically. In this section, a non-Newtonian fluid capable of describing the settling and rheological behavior of activated sludge is used, so that bubble dynamics are investigated in a system closer to the real situation. This fluid has a density close to water. The viscosity of fluids around the single bubble ranges from 0.0065 to 0.02 Pa·s depending on the MLSS concentration. The terminal rise velocity of 3 mm single bubble in sludge is around 0.07 m/s for the investigated the MLSS concentration from 5 to 25 g/L. With the relative constant bubble rising velocity of 0.07 m/s, the fluid density of 1000 kg/m<sup>3</sup>, bubble diameter of 3 mm and viscosity of 0.0065 - 0.02 Pa·s, the non-dimensional numbers can be calculated.  $Re_B$  is in the range of 15 - 46 and  $We$  is around 0.2. In water,  $Re_B$  is about 600 and  $We$  is at 1.7 for the single bubble with a diameter of 3 mm. As mentioned above, for the case with a minor wall effect, if  $Re_B < 400$  or  $We < 1$ , bubble presents spherical form. And if  $400 < Re_B < 5000$ , bubbles have an ellipsoidal shape. That means 3 mm bubbles will present a spherical shape in the sludge system, while they present an ellipsoidal form in water. This can be confirmed in Fig. 29, where 3 mm bubble is spherical in the fluid with a MLSS concentration of 5 g/L (right in Fig. 29), while it is an ellipsoidal bubble in water (left in Fig. 29).

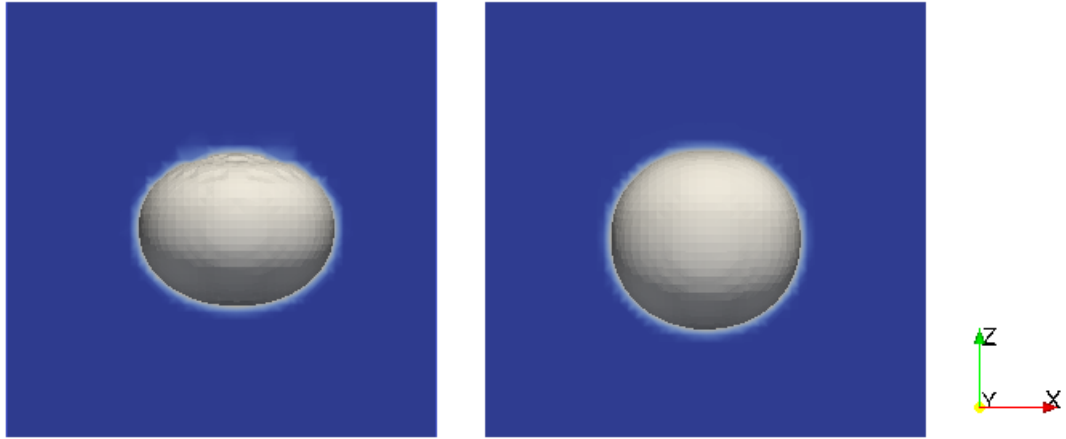


Figure 29: 3 mm bubble in water and sludge with a MLSS concentration of 5 g/L

In the literature, the bubble rise velocity in activated sludge is still unclear, since the activated sludge is not transparent and not suitable for optical measurements. Besides, it is also challenging to determine the fluid properties of activated sludge due to its inhomogeneous properties. Thus, Xanthan solution is usually used instead of activated sludge to investigate the bubble dynamics in non-Newtonian fluid, as their shear-thinning rheological behaviors are close [252]. Boehm et al. [252] chose a Xanthan solution with a concentration of 0.8 g/L to represent activated sludge with a representative MLSS concentration of 11.4 g/L. They found that the terminal rise velocity of 3 mm bubble is around 0.2 m/s in stagnant water and approximately 0.1 m/s in Xanthan solution when this bubble rises in membrane channel with a channel depth of 7 mm [91]. Their results in water agree well with the values in this study, where the rising velocity of 3 mm bubble is modeled to be around 0.2 m/s. The bubble rising velocity in this study is found to be 0.07 m/s at a MLSS concentration of 10 g/L (shown in Fig. 30), which is also close to 0.1 m/s reported in their study. Still, they did not agree with each other completely, since the fluid properties

are different. Besides, the settling behavior of sludge is also considered in this work. Thus, the difference in fluid properties might lead to the difference in bubble rising velocity.

In the study conducted by Boehm et al. [252], they used a specific Xanthan concentration and did not investigate the bubble rising velocities under various Xanthan concentration. Margaritis et al. [291] investigated terminal rising velocities for freely rising bubbles under various Xanthan concentrations and found that the rise velocity of bubbles with an equivalent diameter of 3 mm decreased with increasing Xanthan concentration. This study confirms the observed trend, as shown in Fig. 30, where it reveals that bubble rising velocity decreases as the MLSS concentration increases. This can be explained by Stokes' law, even though the hydraulic conditions can not fully fulfill its assumptions. For the simple case, the bubble terminal rising velocity is reached when the frictional force and the buoyancy force are balanced. The friction force is a function of fluid viscosity. As the MLSS concentration increases, the viscosity of the fluid increases, and so does the friction force.

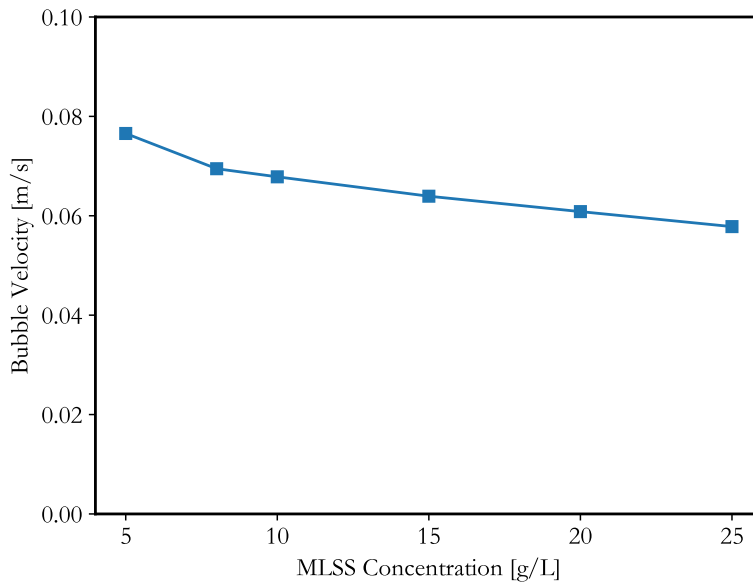


Figure 30: 3 mm bubble rising velocity in sludge at different MLSS concentrations

In short, the bubble rising behavior changes in sludge compared to that in water. The bubble rising velocity is lower in sludge and decreases with an increase in the MLSS concentration.

The viscosity field depends significantly on the flow field due to the rheological property of non-Newtonian fluids. In this study, the shear-thinning Ostwald-de Waele model liquids are used in the simulation to evaluate the shear-thinning effect on bubble rising behavior. The local viscosity distribution at the membrane wall due to the motion of the 3 mm bubble can be obtained from numerical results. The color bar at the right side of Fig. 31 depicts the range of apparent viscosity, where red represents high viscosity, and blue represents low viscosity. As shown in Fig. 31, the region with the lowest viscosity is bubble projection on the membrane wall. This low viscosity region corresponds to the high shear behavior region, where the regions around the bubble and behind bubble tend to have higher SS, as shown in Fig. 23 and Fig. 24. In these regions, the shear-thinning effect of the liquid becomes very strong, as the apparent viscosity decreases with increasing shear rate. Other researchers [292, 293] also found a low viscosity of

shear-thinning liquid around the bubble and in the wake regions of bubbles, where the shear rate is high. Besides, the contour pictures in Fig. 31 illustrates the effect of bubble motion on viscosity distribution at different MLSS concentrations. At a low MLSS concentration where the viscosity of the fluid is also low, the influence zone (orange and blue regions in Fig. 31) due to bubble motion is much larger, while at a high MLSS concentration above 20 g/L, no influence zone can be observed. If the influence zone, where the shear rate is high, can be used as an indicator for membrane fouling control performance, the scouring effect of a 3mm single bubble on membrane surface is minor in sludge with a high MLSS concentration, as the area of influence zone becomes smaller in Fig. 31 from left to right.

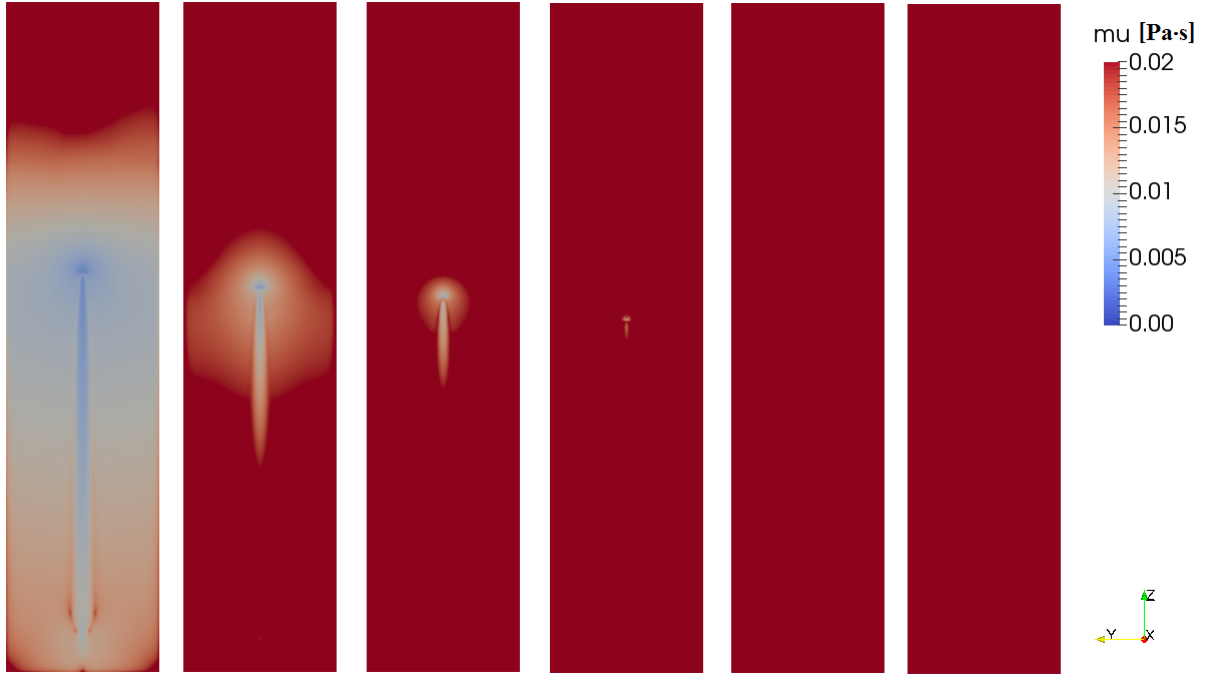


Figure 31: Viscosity distribution at membrane walls in sludge with different MLSS concentrations (MLSS concentrations from left to right: 5, 8, 10, 15, 20, 25 g/L)

As analyzed above, the cleaning effect of the 3 mm single bubble decreases as the MLSS concentration increases. However, if SS is used as an indicator, bubble cleaning effect increases with the MLSS concentration, as illustrated in Fig. 32, where the max. SS values increase as the MLSS concentration increases. Thus, SS is not a plausible indicator, as it is the product of wall shear rate and viscosity, as shown in Eq. 73. Instead of SS, researchers [33, 122, 182] related membrane fouling to the cross flow velocity, because it plays an important role in the determination of a particle, whether it is attracted to or detached from the membrane. As analyzed in section 4.1.3, the mechanism is the force balance between the back diffusion force and the drag force. If the back diffusion force is smaller than the drag force, the particle will be attracted to the membrane surface. The ratio of the back diffusion force to the drag force can show the membrane fouling potential. If the ratio is much larger than 1, solids can scour away from membrane surface resulting in a high membrane fouling performance. Substituting Eq. 84 and Eq. 83 into this ratio, it is found that the force ratio is directly proportional to wall shear rate and inversely proportional to fluid viscosity, shown in Eq. 86. As the MLSS concentration increases, fluid viscosity increases resulting in a lower force ratio, thus lower fouling mitigation performance.

$$\frac{f_{bd}}{f_{drag}} = \frac{0.761\tau_w^{1.5}d_p^3\rho^{0.5}/\mu}{3\mu d_p J} = \frac{0.254\gamma_w^{1.5}d_p^2\rho^{0.5}}{\mu^{0.5}J} \quad (86)$$

where,  $f_{drag}$  is the drag force [ $\text{kg}\cdot\text{m}/\text{s}^2$ ],  $f_{bd}$  is the back diffusion force [ $\text{kg}\cdot\text{m}/\text{s}^2$ ],  $\mu$  is the dynamic viscosity of the feed flow [ $\text{Pa}\cdot\text{s}$ ],  $d_p$  is the particle diameter [ $\text{m}$ ],  $J$  is the permeate flux [ $\text{m}/\text{s}$ ],  $\tau_w$  is SS [ $\text{Pa}$ ],  $\gamma_w$  is wall shear rate [ $\text{s}^{-1}$ ] and  $\rho$  is the fluid density [ $\text{kg}/\text{m}^3$ ].

Besides, it can be seen from Eq. 86 that wall shear rate is more suitable than SS to indicate membrane fouling performance when it involves different fluid viscosity. Fig. 32 illustrates the relationship between the max. shear rate at membrane walls and the MLSS concentration. As the MLSS concentration increases, the max. shear rate drops, so does the membrane fouling mitigation.

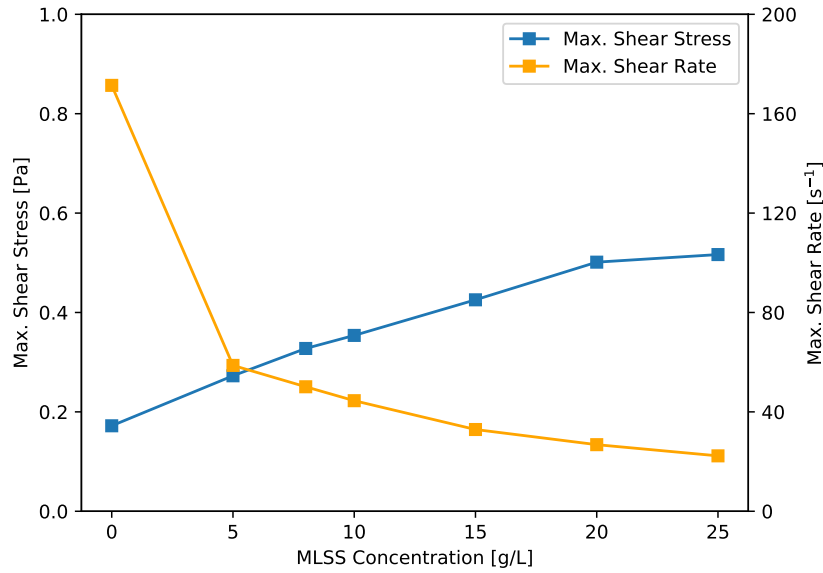


Figure 32: Max. SS and max. shear rate in sludge with different MLSS concentrations

## 4.2 Influencing parameters of bubble swarms

After the single bubbles' behavior in membrane channel and the hydrodynamic influence on membrane fouling mitigation are investigated fundamentally, bubble swarms behaviors and their influence on fouling control will be described in this chapter. In contrast to the simulation of single bubbles, the interaction between bubbles and its impact on bubble dynamics is discussed first. As concluded from the simulation of single bubbles, bubble size affects bubble dynamics and hydrodynamic conditions around bubbles significantly, the influence of parameters determining the bubble size in bubble swarms, e.g. air flow rate, is described. Additionally, the impacts of superimposed liquid velocity, gap distance, and MLSS concentration are discussed in Section 4.2.2, Section 4.2.3, and Section 4.2.4, respectively.

### 4.2.1 Bubble swarm dynamics

Bubbles are the most critical component in the aeration process in MBRs. Parameters that affect the size and number of generated bubbles and their effects on SS are discussed here.



---

## Bubble generation

In a submerged FS membrane module, bubble swarms are generated through the nozzles underneath membranes. The nozzle size can affect the sizes and distributions of generated bubble swarms. Nozzles of different size are simulated to investigate their effect on the size of the generated bubbles and ultimately on SS induced by them. It is found that under the same aeration intensity, coarser bubbles are produced by large nozzles, while finer bubbles are generated by small orifices. For the nozzle size with a cross section in the range of 1 - 3 mm<sup>2</sup>, the generated bubbles have a diameter around 3 mm at a gas inlet velocity of 0.2 m/s. Many studies [294–296] have been done to illustrate the relationship between generated bubble size and nozzle size with mathematical expressions. Analog to the model proposed by Jamialahmadi et al. [295], a similar model (Eq. 87) is given including all possible influencing parameters with modifying coefficients to fit the numerical data in this study.

$$\frac{d_B}{d_o} = \left( \frac{0.807}{Bd_o^{1.677}} - \frac{2045Fr^{0.756}}{Ga^{0.486}} + 50.78Fr^{0.756} \right)^{\frac{1}{3}}, \quad R^2 = 0.993 \quad (87)$$

where,  $d_o$  is the equivalent orifice, and  $Bd_o$  is bond number in terms of the orifice, as defined in Eq. 88.

$$Bd_o = \frac{\rho_l g d_o^2}{\sigma} \quad (88)$$

Galileo number at the orifice is given by Eq. 89.

$$Ga = \frac{\rho_l g d_o^3}{\mu_l^3} \quad (89)$$

Froude number is calculated with Eq. 90.

$$Fr = \frac{u_{in}^2}{d_o g} \quad (90)$$

where,  $u_{in}$  is the inlet velocity [m/s].

This model indicates that coarser bubbles are produced through the same nozzle at a higher air flow rate. Bubbles generated from aerators with a cross-section of 1 mm<sup>2</sup> at a gas inlet velocity of 0.02 m/s have an average diameter of 2.92 mm, while those produced through the same nozzle at 0.2 m/s gas inlet velocity is 3.10 mm in average. Despite the increase in air flow rate by a factor of 9, the increase in bubble size is slight. However, the numbers of bubbles in the membrane channel increases dramatically, from 12 at 0.02 m/s to 88 at 0.2 m/s. A higher air flow rate leads to a larger number of bubbles, which was also observed experimentally [26]. Bubble-induced ave. SS on the influencing membrane surfaces with a width of 30 mm depends on the size and the number of bubbles ringing in the membrane channel. Since the generated bubbles at the same nozzle have more or less the same diameter, the ave. SS is significantly affected by the number of bubbles. As air flow rate increases, the number of bubbles rising in the channel increases, so does the ave. SS, as shown in Fig. 33. Bayat et al. [161] and Amiraftehi et al. [160] also found a positive correlation between air flow rate and exerted SS. In Fig. 33, a decreasing growth rate of the ave.

SS can be seen. It can be predicted that the ave. SS stays stable when the air flow rate further increases above a specific critical value. This supposition agrees well with the observations by Ndinisa et al. [25, 26] and Boehm et al. [82], who reported the enhancement of membrane filtration performance with increasing aeration intensities and minor improvement with a further increase in air flow rate beyond some specific critical values.

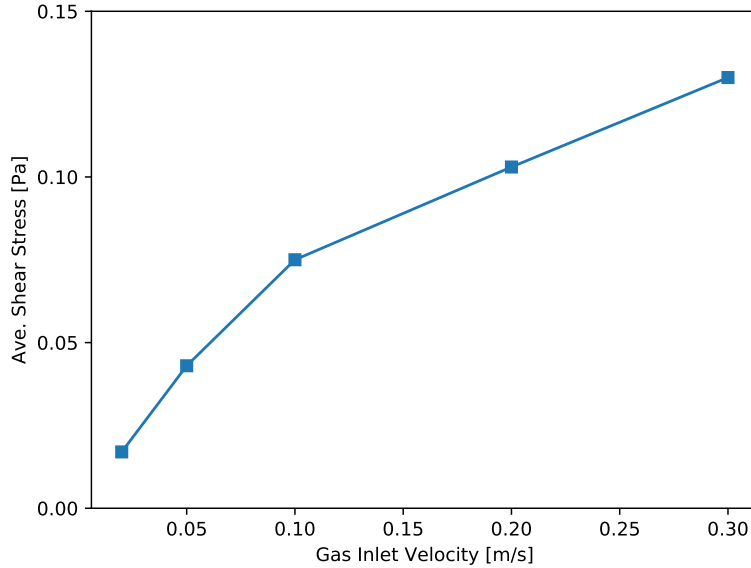


Figure 33: Ave. SS induced by bubble swarms generated at various gas inlet velocities

The described relationship between the ave. SS on the membrane surface and air flow rate agrees with a power-law correlation. Therefore, the ave. SS and aeration intensities are fitted with a power-law function, as illustrated in Eq. 91.

$$\tau_w = 0.2783u_{in}^{0.6178} \quad , \quad R^2 = 0.9842 \quad (91)$$

This fitted function suggests that at a low gas inlet velocity, the ave. SS increases significantly, and upon a certain critical value, a further increase in aeration intensity has an only minor effect on SS, hence fouling control. A power-law correlation between air flow rate and SS was also found in previous studies [110, 121], despite that they used a different numerical approach for modeling multi-phase flow. As suggested by Yan et al. [121], this relationship provided a clue of exploring the critical value of air flow rate. Besides, Ndinisa et al. [25, 26] and Boehm et al. [82] also found the critical aeration intensity experimentally. If the critical air flow rate is found in practice, and MBR is operated under the critical value, it would achieve satisfying membrane filtration performance while saving energy.

Aeration intensity affects the ave. SS significantly, while the effect of nozzle size on membrane fouling control is not so noticeable, even though both the size and the number of bubbles are affected by the nozzle size significantly. As the nozzle becomes larger, the generated bubble size increases from 3.1 to 3.76 mm, while the number of bubbles increases from 43 to 88. However, under the same aeration intensity, an increase in nozzle size can increase the ave. SS only slightly. As the cross-section of the nozzle increases

from 1 to 3 mm<sup>2</sup>, the ave. SS increases from 0.103 to 0.115 Pa, which are in the range of the obtained SS in the literature, as listed in Table 12. Thus, it can be concluded that large nozzles are more beneficial for membrane fouling control. This finding is consistent with the observation by Ndinisa et al. [25, 26], who found an enhancement in membrane fouling mitigation in an aerated FS membrane module with an increase in the nozzle size. Besides, the beneficial effect of the larger nozzle on the ave. SS under the same gas superficial velocity was also obtained by Yamanoi and Kageyama [92], as they compared the SS of the nozzle aerator and the glass ball filter aerator, which produce bubbles in centimeter and millimeter range, respectively.

Table 12: SS exerted by bubble swarms in the FS membrane module

Reference	Methods	Geometry d × w × h [mm]	System	Flow rate	SS
Yamanoi et al. [92]	Exp.	(5 - 10)×100×340	Water	1.2 - 9.6 L/min	9 - 1.6 Pa Ave. 0.4 Pa
Ducom et al. [88, 89]	Exp.	5×70×147	Water	0 - 0.4 m/s	0.7 - 3.5 (Ratio)
Ndinisa et al. [25, 26]	Exp. + Num.	(7 - 14)×10×290	Water	2, 4, 6, 8 L/min	0 - 0.85 Pa
Boehm et al. [82, 91]	Exp.	(5, 7)×160×1500	Water + Xanthan	0 - 0.21 m/s	0 - 3.4 Pa in water 0.8 - 2.3 Pa in Xanthan
Yang et al. [58, 110]	Exp. + Num.	220×320×10	Water + sludge		Max. 3.17 Pa Ave. 0 - 2.2 Pa
Ibrahim [158]	Exp. + Num.		Water		1.8 - 5 Pa
Amini et al. [33]	Exp. + Num.	8×500×1000	Sludge		Ave. 5.4 - 6.5 Pa
Amirafatabi et al. [160]					Ave. 0.6 - 0.85 Pa
Khalili-Garakani et al. [144]	Exp. + Num.	8×310×230			Ave. 2.819 - 3.901 Pa

The ave. SS induced by bubble swarms generated through one nozzle ranges from 0.04 to 0.12 Pa. Table 12 shows the ave. SS in this study compared to the values reported in previous studies. The SS obtained by Ibrahim [158] at an air flow rate of 5 L/min with bubbles of different size through different types of diffusers in a 3 mm spaced membrane channel was in the range 1.8 - 5 Pa. However, it is not mentioned in his study, if the SS refers to the ave. or the max. SS. Anyway, the membrane channel is very narrow,

and bubbles with a diameter of 3 - 4 mm can exert higher SS on the membrane surface due to the thin liquid film between bubble rim and membrane wall. Amini et al. [33] also reported a relatively high ave. SS on 8 mm spaced membrane sheets since they used a much higher air velocity of 1.5 m/s. Besides, in this study, there is only one nozzle, and the gas holdup in the influencing zone is only 0.3% at an air inlet velocity of 0.2 m/s through the smallest orifice, while it is 4% - 5% in their study. The gas holdup is defined as the ratio of the gas phase volume to the total investigated volume. The gas holdup in their research is more than 10 times higher than that in this study. This can explain the enormous difference in the ave. SS. High ave. SS on the membrane surface was also found by Khalili-Garakani et al. [144], who did simulations with activated sludge at a MLSS concentration of 10 g/L under various aeration intensities. The high values in SS can be attributed to the high viscosity of activated sludge. This is confirmed by the conclusions of Boehm [91], who revealed higher ave. SS in Xanthan solution than in water under the same conditions. Lower ave. SS on the membrane surface was also reported in the literature, as listed in Table 12. Amiraftabi et al. [160] found the ave. SS varied in the range of 0.6 - 0.85 Pa at an air velocity of 1.47 - 6.11 m/s, which is much higher than the air velocity in this study. If air velocity of this range is substituted in Eq. 91 to predict the ave. SS, the predicted values are in the range of 0.35 - 0.85 Pa, which agrees well with the values in their study. Other studies found the ave. SS on FS membrane surfaces in water varied between 0 and 2.2 Pa [58, 110]. Despite relative low values of SS, the ave. SS in this study is still in this range. The low values, as analyzed before, can be attributed to single nozzle and low air flow rate in this study, compared to the operation of MBRs in other studies, where multiple nozzles are used, or the FS modules are intensively aerated.

### Bubble interactions

The interaction and coalescence of many bubbles rising in a narrow channel is a fundamental aspect to understand the hydrodynamics of the aeration process in MBRs. As bubbles are patched in the model bottom or generated through one orifice, they are in-line configured rising in the membrane channel, as illustrated in Fig. 34.

At first, bubbles rise upwards due to buoyancy force through the stagnant liquid and form their wake regions, which can affect the hydrodynamics of the neighboring bubbles significantly. For in-line configured bubbles, the trailing bubble (the bubble behind the leading bubble in Fig. 34 at 0.1s) is attracted in the wake region of the leading bubble (the upmost bubble in Fig. 34 at 0.1 s), resulting in a higher rising velocity of the trailing bubble than that of the leading bubble and a coalescence tendency of this two bubbles. This can be interpreted by the small interval distance between these two bubbles at 0.1 s and the formation of one giant bubble by these two bubbles at 0.15 s in Fig. 34. As time advances, the merged large bubble becomes the leading bubble, and its strong wake interaction promotes the trailing bubble to merge into the leading bubble, hence forming an even larger bubble. As presented in Fig. 34, we can see that from 0.15 to 0.4 s, the coalesced bubble becomes larger and larger and expands in the horizontal direction.

When bubbles rise in line, the trailing bubble gets closer to and finally merges with the preceding bubble, which was observed by Katz and Meneveau [297] experimentally for bubbles with a diameter above 0.349 mm rising in pure water and distilled water. They found that the trailing bubble accelerates and the wake-induced relative motion between the trailing bubble and the leading bubble increases as the trailing bubble becomes closer to the leading bubble, resulting in the collision and coalescence between these two

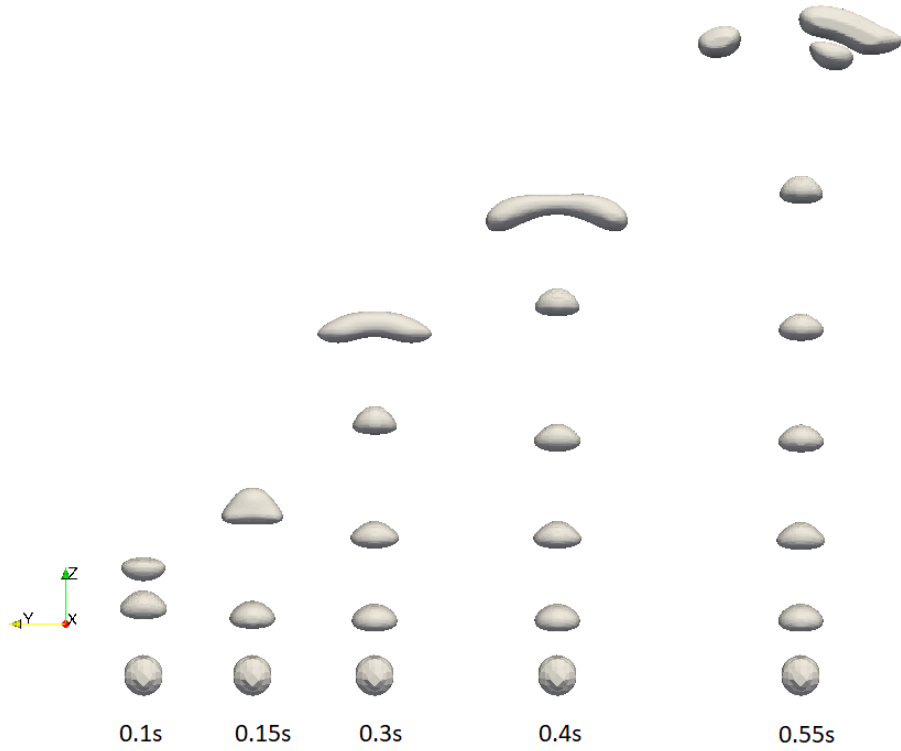


Figure 34: Snapshots of 6 mm bubble swarms at different time steps

bubbles. The acceleration of the trailing bubble was found to be related to the velocity field in the wake region of the leading bubble [298]. De Nevers and Wu [299] attributed this acceleration also to the wake effect of the leading bubble. Lin and Lin[300] concluded that the coalescing interactions are due to the negative pressure in the wake region of the preceding bubble, the circulated upwards flow by the leading bubble and the rheological effect of fluid properties. All of these generates a pushing force to push the trailing bubble to approach the preceding bubble.

Given enough time, small bubbles can form giant bubbles, as shown in Fig. 35, where it presents the snapshot of a large coalesced bubble formed by merging several 6 mm bubbles. This large bubble has a typical spherical-cup shape in front view, while in a side view it looks like a Taylor bubble whose form develops into a bubble body with an oval-shaped nose and a flat tail due to the constraint of the channel and its width spans the channel gap almost completely.

Besides, this giant bubble is followed by a serial of tiny bubbles, as presented in Fig. 35. The occurrence of this type large bubble due to the agglomeration of small bubbles along with tiny bubbles indicates the transition from bubbly flow (small discrete bubbles reasonably distributed in the liquid phase) to slug flow (large Taylor bubbles carrying small bubbles in the liquid phase) based on the classification criteria of two-phase flow regimes in narrow channels [24, 301]. Since the slug bubble is squeezed in the narrow gap, the liquid film between bubbles' rim and membrane walls should be very thin. As a result, SS induced by this bubble is much higher. The local ave. SS of membranes in the box regions only containing this bubble is approximately 1.4 Pa, while the local ave. SS of a 6 mm bubble is only around 1.29 Pa. SS above 1.0 Pa exerted by slug bubbles with a volume over 60 mL was also obtained in the previous study [93], where slug bubbles are regarded to be able to enhance fluxes better due to the high bubble-induced SS and large



Figure 35: Snapshot of a giant bubble with a serial of tiny bubbles in the simulation of 6 mm bubble swarm rising in stagnant water (left: in front view; right: in a side view)

covering area. Despite high SS in the region near individual slug bubbles, the ave. SS induced by slug flow on the whole membrane surfaces is not necessarily higher than that by bubbly flow, as smaller bubbles are more uniform and densely distributed in bubbly flow. In this study slug flow is found to be able to control fouling better, for the ave. SS on the whole membrane surface is higher in slug flow (0.347 Pa) than that in bubbly flow (0.234 Pa) under the same aeration intensity. This finding agrees well with the conclusion from experimental studies on the anti-fouling performance of bubbles in the FS membrane module, where slug bubbles are experimentally found to be more effective and economical than small bubbles under the same aeration operation [92, 165]. Besides, Javid et al. [164] also found that the slug flow enhanced more permeate flux in the FS membrane module than the bubbly flow.

### Bubble size

When the gas flow rate increases, it can be observed a rising trend of the ave. SS on the membrane surface, as shown in Fig. 33. Besides, it is also found out that the bubble frequency and the size of generated bubbles increases with an increase in air flow rate. How do these two parameters affect the SS cannot be derived from Fig. 33. In this section, only the impact of bubble size is investigated by patching bubbles of different size at the same frequency in the bottom of the model. It is found that the rising velocity of bubble swarms are higher than that of single bubbles of the same size. The velocity of 6 mm bubble swarms is double of that of 6 mm single bubble. The acceleration effect of bubble swarms was experimentally observed by Krishna et al. [274], who revealed an increase factor of 3 - 6 in the rising velocity of the large bubble swarm compared to that of a single bubble. This acceleration effect of bubble swarms owes to the trailing bubbles, which can rise with a higher velocity due to the influence of bubble ahead of it. Bubbles in the membrane channel can be treated as a trailing bubble since each of them has a bubble above it. However, the deceleration effect of membrane walls still exists. Despite of the large size, the velocity of a slug bubble is about 20% lower than that of a single 6 mm bubble. The low velocity of the slug bubble is another advantage. As the velocity is low, the retention time of the slug bubble in

membrane channel becomes high. In addition, the SS induced by slug bubble is higher. As a result, the scouring effect of slug bubble on membrane surfaces is more prolonged and stronger.

To describe the effect of bubble size on the ave. SS more accurately, an influence zone with a width of 4 times of bubble size is defined. This zone includes possibly all the bubble swarms that are patched in the bottom and rises due to buoyancy force. The ave. SS is calculated with regard to the membrane surfaces in this influence zone. Fig. 36 illustrates the ave. SS exerted by bubble swarms of different size on membrane surfaces in the defined zone where it reveals a growing trend of SS by increasing bubble size. This is in agreement with findings in previous work taken out by Wei et al. [93].

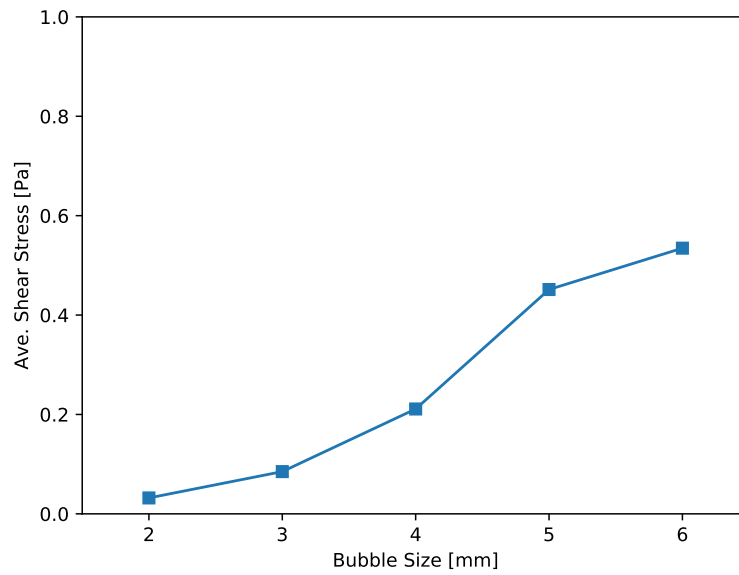


Figure 36: Ave. SS induced by bubble swarms with varying sizes in stagnant water at 7 mm spaced membrane channel

Besides, similar to air flow rate, the ave. SS increases sharply with an increase in bubble size at first, and then slowly. This can be attributed to the relationship between the air flow rate and bubble size. As air flow rate can be calculated based on bubble size and frequency, the effect of bubble size can be converted into the impact of air flow rate when bubbles are patched at the same frequency.

### Bubble frequency

As mentioned above, the bubble frequency and the bubble size increase, as the air flow rate increases. With a focus on the effect of bubble frequency, 6 mm bubbles are patched at the bottom of the model at different time interval ranging from 0.05 to 0.5 s, which corresponds to the bubbling frequency from 20 to 2 Hz. The ave. SS on membrane surfaces in the influence zone of 6 mm bubble swarms is plotted in Fig. 37 against bubbling frequency. From the graph, it can be seen a general rising trend of the ave. SS with bubbling frequency. The possible reason for the rising trend lies in the number of bubbles intended in the membrane channel. Increasing the bubbling frequency, the time interval for patching bubbles reduces, so does the vertical interval of successive bubbles. Thus the number of bubble swarms in the membrane channel increases. As analyzed in Section 4.1.1, the motion of a single bubble affects mainly the flow field around the bubble and the bubble wake region. The SS on membrane surfaces in this influence zone of a single bubble is much higher than other places. As the number of bubbles increases, the sum of the

membrane regions in the influence zone of all bubbles in the membrane channel increases. Thus the ave. SS on membrane surfaces will increase by increasing the sparging frequency. This suggests that membrane fouling can be reduced more at a high bubbling frequency. The beneficial effect of high sparging frequency on membrane SS was observed in the study by Jankhah et al. [302, 303] and by Radaei et al. [304].

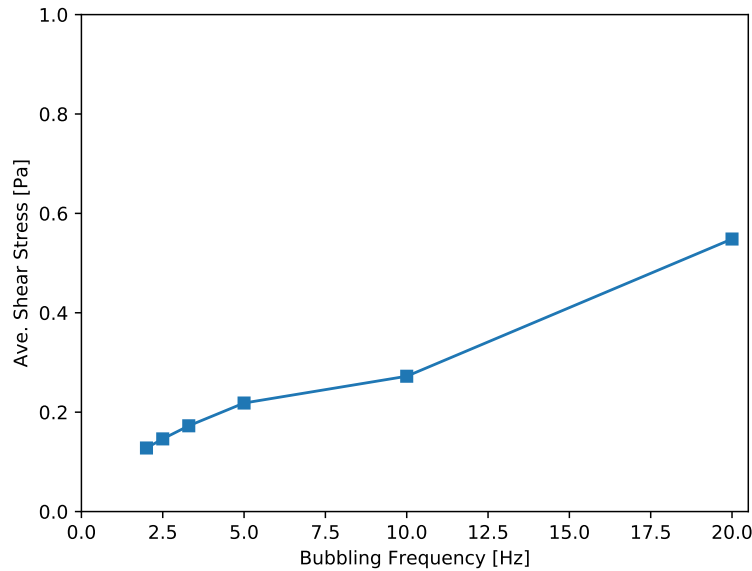


Figure 37: Ave. SS induced by 6 mm bubble swarms with varying patching frequencies at 7 mm spaced membrane channel

Fig. 37 also displays a nearly linear relationship between the ave. SS and bubble frequency. As the frequency increases from 2 to 5 Hz, the number of bubbles in membrane channel in the influence zone for 6 mm bubble, where the ave. SS is calculated, is almost doubled, so does the ave. SS. When successive bubbles have enough distance, and the interaction between bubbles is weak, the ave. SS is directly linked to the number of bubbles in the membrane channel. However, at a high bubbling frequency, the trailing bubbles will be affected by the leading bubble and rise in the wake region of the preceding bubble, when the vertical interval of successive bubbles is smaller than the wake region of the preceding bubble. That means the influence zones of these two bubbles overlap, so do the membrane surfaces in these two influence zones. As a result, the ave. SS does not increase linearly with the number of bubbles in the membrane channel. Thus, when the bubbling frequency increases from 5 to 20 Hz, the ave. SS increases only by a factor of 2, as illustrated in Fig. 37.

### Bubble distribution

As bubbles detach from the nozzle or are patched into the system, they rise in the membrane channel due to the buoyant force. In an air-water system, bubbles with diameters investigated in this study (2 - 6 mm) are surface tension force dominant regime [305], which is characterized by non-rectilinear motion of bubbles such as zigzagging and helical trajectory. In this study, the motion of bubbles in one of the horizontal directions is constrained by membrane walls. Thus, no helical motion of bubbles but only only zigzagging motions can be observed. Fig. 38 exemplarily illustrates the rising paths of 6 mm bubble swarms in different scenarios.



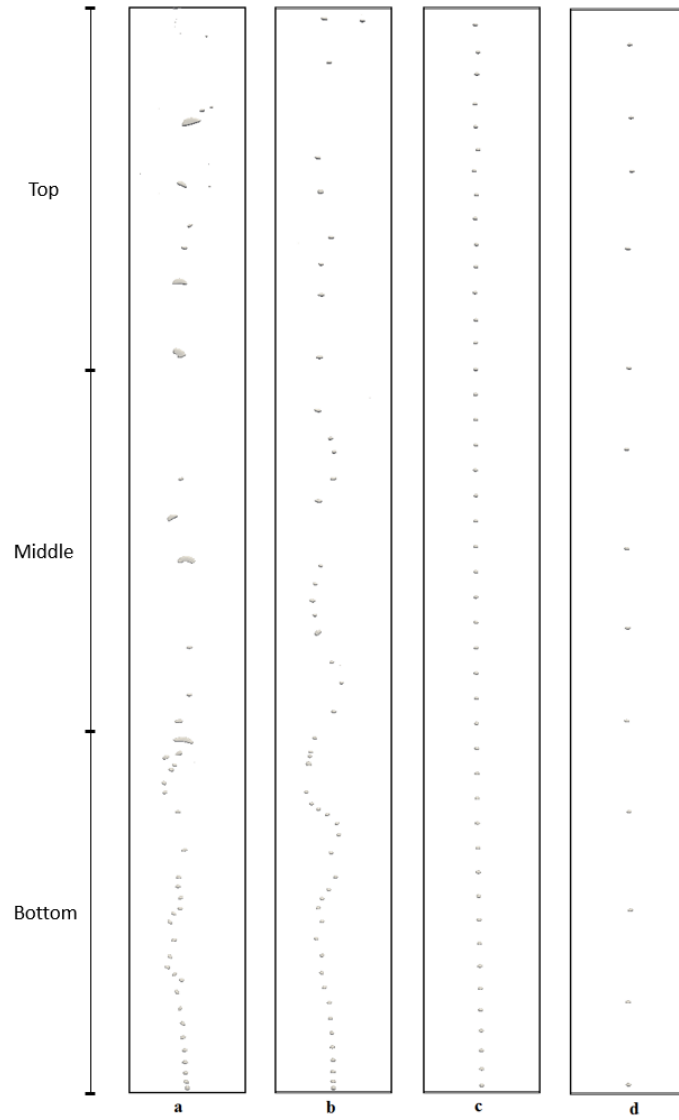


Figure 38: Snapshot of 6 mm bubble swarms in different scenarios: in 6 mm membrane channel with stagnant water, in 7 mm membrane channel with stagnant water, in 7 mm membrane channel with a liquid velocity of 0.3 m/s, and patching in 7 mm membrane channel with a low frequency(from left to right)

At a low frequency (Fig. 38 d) and a high liquid velocity (Fig. 38 c), the trajectory of 6 mm bubble swarms is rectilinear, while at a high frequency (Fig. 38 b) and in narrow membrane channel (Fig.38 a), bubbles rise linearly at first, then begin to oscillate and to deviate from the straight line, and at last exhibit zigzag rising behavior above a certain distance due to their sensitivity to disturbance [306]. The linear path at a high liquid velocity can be attributed to the fact that bubbles tend to rise along with the liquid phase and not drift away when the liquid phase around the bubble flow upwards uniformly. Wake dynamics can induce asymmetric vortexes and play an important role in bubble path instabilities. When bubbles are patched at a low frequency or rise with a high superimposed liquid velocity, the vertical interval of successive bubbles is large, as displayed in Fig. 38. Thus, the trailing bubble might not be affected by the wake region of the proceeding bubble due to the large distance. As a result, bubbles can keep rising linearly. The zigzagging rising paths at high frequencies with no superimposed liquid velocity are explained by the

---

asymmetry generated by the vortexes in the wake region and the associated back diffusion forces [307]. Under the same flow condition, bubbles retain the zigzagging motion in 7 mm spaced membrane channel (as shown in Fig. 38 b), whereas the flow pattern in narrower membrane channel transformed from bubbly flow to slug flow, where bubbles rise in the zigzag path. A maintaining linear trajectory or a zigzagging trajectory of bubbles after a certain linear rising path was also observed in previous studies [269, 307, 308]. However, they did not point out a transform of bubbly flow to slug flow, since none of them investigated the trajectory of bubble swarms rising in narrow channels. The transition of bubbly flow to slug flow occurs owing to the coalescence of bubbles when small bubbles merge into the typical slug bubbles. In a narrower membrane channel, the deceleration effect of membrane walls on large bubbles is more significant. This might lead to more coalescence of bubbles, as the vertical distance between successive bubbles becomes smaller due to the lower rising velocity of bubbles and the fixed patch time.

Apart from the non-linear motion of bubbles, significant shape fluctuations can also be observed in Fig. 38 a and Fig. 38 b, where 6 mm bubbles rise in stagnant water at a higher frequency. When bubbles are in zigzagging motion, they tend to tilt with the surface oscillation, as shown in Fig. 38. The deformation of bubbles in zigzag motion was also observed in previous studies [269, 307] and can be associated with the shedding vortexes behind bubbles and the transformation of the stream-wise vorticity [307]. In Fig. 38 b, bubbles in the bottom part are relatively small and densely distributed, while in the upper part, the volume is roughly doubled and the vertical distance between successive bubbles becomes larger as well. Two bubbles might be merged into one large bubble, and the coalesced bubble is away from the bubbles near it with enough space, so that the impact of wake region of the bubbles above is not strong enough to track the bubbles below. As a result, the coalesced bubbles rising along the zigzagging path in the upper part of the membrane channel. In a narrower membrane channel, even distributed 6 mm bubbles can be observed in the bottom, which is similar to that observed in Fig. 38 b. However, in the middle and upper part of the model, giant bubbles and tiny bubbles exist, as displayed in Fig. 38 a. It can be interpreted that the coalesced bubble of two 6 mm bubbles can not reach the stable state like that in case b, so that the coalesced bubble further merges with other bubbles. As a result, giant bubbles rise in the narrow gap with a very large vertical interval and shear off tiny bubbles during their rise.

The coalesce of bubbles can be seen from Fig. 39, where about 15 among 54 bubbles have a diameter larger than 6 mm when bubbles rise in 7 mm spaced membrane channel at a high bubbling frequency without any superimposed liquid velocity. Bubbles in the interval between 5 and 6 mm are those who do not break up and coalesce. Bubbles with a size less than 5 mm are generated by the breakup process. In 7 mm channel, it is dominant by those bubbles, particularly in the bottom part where large bubbles outnumber small bubbles, as demonstrated in Fig. 38 and Fig. 39. It should be noted that the high percentage might not agree with reality due to the limitations of the algorithm of VOF, which tends to over-predict the merging process between bubbles. When the distance of two separate bubbles is less than one mesh size, it will form one large bubble. In reality, they might get away from each other or even if they contact or colloid with each other, they might bounce away instead of forming one giant bubble. In 7 mm membrane channel, all coalesced bubbles have a diameter in the range of 6 - 8 mm, indicating that most of the large bubbles are generated by merging two 6 mm bubbles. However, in 6 mm membrane channel, the coalesced bubbles are relatively large with a diameter above 8 mm, as displayed in Fig. 39. The largest bubble there

has an equivalent volumetric diameter of 12 mm. To form such a giant bubble, it needs to merge eight bubbles with a diameter of 6 mm.

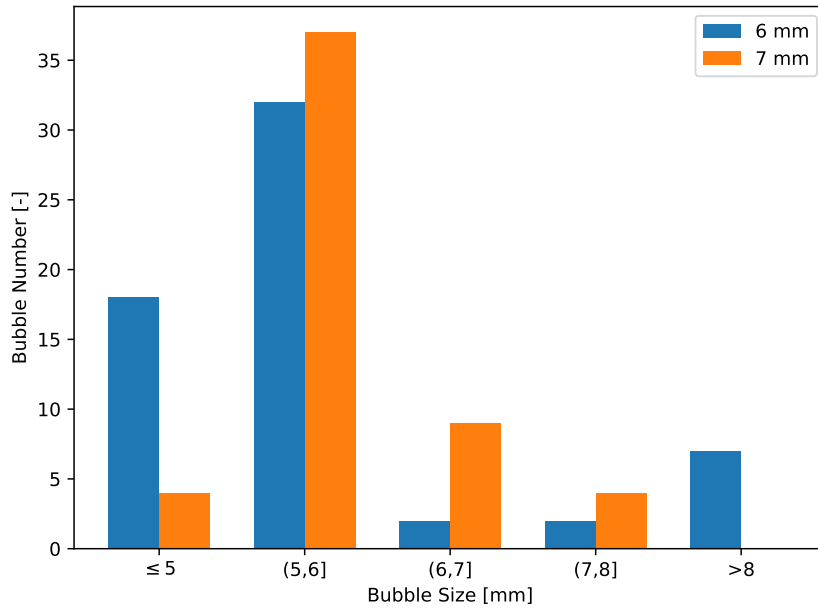


Figure 39: Bubbles size distribution in 6 mm and 7 mm spaced membrane channel

In contrast to bubble coalescence, bubble breakups seem to occur rarely in 7 mm membrane channel since there are less than five bubbles smaller than bubbles with a size less than 5 mm. This can also be attributed to the limitations in the algorithm of VOF. Bubbles are a group of mesh cells with *alpha.water* less than a fixed value, which can be chosen at will from 0 to 1. But this value affects the bubble numbers and bubble size. Bubbles are larger at a high *alpha.water* value and the number of small bubbles is higher as well. In this post-processing, *alpha.water* is 0.5, at which very tiny bubbles cannot be caught. In 7 mm spaced membrane channel, the relative small coalesced bubbles rise in the gap in a relatively stable state, and a few tiny bubbles are generated, while in the narrower membrane channel, the giant bubbles are too large to keep their stable form, so that tiny bubbles are generated from them, as illustrated in Fig. 39. As a result, tiny bubbles in 6 mm membrane channel outnumbered that in 7 mm membrane channel under the same aeration conditions. It should be noted that the actual number of tiny bubbles in 6 mm membrane channel should be higher because bubbles whose size is smaller than 0.5 mm are ignored in the post-process.

Bubble distribution can affect SS distribution as well. An uneven distribution of bubbles tends to cause an uneven distribution of SS, hence an uneven fouling reduction performance [309]. The models are divided into bottom, middle and top parts, which corresponds to the zone in the membrane channel with a height of 0 - 0.5 m, 0.5 - 1.0 m, and 1.0 - 1.5 m, respectively, as displayed in Fig. 38. When 6 mm bubbles are evenly distributed (Fig. 38 c and d), the ave. SS on membrane surfaces in the bottom, middle, and top parts remains nearly the same. When bubbles rise in 7 mm spaced channel at a high frequency without superimposed liquid velocity, in the bottom bubbles are smaller but more densely distributed compared to the loosely distributed large bubbles in the top part, as analyzed above and demonstrated in Fig. 38 b. The ave. SS in the middle and the bottom is more or less the same, while it is about 40% lower in

the top part. The low values of SS might be associated with the low gas hold-up in this part. In the case of 6 mm spaced membrane channel, massive difference in bubbles size, shape, and distribution can be observed between the bottom part and the other parts. Despite the considerable variation of bubbles in the middle part and the bottom part, the ave. SS is roughly the same, whereas the ave. SS in the top part is about 30% higher. High SS in the top part might be caused by the stronger impact of slug bubbles. In one word, densely distributed small bubbles, and slug bubbles can induce a higher SS under the same aeration intensity, and SS distribution is determined by bubble distribution in the FS membrane module. This can be confirmed by Liu et al. [309] who studied on the relationship between SS distribution and bubble distribution in the membrane module.

Since the bubble distribution affects the SS, and bubble distribution is directly affected by the arrangement of aerators, a proper arrangement might be one of the simplest but also the most effective ways to improve the hydraulic conditions in the FS membrane module. In previous studies, the bottom distance between the aerator and the bottom of membrane sheets is proven to be an important design variable in MBRs [39, 110, 159, 309]. As the traveling time of bubble increases, bubbles tend to coalesce and distribute unevenly, as shown in Fig. 38 a and b, where small bubbles are evenly distributed in the bottom part, and large bubbles are unevenly distributed in the top part. In this research, the ave. SS on membrane surfaces in the influence zone with a width of 30 mm is investigated at various bottom distances ranging from 0.1 to 0.5 m. Fig. 40 exemplarily depicts the ave. SS at various bottom distances under the same aeration conditions.

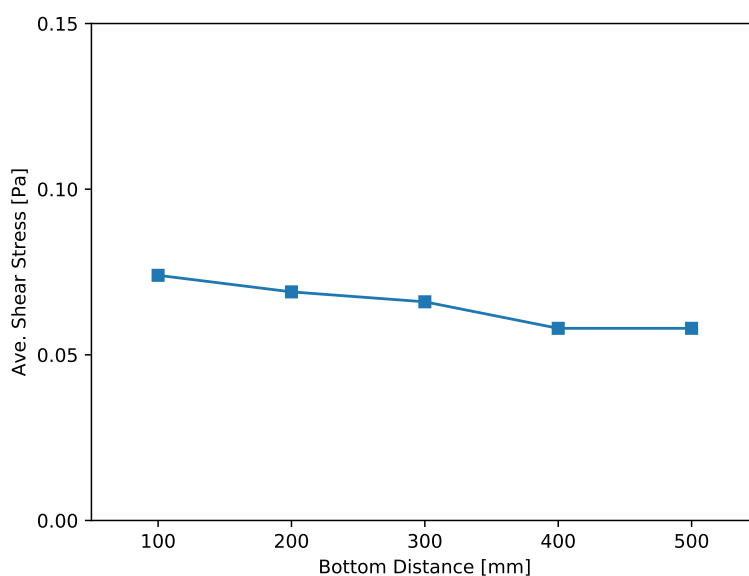


Figure 40: Ave. SS at the same aeration intensity in FS membrane modules with varying distances between the aerators and the bottom of the membrane sheets

The SS is found to decline from 0.074 to 0.058 Pa continually when the bottom distance between the aerator and the membrane sheets bottom increases from 100 to 500 mm, as demonstrated in Fig. 40. However, this is inconsistent with the numerical results for the FS membrane module reported by Liu et al. [309], who found an opposite trend, where the ave. SS in the FS membrane module increases as the bottom distance increases. Other researchers found an optimal bottom distance in the range of 300 - 450 mm [39, 110]. The

nontraditional conclusions in previous studies and this study can be attributed to the different models and different numerical methods used among researchers. Researchers used either lab-scale models or limited nozzles. Due to the limitation in computing resource, there are some assumptions for simplification of the numerical problem in all studies, which do not match the real situation in the aeration process. In this research, only one nozzle is investigated. When this nozzle is far away from the membrane sheet bottom, bubbles in the membrane channel will be loosely distributed, so that some bubbles can not be included in the investigated influence zone. As a result, the ave. SS is lower at a large bottom distance. However, when there are plenty of nozzles in the aeration process, bubbles from one nozzle can leave the influence zone of this nozzle and bubbles from other nozzles can also enter this zone. It faces no problem of losing bubbles during calculating the ave. SS along the membrane surface when bottom distance increases. If so, the ave. SS is probably not sensitive to the bottom distance. This interpretation can be confirmed by the study conducted by Yang et al. [39], who found SS not sensitive to the bottom distance in a full-scale FS membrane module owing to the fact that FS modules are very high for a full-scale application.

---

#### 4.2.2 Superimposed liquid velocity

---

The SS due to the superimposed liquid velocity ranges from 0.17 to 0.95 Pa, as illustrated in the blue line in Fig. 41, where it reveals a general rising trend of SS with an increase in superimposed liquid velocity. In two-phase flow, the contribution of air sparging on ave. SS can be derived from Fig. 41, where the green and orange lines, which represent the ave. SS with aeration of 4 and 6 mm bubble swarms at different upwards liquid velocities, are above the blue line representing the condition without aeration. The difference of the green and the orange lines to the blue line at a specific superimposed liquid velocity represents the contribution of the gas phase on SS. For 6 mm bubble swarms, this contribution of gas phase remains at about 0.5 Pa regardless of liquid velocity. For 4 mm bubble swarms, gas phase contributes more to ave. SS at a low liquid velocity, while at a high liquid velocity of 0.3 m/s, the effect of liquid phase movement on ave. SS dominates, as illustrated in Fig. 41. The ave. SS due to aeration in stagnant water is about 0.2 Pa. At a low liquid velocity, the SS of two-phase flow is roughly equal to the sum of the SS due to the liquid phase and the SS due to the gas phase. However, at a high liquid velocity, the effect of liquid movement is too strong, and the effect of bubbles motion is becoming less significant. At a given aeration intensity, the contribution of the gas phase on the ave. SS can be neglected above a certain superimposed liquid velocity. This conjecture was experimentally observed by Ducom et al. [89] that the ave. SS of two-phase flow is nearly equal to the SS of liquid phase at a liquid velocity above 0.24 m/s regardless of the aeration intensities. The small contribution of aeration at a high superimposed liquid velocity can be attributed to the numbers of bubbles in the membrane channel. The absolute rising velocity of bubbles equals to the sum of the relative rising velocity and the velocity imposed in the liquid phase. For bubbles with the same diameter, the relative rising velocity is more or less the same. As the liquid velocity increases, the absolute rising velocity of individual bubbles increases. At a high liquid velocity, bubbles tend to flow along with the liquid phase. With the same bubbling frequency, the vertical interval between successive bubbles increases, resulting in a decline in the number of bubbles and the retention time of individual bubbles in the membrane channel with a fixed height. While at a low liquid velocity, bubbles tend to oscillate. Despite an increase in the absolute bubble rising velocity, the actual number of bubbles does not reduce much due to the oscillatory movement of bubbles.

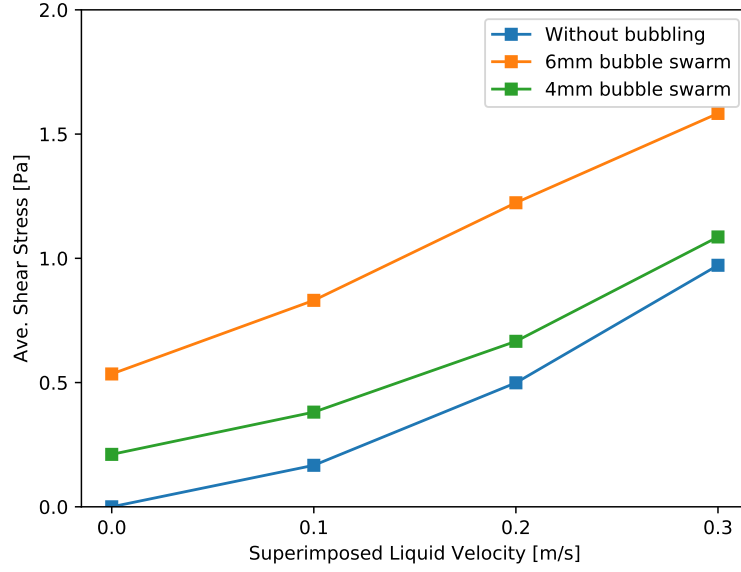


Figure 41: Ave. SS on 7 mm spaced membrane sheets with and without bubbling at various liquid velocities

To investigate whether the SS is due to single-phase flow or due to aeration, Ducom et al. [88, 89] defined a non-dimensional hydrodynamic variable, the parameter  $A$  (Eq. 92), which is the ratio of the ave. SS under aeration to the SS without air bubbling.

$$A = \frac{\overline{\tau_{2p}}}{\tau_{1p}} \quad (92)$$

where,  $\overline{\tau_{2p}}$  is the ave. SS induced by two-phase flow, [Pa], and  $\tau_{1p}$  is the SS induced by liquid phase, [Pa].

Ducom et al. [88, 89] established a positive correlation between the parameter  $A$  and flux enhancement during membrane filtration. The parameter  $A$  is found to be 2.28, 1.33, and 1.11 for 4 mm bubble swarms, 4.98, 2.45 and 1.63 for 6 mm bubble swarms at a superimposed liquid velocity of 0.1, 0.2, and 0.3 m/s. The ratio here represents the contribution of gas phase and liquid phase to the ave. SS directly. When  $A$  is close to 1, the SS induced by the liquid movement is dominant, while the gas phase contributes more than the liquid phase to the ave. SS, when  $A$  is above 2. Thus, at 0.1 m/s liquid velocity, SS induced by the motion of bubble swarms is more significant, while at a higher liquid velocity of 0.3 m/s, SS is mainly generated by the liquid phase, especially for bubble swarms of smaller size. Ducom et al. [88, 89] discussed parameter  $A$  in their study and observed a higher SS ratio at the lowest liquid velocity, which is confirmed in this work.

Since a high cross flow rate is induced with a higher energy input in the FS membrane module and bubble retention time in the membrane channel reduces at a high superimposed liquid velocity, extremely superimposed liquid velocity is not recommended, although the ave. SS is much higher at a high liquid velocity. It is recommended to keep the superimposed liquid velocity around 0.1 m/s in the membrane channel, since the energy consumption is less and the retention time of bubbles is longer due to the oscillation of bubbles, compared to that at a high superimposed liquid velocity.

### 4.2.3 Channel depth

In previous studies, many researchers found an optimal membrane gap distance. Prieske et al. [139–141] reported that SS decreased significantly with an increase in the distance between the two membrane plates and the optimal condition for the FS membrane is found to be 5 mm bubbles with a channel depth of 5 mm. Wang et al. [40, 83] investigated large sized bubbles produced with a novel slug bubbling approach entering membrane sheets with different gap distances, and identified the optimal configuration was at a channel gap of 6 mm in terms of high SS. And in the study conducted by Wei et al. [93], the optimal gap distance between two sheets was around 8 mm, where the max. SS was achieved by slug bubbles with a volume of 60 mL and 100 mL in the FS membrane module for an industrial application. Ndinisa et al. [25, 26] reported the beneficial effect of the narrow membrane channel on fouling control performance, which was found to be reduced by at least 40% when the gap distance increases from 7 to 14 mm. However, the optimal membrane gap distance can not be found in this research in terms of the ave. SS induced by bubble swarms. Fig. 42 demonstrates the impact of membrane channel gap distance on the ave. SS caused by 3 mm and 6 mm bubble swarms, where it reveals a generally unchanged trend of SS by widening the channel gaps in the FS membrane module. The insensitivity of SS to channel distances was observed by Yamanoi and Kageyama [92] in their experiment. They found about a 5% increase in SS by widening the membrane channel from 5 to 7 mm. No significant influence of membrane spacing distance on SS was also found in full-scale MBRs numerically, where SS increased only by 4.2% by narrowing the membrane space from 10 to 7 mm [39].

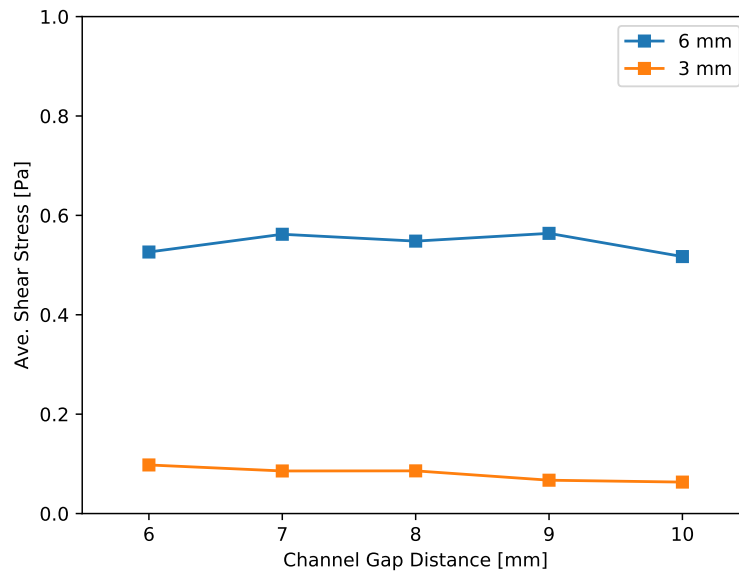


Figure 42: Ave. SS induced by 3 mm or 6 mm bubble swarms in membrane channels with various gap distances

Despite the slight change in SS by increasing membrane channel depth, the optimal gap distance, where the highest SS is achieved, is 6 mm for 3 mm bubble swarms and 7 mm for 6 mm bubble swarms, as illustrated in Fig. 42. This proves that the optimal configuration of the FS membrane module is associated with the operating conditions. Thus, various optimal membrane channels are identified in previous studies, where the operating conditions and membrane models are different. While the ave. SS is not sensitive

to membrane channel distance, as displayed in Fig. 42, the the max. SS induced by individual bubbles decreases by widening the membrane gap, as shown in Fig. 26. Based on the results in terms of the max. SS, membrane channel distance of 6 mm is recommended.

#### 4.2.4 MLSS concentration

In chapter 4.1.4, the effect of bubble motion on local viscosity distribution at the membrane surfaces around the 3 mm bubble single bubble in sludge with a MLSS concentration of 5 g/L is analyzed. As shown in Fig. 31, due to the shear-thinning rheological property of non-Newtonian fluids the low shear region corresponds to the high viscous region, where they are not yet affected by the motion of the 3 mm single bubble in the top part or they are far away from bubble position changed only slightly. And the influence zone of 3 mm single bubble becomes smaller as the MLSS concentration increases (Fig. 31). This is also valid for 3 mm bubble swarms, as shown in Fig. 43, where it displays the viscosity distribution at the whole membrane wall due to the motion of bubble swarms in sludge with different MLSS concentrations ranging from 5 to 25 g/L. In these contour plots, red areas represent regions with a high viscosity, while blue areas represents low viscosity regions. In Fig. 43, the color of the pictures from left to right changes from blue to red, indicating the growth of dynamic viscosity at membrane surfaces, thus a decrease in the impact of 3 mm bubble swarms motion, with an increase of the MLSS concentration. Among all these plots, lines with an extremely low viscosity can be observed in the middle of membrane walls, where bubbles are in line distributed in the membrane channel. The lines represent regions at membrane walls, where the scouring effect of 3 mm bubble swarms are stronger. At the same time, these lines in graphs from left to right become thinner and shorter, indicating that the scouring effect under the same aeration conditions drops as the MLSS concentration increases.

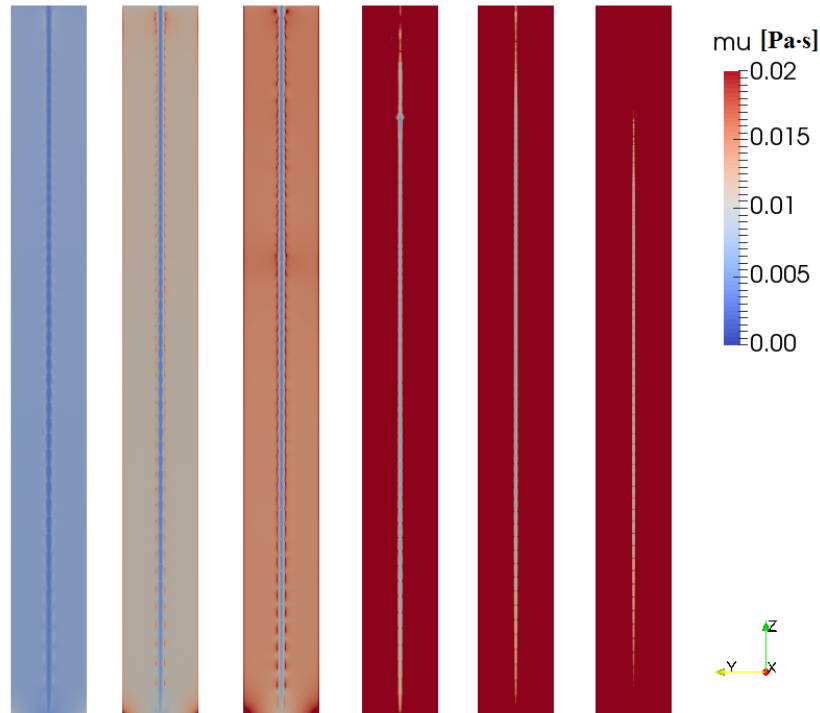


Figure 43: Viscosity distribution around 3 mm bubble swarms at the whole membrane wall in sludge with different MLSS concentrations (from left to right: 5, 8, 10, 15, 20, 25 g/L)



The ave. SS is plotted against the MLSS concentration in Fig. 44. As the MLSS concentration increases, the ave. SS increases, while the ave. shear rate drops continuously, as illustrated in Fig. 44. A similar relationship is found between the max. shear rate induced by the rise of 3 mm single bubble and the MLSS concentration. Since high shear rate is found in a low MLSS concentration and a high shear rate can scour more particles away from membrane fouling, a low MLSS concentration is recommended only with respect to hydraulic conditions. In the literature, little is known in SS or wall shear rate induced by bubble swarms rising in activated sludge in FS membrane modules. Boehm et al. [82, 91] measured SS and wall shear rate in water and in Xanthan solutions, which corresponds to activated sludge with a MLSS concentration of 11.4 g/L. Despite the simplification by replacing activated sludge with Xanthan solution, they found that under the same aeration conditions, the SS is higher in Xanthan solution than in water, while the wall shear rate is higher in water than in Xanthan solution. Their findings agree well with Fig. 44. At a MLSS concentration of 0 g/L, i.e. in water, the ave. SS is lower, while the ave. shear rate is higher than that at a MLSS concentration of 11.4 g/L.

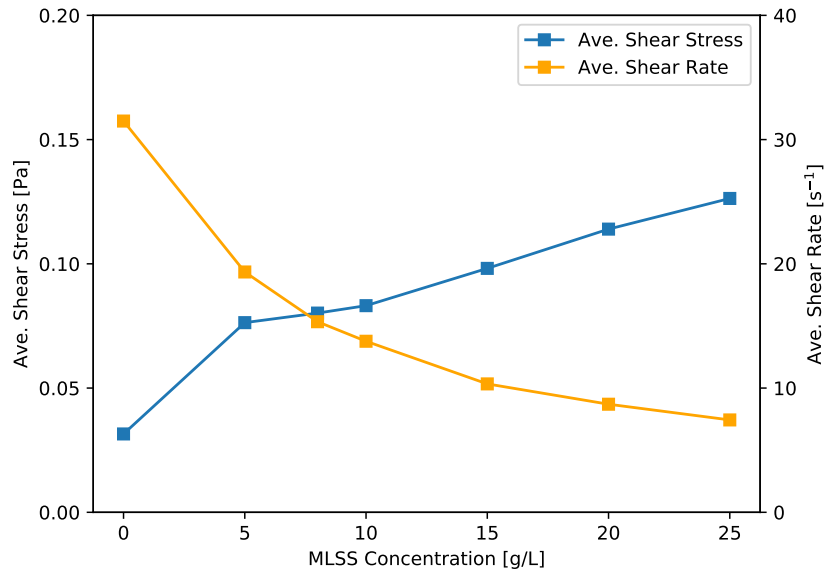


Figure 44: Ave. SS and ave. shear rate of 3 mm bubble swarms rising in sludges

Bubble distribution can affect shear rate distribution, as illustrated in Fig. 45, where a high shear rate occurs always around bubbles and an uneven distribution of bubbles results in an uneven distribution of the shear rate. In water, bubbles are deviated from the straight line and are distributed non-uniformly, while bubbles in sludge rise in a straight line without oscillation. Boehm et al. [91] also found that the oscillation of bubble swarms is negligibly small. They attributed the lack of oscillation to the symmetrical flow field near the bubble in Xanthan solution. A symmetrical flow field near bubbles in sludge is also observed in this study. This might be the reason why bubbles rise in a straight line in sludge.

Besides, it is shown in Fig. 45 that the shear rate around bubbles in water is much higher than that in sludge. High values of shear rate in water are because of the high rising velocity of bubbles in water, as the shear rate is positively linked to the velocity. Due to the viscous effect of sludge, bubbles of the same size rise slowly. As a result, the gas hold-up in sludge is higher than in water under the same aeration

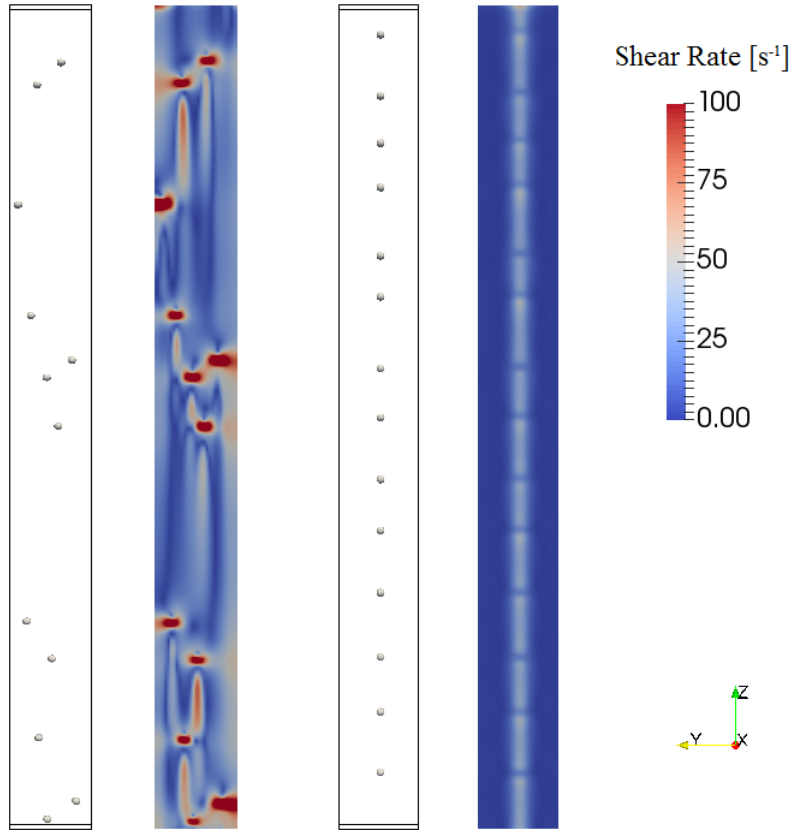


Figure 45: Bubble distribution and shear rate distribution in the top part of the model in water (left two pictures) and in sludge with a MLSS concentration of 5 g/L (right two pictures)

condition. This finding was also reported by Boehm et al. [82, 91], who studied the gas hold-up in water and in Xanthan solution at same air-flow rates and observed a higher gas hold-up in Xanthan than in water. Speaking of bubble rise velocity in sludge with a MLSS concentration of 10 g/L, the velocity of bubble swarms (0.097 m/s) is found to be much higher than that of a single bubble (0.07 m/s). This might be attributed to the acceleration effect of trailing bubbles, when bubbles are in-line reconfigured, as explained in section 4.1.1. The rising velocity of 3 mm bubble swarms is very close to the measured velocity (approximately 0.1 m/s) for single 3 mm bubbles rising in Xanthan solution with a representative MLSS concentration of 11.4 g/L [91, 252]. Maybe they measured the rising velocity of single bubbles with successive bubbles through one inlet. However, they did not describe the quantity of bubbles in the whole membrane channel when measuring the rising velocity of single bubbles. If there is more than one bubble rising in the gap, the measured value of rising velocity might be inaccurate due to the interaction between bubbles.

---

#### 4.3 Discussion referring to research questions

---

**Which parameters can affect the hydrodynamics in an aerated the FS membrane module, and how do they affect SS?**

Fundamental parametric studies are performed under various conditions to investigate the hydrodynamics of the FS membrane module and to predict SS on membrane surfaces. Parameters, e.g. bubble diameter, channel depth, nozzle configuration, superimposed liquid velocity, and the MLSS concentration are found

---

to affect SS and the hydrodynamics in FS modules significantly. Based on the numerical results of this research, the main findings of the influence of these critical parameters are described before, and can be summarized as follows.

- Bubble generation

When air is introduced into the liquid phase, bubbles are generated through orifices. This study conducts simulations of the bubble generation process and their subsequent ascent between membrane sheets, in order to investigate the effect of nozzle size, nozzle position, and airflow rate on bubble size and SS. It is found out that the sizes of generated bubbles are dependent on nozzle size and airflow rate. Using non-dimensional parameters to include all possible hydraulic factors, a model is proposed in this work to predict bubble size based on nozzle configuration and air inlet velocity. The expression fits the numerical data well, and it indicates that coarser bubbles are formed through larger orifices or at a higher airflow rate. As for the ave. SS, the nozzle size does not show a noticeable impact on it, and the nozzle position affects it slightly. When the nozzle locates near the membrane cassette bottom, the ave. SS tends to be slightly higher. While the minor effect of the nozzle is found on the ave. SS, while it depends on inlet velocity greatly. Their relationship agrees well with a power-law correlation, which suggested that the ave. SS increases significantly at a low gas inlet velocity, and it only increases slightly with a further increase in aeration intensity upon a certain critical value.

- Bubble dynamics

Bubble size is a decisive parameter, as bubble shape in a fluid depends greatly on bubble size. In the literature, the general classification of bubble shape regimes is studied for bubbles rising in an unconfined environment. However, the general classifications are not suitable for bubbles rising in a narrow channel. Unlike other researches, non-dimensional parameters  $E$  together with  $Le$  are suggested in this work to apply to estimate bubble shapes, when bubbles rise in an aerated FS membrane channel. Further findings are: At a  $Le$  above 0.8 and  $E$  below 0.55, bubbles present a spherical-cap form. Otherwise, bubbles tend to be ellipsoidal. For bubble swarms, they rise between membrane walls in line. Due to the wake region influence of the leading bubble, the trailing bubbles tend to merge with the preceding bubble. This observation during simulations confirms the experimental observation in the literature. Given enough time, giant Taylor bubbles can be formed by merging small bubbles. A series of tiny bubbles following it can also be observed in the simulation of rising bubble swarms. Thus, due to bubble coalesce and breakups, bubble size of bubble swarms span a wide range.

Bubble shape affects the flow fields around it significantly. The flow fields behind an ellipsoidal bubble and a spherical-cap shaped bubble are found to be different. In this work, helical vortexes could be observed behind a spherical-cap bubble, while no apparent eddies could be identified behind an ellipsoidal bubble. Besides, the wake region of the spherical-cap bubble has a stronger influence. The max. SS occurs in the falling film region for small bubbles, while it is in the wake region with a much higher value for large bubbles. The power-law relationship between SS and bubble size obtained in this work shows clearly the crucial role of bubble size. In bubble swarms, slug bubbles can be found during the simulation. High ave. SS is found near them, but regarding the whole membrane surfaces, slug flow does not necessarily create higher SS than bubbly flow.

For bubble swarms, bubbling frequency and bubble distribution are also investigated in this study. Ave. SS increases nearly linearly with an increase in bubbling frequency. As for bubble distribution, different rising paths of bubbles are presented under different conditions. Under some conditions, uneven distribution of bubbles is found, which leads to uneven distribution of ave. SS, hence an uneven fouling reduction performance.

- Superimposed liquid velocity

Simulations are conducted at different superimposed liquid velocities. Based on the max. SS induced by single bubbles, the forces acting on a particle are analyzed, and the critical particle size is calculated based on forces balance. The calculated critical particle size is found to be very small in the range of  $\mu\text{m}$  under the conditions investigated in this work. A non-dimensional hydrodynamic parameter  $B$  found in the literature to quantities the SS fluctuation is calculated in this study. The parameter  $B$  is found to decline as the superimposed liquid velocity increases or the bubble size increases. For bubble swarms, the ave. SS increases with increasing superimposed liquid velocity with and without bubbling. Another dimensionless hydrodynamic variable, parameter  $A$ , to compare the contribution of air bubbling and liquid movement on the ave. SS, is calculated. It is found that the contribution of air bubbling is more significant at a low upwards liquid velocity, while at a higher liquid velocity of 0.3 m/s, SS is mainly induced by the motion of the liquid phase. Based on the conclusions drawn from simulations of single bubbles and large bubbles, it is recommended to use small bubbles and low upwards liquid velocity, where higher values of parameter  $A$  and parameter  $B$  can be achieved, where is found in the literature to be beneficial for membrane fouling control.

- Gap distance

Gap distance affects the max. SS created by single bubbles significantly, while it has only minor influence on the ave. SS induced by bubble swarms. Given a constant bubble size, the max. SS induced by single bubbles decreases, as the gap distance increases from 6 to 10 mm. For bubbles of different diameters rising in the membrane channel with different membrane gaps, the falling film thickness affects the max. SS more directly than bubble size or channel gaps. A model with a non-dimensional parameter  $Le$  is fitted to predict the max. SS induced by bubbles of different size in various membrane channels. Besides, the max. SS is found in the range of 0.02 to 3.06 Pa, which agrees well with previous studies.

However, the effect of membrane channel depths on the ave. SS is not so noticeable for 3 or 6 mm bubble swarms. Despite the slight change in the ave. SS by increasing membrane channel depth, the highest SS is achieved when 6 mm bubble swarms rise in the narrowest membrane channel.

Therefore, the narrowest membrane channel of 6 mm and the larger bubble size of 6 mm is recommended in this study, since both the max. and ave. SS are highest under this condition. Based on the general trend observed, a further decrease in membrane channel should increase both the max. and ave. SS. However, it is not recommended considering the clogging problem in practical applications of FS membrane modules.

- MLSS concentration

---

Since the MLSS concentration determines the rheological behavior of the non-Newtonian fluid, bubble dynamics and hydrodynamics due to bubble motion in sludge are quite different from that in water. The 3 mm single bubble presents spherical form in sludge, while it has an ellipsoidal shape in the water. The bubble rising velocity of a single bubble is much lower in sludge than in water, and it drops continually when MLSS concentration increases. The rising velocity of bubble swarms is higher than that of a single bubble of the same size. SS turns out to be an inappropriate indicator of membrane fouling control performance when it involves fluid viscosity. Instead, the wall shear rate is used as an indicator. With an increase in the MLSS concentration, the max. shear rate induced by single bubble drops, as well as the ave. shear rate induced by bubble swarms.

Among all of the varied parameters, the superimposed liquid velocity and airflow rate (including different bubble sizes at the same bubbling frequency) have the strongest influence on the ave. SS on the membrane surface. The MLSS concentration or the rheology of non-Newtonian fluid affects the bubble ascent behavior the most.



---

## 5 Summary

---

MBR systems with FS modules, as an established technology, are of widespread in various industrial processes, especially in the field of domestic and industrial wastewater treatment. Since their widespread is limited by membrane fouling, the bioreactors are often aerated despite high energy demand to create SS scouring solids away from membrane surface. The efficient fouling reduction or high SS values in FS modules are because of high velocity gradients along membrane surfaces induced by bubbles' motion in the narrow membrane channels. However, the cleaning effect of aeration in FS membrane modules are still not fully understood due to the complex hydrodynamic flow fields in the multi-phase fluid. Recently, as a modern analysis tool for fluid simulation, CFD has been widely used to investigate the hydrodynamics in MBRs. It provides possibilities for quantification of hydrodynamic characteristics at a fundamental level that could hardly be done experimentally. CFD has been preferred to characterize the gas-liquid two-phase flow in MBRs for the prediction of membrane fouling control performance by aeration.

This work presents a comprehensive review of the CFD-MBR literature on modeling of MBRs by the use of CFD at different scales. It is found that most of the numerical models developed so far for modeling MBRs, particularly involving multi-phase flows are applied only in lab-scale MBR research, while limited simulations are carried out on full scale due to high computing consumption. However, comparing the numerical results from lab-scale and full-scale simulations, it reveals that hydrodynamic parameters in MBRs demonstrated less sensitivity to geometrical parameters (inclusion of baffles, membrane spacing, aerator to module distance, a module to free water surface distance, etc.) in full-scale simulations than that in lab-scale simulations. The literature is also reviewed in different membrane modules: FS modules, HF modules, and tubular membrane modules. The simulations of tubular membrane modules are mainly found in early studies, where its tubular geometry tends to be simplified as a 2D axisymmetric system to save computing resources. 2D models in a cylinder coordinate are also used coupling with self-developed models to predict the permeate flux or nutrient removal efficiency in HF modules by implementing self-developed models, and no such studies are found for FS modules. Simulations of FS modules are mainly in 3 dimensions.

From a literature review on FS modules using CFD, it is concluded that following shortcomings and gaps still exist in the literature. A systematic investigation of the aeration process by use of CFD modeling bubbles' behavior in the FS membrane module lacks yet in the literature. Simulations with the VOF approach to model bubbles' ascent in the FS membrane channel with a sufficient height under bubbling aeration cannot be found in the literature. Little is known about SS on the FS membrane surface induced by bubble swarms, particularly from a hydrodynamic perspective. Conclusions drawn from the literature about the effects of the critical parameters, bubble size, and MLSS concentration, on membrane fouling mitigation are still controversial. Little is done in the literature to examine the impact of nozzle size in the FS module using CFD. Besides, most CFD studies use water instead of activated sludge in their simulations for simplification. Some take the rheological behavior of activated sludge into consideration, but no one conducted simulations with the VOF method, including the settling property of mixed liquor.

In order to overcome the shortcomings and to fill the research gaps mentioned above, this research presents a numerical study of aeration process in the FS membrane module, targeting bubbles' ascent in water and activated sludge in the FS membrane channel with a adequate length, by performing 3D transient simulations using OpenFOAM. This study is carried out to develop validated predictive models of the

---

aeration process in FS membrane modules, including the properties of activated sludge, and to achieve a fundamental understanding of aeration process on membrane fouling control in FS modules, especially from the hydrodynamic perspective. For this purpose, fundamental parametric studies are carried out under different combinations of geometrical and operational parameters in the validated CFD model in interFoam, in order to investigate the hydrodynamics in the FS membrane module, to predict SS on membrane surfaces and to identify the optimal geometrical and operational conditions in the FS membrane module. Besides, interSolidFoam is developed for modeling the gas-liquid-solid pseudo-three-phase flow, accounting for the influence of activated sludge on the hydrodynamic characteristics in FS modules.

Bubble size, channel depth, nozzle configuration, superimposed liquid velocity, and MLSS concentration are investigated here. Based on the numerical results, the geometrical parameters have a minor effect on membrane fouling reduction, when the ave. SS is regarded as an indicator for fouling control performance. Under the same operational conditions, the ave. SS on membrane wall changes only slightly at various nozzle configurations, nozzle positions, and membrane channel depths. Despite the slight change in the ave. SS, the highest value is found, when bubbles rise in the narrowest membrane gap distance investigated. However, if the fluctuation of SS, namely the max. SS, is regarded as an indicator, channel depth is a powerful parameter, and the best performance (the highest value of the max. SS) is achieved at the narrowest membrane channel. Therefore, for a better membrane fouling control, the narrowest membrane channel of 6 mm is recommended for FS modules. Unlike geometrical parameters, the operational parameters have a significant influence on the hydrodynamics in FS modules. MLSS concentration, namely the activated sludge concentration, affects bubble dynamics the most. Due to the viscous effect, bubbles present a more spherical form and rise much slowly in sludge than in water. It is also found out that wall shear rate is a more appropriate indicator for fouling control performance than SS when the fluid involves varying viscosity. As the MLSS concentration increases, wall shear rates decrease, so does the membrane fouling mitigation. Airflow rate and superimposed liquid velocity have the strongest influence on the ave. SS. A general rising trend of the ave. SS is observed with an increase in superimposed liquid velocity or an increase in airflow rate, including the increase of bubble size under the same bubbling frequency.

Gas-liquid two-phase flow is investigated in detail in this work, and only the rising behaviors of 3 mm single bubble and bubble swarms in sludge with different MLSS concentrations are simulated. The future effort remains to be done with the developed solver (interSolidFoam) to perform simulations of bubbles of different size rising in sludge under various conditions, e.g. at various liquid velocities, in membrane channels with different depths, at various gas flow rates, etc. It is hoped that more validated CFD models will be carried out in interSolidFoam for three-phase flow in MBRs to gain a better understanding of the critical optimizing/designing parameters in MBRs, especially when it involves the rheological and settling behavior of activated sludge. As the constitute of activated sludge and its treatment process are different, the parameters of the sludge model of different sludge type are different. For one specific activated sludge, the sludge model can be determined through experiments and then be implemented in interSolidFoam. In this way, interSolidFoam can calculate bubble dynamics in fluid representing one specific activated sludge.

Apart from the simulation of MBRs, the presented CFD solver can be potentially used to investigate the DO concentration distribution in activated sludge around bubbles by incorporating an oxygen mass transfer model into interSolidFoam. In this way, another function of the aeration process in MBRs to provide biomass with sufficient oxygen can be simulated and investigated numerically. To make the system



---

closer to the real situation, it would be of interest to couple ASM into the source term of momentum equation to account for the biological consumption of DO. However, it should be noted that these coupled models will further increase computational consumption and therefore limit the simulation at a small scale. Moreover, to evaluate the predictive capability of the model, it needs to be validated against experimental data. In this work, the modeled terminal rising velocity of single bubbles is validated against measured bubble rising velocity from the literature. And a satisfying agreement is achieved. However, due to the complexity of bubble swarms and activated sludge, the measurement techniques to determine of the rising velocity of bubble swarms in water, especially in activated sludge, are still limited. As no experimental studies on bubble terminal rising velocity of bubble swarms of different sizes rising in activated sludge have yet been reported in the literature, future experimental research is necessary on this topic to validate the numerical model.



---

## References

---

- [1] A. T. Besha, A. Y. Gebreyohannes, R. A. Tufa, D. N. Bekele, E. Curcio, and L. Giorno, “Removal of emerging micropollutants by activated sludge process and membrane bioreactors and the effects of micropollutants on membrane fouling: A review”, *Journal of environmental chemical engineering*, vol. 5, no. 3, pp. 2395–2414, 2017.
- [2] M. Kraume and A. Drews, “Membrane bioreactors in waste water treatment–status and trends”, *Chemical engineering & technology*, vol. 33, no. 8, pp. 1251–1259, 2010.
- [3] F. Meng, S. Zhang, Y. Oh, Z. Zhou, H.-S. Shin, and S.-R. Chae, “Fouling in membrane bioreactors: An updated review”, *Water research*, vol. 114, pp. 151–180, 2017.
- [4] X. Hao, J. Li, M. van Loosdrecht, and T. Li, “A sustainability-based evaluation of membrane bioreactors over conventional activated sludge processes”, *Journal of Environmental Chemical Engineering*, vol. 6, no. 2, pp. 2597–2605, 2018.
- [5] K. Xiao, Y. Xu, S. Liang, T. Lei, J. Sun, X. Wen, H. Zhang, C. Chen, and X. Huang, “Engineering application of membrane bioreactor for wastewater treatment in china: Current state and future prospect”, *Frontiers of Environmental Science & Engineering*, vol. 8, no. 6, pp. 805–819, 2014.
- [6] J. Sun, P. Liang, X. Yan, K. Zuo, K. Xiao, J. Xia, Y. Qiu, Q. Wu, S. Wu, X. Huang, *et al.*, “Reducing aeration energy consumption in a large-scale membrane bioreactor: Process simulation and engineering application”, *Water research*, vol. 93, pp. 205–213, 2016.
- [7] B. Verrecht, S. Judd, G. Guglielmi, C. Brepols, and J. Mulder, “An aeration energy model for an immersed membrane bioreactor”, *Water research*, vol. 42, no. 19, pp. 4761–4770, 2008.
- [8] P. Le-Clech, “Membrane bioreactors and their uses in wastewater treatments”, *Applied microbiology and biotechnology*, vol. 88, no. 6, pp. 1253–1260, 2010.
- [9] F. Schmitt and K.-U. Do, “Prediction of membrane fouling using artificial neural networks for wastewater treated by membrane bioreactor technologies: Bottlenecks and possibilities”, *Environmental Science and Pollution Research*, vol. 24, no. 29, pp. 22 885–22 913, 2017.
- [10] S. J. Judd, “The status of industrial and municipal effluent treatment with membrane bioreactor technology”, *Chemical Engineering Journal*, vol. 305, pp. 37–45, 2016.
- [11] P. Hillis, *Membrane technology in water and wastewater treatment*. Royal Society of Chemistry, 2007.
- [12] P. Krzeminski, L. Leverette, S. Malamis, and E. Katsou, “Membrane bioreactors—a review on recent developments in energy reduction, fouling control, novel configurations, LCA and market prospects”, *Journal of Membrane Science*, vol. 527, pp. 207–227, 2017.
- [13] RESEARCH and MARKETS, *Global membrane bioreactor systems market size, market share, application analysis, regional outlook, growth trends, key players, competitive strategies and forecasts*, <https://www.researchandmarkets.com/reports/4564636/global-membrane-bioreactor-systems-market-size/>, Accessed October 13, 2018.
- [14] S. Judd, *The MBR book: principles and applications of membrane bioreactors for water and wastewater treatment*. Elsevier, 2010.
- [15] A. Santos and S. Judd, “The commercial status of membrane bioreactors for municipal wastewater”, *Separation Science and Technology*, vol. 45, no. 7, pp. 850–857, 2010.
- [16] TheMBRSite, *When MBR sludge goes bad*, <https://www.thembrsite.com/features/when-sludge-in-membrane-bioreactors-goes-bad-may-2010/>, Accessed October 03, 2019.
- [17] Z. Wang, J. Ma, C. Y. Tang, K. Kimura, Q. Wang, and X. Han, “Membrane cleaning in membrane bioreactors: A review”, *Journal of membrane science*, vol. 468, pp. 276–307, 2014.

- 
- [18] X. Du, Y. Wang, G. Leslie, G. Li, and H. Liang, "Shear stress in a pressure-driven membrane system and its impact on membrane fouling from a hydrodynamic condition perspective: A review", *Journal of Chemical Technology & Biotechnology*, vol. 92, no. 3, pp. 463–478, 2017.
- [19] Z. Cui and T. Taha, "Enhancement of ultrafiltration using gas sparging: A comparison of different membrane modules", *Journal of Chemical Technology & Biotechnology: International Research in Process, Environmental & Clean Technology*, vol. 78, no. 2-3, pp. 249–253, 2003.
- [20] Z. Cui, S. Chang, and A. Fane, "The use of gas bubbling to enhance membrane processes", *Journal of Membrane Science*, vol. 221, no. 1-2, pp. 1–35, 2003.
- [21] I.-S. Chang and S. J. Judd, "Air sparging of a submerged MBR for municipal wastewater treatment", *Process Biochemistry*, vol. 37, no. 8, pp. 915–920, 2002.
- [22] T. Chiu and A. James, "Critical flux enhancement in gas assisted microfiltration", *Journal of membrane science*, vol. 281, no. 1-2, pp. 274–280, 2006.
- [23] J. Wang, A. G. Fane, and J. W. Chew, "Effect of bubble characteristics on critical flux in the microfiltration of particulate foulants", *Journal of Membrane Science*, vol. 535, pp. 279–293, 2017.
- [24] Y. Wibisono, E. Cornelissen, A. Kemperman, W. Van Der Meer, and K. Nijmeijer, "Two-phase flow in membrane processes: A technology with a future", *Journal of membrane science*, vol. 453, pp. 566–602, 2014.
- [25] N. Ndinisa, A. Fane, and D. Wiley, "Fouling control in a submerged flat sheet membrane system: Part I—bubbling and hydrodynamic effects", *Separation science and technology*, vol. 41, no. 7, pp. 1383–1409, 2006.
- [26] N. Ndinisa, A. Fane, D. Wiley, and D. Fletcher, "Fouling control in a submerged flat sheet membrane system: Part II—two-phase flow characterization and CFD simulations", *Separation Science and Technology*, vol. 41, no. 7, pp. 1411–1445, 2006.
- [27] S. Jankhah and P. R. Bérubé, "Pulse bubble sparging for fouling control", *Separation and Purification Technology*, vol. 134, pp. 58–65, 2014.
- [28] R. Iglesias, P. Simón, L. Moragas, A. Arce, and I. Rodriguez-Roda, "Cost comparison of full-scale water reclamation technologies with an emphasis on membrane bioreactors", *Water Science and Technology*, vol. 75, no. 11, pp. 2562–2570, 2017.
- [29] B. Verrecht, T. Maere, I. Nopens, C. Brepols, and S. Judd, "The cost of a large-scale hollow fibre MBR", *Water Research*, vol. 44, no. 18, pp. 5274–5283, 2010.
- [30] H. K. Versteeg and W. Malalasekera, *An introduction to computational fluid dynamics: the finite volume method*. Pearson Education, 2007.
- [31] A. M. Karpinska and J. Bridgeman, "CFD-aided modelling of activated sludge systems—A critical review", *Water research*, vol. 88, pp. 861–879, 2016.
- [32] A. N. Kochevsky, "Possibilities of simulation of fluid flows using the modern CFD software tools", *arXiv preprint physics/0409104*, 2004.
- [33] E. Amini, M. R. Mehrnia, S. M. Mousavi, and N. Mostoufi, "Experimental study and computational fluid dynamics simulation of a full-scale membrane bioreactor for municipal wastewater treatment application", *Industrial & engineering chemistry research*, vol. 52, no. 29, pp. 9930–9939, 2013.
- [34] P. Sousa, A. Soares, E. Monteiro, and A. Rouboa, "A CFD study of the hydrodynamics in a desalination membrane filled with spacers", *Desalination*, vol. 349, pp. 22–30, 2014.
- [35] G. Fimbres-Weihs and D. Wiley, "Review of 3D CFD modeling of flow and mass transfer in narrow spacer-filled channels in membrane modules", *Chemical Engineering and Processing: Process Intensification*, vol. 49, no. 7, pp. 759–781, 2010.

- 
- [36] R. Sengur, G. Deveci, R. Kaya, T. Turken, S. Guclu, D. Y. Imer, and I. Koyuncu, "CFD modeling of submerged membrane bioreactors (sMBRs): A review", *Desalination and Water Treatment*, vol. 55, no. 7, pp. 1747–1761, 2015.
- [37] X. Liu, Y. Wang, T. D. Waite, and G. Leslie, "Numerical simulations of impact of membrane module design variables on aeration patterns in membrane bioreactors", *Journal of Membrane Science*, vol. 520, pp. 201–213, 2016.
- [38] N. Ratkovich, M. Hunze, and I. Nopens, "Hydrodynamic study of a hollow fiber membrane system using experimentally and numerically derived surface shear stresses", *Multiphase Science and Technology*, vol. 24, no. 1, pp. 47–66, 2012.
- [39] M. Yang, M. Liu, D. Yu, J. Zheng, Z. Wu, S. Zhao, J. Chang, and Y. Wei, "Numerical simulation of scaling-up for AEC-MBRs regarding membrane module configurations and cyclic aeration modes", *Bioresource Technology*, vol. 245, pp. 933–943, 2017.
- [40] B. Wang, K. Zhang, and R. W. Field, "Novel aeration of a large-scale flat sheet MBR: A CFD and experimental investigation", *AIChE Journal*, vol. 64, no. 7, pp. 2721–2736, 2018.
- [41] M. W. D. Brannock, H. De Wever, Y. Wang, and G. Leslie, "Computational fluid dynamics simulations of MBRs: Inside submerged versus outside submerged membranes", *Desalination*, vol. 236, no. 1-3, pp. 244–251, 2009.
- [42] O. Kulesha, Z. Maletskyi, and H. Ratnaweera, "State-of-the-art of membrane flux enhancement in membrane bioreactor", *Cogent Engineering*, p. 1489700, 2018.
- [43] J. M. Hassan, W. S. Mohammed, T. A. Mohamed, and W. H. Alawee, "CFD simulation for manifold with tapered longitudinal section", *International Journal of Emerging Technology and Advanced Engineering*, vol. 4, no. 2, pp. 28–35, 2014.
- [44] J. C. K. Tong, E. M. Sparrow, and J. P. Abraham, "Geometric strategies for attainment of identical outflows through all of the exit ports of a distribution manifold in a manifold system", *Applied Thermal Engineering*, vol. 29, no. 17-18, pp. 3552–3560, 2009.
- [45] B. F. McNamara, J. Layne, M. Hyre, D. J. Kinnear, and C. B. Bott, "Evaluation of three full-scale grit removal processes using CFD modeling", *Proceedings of the Water Environment Federation*, vol. 2012, no. 9, pp. 6008–6030, 2012.
- [46] A. Sonnenburg and U. Theilen, "Sandabscheidungen in einer kompakten Walzensandfanganlage Herleitung der physikalischen Wirkmechanismen mithilfe von CFD", *KA Abwasser, Abfall*, vol. 56, 2009.
- [47] A. Sonnenburg and W. Urban, "Der Leitwandsandfang Entwicklung eines neuen, unbelüfteten Sandfangs zur Erreichung hoher Abscheidegrade von Feinsanden", *KA Abwasser, Abfall*, vol. 63, 2016.
- [48] R. W. Samstag, E. A. Wicklein, R. D. Reardon, R. J. Leetch, R. Parks, and C. D. Groff, "Field and CFD analysis of jet aeration and mixing", *Proceedings of the Water Environment Federation*, vol. 2012, no. 12, pp. 4113–4139, 2012.
- [49] H. Xie, J. Yang, Y. Hu, H. Zhang, Y. Yang, K. Zhang, X. Zhu, Y. Li, and C. Yang, "Simulation of flow field and sludge settling in a full-scale oxidation ditch by using a two-phase flow CFD model", *Chemical Engineering Science*, vol. 109, pp. 296–305, 2014.
- [50] Y. Le Moullec, C. Gentric, O. Potier, and J. P. Leclerc, "CFD simulation of the hydrodynamics and reactions in an activated sludge channel reactor of wastewater treatment", *Chemical Engineering Science*, vol. 65, no. 1, pp. 492–498, 2010.
- [51] Y. Le Moullec, O. Potier, C. Gentric, and J. P. Leclerc, "Activated sludge pilot plant: Comparison between experimental and predicted concentration profiles using three different modelling approaches", *Water Res*, vol. 45, no. 10, pp. 3085–97, 2011.
-

- 
- [52] Y. Le Moullec, C. Gentric, O. Potier, and J. Leclerc, "Comparison of systemic, compartmental and CFD modelling approaches: Application to the simulation of a biological reactor of wastewater treatment", *Chemical engineering science*, vol. 65, no. 1, pp. 343–350, 2010.
- [53] U. Rehman, T. Maere, M. Vesvikar, Y. Amerlinck, and I. Nopens, "Hydrodynamic-biokinetic model integration applied to a full-scale WWTP", in *9th IWA World Water Congress and exhibition*.
- [54] L. Lei and J. Ni, "Three-dimensional three-phase model for simulation of hydrodynamics, oxygen mass transfer, carbon oxidation, nitrification and denitrification in an oxidation ditch", *Water Res*, vol. 53, pp. 200–14, 2014.
- [55] I. Takacs, G. G. Patry, and D. Nolasco, "A dynamic model of the clarification-thickening process", *Water research*, vol. 25, no. 10, pp. 1263–1271, 1991.
- [56] R. W. Samstag, J. J. Ducoste, A. Griborio, I. Nopens, D. J. Batstone, J. D. Wicks, S. Saunders, E. A. Wicklein, G. Kenny, and J. Laurent, "CFD for wastewater treatment: An overview", *Water Sci Technol*, vol. 74, no. 3, pp. 549–63, 2016.
- [57] N. Ratkovich, W. Horn, F. Helmus, S. Rosenberger, W. Naessens, I. Nopens, and T. R. Bentzen, "Activated sludge rheology: A critical review on data collection and modelling", *Water research*, vol. 47, no. 2, pp. 463–482, 2013.
- [58] M. Yang, D. Yu, M. Liu, L. Zheng, X. Zheng, Y. Wei, F. Wang, and Y. Fan, "Optimization of MBR hydrodynamics for cake layer fouling control through CFD simulation and RSM design", *Bioresour Technol*, vol. 227, pp. 102–111, 2017.
- [59] S.-H. Yoon, *Membrane bioreactor processes: principles and applications*. CRC press, 2015.
- [60] A. Van Bentem, N. Nijman, P. Schyns, and C. Petri, "MBR Varsseveld: 5 years of operational experience", *Water Practice and Technology*, vol. 5, no. 1, wpt2010013, 2010.
- [61] R. W. BAKER, *Membrane Technology and Applications*. John Wiley and Sons Ltd, 2012.
- [62] T. Melin and R. Rautenbach, *Membranverfahren: Grundlagen der Modul- und Anlagenauslegung*. Springer-Verlag, 2007.
- [63] P. Krzeminski, J. A. Gil, A. F. van Nieuwenhuijzen, J. H. van der Graaf, and J. B. van Lier, "Flat sheet or hollow fibrecomparison of full-scale membrane bio-reactor configurations", *Desalination and Water Treatment*, vol. 42, no. 1-3, pp. 100–106, 2012.
- [64] I. Bodik, A. Blt'áková, L. Danová, and S. Sedlek, "Comparison of flat-sheet and hollow-fiber membrane modules in municipal wastewater treatment.", *Polish Journal of Environmental Studies*, vol. 18, no. 3, 2009.
- [65] A. Santos, W. Ma, and S. J. Judd, "Membrane bioreactors: Two decades of research and implementation", *Desalination*, vol. 273, no. 1, pp. 148–154, 2011.
- [66] B. E. Logan and M. Elimelech, "Membrane-based processes for sustainable power generation using water", *Nature*, vol. 488, no. 7411, p. 313, 2012.
- [67] P. L. McCarty, J. Bae, and J. Kim, *Domestic wastewater treatment as a net energy producer—can this be achieved?*, 2011.
- [68] Z. Wang and Z. Wu, "A review of membrane fouling in MBRs: Characteristics and role of sludge cake formed on membrane surfaces", *Separation Science and Technology*, vol. 44, no. 15, pp. 3571–3596, 2009.
- [69] A. Drews, "Membrane fouling in membrane bioreactorscharacterisation, contradictions, cause and cures", *Journal of membrane science*, vol. 363, no. 1-2, pp. 1–28, 2010.
- [70] J. C. Crittenden, R. R. Trussell, D. W. Hand, K. J. Howe, and G. Tchobanoglous, *MWH's water treatment: principles and design*. John Wiley & Sons, 2012.

- 
- [71] S. Rosenberger, H. Evenblij, S. Te Poele, T. Wintgens, and C. Laabs, “The importance of liquid phase analyses to understand fouling in membrane assisted activated sludge processesix case studies of different european research groups”, *Journal of Membrane Science*, vol. 263, no. 1-2, pp. 113–126, 2005.
- [72] M. Pourbozorg, T. Li, and A. W. Law, “Effect of turbulence on fouling control of submerged hollow fibre membrane filtration”, *Water research*, vol. 99, pp. 101–111, 2016.
- [73] H. Monclus, S. Zacharias, A. Santos, M. Pidou, and S. Judd, “Criticality of flux and aeration for a hollow fiber membrane bioreactor”, *Separation Science and Technology*, vol. 45, no. 7, pp. 956–961, 2010.
- [74] F. Kavousi, E. Syron, M. Semmens, and E. Casey, “Hydrodynamics and gas transfer performance of confined hollow fibre membrane modules with the aid of computational fluid dynamics”, *Journal of Membrane Science*, vol. 513, pp. 117–128, 2016.
- [75] N. C. Pearson, S. L. Waters, J. M. Oliver, and R. J. Shipley, “Multiphase modelling of the effect of fluid shear stress on cell yield and distribution in a hollow fibre membrane bioreactor”, *Biomechanics and modeling in mechanobiology*, vol. 14, no. 2, pp. 387–402, 2015.
- [76] S. Z. Abdullah, H. E. Wray, P. R. Bérubé, and R. C. Andrews, “Distribution of surface shear stress for a densely packed submerged hollow fiber membrane system”, *Desalination*, vol. 357, pp. 117–120, 2015.
- [77] R. Kaya, G. Deveci, T. Turken, R. Sengur, S. Guclu, D. Y. Koseoglu-Imer, and I. Koyuncu, “Analysis of wall shear stress on the outside-in type hollow fiber membrane modules by CFD simulation”, *Desalination*, vol. 351, pp. 109–119, 2014.
- [78] F. Zamani, A. W. Law, and A. Fane, “Hydrodynamic analysis of vibrating hollow fibre membranes”, *Journal of membrane science*, vol. 429, pp. 304–312, 2013.
- [79] X. Yang, H. Yu, R. Wang, and A. G. Fane, “Optimization of microstructured hollow fiber design for membrane distillation applications using CFD modeling”, *Journal of membrane science*, vol. 421, pp. 258–270, 2012.
- [80] L. Xia, A. W.-K. Law, and A. G. Fane, “Hydrodynamic effects of air sparging on hollow fiber membranes in a bubble column reactor”, *Water research*, vol. 47, no. 11, pp. 3762–3772, 2013.
- [81] L. Böhm, A. Drews, and M. Kraume, “Bubble induced shear stress in flat sheet membrane systemsserial examination of single bubble experiments with the electrodiffusion method”, *Journal of membrane science*, vol. 437, pp. 131–140, 2013.
- [82] L. Böhm and M. Kraume, “Fluid dynamics of bubble swarms rising in Newtonian and non-Newtonian liquids in flat sheet membrane systems”, *Journal of Membrane Science*, vol. 475, pp. 533–544, 2015.
- [83] B. Wang, K. Zhang, and R. W. Field, “Slug bubbling in flat sheet MBRs: Hydrodynamic optimization of membrane design variables through computational and experimental studies”, *Journal of Membrane Science*, vol. 548, pp. 165–175, 2018.
- [84] O. Le Berre and G. Daufin, “Skimmilk crossflow microfiltration performance versus permeation flux to wall shear stress ratio”, *Journal of Membrane Science*, vol. 117, no. 1-2, pp. 261–270, 1996.
- [85] C. Chan, P. Bérubé, and E. Hall, “Shear profiles inside gas sparged submerged hollow fiber membrane modules”, *Journal of Membrane Science*, vol. 297, no. 1-2, pp. 104–120, 2007.
- [86] C. Chan, P. Bérubé, and E. Hall, “Relationship between types of surface shear stress profiles and membrane fouling”, *Water research*, vol. 45, no. 19, pp. 6403–6416, 2011.
- [87] H. E. Wray, R. C. Andrews, and P. R. Bérubé, “Surface shear stress and membrane fouling when considering natural water matrices”, *Desalination*, vol. 330, pp. 22–27, 2013.
-



- 
- [88] G. Ducom, F. Puech, and C. Cabassud, “Air sparging with flat sheet nanofiltration: A link between wall shear stresses and flux enhancement”, *Desalination*, vol. 145, no. 1-3, pp. 97–102, 2002.
- [89] G. Ducom, F.-P. Puech, and C. Cabassud, “Gas/liquid two-phase flow in a flat sheet filtration module: Measurement of local wall shear stresses”, *The Canadian Journal of Chemical Engineering*, vol. 81, no. 3-4, pp. 771–775, 2003.
- [90] L. Böhm, S. Jankhah, J. Tihon, P. R. Bérubé, and M. Kraume, “Application of the electrodiffusion method to measure wall shear stress: Integrating theory and practice”, *Chemical Engineering & Technology*, vol. 37, no. 6, pp. 938–950, 2014.
- [91] L. P. Böhm, “Comparison of single bubble and bubble swarm behavior in narrow gaps inside flat sheet membrane modules”, Thesis, 2015.
- [92] I. Yamanoi and K. Kageyama, “Evaluation of bubble flow properties between flat sheet membranes in membrane bioreactor”, *Journal of membrane science*, vol. 360, no. 1-2, pp. 102–108, 2010.
- [93] P. Wei, K. Zhang, W. Gao, L. Kong, and R. Field, “CFD modeling of hydrodynamic characteristics of slug bubble flow in a flat sheet membrane bioreactor”, *Journal of membrane science*, vol. 445, pp. 15–24, 2013.
- [94] X. Liu, Y. Wang, T. D. Waite, and G. Leslie, “Numerical simulation of bubble induced shear in membrane bioreactors: Effects of mixed liquor rheology and membrane configuration”, *Water Research*, vol. 75, pp. 131–145, 2015.
- [95] K. Essemiani, G. Ducom, C. Cabassud, and A. Liné, “Spherical cap bubbles in a flat sheet nanofiltration module: Experiments and numerical simulation”, *Chemical Engineering Science*, vol. 56, no. 21, pp. 6321–6327, 2001.
- [96] M. W. D. Brannock, Y. Wang, and G. Leslie, “Optimising mixing in full-scale MBRs: CFD modelling and validation”, *Water*, vol. 35, no. 2, pp. 114–115, 2008.
- [97] M. Brannock, Y. Wang, and G. Leslie, “Mixing characterisation of full-scale membrane bioreactors: CFD modelling with experimental validation”, *Water Research*, vol. 44, no. 10, pp. 3181–3191, 2010.
- [98] M. W. D. Brannock, Y. Wang, and G. Leslie, “Evaluation of full-scale membrane bioreactor mixing performance and the effect of membrane configuration”, *Journal of Membrane Science*, vol. 350, no. 1-2, pp. 101–108, 2010.
- [99] M. Brannock, G. Leslie, Y. Wang, and S. Buethorn, “Optimising mixing and nutrient removal in membrane bioreactors: CFD modelling and experimental validation”, *Desalination*, vol. 250, no. 2, pp. 815–818, 2010.
- [100] N. Ratkovich, C. C. V. Chan, P. R. Berube, and I. Nopens, “Experimental study and CFD modelling of a two-phase slug flow for an airlift tubular membrane”, *Chemical Engineering Science*, vol. 64, no. 16, pp. 3576–3584, 2009.
- [101] N. Ratkovich, C. C. V. Chan, P. R. Berube, and I. Nopens, “Investigation of the effect of viscosity on slug flow in airlift tubular membranes in search of a sludge surrogate”, *Water Science and Technology*, vol. 61, no. 7, pp. 1801–1809, 2010.
- [102] N. Ratkovich, T. R. Bentzen, P. R. Bérubé, N. Heinen, and M. R. Rasmussen, “Energy consumption related to shear stress for membrane bioreactors used for wastewater treatment”, in *Proceedings of the 24th International Conference on Efficiency, Cost, Optimization, Simulation and Environmental Impact of Energy Systems, ECOS 2011*, 2011, pp. 2195–2206.
- [103] N. Ratkovich, C. C. V. Chan, P. R. Berube, and I. Nopens, “Analysis of shear stress and energy consumption in a tubular airlift membrane system”, *Water Science & Technology*, vol. 64, no. 1, p. 189, 2011.



- 
- [104] T. R. Bentzen, N. Ratkovich, S. Madsen, J. C. Jensen, S. N. Bak, and M. R. Rasmussen, "Analytical and numerical modelling of Newtonian and non-Newtonian liquid in a rotational cross-flow MBR", *Water Sci Technol*, vol. 66, no. 11, pp. 2318–27, 2012.
- [105] W. Naessens, T. Maere, N. Ratkovich, S. Vedantam, and I. Nopens, "Critical review of membrane bioreactor models - Part 2: Hydrodynamic and integrated models", *Bioresource Technology*, vol. 122, pp. 107–118, 2012.
- [106] N. Ratkovich, T. R. Bentzen, and M. R. Rasmussen, "Energy consumption in terms of shear stress for two types of membrane bioreactors used for municipal wastewater treatment processes", *Archives of Thermodynamics*, vol. 33, no. 2, pp. 85–106, 2012.
- [107] N. Ratkovich, C. C. Chan, T. R. Bentzen, and M. R. Rasmussen, "Experimental and CFD simulation studies of wall shear stress for different impeller configurations and MBR activated sludge", *Water Sci Technol*, vol. 65, no. 11, pp. 2061–70, 2012.
- [108] N. Ratkovich and T. R. Bentzen, "Comparison of four types of membrane bioreactor systems in terms of shear stress over the membrane surface using computational fluid dynamics", *Water Sci Technol*, vol. 68, no. 12, pp. 2534–44, 2013.
- [109] X. Liu, Y. Wang, T. D. Waite, and G. Leslie, "Fluid structure interaction analysis of lateral fibre movement in submerged membrane reactors", *Journal of Membrane Science*, vol. 504, pp. 240–250, 2016.
- [110] M. Yang, Y. Wei, X. Zheng, F. Wang, X. Yuan, J. Liu, N. Luo, R. Xu, D. Yu, and Y. Fan, "CFD simulation and optimization of membrane scouring and nitrogen removal for an airlift external circulation membrane bioreactor", *Bioresource Technology*, vol. 219, pp. 566–575, 2016.
- [111] A. J. Karabelas, C. P. Koutsou, and S. G. Yiantsios, "Direct numerical simulation of flow in spacer-filled channels: Effect of spacer geometrical characteristics", *Journal of Membrane Science*, vol. 291, no. 1-2, pp. 53–69, 2007.
- [112] S. S. Bucs, R. V. Linares, J. O. Marston, A. I. Radu, J. S. Vrouwenvelder, and C. Picioreanu, "Experimental and numerical characterization of the water flow in spacer-filled channels of spiral-wound membranes", *Water research*, vol. 87, pp. 299–310, 2015.
- [113] N. Horstmeyer, T. Lippert, D. Schön, F. Schlederer, C. Picioreanu, K. Achterhold, F. Pfeiffer, and J. E. Drewes, "CT scanning of membrane feed spacers Impact of spacer model accuracy on hydrodynamic and solute transport modeling in membrane feed channels", *Journal of Membrane Science*, vol. 564, pp. 133–145, 2018.
- [114] B. Gu, C. S. Adjiman, and X. Y. Xu, "The effect of feed spacer geometry on membrane performance and concentration polarisation based on 3D CFD simulations", *Journal of Membrane Science*, vol. 527, pp. 78–91, 2017.
- [115] Y. Yu, Z. Yang, and Y. Duan, "Structure and flow calculation of cake layer on microfiltration membranes", *Journal of Environmental Sciences*, vol. 56, pp. 95–101, 2017.
- [116] L. Fortunato, A. Qamar, Y. Wang, S. Jeong, and T. Leiknes, "In-situ assessment of biofilm formation in submerged membrane system using optical coherence tomography and computational fluid dynamics", *Journal of Membrane Science*, vol. 521, pp. 84–94, 2017.
- [117] A. A. Poostchi, M. Bayat, M. Rezaei, E. Amini, and M. R. Mehrnia, "Formation of pre-coating dynamic membrane on mesh filter by cross-flow filtration of PAC–water suspension in a bioreactor: Experimental and modeling", *Desalination and Water Treatment*, vol. 55, no. 1, pp. 17–27, 2015.
- [118] M. Rahimi, S. Madaeni, and K. Abbasi, "CFD modeling of permeate flux in cross-flow microfiltration membrane", *Journal of membrane science*, vol. 255, no. 1-2, pp. 23–31, 2005.
- [119] C. Kang, J. Hua, J. Lou, W. Liu, and E. Jordan, "Bridging the gap between membrane bio-reactor (MBR) pilot and plant studies", *Journal of Membrane Science*, vol. 325, no. 2, pp. 861–871, 2008.

- 
- [120] X. Yan, Q. Wu, J. Sun, P. Liang, X. Zhang, K. Xiao, and X. Huang, "Hydrodynamic optimization of membrane bioreactor by horizontal geometry modification using computational fluid dynamics", *Bioresource Technology*, vol. 200, pp. 328–334,
- [121] X. Yan, K. Xiao, S. Liang, T. Lei, P. Liang, T. Xue, K. Yu, J. Guan, and X. Huang, "Hydraulic optimization of membrane bioreactor via baffle modification using computational fluid dynamics", *Bioresource technology*, vol. 175, pp. 633–637, 2015.
- [122] Y. Wang, M. Brannock, S. Cox, and G. Leslie, "CFD simulations of membrane filtration zone in a submerged hollow fibre membrane bioreactor using a porous media approach", *Journal of Membrane Science*, vol. 363, no. 1-2, pp. 57–66, 2010.
- [123] N. Ratkovich, M. Hunze, H. Futselaar, and I. Nopens, "Use of CFD to model and optimize the hydrodynamics of an airlift MBR side-stream module", *Proceedings of the Water Environment Federation*, vol. 2009, no. 14, pp. 2812–2818, 2009.
- [124] Y. Wang, M. Brannock, and G. Leslie, "Membrane bioreactors: Overview of the effects of module geometry on mixing energy", *Asia-Pacific Journal of Chemical Engineering*, vol. 4, no. 3, pp. 322–333, 2009.
- [125] Q. Wu, X. Yan, K. Xiao, J. Guan, T. Li, P. Liang, and X. Huang, "Optimization of membrane unit location in a full-scale membrane bioreactor using computational fluid dynamics", *Bioresource technology*, vol. 249, pp. 402–409, 2018.
- [126] J. Saalbach and M. Hunze, "Flow structures in MBR-tanks", *Water Science and Technology*, vol. 57, no. 5, pp. 699–705, 2008.
- [127] E. Amini, M. R. Mehrnia, S. M. Mousavi, H. Azami, and N. Mostoufi, "Investigating the effect of sparger configuration on the hydrodynamics of a full-scale membrane bioreactor using computational fluid dynamics", *RSC Advances*, vol. 5, no. 127, pp. 105 218–105 226, 2015.
- [128] N. Liu, Q. Zhang, G.-L. Chin, E.-H. Ong, J. Lou, C.-W. Kang, W. Liu, and E. Jordan, "Experimental investigation of hydrodynamic behavior in a real membrane bio-reactor unit", *Journal of Membrane Science*, vol. 353, no. 1-2, pp. 122–134, 2010.
- [129] Z. Cui, J. Wang, H. Zhang, H. H. Ngo, H. Jia, W. Guo, F. Gao, G. Yang, and D. Kang, "Investigation of backwashing effectiveness in membrane bioreactor (MBR) based on different membrane fouling stages", *Bioresource technology*, vol. 269, pp. 355–362, 2018.
- [130] X. Guo, Y. Wang, H. Zhang, P. Li, and C. Ma, "Numerical and experimental investigation for cleaning process of submerged outside-in hollow fiber membrane", *Water Science and Technology*, wst2017228, 2017.
- [131] Z. Wang, K. Su, T. Shu, and W. Wang, "Numerical simulation of filtration performance in submerged membrane bioreactors: Effect of particle packed structure", *Water Science and Technology*, wst2017426, 2017.
- [132] T. Taha, W. L. Cheong, R. W. Field, and Z. F. Cui, "Gas-sparged ultrafiltration using horizontal and inclined tubular membranesA CFD study", *Journal of Membrane Science*, vol. 279, no. 1-2, pp. 487–494, 2006.
- [133] T. Taha and Z. F. Cui, "CFD modelling of slug flow in vertical tubes", *Chemical Engineering Science*, vol. 61, no. 2, pp. 676–687, 2006.
- [134] Z. Trad, C. Vial, J. P. Fontaine, and C. Larroche, "CFD optimization of a submerged membrane reactor for biohydrogen production", in *Lecture Notes in Engineering and Computer Science*, vol. 2, 2014, pp. 595–600.
- [135] Z. Trad, C. Vial, J. P. Fontaine, and C. Larroche, "Modeling of hydrodynamics and mixing in a submerged membrane bioreactor", *Chemical Engineering Journal*, vol. 282, pp. 77–90, 2015.

- 
- [136] S. D. Vlaev and I. Tsibranska, "Shear stress generated by radial flow impellers at bioreactor integrated membranes", *Theoretical Foundations of Chemical Engineering*, vol. 50, no. 6, pp. 959–968, 2016.
- [137] S. Ahmed, M. T. Seraji, J. Jahedi, and M. Hashib, "CFD simulation of turbulence promoters in a tubular membrane channel", *Desalination*, vol. 276, no. 1-3, pp. 191–198, 2011.
- [138] M. K. Moraveji, B. Sajjadi, and R. Davarnejad, "CFD simulation of hold-up and liquid circulation velocity in a membrane airlift reactor", *Theoretical Foundations of Chemical Engineering*, vol. 46, no. 3, pp. 266–273, 2012.
- [139] H. Prieske, A. Drews, and M. Kraume, "Prediction of the circulation velocity in a membrane bioreactor", *Desalination*, vol. 231, no. 1-3, pp. 219–226, 2008.
- [140] H. Prieske, L. Böhm, A. Drews, and M. Kraume, "Optimised hydrodynamics for membrane bioreactors with immersed flat sheet membrane modules", *Desalination and Water Treatment*, vol. 18, no. 1-3, pp. 270–276, 2010.
- [141] A. Drews, H. Prieske, E.-L. Meyer, G. Senger, and M. Kraume, "Advantageous and detrimental effects of air sparging in membrane filtration: Bubble movement, exerted shear and particle classification", *Desalination*, vol. 250, no. 3, pp. 1083–1086, 2010.
- [142] A. Khalili, M. R. Mehrnia, N. Mostoufi, and M. Sarrafzadeh, "Flow characteristics in an airlift membrane bioreactor", *Chemical Product and Process Modeling*, vol. 4, no. 5, 2009.
- [143] D. C. Kim and K. Y. Chung, "Numerical simulation of aeration flow phenomena in bench-scale submerged flat membrane bioreactor", *Journal of Industrial and Engineering Chemistry*, 2018.
- [144] A. Khalili-Garakani, M. R. Mehrnia, N. Mostoufi, and M. H. Sarrafzadeh, "Analyze and control fouling in an airlift membrane bioreactor: CFD simulation and experimental studies", *Process Biochemistry*, vol. 46, no. 5, pp. 1138–1145, 2011.
- [145] N. Hilal, O. O. Ogunbiyi, and N. J. Miles, "Experimental investigation on the separation of bentonite using ceramic membranes: Effect of turbulence promoters", *Separation Science and Technology*, vol. 43, no. 2, pp. 286–309, 2008.
- [146] A. Joki, Z. Zavargo, Z. ere, and M. Teki, "The effect of turbulence promoter on cross-flow micro-filtration of yeast suspensions: A response surface methodology approach", *Journal of Membrane Science*, vol. 350, no. 1-2, pp. 269–278, 2010.
- [147] S. Popovi and M. N. Teki, "Twisted tapes as turbulence promoters in the microfiltration of milk", *Journal of membrane science*, vol. 384, no. 1-2, pp. 97–106, 2011.
- [148] Z. Cao, D. Wiley, and A. Fane, "CFD simulations of net-type turbulence promoters in a narrow channel", *Journal of Membrane Science*, vol. 185, no. 2, pp. 157–176, 2001.
- [149] D. E. Wiley and D. F. Fletcher, "Computational fluid dynamics modelling of flow and permeation for pressure-driven membrane processes", *Desalination*, vol. 145, no. 1-3, pp. 183–186, 2002.
- [150] S. K. Karode and A. Kumar, "Flow visualization through spacer filled channels by computational fluid dynamics I.: Pressure drop and shear rate calculations for flat sheet geometry", *Journal of Membrane science*, vol. 193, no. 1, pp. 69–84, 2001.
- [151] F. Xie, J. Wang, and J. Liu, "CFD simulation of micro-channel turbulence promoters in a flat sheet membrane bioreactor", *Chinese Journal of Environmental Engineering*, vol. 9, no. 8, pp. 3841–3846, 2015.
- [152] F. Xie, J. Wang, and J. Liu, "Effects of aeration rate on hydrodynamic performance of SMBR equipped with micro-channel turbulence promoters", *Chinese Journal of Environmental Engineering*, vol. 9, no. 9, pp. 4391–4397, 2015.

- 
- [153] F. Xie, W. Chen, J. Wang, and J. Liu, "Fouling characteristics and enhancement mechanisms in a submerged flat-sheet membrane bioreactor equipped with micro-channel turbulence promoters with micro-pores", *Journal of Membrane Science*, vol. 495, pp. 361–371, 2015.
- [154] F. Xie, W. Chen, J. Wang, and J. Liu, "CFD and experimental studies on the hydrodynamic performance of submerged flat-sheet membrane bioreactor equipped with micro-channel turbulence promoters", *Chemical Engineering and Processing: Process Intensification*, vol. 99, pp. 72–79, 2016.
- [155] F. Xie, J. Liu, J. Wang, and W. Chen, "Computational fluid dynamics simulation and particle image velocimetry experimentation of hydrodynamic performance of flat-sheet membrane bioreactor equipped with micro-channel turbulence promoters with micro-pores", *Korean Journal of Chemical Engineering*, vol. 33, no. 7, pp. 2169–2178, 2016.
- [156] F. Xie, H. Ge, J. Liu, W. Chen, and H. Song, "CFD and experimental studies the effect of micro-channel turbulence promoter installation on the hydrodynamic performance of submerged flat-sheet membrane bioreactor", *Chemical Engineering and Processing - Process Intensification*, vol. 127, pp. 28–35, 2018.
- [157] R. Iwatsu, J. M. Hyun, and K. Kuwahara, "Analyses of three-dimensional flow calculations in a driven cavity", *Fluid dynamics research*, vol. 6, no. 2, p. 91, 1990.
- [158] R. Ibrahim, "Improving energy efficiency and fouling mitigation for membrane bioreactor in al-rustamiyah sewage treatment plant based on hydrodynamics", *International Journal of Environmental Science and Technology*, vol. 15, no. 11, pp. 2369–2380, 2018.
- [159] Q. Zhang, Y. Fan, Y. Wei, D. Yu, and R. Xu, "Simulation and optimization of airlift external circulation membrane bioreactor using CFD", *Membrane Science and Technology*, vol. 4, p. 028, 2013.
- [160] M. S. Amiraftebi, N. Mostoufi, M. Hosseinzadeh, and M. R. Mehrnia, "Reduction of membrane fouling by innovative method (injection of air jet)", *Journal of Environmental Health Science and Engineering*, vol. 12, no. 1, 2014.
- [161] M. Bayat, M. R. Mehrnia, N. Mostoufi, and M. R. Hamaneh, "Investigating wastewater treatment in MBRs using computational fluid dynamics", *Journal of Environmental Studies*, vol. 41, no. 1, pp. 1–12, 2015.
- [162] A. Boyle-Gotla, P. Jensen, S. Yap, M. Pidou, Y. Wang, and D. Batstone, "Dynamic multidimensional modelling of submerged membrane bioreactor fouling", *Journal of Membrane Science*, vol. 467, pp. 153–161, 2014.
- [163] J. Wu and C. He, "Effect of cyclic aeration on fouling in submerged membrane bioreactor for wastewater treatment", *Water research*, vol. 46, no. 11, pp. 3507–3515, 2012.
- [164] S. M. Javid, M. Passandideh-Fard, A. Faezian, and M. Goharimanesh, "Slug and bubble flows in a flat sheet ultrafiltration module: Experiments and numerical simulation", *International Journal of Multiphase Flow*, vol. 91, pp. 39–50, 2017.
- [165] K. Zhang, P. Wei, M. Yao, R. W. Field, and Z. Cui, "Effect of the bubbling regimes on the performance and energy cost of flat sheet MBRs", *Desalination*, vol. 283, pp. 221–226, 2011.
- [166] L. Bohm, H. Prieske, and M. Kraume, "Fluid dynamic optimization of flat sheet membrane modules—Movement of bubbles in vertical channels", *Chem. Eng. Trans*, vol. 32, pp. 1501–1507, 2013.
- [167] B. Jajuee, A. Margaritis, D. Karamanev, M. A. Bergougnou, and S. A. M. Karimian, "Measurements and CFD simulations of gas holdup and liquid velocity in novel aircraft membrane contactor", *AIChE Journal*, vol. 52, no. 12, pp. 4079–4089, 2006.
- [168] K. Praneeth, S. Moulik, P. Vadthya, S. K. Bhargava, J. Tardio, and S. Sridhar, "Performance assessment and hydrodynamic analysis of a submerged membrane bioreactor for treating dairy industrial effluent", *Journal of hazardous materials*, vol. 274, pp. 300–313, 2014.

- 
- [169] J. Günther, P. Schmitz, C. Albasi, and C. Lafforgue, "A numerical approach to study the impact of packing density on fluid flow distribution in hollow fiber module", *Journal of membrane science*, vol. 348, no. 1-2, pp. 277–286, 2010.
- [170] J. Günther, D. Hobbs, C. Albasi, C. Lafforgue, A. Cockx, and P. Schmitz, "Modeling the effect of packing density on filtration performances in hollow fiber microfiltration module: A spatial study of cake growth", *Journal of membrane science*, vol. 389, pp. 126–136, 2012.
- [171] L. Zhuang, H. Guo, P. Wang, and G. Dai, "Study on the flux distribution in a dead-end outside-in hollow fiber membrane module", *Journal of Membrane Science*, vol. 495, pp. 372–383, 2015.
- [172] K. B. Lim, P. C. Wang, H. An, and S. C. M. Yu, "Computational studies for the design parameters of hollow fibre membrane modules", *Journal of Membrane Science*, vol. 529, pp. 263–273, 2017.
- [173] S. M. Nowee, M. Taherian, M. Salimi, and S. M. Mousavi, "Modeling and simulation of phenol removal from wastewater using a membrane contactor as a bioreactor", *Applied Mathematical Modelling*, vol. 42, pp. 300–314, 2017.
- [174] S. Buethorn, D. Volmering, K. Vossenkaul, T. Wintgens, M. Wessling, and T. Melin, "CFD simulation of single-and multi-phase flows through submerged membrane units with irregular fiber arrangement", *Journal of membrane science*, vol. 384, no. 1-2, pp. 184–197, 2011.
- [175] H. Sanaeepur, O. Hosseinkhani, A. Kargari, A. E. Amooghin, and A. Raisi, "Mathematical modeling of a time-dependent extractive membrane bioreactor for denitrification of drinking water", *Desalination*, vol. 289, pp. 58–65, 2012.
- [176] R. Ghidossi, J. Daurelle, D. Veyret, and P. Moulin, "Simplified CFD approach of a hollow fiber ultrafiltration system", *Chemical Engineering Journal*, vol. 123, no. 3, pp. 117–125, 2006.
- [177] Z. Tao, S. Xing, C. Li, G. Qiu, and R. Tian, "Three-dimensional CFD simulation of gas-liquid two phase flow in SMBR", *Chinese Journal of Environmental Engineering*, vol. 8, no. 6, pp. 2251–2256, 2014.
- [178] J. Wang, Y. Wu, L. Luo, H. Zhang, Z. Xiao, and G. Huan, "CFD simulation and optimization of internal hydrodynamic characteristics and aerating distribution in membrane bioreactor", *Tumu Jianzhu yu Huanjing Gongcheng/Journal of Civil, Architectural and Environmental Engineering*, vol. 36, no. 2, pp. 119–125, 2014.
- [179] L. Martinelli, C. Guigui, and A. Line, "Characterisation of hydrodynamics induced by air injection related to membrane fouling behaviour", *Desalination*, vol. 250, no. 2, pp. 587–591, 2010.
- [180] A. Sofia, W. Ng, and S. Ong, "Engineering design approaches for minimum fouling in submerged MBR", *Desalination*, vol. 160, no. 1, pp. 67–74, 2004.
- [181] P. Culfaz, M. Wessling, and R. G. Lammertink, "Fouling behavior of microstructured hollow fiber membranes in submerged and aerated filtrations", *Water research*, vol. 45, no. 4, pp. 1865–1871, 2011.
- [182] E. Braak, C. Albasi, D. Anne-Archard, S. Schetrite, and M. Alliet, "Impact of aeration on mixed liquor in submerged-membrane bioreactors for wastewater treatment", *Chemical Engineering & Technology*, vol. 40, no. 8, pp. 1453–1465, 2017.
- [183] S. L. Xing, Z. L. Tao, J. M. Niu, R. Tian, and C. L. Li, "Effect of aeration conditions on the flow field in the submerged membrane bioreactor", in *Applied Mechanics and Materials*, Trans Tech Publ, vol. 535, 2014, pp. 539–546.
- [184] T. Li, H. Nagaoka, T. Itonaga, and Y. Nakahara, "Estimation of shear stress working on submerged vertically set hollow fibre membrane in MBRs", *Journal of Water Supply: Research and Technology - AQUA*, vol. 59, no. 2-3, pp. 191–197, 2010.
- [185] N. Ratkovich, "Industrial wastewater treatment using CFD simulation of an anaerobic membrane bio reactor (AnMBR)", *Boletín Técnico*, vol. 54, no. 3, 2016.
-



- 
- [186] S. D. Vlaev, I. Tsibranska, and D. Dzhonova-Atanasova, "Hydrodynamic characterization of dual-impeller submerged membrane bioreactor relevant to single-use bioreactor options", *Chemical Engineering Research and Design*, vol. 132, pp. 930–941, 2018.
- [187] Y. Liu, G. He, X. Liu, G. Xiao, and B. Li, "CFD simulations of turbulent flow in baffle-filled membrane tubes", *Separation and Purification Technology*, vol. 67, no. 1, pp. 14–20, 2009.
- [188] Y.-L. Li, P.-J. Lin, and K.-L. Tung, "CFD analysis of fluid flow through a spacer-filled disk-type membrane module", *Desalination*, vol. 283, pp. 140–147, 2011.
- [189] J. Yang, S. Vedantam, H. Spanjers, I. Nopens, and J. B. van Lier, "Analysis of mass transfer characteristics in a tubular membrane using CFD modeling", *Water research*, vol. 46, no. 15, pp. 4705–4712, 2012.
- [190] J. D. Anderson and J. Wendt, *Computational fluid dynamics*. Springer, 1995, vol. 206.
- [191] J. Blazek, *Computational fluid dynamics: principles and applications*. Butterworth-Heinemann, 2015.
- [192] F. Moukalled, L. Mangani, M. Darwish, *et al.*, *The finite volume method in computational fluid dynamics: An Advanced Introduction with OpenFOAM and Matlab*. Springer, 2016.
- [193] A. N. Kolmogorov, "Dissipation of energy in isotropic turbulence", in *Dokl. Akad. Nauk SSSR*, vol. 32, 1941, pp. 325–327.
- [194] A. N. Kolmogorov, "The local structure of turbulence in incompressible viscous fluid for very large reynolds numbers", in *Dokl. Akad. Nauk SSSR*, vol. 30, 1941, pp. 299–303.
- [195] S. B. Pope and S. B. Pope, *Turbulent flows*. Cambridge university press, 2000.
- [196] M. Schäfer, *Computational engineering: introduction to numerical methods*. Springer, 2006.
- [197] G. P. Keir, "Coupled modelling of hydrodynamics and mass transfer in membrane filtration", Deakin University, Tech. Rep., 2012.
- [198] T. Chung, *Computational fluid dynamics*. Cambridge university press, 2010.
- [199] R. R. Hwang and S.-Y. Jaw, "Second-order closure turbulence models: Their achievements and limitations", in *Proc. Natl. Sci. Counc. ROC(A)*, vol. 22, 1998, pp. 703–722.
- [200] J. Boussinesq, "Essa sur latheories des eaux courantes. Memoires presentes par divers savants a lAcademic des Sciences de lInstitut National de France", *Tome XXIII*, no. 1, 1877.
- [201] A. Fluent, "12.0 theory guide", *Ansys Inc*, vol. 5, no. 5, 2009.
- [202] A. Jones and D. Launder, *Lectures in mathematical models of turbulence*, 1972.
- [203] D. C. Wilcox *et al.*, *Turbulence modeling for CFD*. DCW industries La Canada, CA, 1998, vol. 2.
- [204] F. R. Menter, "Two-equation eddy-viscosity turbulence models for engineering applications", *AIAA journal*, vol. 32, no. 8, pp. 1598–1605, 1994.
- [205] E. B. Christopher, "Fundamentals of multiphase flows", *Cambridge University, Press UK*, 2005.
- [206] N. Rios Ratkovich, *Understanding hydrodynamics in Membrane Bioreactor systems for wastewater treatment: Two-phase empirical and numerical modelling and experimental validation*. Ghent University, 2010.
- [207] C. Hirt and B. Nichols, "A computational method for free surface hydrodynamics", *Journal of pressure vessel technology*, vol. 103, no. 2, pp. 136–141, 1981.
- [208] P. Zahedi, R. Saleh, R. Moreno-Atanasio, and K. Yousefi, "Influence of fluid properties on bubble formation, detachment, rising and collapse; Investigation using volume of fluid method", *Korean Journal of Chemical Engineering*, vol. 31, no. 8, pp. 1349–1361, 2014.

- 
- [209] A. Ahmadi Nadooshan and E. Shirani, “Interface pressure model for surface tension force for VOF-based methods in interfacial flows”, *Engineering Applications of Computational Fluid Mechanics*, vol. 2, no. 4, pp. 496–513, 2008.
- [210] J. U. Brackbill, D. B. Kothe, and C. Zemach, “A continuum method for modeling surface tension”, *Journal of computational physics*, vol. 100, no. 2, pp. 335–354, 1992.
- [211] A. Albadawi, Y. Delauré, D. B. Donoghue, A. Robinson, and D. B. Murray, “Numerical investigation of volume of fluid and level set interface capturing methods for bubble growth and detachment”, in *Journal of Physics: Conference Series*, IOP Publishing, vol. 395, 2012, p. 012 166.
- [212] N. Ndinisa, D. Wiley, and D. Fletcher, “Computational fluid dynamics simulations of taylor bubbles in tubular membranes: Model validation and application to laminar flow systems”, *Chemical Engineering Research and Design*, vol. 83, no. 1, pp. 40–49, 2005.
- [213] S. Rosenberger, K. Kubin, and M. Kraume, “Rheology of activated sludge in membrane bioreactors”, *Engineering in life sciences*, vol. 2, no. 9, pp. 269–275, 2002.
- [214] G. Laera, C. Giordano, A. Pollice, D. Saturno, and G. Mininni, “Membrane bioreactor sludge rheology at different solid retention times”, *Water Research*, vol. 41, no. 18, pp. 4197–4203, 2007.
- [215] C. Durán, Y. Fayolle, Y. Pechaud, A. Cockx, and S. Gillot, “Impact of suspended solids on the activated sludge non-newtonian behaviour and on oxygen transfer in a bubble column”, *Chemical Engineering Science*, vol. 141, pp. 154–165, 2016.
- [216] F. Yang, A. Bick, S. Shandalov, A. Brenner, and G. Oron, “Yield stress and rheological characteristics of activated sludge in an airlift membrane bioreactor”, *Journal of Membrane Science*, vol. 334, no. 1-2, pp. 83–90, 2009.
- [217] A. Pollice, C. Giordano, G. Laera, D. Saturno, and G. Mininni, “Rheology of sludge in a complete retention membrane bioreactor”, *Environmental technology*, vol. 27, no. 7, pp. 723–732, 2006.
- [218] N. Rios Ratkovich, I. Nopens, V. De Schepper, T. Jiang, W. Verstraete, and P. A. Vanrolleghem, “A rheological model for activated sludge in a side-stream MBR”, in *4th IWA International Membranes Conference*, 2007.
- [219] R. I. Dick and B. B. Ewing, “The rheology of activated sludge”, *Journal (Water Pollution Control Federation)*, pp. 543–560, 1967.
- [220] I. Seyssiecq, J.-H. Ferrasse, and N. Roche, “State-of-the-art: Rheological characterisation of wastewater treatment sludge”, *Biochemical Engineering Journal*, vol. 16, no. 1, pp. 41–56, 2003.
- [221] D. Brennan, “The numerical simulation of two phase flows in settling tanks”, PhD thesis, Imperial College London (University of London), 2001.
- [222] A. K. Garakani, N. Mostoufi, F. Sadeghi, M. Hosseinzadeh, H. Fatourehchi, M. Sarrafzadeh, and M. Mehrnia, “Comparison between different models for rheological characterization of activated sludge”, *Iranian journal of environmental health science & engineering*, vol. 8, no. 3, p. 255, 2011.
- [223] H. Hasar, C. Kinaci, A. Ünlü, H. Torul, and U. Ipek, “Rheological properties of activated sludge in a sMBR”, *Biochemical Engineering Journal*, vol. 20, no. 1, pp. 1–6, 2004.
- [224] H. Ozogul, P. Jay, and A. Magnin, “Slipping of a viscoplastic fluid flowing on a circular cylinder”, *Journal of Fluids Engineering*, vol. 137, no. 7, p. 071 201, 2015.
- [225] T. C. Papanastasiou, “Flows of materials with yield”, *Journal of Rheology*, vol. 31, no. 5, pp. 385–404, 1987.
- [226] P. Ohle, *Bemessungen von Membranbioreaktoren für die kommunale Abwasserreinigung*. Ges. zur Förderung der Siedlungswasserwirtschaft an der RWTH Aachen, 2002.
- [227] G. J. Kynch, “A theory of sedimentation”, *Transactions of the Faraday society*, vol. 48, pp. 166–176, 1952.
-

- 
- [228] A. M. Egala, D. Kinnear, S. Murthy, and K. Jones, "Settling transition concentration measurement to quantify sludge settling behavior", *Proceedings of the Water Environment Federation*, vol. 2012, no. 10, pp. 5735–5746, 2012.
- [229] P. François, F. Locatelli, J. Laurent, and K. Bekkour, "Experimental study of activated sludge batch settling velocity profile", *Flow Measurement and Instrumentation*, vol. 48, pp. 112–117, 2016.
- [230] D.-H. Li and J. J. Ganczarczyk, "Stroboscopic determination of settling velocity, size and porosity of activated sludge flocs", *Water Research*, vol. 21, no. 3, pp. 257–262, 1987.
- [231] L. Guo, D. Zhang, D. Xu, and Y. Chen, "An experimental study of low concentration sludge settling velocity under turbulent condition", *water research*, vol. 43, no. 9, pp. 2383–2390, 2009.
- [232] P. A. Vesilind, "Design of prototype thickeners from batch settling tests", *Water Sewage Works*, vol. 115, no. 7, pp. 302–307, 1968.
- [233] C. M. Bye and P. L. Dold, "Sludge volume index settleability measures: Effect of solids characteristics and test parameters", *Water environment research*, vol. 70, no. 1, pp. 87–93, 1998.
- [234] G. Daigger and R. Roper Jr, "The relationship between SVI and activated sludge settling characteristics", *Journal (Water Pollution Control Federation)*, pp. 859–866, 1985.
- [235] L. Härtel and H. Pöpel, "A dynamic secondary clarifier model including processes of sludge thickening", *Water science and technology*, vol. 25, no. 6, pp. 267–284, 1992.
- [236] L. Akca, C. Kinaci, and M. Karpuzcu, "A model for optimum design of activated sludge plants", *Water Research*, vol. 27, no. 9, pp. 1461–1468, 1993.
- [237] D. Zhang, Z. Li, P. Lu, T. Zhang, and D. Xu, "A method for characterizing the complete settling process of activated sludge", *Water Research*, vol. 40, no. 14, pp. 2637–2644, 2006.
- [238] K. Grijspeerdt, P. Vanrolleghem, and W. Verstraete, "Selection of one-dimensional sedimentation: Models for on-line use", *Water science and technology*, vol. 31, no. 2, pp. 193–204, 1995.
- [239] R. W. Watts, S. A. Svoronos, and B. Koopman, "One-dimensional modeling of secondary clarifiers using a concentration and feed velocity-dependent dispersion coefficient", *Water Research*, vol. 30, no. 9, pp. 2112–2124, 1996.
- [240] B. De Clercq, "Computational fluid dynamics of settling tanks: Development of experiments and rheological, settling, and scraper submodels.", 2004.
- [241] S. Cho, F. Colin, M. Sardin, and C. Prost, "Settling velocity model of activated sludge", *Water research*, vol. 27, no. 7, pp. 1237–1242, 1993.
- [242] K. J. Scott, "Mathematical models of mechanism of thickening", *Industrial & Engineering Chemistry Fundamentals*, vol. 5, no. 1, pp. 109–113, 1966.
- [243] A. Vanderhasselt and P. A. Vanrolleghem, "Estimation of sludge sedimentation parameters from single batch settling curves", *Water Research*, vol. 34, no. 2, pp. 395–406, 2000.
- [244] G. Keir and V. Jegatheesan, "A review of computational fluid dynamics applications in pressure-driven membrane filtration", *Reviews in Environmental Science and Bio/Technology*, vol. 13, no. 2, pp. 183–201, 2014.
- [245] M. W. D. Brannock, *Computational fluid dynamics tools for the design of mixed anoxic wastewater treatment vessels*. University of Queensland, 2003.
- [246] T. Wang, J. Wang, and Y. Jin, "A CFD–PBM coupled model for gas–liquid flows", *AIChE Journal*, vol. 52, no. 1, pp. 125–140, 2006.
- [247] T. Wang, "Simulation of bubble column reactors using CFD coupled with a population balance model", *Frontiers of Chemical Science and Engineering*, vol. 5, no. 2, pp. 162–172, 2011.



- 
- [248] L. Fan, N. Xu, Z. Wang, and H. Shi, “PDA experiments and CFD simulation of a lab-scale oxidation ditch with surface aerators”, *Chemical Engineering Research and Design*, vol. 88, no. 1, pp. 23–33, 2010.
- [249] I. Nopens, C. Biggs, B. De Clercq, R. Govoreanu, B.-M. Wilén, P. Lant, and P. A. Vanrolleghem, “Modelling the activated sludge flocculation process combining laser light diffraction particle sizing and population balance modelling (PBM)”, *Water Science and Technology*, vol. 45, no. 6, pp. 41–49, 2002.
- [250] L. Böhm and M. Kraume, “Hydrodynamic investigation of single bubbles”, *Czasopismo Techniczne. Mechanika*, vol. 109, no. 1-M, pp. 21–29, 2012.
- [251] L. Böhm, T. Kurita, K. Kimura, and M. Kraume, “Rising behaviour of single bubbles in narrow rectangular channels in Newtonian and non-Newtonian liquids”, *International Journal of Multiphase Flow*, vol. 65, pp. 11–23, 2014.
- [252] L. Böhm, M. Brehmer, and M. Kraume, “Comparison of the single bubble ascent in a Newtonian and a non-Newtonian liquid: A phenomenological PIV study”, *Chemie Ingenieur Technik*, vol. 88, no. 1-2, pp. 93–106, 2016.
- [253] Y. Cao, “Examinations of the shear stress on MBR-membrane plates by a single bubble using CFD”, Master’s thesis, Technische Universität, 2015.
- [254] P. Higuera, J. L. Lara, and I. J. Losada, “Simulating coastal engineering processes with OpenFOAM”, *Coastal Engineering*, vol. 71, pp. 119–134, 2013.
- [255] T.-H. Bae and T.-M. Tak, “Interpretation of fouling characteristics of ultrafiltration membranes during the filtration of membrane bioreactor mixed liquor”, *Journal of Membrane Science*, vol. 264, no. 1-2, pp. 151–160, 2005.
- [256] F. Meng, F. Yang, B. Shi, and H. Zhang, “A comprehensive study on membrane fouling in submerged membrane bioreactors operated under different aeration intensities”, *Separation and Purification Technology*, vol. 59, no. 1, pp. 91–100, 2008.
- [257] R. Bannari, F. Kerdouss, B. Selma, A. Bannari, and P. Proulx, “Three-dimensional mathematical modeling of dispersed two-phase flow using class method of population balance in bubble columns”, *Computers & chemical engineering*, vol. 32, no. 12, pp. 3224–3237, 2008.
- [258] J. Cheng, Q. Li, C. Yang, Y. Zhang, and Z. Mao, “CFD-PBE simulation of a bubble column in OpenFOAM”, *Chinese Journal of Chemical Engineering*, vol. 26, no. 9, pp. 1773–1784, 2018.
- [259] P. Higuera, J. L. Lara, and I. J. Losada, “Realistic wave generation and active wave absorption for Navier–Stokes models: Application to OpenFOAM”, *Coastal Engineering*, vol. 71, pp. 102–118, 2013.
- [260] R. Rzehak and S. Kriebitzsch, “Multiphase CFD-simulation of bubbly pipe flow: A code comparison”, *International Journal of Multiphase Flow*, vol. 68, pp. 135–152, 2015.
- [261] T. Holzmann, “Mathematics, numerics, derivations and OpenFOAM”, *Loeben, Germany: Holzmann CFD*, URL: <https://holzmann-cfd.de> (visited on Nov. 29, 2017), 2016.
- [262] R. Clift, J. R. Grace, and M. E. Weber, *Bubbles, drops, and particles*. Courier Corporation, 2005.
- [263] M. Brenda, *Hybrid Sludge Modeling in Water Treatment Processes*. Technische Universität, 2015, vol. 231.
- [264] J. Cooke, L. Armstrong, K. Luo, and S. Gu, “Adaptive mesh refinement of gas–liquid flow on an inclined plane”, *Computers & Chemical Engineering*, vol. 60, pp. 297–306, 2014.
- [265] A. Theodorakakos and G. Bergeles, “Simulation of sharp gas–liquid interface using VOF method and adaptive grid local refinement around the interface”, *International Journal for Numerical Methods in Fluids*, vol. 45, no. 4, pp. 421–439, 2004.
-

- 
- [266] L. O. Keudel, *Bestimmung des Absetzverhaltens von belebtem Schlamm zur Bemessung von Kläranlagen nach dem Sequencing Batch Reactor (SBR)-Verfahren*. na, 2002.
- [267] S. Schumacher, *Leistungsbestimmende Prozesse in Nachklärbecken: Einflussgrößen, Modellbildung und Optimierung*. Univ., Inst. für Strömungsmechanik und Elektronisches Rechnen im Bauwesen, 2006.
- [268] D. Mikaelian, A. Larcy, S. Dehaeck, *et al.*, “A new experimental method to analyze the dynamics and the morphology of bubbles in liquids: Application to single ellipsoidal bubbles”, *Chemical Engineering Science*, vol. 100, pp. 529–538, 2013.
- [269] L. Liu, H. Yan, and G. Zhao, “Experimental studies on the shape and motion of air bubbles in viscous liquids”, *Experimental Thermal and Fluid Science*, vol. 62, pp. 109–121, 2015.
- [270] R. Wellek, A. Agrawal, and A. Skelland, “Shape of liquid drops moving in liquid media”, *AIChE Journal*, vol. 12, no. 5, pp. 854–862, 1966.
- [271] D. Legendre, R. Zenit, and J. R. Velez-Cordero, “On the deformation of gas bubbles in liquids”, *Physics of Fluids*, vol. 24, no. 4, p. 043303, 2012.
- [272] N. Aybers and A. Tapucu, “Studies on the drag and shape of gas bubbles rising through a stagnant liquid”, *Wärme-und Stoffübertragung*, vol. 2, no. 3, pp. 171–177, 1969.
- [273] E. Loth, “Quasi-steady shape and drag of deformable bubbles and drops”, *International Journal of Multiphase Flow*, vol. 34, no. 6, pp. 523–546, 2008.
- [274] R. Krishna, M. Urseanu, J. Van Baten, and J. Ellenberger, “Rise velocity of a swarm of large gas bubbles in liquids”, *Chemical Engineering Science*, vol. 54, no. 2, pp. 171–183, 1999.
- [275] R. Krishna and J. Van Baten, “Scaling up bubble column reactors with the aid of CFD”, *Chemical Engineering Research and Design*, vol. 79, no. 3, pp. 283–309, 2001.
- [276] M. Rastello, J.-L. Marié, and M. Lance, “Drag and lift forces on clean spherical and ellipsoidal bubbles in a solid-body rotating flow”, *Journal of Fluid Mechanics*, vol. 682, pp. 434–459, 2011.
- [277] F. Liang-Shih and K. Tsuchiya, *Bubble wake dynamics in liquids and liquid-solid suspensions*. Butterworth-Heinemann, 2013.
- [278] M. Khan, M. Hussain, Z. Mansourpour, N. Mostoufi, N. Ghasem, and E. Abdullah, “CFD simulation of fluidized bed reactors for polyolefin production—A review”, *Journal of Industrial and Engineering Chemistry*, vol. 20, no. 6, pp. 3919–3946, 2014.
- [279] R. Davies and G. I. Taylor, “The mechanics of large bubbles rising through extended liquids and through liquids in tubes”, *Proceedings of the Royal Society of London. Series A. Mathematical and Physical Sciences*, vol. 200, no. 1062, pp. 375–390, 1950.
- [280] D. T. Dumitrescu, “Strömung an einer luftblase im senkrechten Rohr”, *ZAMM-Journal of Applied Mathematics and Mechanics/Zeitschrift für Angewandte Mathematik und Mechanik*, vol. 23, no. 3, pp. 139–149, 1943.
- [281] G. Bozzano and M. Dente, “Shape and terminal velocity of single bubble motion: A novel approach”, *Computers & chemical engineering*, vol. 25, no. 4-6, pp. 571–576, 2001.
- [282] A. Filella, P. Ern, and V. Roig, “Oscillatory motion and wake of a bubble rising in a thin-gap cell”, *Journal of Fluid Mechanics*, vol. 778, pp. 60–88, 2015.
- [283] T. Taha and Z. Cui, “CFD modelling of gas-sparged ultrafiltration in tubular membranes”, *Journal of membrane science*, vol. 210, no. 1, pp. 13–27, 2002.
- [284] L. Böhm, A. Drews, H. Prieske, P. R. Bérubé, and M. Kraume, “The importance of fluid dynamics for MBR fouling mitigation”, *Bioresource technology*, vol. 122, pp. 50–61, 2012.

- 
- [285] T. Jiang, M. D. Kennedy, C. Yoo, I. Nopens, W. van der Meer, H. Futselaar, J. C. Schippers, and P. A. Vanrolleghem, "Controlling submicron particle deposition in a side-stream membrane bioreactor: A theoretical hydrodynamic modelling approach incorporating energy consumption", *Journal of membrane science*, vol. 297, no. 1-2, pp. 141–151, 2007.
- [286] G. Foley, *Membrane filtration: a problem solving approach with MATLAB*. Cambridge University Press, 2013.
- [287] H. K. Vyas, R. Bennett, and A. Marshall, "Cake resistance and force balance mechanism in the crossflow microfiltration of lactalbumin particles", *Journal of Membrane Science*, vol. 192, no. 1-2, pp. 165–176, 2001.
- [288] J. Altmann and S. Ripperger, "Particle deposition and layer formation at the crossflow microfiltration", *Journal of Membrane Science*, vol. 124, no. 1, pp. 119–128, 1997.
- [289] H. E. Wray, R. C. Andrews, and P. R. Bérubé, "Surface shear stress and retention of emerging contaminants during ultrafiltration for drinking water treatment", *Separation and Purification Technology*, vol. 122, pp. 183–191, 2014.
- [290] G. Rubin, "Widerstands- und Auftriebsbeiwerte von ruhenden, kugelförmigen Partikeln in stationären, wandnahen laminaren Grenzschichten", PhD thesis, Verlag nicht ermittelbar, 1977.
- [291] A. Margaritis, D. W. te Bokkel, and D. G. Karamanev, "Bubble rise velocities and drag coefficients in non-Newtonian polysaccharide solutions", *Biotechnology and bioengineering*, vol. 64, no. 3, pp. 257–266, 1999.
- [292] A. R. Gollakota and N. Kishore, "CFD study on rise and deformation characteristics of buoyancy-driven spheroid bubbles in stagnant carreau model non-Newtonian fluids", *Theoretical and Computational Fluid Dynamics*, vol. 32, no. 1, pp. 35–46, 2018.
- [293] L. Zhang, C. Yang, and Z.-S. Mao, "Numerical simulation of a bubble rising in shear-thinning fluids", *Journal of Non-Newtonian Fluid Mechanics*, vol. 165, no. 11-12, pp. 555–567, 2010.
- [294] N. Dietrich, N. Mayoufi, S. Poncin, and H.-Z. Li, "Experimental investigation of bubble and drop formation at submerged orifices", *Chemical Papers*, vol. 67, no. 3, pp. 313–325, 2013.
- [295] M. Jamialahmadi, M. Zehtaban, H. Müller-Steinhagen, A. Sarrafi, and J. Smith, "Study of bubble formation under constant flow conditions", *Chemical Engineering Research and Design*, vol. 79, no. 5, pp. 523–532, 2001.
- [296] A. A. Kulkarni and J. B. Joshi, "Bubble formation and bubble rise velocity in gas- liquid systems: A review", *Industrial & Engineering Chemistry Research*, vol. 44, no. 16, pp. 5873–5931, 2005.
- [297] J. Katz and C. Meneveau, "Wake-induced relative motion of bubbles rising in line", *International journal of multiphase flow*, vol. 22, no. 2, pp. 239–258, 1996.
- [298] M. Gumulya, R. Utikar, G. Evans, J. Joshi, and V. Pareek, "Interaction of bubbles rising inline in quiescent liquid", *Chemical Engineering Science*, vol. 166, pp. 1–10, 2017.
- [299] N. de Nevers and J.-L. Wu, "Bubble coalescence in viscous fluids", *AIChE Journal*, vol. 17, no. 1, pp. 182–186, 1971.
- [300] T.-J. Lin and G.-M. Lin, "Mechanisms of in-line coalescence of two-unequal bubbles in a non-Newtonian fluid", *Chemical Engineering Journal*, vol. 155, no. 3, pp. 750–756, 2009.
- [301] T. Wilmarth and M. Ishii, "Two-phase flow regimes in narrow rectangular vertical and horizontal channels", *International Journal of Heat and Mass Transfer*, vol. 37, no. 12, pp. 1749–1758, 1994.
- [302] S. Jankhah and P. R. Bérubé, "Power induced by bubbles of different sizes and frequencies on to hollow fibers in submerged membrane systems", *Water research*, vol. 47, no. 17, pp. 6516–6526, 2013.

- 
- [303] S. Jankhah, “Effect of bubble size and sparging frequency on the power transferred onto membranes for fouling control”, PhD thesis, University of British Columbia, 2013.
- [304] E. Radaei, X. Liu, K. H. Tng, Y. Wang, F. J. Trujillo, and G. Leslie, “Insights on pulsed bubble control of membrane fouling: Effect of bubble size and frequency”, *Journal of Membrane Science*, vol. 554, pp. 59–70, 2018.
- [305] A. Tomiyama, G. Celata, S. Hosokawa, and S. Yoshida, “Terminal velocity of single bubbles in surface tension force dominant regime”, *International Journal of Multiphase Flow*, vol. 28, no. 9, pp. 1497–1519, 2002.
- [306] P. Saffman, “On the rise of small air bubbles in water”, *Journal of Fluid Mechanics*, vol. 1, no. 3, pp. 249–275, 1956.
- [307] C. Brücker, “Structure and dynamics of the wake of bubbles and its relevance for bubble interaction”, *Physics of fluids*, vol. 11, no. 7, pp. 1781–1796, 1999.
- [308] K. Ellingsen and F. Risso, “On the rise of an ellipsoidal bubble in water: Oscillatory paths and liquid-induced velocity”, *Journal of Fluid Mechanics*, vol. 440, pp. 235–268, 2001.
- [309] X. Liu, Y. Wang, Y. Shi, Q. Li, P. Dai, J. Guan, T. D. Waite, and G. Leslie, “CFD modelling of uneven flows behaviour in flat-sheet membrane bioreactors: From bubble generation to shear stress distribution”, *Journal of Membrane Science*, vol. 570, pp. 146–155, 2019.